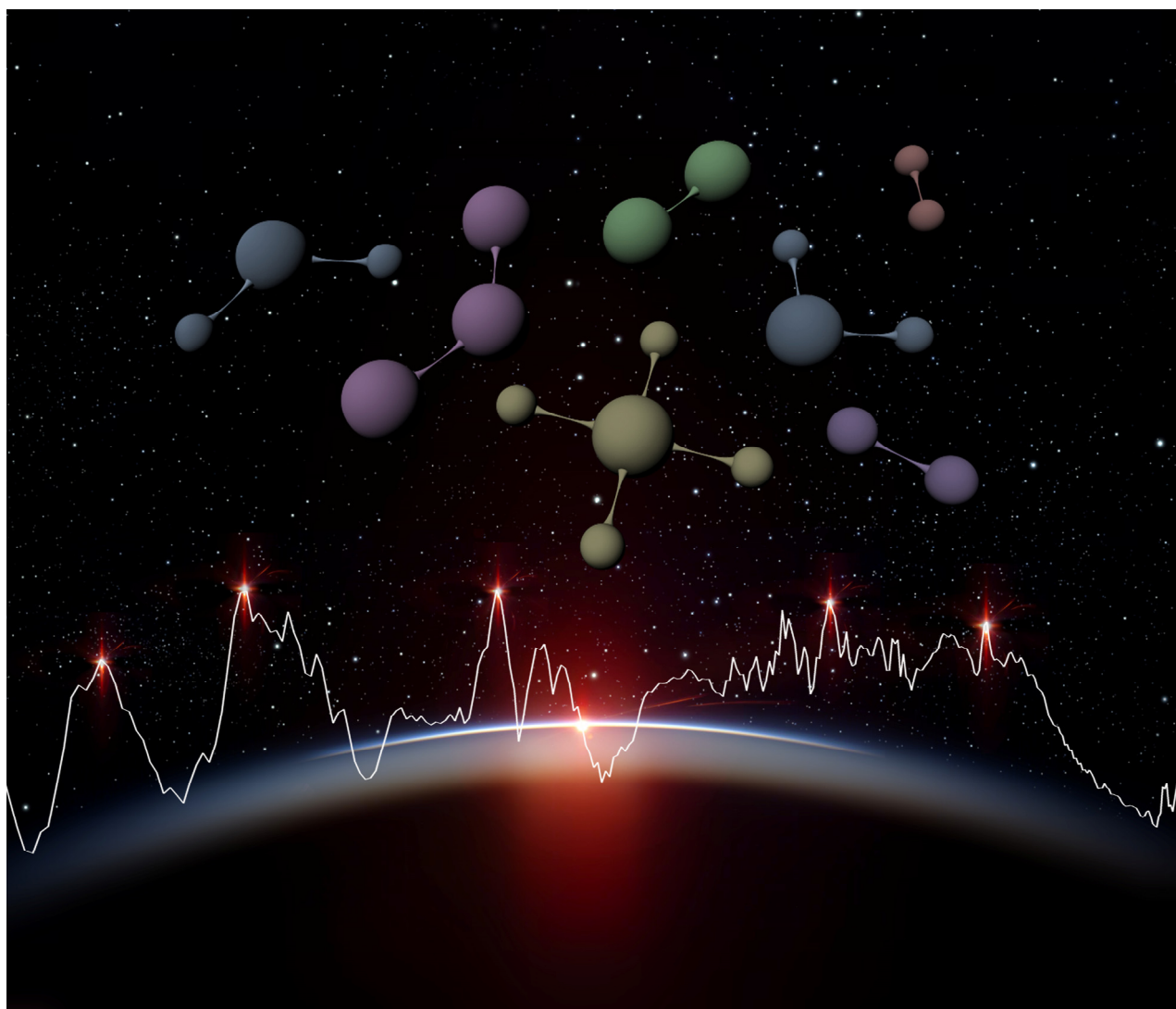


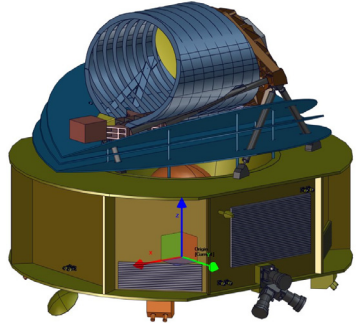
# ARIEL

**Atmospheric Remote-sensing Infrared Exoplanet Large-survey**  
*Enabling Planetary Science across Light-years*



Assessment Study Report

----- PAGE INTENTIONALLY LEFT BLANK -----

ARIEL Mission Summary	
<b>Key Science Questions to be Addressed</b>	<ul style="list-style-type: none"> <li>• <b>What are exoplanets made of?</b></li> <li>• <b>How do planets and planetary systems form?</b></li> <li>• <b>How do planets and their atmospheres evolve over time?</b></li> </ul>
<b>Science Objectives</b> (Chapter 2)	<ul style="list-style-type: none"> <li>• Detect and determine the composition and structure of a large number of planetary atmospheres</li> <li>• Constrain planetary interiors by removing degeneracies in the interpretation of mass-radius diagrams</li> <li>• Constrain planetary formation and evolution models through measurements of the elemental composition (evidence for migration)</li> <li>• Determine the energy budget of planetary atmospheres (albedo, vertical and horizontal temperature structure, weather/temporal variations)</li> <li>• Identify and constrain chemical processes at work (thermochemistry, photochemistry, transport, quenching, etc.)</li> <li>• Constrain the properties of clouds (cloud type, particle size, distribution, patchiness, etc.)</li> <li>• Investigate the impact of stellar and planetary environment on exoplanet properties</li> <li>• Identification of different populations of planets and atmospheres (for example, through colour-colour diagrams)</li> <li>• Capacity to do a population study AND go into a detailed study of select planets</li> </ul>
<b>ARIEL Core Survey</b> (Chapters 2.2 & 7.4.3)	<ul style="list-style-type: none"> <li>• Survey of ~ 1000 transiting exoplanets from gas giants to rocky planets, in the hot to temperate zones of F to M-type host stars</li> <li>• Target selection before launch based on ESA science team and community inputs</li> <li>• Delivery of a homogeneous catalogue of planetary spectra, yielding refined molecular abundances, chemical gradients and atmospheric structure; diurnal and seasonal variations; presence of clouds and measurement of albedo</li> </ul>
<b>Observational Strategy</b> (Chapter 2.4.2)	<ul style="list-style-type: none"> <li>• Transit, eclipse and phase-curve spectroscopy with broad (0.5-7.8<math>\mu</math>m), instantaneous, uninterrupted spectra</li> <li>• High photometric stability on transit timescales</li> <li>• Large instantaneous sky coverage</li> <li>• Focus on planets around very bright stellar hosts.</li> <li>• Three-tiered approach: 3 different samples are observed at optimised spectral resolutions and SNRs.</li> <li>• Required SNR obtained by summing a number of transits or eclipses (typically &lt; 10 events)</li> </ul>
<b>Payload</b> (Chapter 4)	<ul style="list-style-type: none"> <li>• Off-axis Cassegrain telescope, 1.1m x 0.7m elliptical M1; diffraction limited at 3<math>\mu</math>m. Mirrors, optical bench and telescope all manufactured from Aluminium alloy for isothermal design with minimal thermo-elastic deformation.</li> <li>• ARIEL InfraRed Spectrometer (AIRS) provides low/medium resolution (R = 30 – 200) spectroscopy between 1.95 and 7.8 <math>\mu</math>m.</li> <li>• FGS module includes 3 photometric channels (two used for guiding as well as science) between 0.5 and 1.2 <math>\mu</math>m and low resolution NIR spectrometer from 1.2 – 1.95 <math>\mu</math>m.</li> <li>• Thermal: Warm SVM, cryogenic PLM cooled passively to ~55K with the thermal shield assembly. Active cooler (Neon JT) included to ensure AIRS detector operating temperature of <math>\leq</math>42K</li> </ul> 
<b>Spacecraft</b> (Chapter 5)	<ul style="list-style-type: none"> <li>• Spacecraft budgets: &lt;1.3 t launch mass, ~1 kW power</li> <li>• Communications: X-band, 180 Gbit / week of science and housekeeping data</li> <li>• Fine pointing requirements across instrument LoS (3 sigma): APE <math>\leq</math> 1"; RPE <math>\leq</math> 200 mas up to 90 s; PDE <math>\leq</math> 100 mas up to 10 hrs for integrations of 90 s</li> <li>• AOCS: Fine Guidance Sensor and Reaction Wheels on dampers used in a narrow angular speed operating range to minimise micro-vibrations</li> </ul>
<b>Launch and Operations</b> (Chapters 5.1 & 6)	<ul style="list-style-type: none"> <li>• A62 launch from Kourou in 2026 to operational large amplitude orbit around L2</li> <li>• 4 years nominal lifetime (6 years goal)</li> <li>• MOC as ESOC, SOC at ESAC, and Instrument Operations and Science Data Centre distributed across consortium member states</li> <li>• 14 hrs split in 3 ground contacts per week with 35 m ESTRACK ground stations</li> </ul>
<b>Data Policy</b> (Chapter 7.4.4)	<ul style="list-style-type: none"> <li>• It is recognized that ARIEL data will be of great interest to the general astronomical &amp; exoplanet community.</li> <li>• ARIEL wants to embrace the general community, we will do this by offering open involvement in target selection, and by providing a very open data policy.</li> <li>• Regular timely public releases of high quality data products at various processing levels will be provided throughout the mission.</li> </ul>

## Foreword

The concept of a mission devoted to atmospheric characterization of exoplanets through transit spectroscopy was first considered in Europe in 2007, shortly after the DARWIN proposal submitted to ESA for the first Cosmic Vision call for L-class missions was rejected because of the need for further scientific and technical developments. Following the decision, both ESA (EP-RAT panel – report in October 2010) and the Exoplanetary Community (Blue Dot Team – Barcelona conference in September 2009) started a discussion to define a scientific and technological roadmap for exoplanetary research. Both groups concluded that an intermediate step was needed, both scientifically and technically, before the characterisation of Earth-like planets could be tackled, and recommended a transit spectroscopy mission as a first step to atmospheric characterisation. A short study was undertaken at ESTEC in the context of the ExoPlanet Roadmap Advisory Team mandate: the THESIS mission concept, the subject of one of the EP-RAT white papers, was studied under the name ESM (Exoplanet Spectroscopy Mission). Following this study the Exoplanet Characterisation Observatory (EChO) was proposed and accepted for assessment phase study for the M3 mission opportunity. Although eventually not selected, the EChO study allowed further development of the technical building blocks and the science case for an eventual transit spectroscopy mission ([EChO – Exoplanet Characterisation Observatory, \*Experimental Astronomy\*, Special Issue, Volume 40, Nos. 2-3, 2015](#)).

In response to the call for the next medium class mission, M4, in the Cosmic Vision 2015 – 2025 programme a proposal was submitted in January 2015 for the ARIEL, Atmospheric Remote-sensing InfraRed Large survey mission. The mission was one of the three selected in June 2015 for study in a Phase 0/A assessment phase. Soon after, an ESA study team, and an ARIEL Study Science Team (SST) comprising scientists from the proposing consortium and beyond, were assembled, and work began on the ARIEL assessment study.

In the summer of 2015, an internal ESA pre-assessment study of ARIEL was undertaken in the Concurrent Design Facility at ESTEC that provided a baseline mission concept primarily used to consolidate requirements for the Invitation to Tender for the subsequent study. This CDF study drew input from the mission proposal, the previous studies conducted on EChO, ESM and THESIS, and input from the payload consortium. The Invitation to Tender was then released for a 15-month industrial phase A study. Tenders were accepted from consortiums led by Airbus Defence and Space (Toulouse) and TAS-F (Cannes); these studies started in early 2016.

The industrial teams and payload consortium studies concluded in February 2017. The payload consortium study included a review of the mission requirements, the technical design and analysis of the complete payload module (including telescope, spectrometer instruments, guidance system and supporting infrastructure) and development of an end-to-end performance simulator of the complete system. The industrial studies included a review of the mission requirements, the technical design and analysis of the S/C (including a conceptual design of a backup telescope) and a programmatic analysis of the mission. Dedicated iterations were done in conjunction with both industrial and instrument studies to harmonise the interfaces between the S/C and the payload, and to consolidate the payload accommodation. At the time of writing, the results of these studies are under review as part of the Mission Selection Review.

A successful open ARIEL community workshop (<http://arielconference.eu/>) was held in Brussels in late November 2016 to share the preliminary results of the Assessment Phase study with the general astronomy and solar system communities, to inform them of the capabilities of the ARIEL mission and to have an open discussion as to how ARIEL involve and serve the general community and can work in conjunction with other ground-based and space-based observatories to best further our knowledge of exoplanetary science.

This assessment study report presents a summary of the very large body of work that has been undertaken on the ARIEL mission at scientific and technical levels over the 21-month period of the ARIEL assessment phase. As such, it represents the contributions of a large number of parties (ESA, industry, institutes and universities from many ESA member states), encompassing a very large number of people. Within the three years since ARIEL was first conceived in 2014, the number of confirmed exoplanets has increased from ~1000 to over 3500, providing an ever more tantalising prospect of looking beyond our solar system & enabling planetary science across the light years.

## Authorship, acknowledgements

This report has been prepared by the ARIEL Team listed below:

ESA Science Study Team (SST)		
<i>Name</i>	<i>Affiliation</i>	<i>City, Country</i>
Giovanna Tinetti	UCL	London, UK
Pierre Drossart	LESIA / Paris Observatory	Paris, FR
Paul Eccleston	STFC / RAL Space	Harwell, UK
Paul Hartogh	MPS	Göttingen, DE
Jérémy Leconte	CNRS / University of Bordeaux	Bordeaux, FR
Giusi Micela	INAF / Observatory of Palermo	Palermo, IT
Marc Ollivier	IAS & LESIA / Paris Observatory	Orsay/Paris, FR
Diego Turrini	INAF / IAPS	Rome, IT
Bart Vandenbussche	University of Leuven	Leuven, BE
Paulina Wolkenberg	CBK-PAN	Warsaw, PL

The ESA Team supporting the activities comprises:

ESA study team		
Ludovic Puig (Study Manager)	ESTEC	Noordwijk, NL
Göran Pilbratt (Study Scientist)		
Astrid Heske (Payload Manager)		
Isabel Escudero Sanz (Optical Engineer)		
Pierre-Elie Crouzet (Detector Engineer)		
Ralf Kohley (SOC)	ESAC	Madrid, ES
Kate Symonds (MOC)	ESOC	Darmstadt, DE
ESA Coordinator		
Luigi Colangeli	ESA	Noordwijk, NL

A detailed list of consortium members and their roles is included in Appendix A.

The payload consortium is supported by their respective national funding agencies. The team would like to thank the agencies for their support during the assessment study.

We would like to thank the ESA CDF team, as well as TEC and SRE directorate colleagues who provided support during the course of the study.

The sections on mission design were compiled by the ESA study team based on the outputs of the industrial studies, led by:

- Airbus Defense and Space, France
- TAS, France

The graphics of the title page were prepared by ESA/C.Carreau and ATG medialab

## Table of contents

<b>1</b>	<b>EXECUTIVE SUMMARY</b> .....	<b>9</b>
<b>2</b>	<b>SCIENTIFIC OBJECTIVES</b> .....	<b>12</b>
2.1	The ARIEL Mission as Part of Cosmic Vision.....	12
2.1.1	Highlights & limits of current knowledge of planets.....	12
2.1.1.1	<i>The way forward: the chemical composition of a large sample of planets</i> .....	13
2.1.1.2	<i>The way forward: ARIEL</i> .....	14
2.1.2	Planetary classes & ARIEL.....	14
2.1.2.1	<i>Planetary migration: an ARIEL ally</i> .....	16
2.1.3	Planet density: an inaccurate indicator of exoplanets' nature.....	17
2.1.4	Current observations of exo-atmospheres: strengths & pitfalls.....	18
2.2	Key Science Questions Addressed by ARIEL.....	20
2.2.1	How ARIEL will place the Solar System into a broader context.....	20
2.2.2	Formation-evolution of gas-rich planets & ARIEL.....	21
2.2.2.1	<i>How ARIEL observations will help overcome degeneracies in the study of the exoplanet interior</i> .....	21
2.2.2.2	<i>Gas-rich exoplanets: ARIEL ability to measure atmospheric chemistry</i> .....	23
2.2.2.3	<i>Gas-rich exoplanets: ARIEL ability to measure atmospheric dynamics &amp; cloud distribution</i> .....	25
2.2.2.4	<i>Gas-rich exoplanets: ARIEL ability to constrain exoplanet provenance &amp; formation mechanisms</i> .....	27
2.2.3	Formation-evolution of transitional planets & ARIEL.....	28
2.2.3.1	<i>Why mass-radius determination is not enough to constrain the transitional planets' composition</i> .....	29
2.2.3.2	<i>How the atmospheric composition can solve the issue</i> .....	30
2.2.4	Formation-evolution of rocky/icy planets & ARIEL.....	31
2.2.5	Planets in rare and/or extreme conditions & ARIEL.....	33
2.3	Extended use of ARIEL observations.....	34
2.4	Strategy to achieve the science objectives.....	34
2.4.1	How do we observe exo-atmospheres?.....	34
2.4.2	ARIEL observational strategy: a 3-tier approach.....	36
2.4.3	ARIEL Tier 1: exoplanet population analysis.....	36
2.4.4	ARIEL Tier 2: single planets & population analysis.....	39
2.4.4.1	<i>Phase-curves</i> .....	41
2.4.5	ARIEL Tier 3: very detailed study of select planets.....	41
2.4.6	Targets available for ARIEL today.....	43
2.4.7	The ARIEL Mission Reference Sample in 2026.....	43
2.5	Uniqueness of ARIEL & Synergies with other facilities.....	45
2.5.1	Complementarity ARIEL-JWST.....	46
2.5.2	Complementarity ARIEL-E-ELT.....	47
2.6	Conclusions.....	48
<b>3</b>	<b>SCIENTIFIC REQUIREMENTS</b> .....	<b>49</b>
3.1	Required wavelength coverage, spectral resolution and S/N.....	49
3.2	Dealing with Systematic and Astrophysical Noise.....	51
3.2.1	ARIEL performance requirements.....	51
3.2.1.1	<i>The ARIEL end-to-end instrument simulator: ARIEL-Sim</i> .....	52
3.2.1.2	<i>Postprocessing analysis techniques</i> .....	52
3.2.2	Correcting for stellar activity.....	53
3.2.2.1	<i>ARIEL-Sim simulations of impact of stellar variability on ARIEL observations</i> .....	53
3.2.2.2	<i>Methods to correct the effect of star spots on transit spectra</i> .....	55
3.2.2.3	<i>Flares</i> .....	56
3.3	Conclusions.....	57

3.4	Key Questions and Answers about ARIEL.....	58
<b>4</b>	<b>PAYLOAD.....</b>	<b>61</b>
4.1	Payload Architecture.....	61
4.2	Payload Module Structural Design and Analysis .....	62
4.2.1	Common Optical Bench Design .....	62
4.2.2	Support Bi-pods Design and Sizing.....	62
4.2.3	V-Groove Radiation Shields .....	62
4.3	Payload Module Thermal Design and Analysis.....	63
4.3.1	Thermal Architecture.....	63
4.3.2	Thermal Analysis Results and Margin Analysis.....	63
4.3.3	Transient Thermal Analyses .....	64
4.4	The ARIEL Active Cooler System .....	64
4.5	The ARIEL Telescope Design .....	65
4.5.1	Optical Design .....	65
4.5.2	Preliminary Mechanical & Thermal Design and Modelling.....	66
4.5.3	Pathfinder Telescope Mirror .....	66
4.5.4	M2 Mirror (M2M) Mechanism.....	67
4.6	Common Optics, Dichroics and In-Flight Calibration Unit.....	68
4.7	The ARIEL InfraRed Spectrometer (AIRS) Design.....	68
4.7.1	Functional Design and Architecture .....	68
4.7.2	Optical Design .....	69
4.7.3	Mechanical and Thermal Design .....	70
4.7.4	Detector and Signal Chain System .....	70
4.7.4.1	<i>Baseline Detectors: Teledyne HIRG</i> .....	70
4.7.4.2	<i>Option European detector developments</i> .....	71
4.7.4.3	<i>Cold and Warm Detector Electronics</i> .....	71
4.8	Instrument Control Unit.....	72
4.8.1	Architecture & Functionality .....	72
4.8.2	Telescope Control Unit.....	72
4.9	The Fine Guidance System (FGS), Visible Photometer (VISPhot) and Near-IR Spectrometer (NIRSpec) Design.....	73
4.9.1	Functional Design and Architecture .....	73
4.9.2	Optical Design and Performance .....	73
4.9.3	Mechanical Design .....	74
4.9.4	Detector System.....	74
4.9.5	FGS Control Unit (FCU) .....	74
4.9.6	Centroiding and Guidance Software.....	75
4.10	The Payload Noise Budget and Performance Simulation.....	75
4.11	Payload Budgets.....	77
4.11.1	Power and Data Rate Budgets .....	77
4.11.2	Payload Mass Budget .....	77
4.11.3	Throughput Budget.....	77
<b>5</b>	<b>MISSION DESIGN .....</b>	<b>78</b>
5.1	Mission Analysis.....	79
5.2	Spacecraft Design .....	81
5.2.1	Structures, configuration and thermal.....	81
5.2.2	Attitude and Orbit Control Subsystem.....	83
5.2.3	Propulsion.....	85
5.2.4	SVM Electrical Architecture .....	85
5.3	Spacecraft Budgets.....	85
5.3.1	Mass Budget .....	85
5.3.2	Power Budget.....	86
5.4	Spacecraft and Payload AIV and Development Plans .....	87
5.5	Technology Readiness .....	89

---

5.5.1	ESA Developments.....	89
5.5.2	Payload Consortium Development Status and Plans.....	89
<b>6</b>	<b>MISSION OPERATIONS AND GROUND SEGMENT.....</b>	<b>90</b>
6.1	Overview.....	90
6.1.1	Overview of the operational centres.....	90
6.1.2	Mission Operations Centre.....	91
6.1.3	Ground Stations.....	91
6.1.4	Science Operations Centre.....	91
6.1.5	Instrument Operations and Science Data Centre.....	92
6.2	Mission operations.....	92
6.3	Science operations, calibration and data handling/archiving.....	93
6.3.1	Mission planning.....	93
6.3.2	Instrument operations and calibration.....	93
6.3.2.1	Ground Calibration:.....	94
6.3.2.2	Flight Calibration.....	94
6.3.3	Data level products.....	94
6.3.4	Science data processing.....	95
6.3.5	ARIEL archive and scientific community support.....	96
<b>7</b>	<b>MANAGEMENT.....</b>	<b>97</b>
7.1	Project management.....	97
7.1.1	Overview.....	97
7.1.2	Management of operations.....	97
7.2	Procurement philosophy.....	97
7.3	ARIEL schedule.....	98
7.4	Science Management.....	99
7.4.1	Project Scientist.....	99
7.4.2	Science Team.....	99
7.4.3	Target List.....	99
7.4.4	Data Rights and Proprietary Periods.....	100
<b>8</b>	<b>COMMUNICATIONS AND OUTREACH.....</b>	<b>101</b>
<b>9</b>	<b>REFERENCES.....</b>	<b>103</b>
9.1	References for Sections 2 & 3 – Science Case and Requirements.....	103
9.2	References for Section 4 & 5 – Payload, Mission and Spacecraft Design.....	106
9.3	References for Section 6 – Mission Operations.....	106
<b>10</b>	<b>LIST OF ACRONYMS.....</b>	<b>107</b>
<b>11</b>	<b>APPENDIX A: ARIEL PAYLOAD CONSORTIUM.....</b>	<b>109</b>
11.1	Consortium Management Team.....	109
11.1.1	Co-PI’s & Co-I’s.....	109
11.1.2	National Project Managers.....	109
11.2	Consortium Technical Team Coordinators.....	109
11.3	Consortium Science Team Coordinators.....	109
11.4	Consortium Contributing Scientists & Engineers.....	109
11.5	International Participating Scientists.....	110

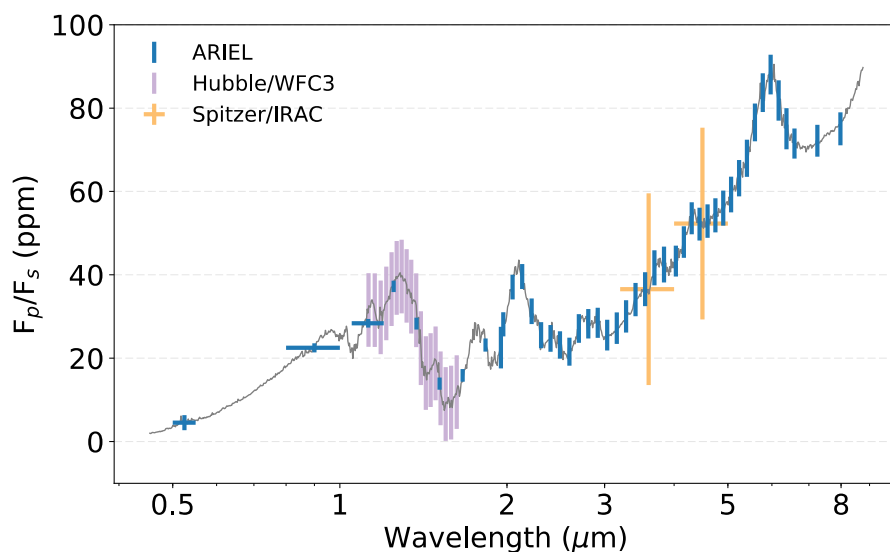
# 1 Executive Summary

The ARIEL mission will address the fundamental questions on **what exoplanets are made of** and **how planetary systems form and evolve** by investigating the atmospheres of many **hundreds of diverse planets** orbiting different types of stars. This unbiased survey will contribute to the progress in answering the first of the four ambitious topics listed in the ESA's Cosmic Vision: “*What are the conditions for planet formation and the emergence of life?*”

Thousands of exoplanets have now been discovered with a huge range of masses, sizes and orbits: from rocky Earth-like planets to large gas giants grazing the surface of their host star. However, the essential **nature of these exoplanets remains largely mysterious**: there is no known, discernible pattern linking the presence, size, or orbital parameters of a planet to the nature of its parent star. We have little idea whether the chemistry of a planet is linked to its formation environment, or whether the type of host star drives the physics and chemistry of the planet's birth, and evolution.

**ARIEL will observe a large number (~1000) of transiting planets for statistical understanding**, including gas giants, Neptunes, super-Earths and Earth-size planets around a range of host star types using transit spectroscopy in the 1.25-7.8  $\mu\text{m}$  spectral range and multiple narrow-band photometry in the optical. We will focus on warm and hot planets to take advantage of their well-mixed atmospheres which should show minimal condensation and sequestration of high-Z materials and thus reveal their bulk and elemental composition (especially C, O, N, S, Si). Observations of these warm/hot exoplanets will allow the understanding of the early stages of planetary and atmospheric formation during the nebular phase and the following few million years. ARIEL will thus provide a truly representative picture of the chemical nature of the exoplanets and relate this directly to the type and chemical environment of the host star.

For this ambitious scientific programme, **ARIEL is designed as a dedicated survey mission for transit and eclipse spectroscopy**, capable of observing a large and well-defined planet sample within its 4-year mission lifetime. Transit, eclipse and phase-curve spectroscopy methods, whereby the signal from the star and planet are differentiated using knowledge of the planetary ephemerides, allow us to measure atmospheric signals from the planet at levels of 10-100 part per million (ppm) relative to the star and, given the bright nature of targets, also allows more sophisticated techniques, such as eclipse mapping, to give a deeper insight into the nature of the atmosphere. *These types of observations require a specifically designed, stable payload and satellite platform with broad, instantaneous wavelength coverage to detect many molecular species, probe the thermal structure, identify clouds and monitor the stellar activity.* The wavelength range proposed covers all the expected major atmospheric gases from e.g. H<sub>2</sub>O, CO<sub>2</sub>, CH<sub>4</sub>, NH<sub>3</sub>, HCN, H<sub>2</sub>S through to the more exotic metallic compounds, such as TiO, VO, and condensed species.



*Expected output (with error bars) from the ARIEL processed data product compared with the input model assumption for a hot super-Earth similar to 55-Cnc-e around a G-type star with  $K_{\text{mag}}$  of 4. ARIEL performances using 8 eclipses (~32 hours of observation) are compared to currently available data for 55 Cnc e from Spitzer-IRAC (8 eclipses, [Demory et al., 2016](#)) and performances of Hubble-WFC3 extrapolated from transit observations of 55 Cnc e ([Tsiaras et al., 2016](#)).*

**Performance Evaluation** – Simulations of ARIEL performance in conducting exoplanet surveys have been performed – using conservative estimates of mission performance and a full model of all significant noise sources in the measurement – using a list of potential ARIEL targets that incorporates the latest available exoplanet statistics. The conclusion is that ARIEL – in line with the stated mission objectives – will be able to observe 500-1000 exoplanets depending on the details of the adopted survey strategy, thus confirming the feasibility of the main science objectives.

**The ARIEL data policy** – has been designed to embrace the astronomy community in general and the exoplanet community in particular. It is recognised that ARIEL data and data products will be of huge interest to the entire exoplanet community, not only to those directly involved in the mission. The intention is to provide high quality data in a timely manner and to have a continuous dialogue with the wider community, maximising the science that can be achieved by the mission.

*Inputs to the target list* – to be observed will be solicited from the wider community (e.g. through whitepapers, meetings, and other mechanisms), the community will be kept informed about the status of the target list, as will the ESA Advisory Bodies whose feedback will be solicited.

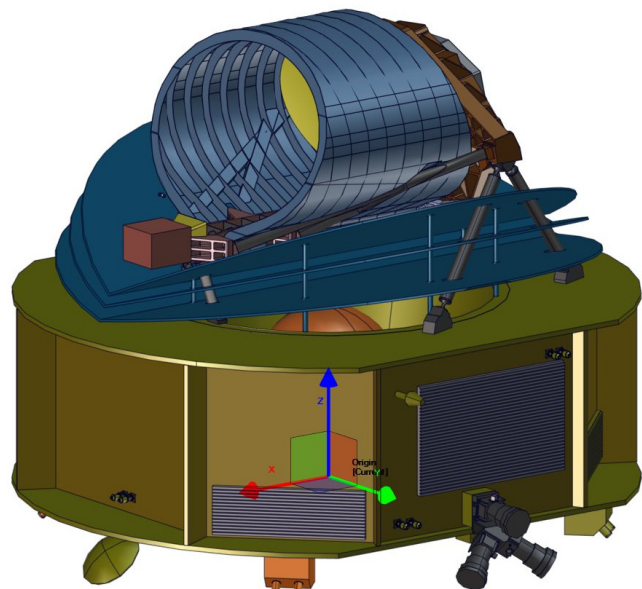
*A Science Demonstration Phase (SDP)* will be conducted as the final step before routine science phase operations commence. The SDP is foreseen to provide approximately one month's worth of data observed in the same manner that the core survey will be conducted. These data will be made public on a timescale of about a month, in conjunction with organisation of a major public workshop.

*Regular timely public releases* of high quality data products at various processing levels will be provided throughout the mission. The data will be pipeline processed to different levels of data products labelled 'raw telemetry' (level 0), 'raw spectral frame cubes' (level 1), 'target (star + planet) spectra' (level 2), and 'individual planet spectra' (level 3), respectively. The lower levels can generally be released quicker than higher levels, but the objective is to release all levels timely in order to maximise the science return and impact of ARIEL.

Beyond the science community, ARIEL's mission to characterise distant worlds offers an immense opportunity to capture the public imagination and inspire the next generation of scientists and engineers. Through the provision of enquiry-based educational programmes and citizen science platforms, school students and members of the public will have the opportunity to participate directly in the analysis of ARIEL data.

**Mission and spacecraft design** – ARIEL will be launched from Kourou (FR) on board an Ariane 62 in 2026. Its nominal operations orbit is a large amplitude orbit around the Sun-Earth L2 point. This orbit provides a stable environment, along with a large instantaneous field of regard, both of which are key to allowing ARIEL to meet its science objectives. The spacecraft is designed in a modular way, with a service module (SVM) and a payload module (PLM) that can be procured and tested in parallel. A payload consortium funded by national agencies will provide the full ARIEL payload (telescope and instrument) and ESA will provide the spacecraft. An illustration of the baseline payload module and a representative SVM is shown to the right.

*The SVM* contains all the units required to operate the spacecraft and maintain the payload in its nominal operating conditions. The spacecraft has a wet mass of ~1.2 t and a power generation capability of ~1 kW. 180 Gbit of science data will be generated every week, and are down-linked in 3 ground contacts totalling 14 hrs/week using an X-band system and the 35 m ESTRACK ground stations. The fine pointing requirements achieved by the AOCS system are (3 sigma): APE  $\leq 1''$ ; RPE  $\leq$



200 mas up to 90 s; PDE  $\leq$  100 mas up to 10 hrs for integrations of 90 s. This is achieved with a Fine Guidance Sensor (FGS, part of the payload instrument suite) and reaction wheels only as the sole actuators (accommodated on dampers, and operated within a narrow angular speed range to minimise any micro-vibrations and avoid exciting structural modes of the S/C).

*The PLM* design is optimised to fulfil the science requirements while keeping the technical risks and costs within the M4 programmatic constraints of the payload consortium. The baseline integrated payload consists of an all-Aluminium off-axis Cassegrain telescope (primary mirror 1100 mm x 730 mm ellipse) with a re-focussing mechanism accommodated behind the M2 mirror and allows correction for any misalignment generated during the telescope assembly or launch and cool down. The telescope feeds a collimated beam into two separate instrument modules. A combined Fine Guidance System / VIS-Photometer / NIR-Spectrometer contains 3 channels of photometry between 0.50  $\mu\text{m}$  and 1.2  $\mu\text{m}$ , of which two will also be used as a redundant system for providing guidance and closed-loop feedback to the high stability pointing of the spacecraft. The FGS provides simultaneous information on the photometric stability of the target stars. One further low resolution ( $R = \sim 10$ ) spectrometer in the 1.2  $\mu\text{m}$  – 1.95  $\mu\text{m}$  waveband, optimized for cloud characterisation, is also accommodated here. The other instrument module, the ARIEL IR Spectrometer (AIRS), provides spectral resolutions of between 30 – 100 for a waveband between 1.95  $\mu\text{m}$  and 7.8  $\mu\text{m}$ . The payload module is passively cooled to  $\sim 55$  K by isolation from the spacecraft bus via a series of V-Groove radiators; the detectors for the AIRS are the only items that require active cooling to  $< 42$  K via an active Ne JT cooler.

The instrument design uses only technologies with a high degree of technical maturity. Transit spectroscopy means that no angular resolution is required and detailed performance studies show that a telescope collecting area of 0.64 m<sup>2</sup> is sufficient to achieve the necessary observations on all the ARIEL targets within the mission lifetime. The satellite is best placed into an L2 orbit to maximise the thermal stability and field of regard. ARIEL is complementary to other international facilities (such as TESS, to be launched in 2017) and will build on the success of ESA exoplanet missions such as Cheops and PLATO, which will provide an optimised target list prior to launch.

**Ground segment** – Responsibility for, and provision of, the ARIEL ground segment is split between ESA and a payload consortium provided, nationally-funded, Instrument Operations and Science Data Centre (IOSDC). The ground segment and operations infrastructure for the Mission Operations Centre (MOC) will be set up at the European Space Operations Centre (ESOC) in Darmstadt, and the ARIEL Science Operations Centre (SOC) set up at the European Space Astronomy Centre (ESAC) near Madrid, which will also host the ARIEL archive comprising mission data base and science data archive. Lower-level data products will be produced at the SOC using processing pipelines based on algorithms and software models that will be developed by the IOSDC, and delivered to the SOC. Final exoplanet spectra will be produced using state-of-the-art tools developed at the IOSDC, and delivered to the SOC for ingestion into the ARIEL science data archive. The pipeline, as well as scripts with critical parameters used to generate the final exoplanet spectra, will be clearly and thoroughly documented and available to users to enable reprocessing of data taken with ARIEL. Long-term mission planning, which will include scheduling of the time-critical observations of ARIEL target transits, will be a joint MOC-SOC-IOSDC activity with scientific guidance provided by the ARIEL Science Team.

Planetary science stands at the threshold of a **revolution in our understanding of our place in the Universe**: just how special are the Earth and our Solar System, and why? It is only by undertaking a comprehensive spectral survey of exoplanets, in a wide variety of environments, that we will answer these fundamental questions. ARIEL represents a once in a generation opportunity to make a major impact on the knowledge of our place in the Cosmos – we intend to seize it.

## 2 Scientific Objectives

Thousands of exoplanets have now been discovered with a huge range of masses, sizes and orbits: from rocky Earth-size planets to large gas giants grazing the surface of their host star. However, the essential nature of these exoplanets remains largely mysterious: there is no known, discernible pattern linking the presence, size, or orbital parameters of a planet to the nature of its parent star. We have little idea whether the chemistry of a planet is linked to its formation environment, or whether the type of host star drives the physics and chemistry of the planet's birth, and evolution.

Progress with these science questions demands a large, unbiased spectroscopic survey of exoplanets.

The ARIEL candidate mission has been conceived to conduct such a survey and to explore the nature of exoplanet atmospheres and interiors and, through this, the key factors affecting the formation and evolution of planetary systems.

### 2.1 The ARIEL Mission as Part of Cosmic Vision

The first major theme of ESA's Cosmic Vision program (ESA BR-247, 2005) poses the questions of how do planets form and what are the conditions that might make them (or their moons) habitable. Even within the limits of our current observational capabilities, studies of extrasolar planets have provided a unique contribution to improving our understanding of these subjects and provided us with a clearer view of the place that the Solar System and the Earth occupy in the galactic context. As a result, a great deal of effort has been, and is being, spent to increase the number of known extrasolar planets (~3500 at the time of writing) and overcome the limits imposed by the incomplete sample, due to observational bias, currently available (Figure 2-1).

The information provided by the presently planned efforts, however, mainly deals with the orbital data and the basic physical parameters (e.g. mass, size) of the discovered planets. In the next decade, emphasis in the field of exo-planetary science must shift from "discovery" to "understanding", by which we mean understanding the nature of the exo-planetary bodies and their formation and evolutionary history. It is in this context that the *Atmospheric Remote-sensing Infrared Exoplanet Large-survey* (ARIEL) has been selected as M4 mission candidate.

#### 2.1.1 Highlights & limits of current knowledge of planets

Since their discovery in the early 1990's, planets have been found around every type of star, including pulsars and binaries. As they form in the late stage of the stellar formation process, planets appear to be rather ubiquitous. Current statistical estimates indicate that, on average, every star in our Galaxy hosts at least one planetary companion (Cassan et al., 2012; Batalha et al, 2014) and therefore  $\sim 10^{12}$  planets should exist just in our Milky Way.

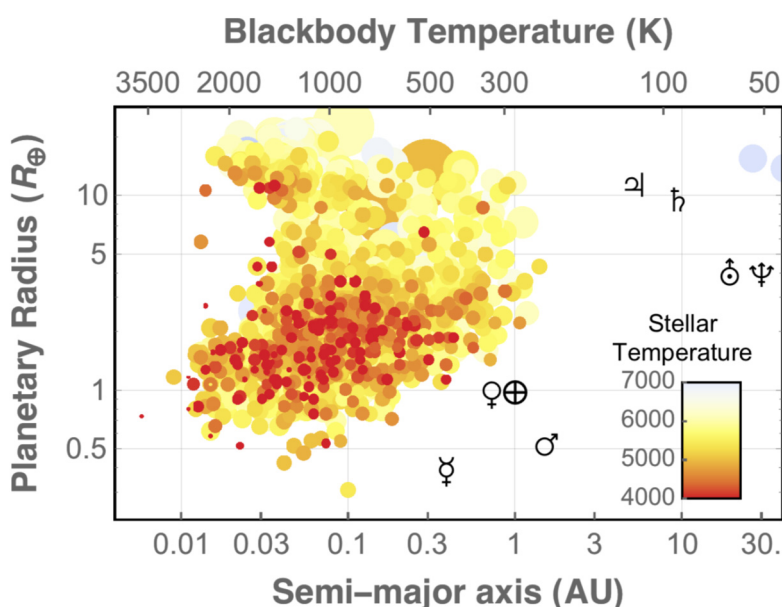


Figure 2-1: Currently known exoplanets, plotted as a function of distance to the star (up to 30 AU) and planetary radii. The graph suggests a continuous distribution of planetary sizes – from sub-Earths to super-Jupiters – and planetary temperatures that span two orders of magnitude.

On the same plot we show the conversion of the orbital period into planetary equilibrium temperature, i.e. the temperature that a black body would have at the given distance of a Sun-like star. Notice that in general a planet is not a black body: the albedo and atmospheric greenhouse effect, which are currently unknown for most exoplanets, have a great impact on its real temperature.

While the number of planets discovered is still far from the thousands of billions mentioned above, the ESA GAIA mission is expected to discover tens of thousands new planets (Perryman et al., 2014). In addition to the ongoing release of results from Kepler (Batalha, 2014), ground-based surveys and the continuing K2 mission (Crossfield et al., 2016) will add to the current ground and space based efforts (see Table 2-6). In the future, we can look forward to many more discoveries from the TESS (NASA), Cheops (ESA) and PLATO (ESA) missions (Ricker et al., 2014; Broeg et al., 2013; Rauer et al., 2014).

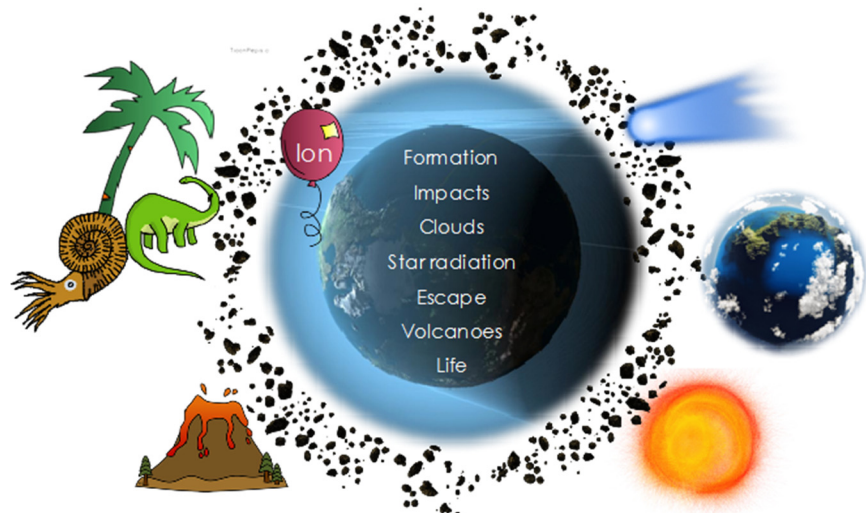
In all scientific disciplines, taxonomy is often the first step toward understanding, yet to date we do not have even a simple taxonomy of planets and planetary systems in our galaxy. In comparison, astrophysics faced a similar situation with the classification of stars in the late 19<sup>th</sup> and early 20<sup>th</sup> century. Here it was the systematic observations of stellar luminosity and colours of large numbers of stars that led to the breakthrough in our understanding and the definition of the classification schemes that we are so familiar with today. The striking observational phenomenon that the brightness of a star correlates with its perceived colours, as first noted by Hertzsprung (1911) and Russell (1914), led to a link between observation and theoretical understanding of interior structure of a star and their nuclear power sources (Eddington, 1924; Bethe, 1939). Thus, observation of a few basic observables in a large sample allowed scientists to predict both the physical and chemical parameters and subsequent evolution of virtually all stars. This has proved to be an immensely powerful tool, not only in studying “local” stellar evolution, but also in tracing the chemical history of the universe and even large scale cosmology.

We seek now a similar approach (i.e. the study of a large sample of objects to seek the underlying physical properties) to understand the formation and evolution of planets. Interestingly, planets do not appear to be as well behaved as stars in terms of parameter-space occupancy: what is certain, though, is that without observing a large number of planets, we will never be able to identify any trend allowing us to pinpoint the general principles underlying their formation.

#### 2.1.1.1 The way forward: the chemical composition of a large sample of planets

The lesson taught us by the study of the planets in the Solar System is that to explore the formation and evolution of a planetary body we need to characterise its composition. The lesson taught us by exoplanets is that to grasp the extreme diversity existing in our galaxy we need large and statistically representative samples. A breakthrough in our understanding of the planet formation and evolution mechanisms – and therefore of the origin of their diversity – will only happen through the direct observation of the chemical composition of a statistically large sample of planets. This is achievable through the remote sensing observation of their gaseous envelop, i.e. through the characterisation of their atmospheres. Knowing what exoplanets are made of is essential to clarify not only their individual histories (e.g. whether a planet was born in the orbit it is observed in or whether it has migrated over a large distance), but also those of the planetary systems they belong to. Knowledge of the chemical makeup of a large sample of planets will also allow us to determine the key mechanisms that govern planetary evolution at different time scales (see Figure 2-2).

*Figure 2-2: Key physical processes influencing the composition and structure of a planetary atmosphere. While the analysis of a single planet cannot establish the relative impact of all these processes on the atmosphere, by expanding observations to a large number of very diverse exoplanets, we can use the information obtained to disentangle the various effects.*



A statistically significant number of planets need to be observed in order to fully test models and understand which physical parameters are most relevant. This aim requires observations of a large sample of

objects (hundreds), generally repeatedly or on long timescales, which can only be done with a dedicated instrument from space, rather than with multi-purpose telescopes, such as JWST and E-ELT (see §2.5 for details).

2.1.1.2 The way forward: ARIEL

In order to fulfil the ambitious scientific program outlined in the previous section, ARIEL has been conceived as a dedicated survey mission for transit, eclipse & phase-curve spectroscopy capable of observing a large, diverse and well-defined planet sample. The transit and eclipse spectroscopy method, whereby the signal from the star and planet are differentiated using knowledge of the planetary ephemerides, allows us to measure atmospheric signals from the planet at levels of 10-50 ppm relative to the star. It is necessary to provide broad instantaneous wavelength coverage to detect as many molecular species as possible, to probe the thermal structure and cloud distribution and to correct for potential contaminating effects of the stellar photosphere (see §3 for details). This can only be achieved with a carefully designed stable payload and satellite platform.

2.1.2 Planetary classes & ARIEL

An attempt at classifying how planets form and evolve, as derived from observations and theoretical results, is summarised in Figure 2-3. A similar convention is used in this report. Because we do not know yet the internal composition of the planets observed, planets in the same area of the parameter space have often received very different names based on some assumption on their nature. The three categories shown in Figure 2-2, for instance, divide the planets depending on their mass with respect to the critical mass range (5-15 Earth masses). Theoretical models indicate that when this critical mass range is reached, planetary bodies embedded in a circumstellar disc start accreting gravitationally nebular gas to become giant planets (like their Solar System analogues Jupiter, Saturn, Uranus and Neptune).

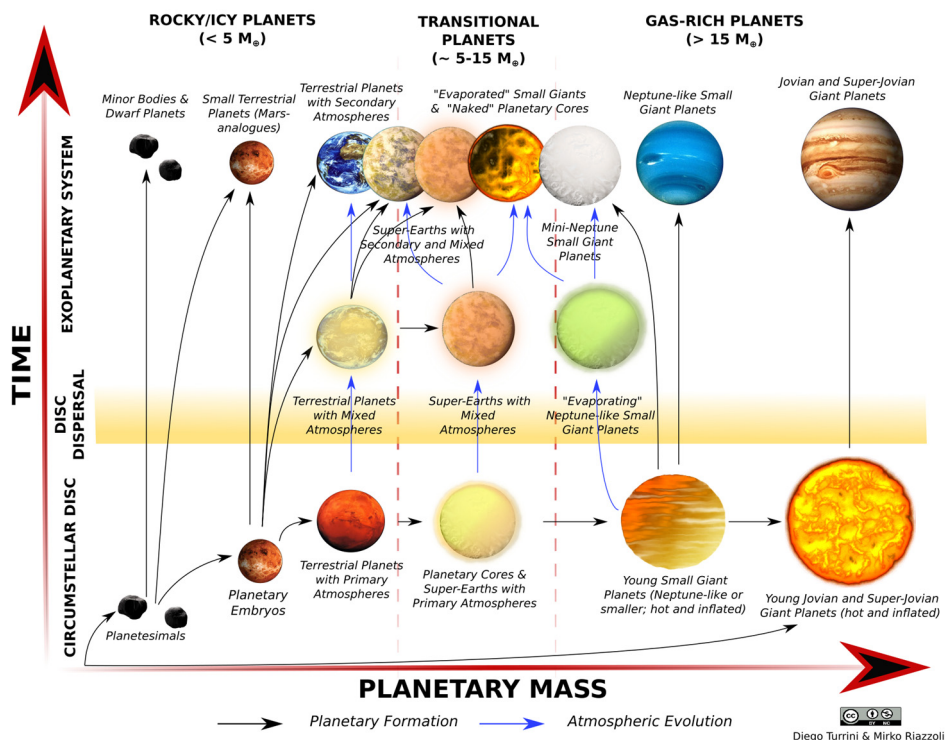


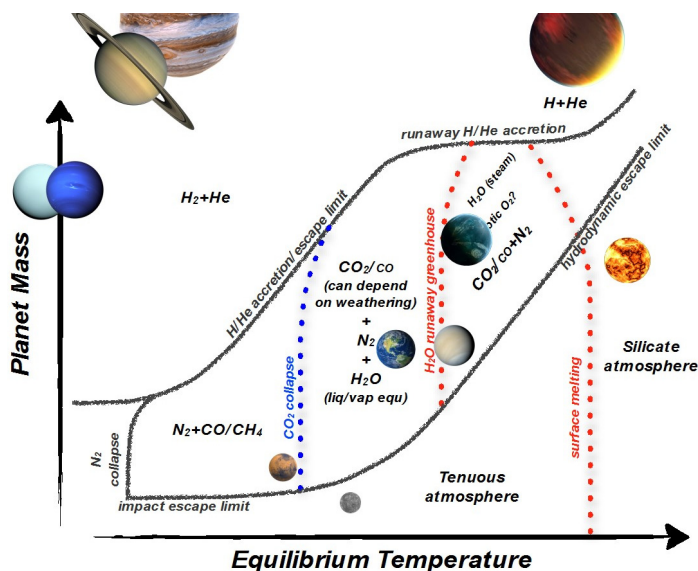
Figure 2-3: Schematic representation of our current understanding of the formation and evolutionary paths that, starting from the gas and dust in circumstellar discs (the bottom left corner of the diagram), create the different kinds of planets currently observed and theorised to now. Black arrows indicate the paths linked to the formation process (e.g. disc instability, solid accretion, gas capture) while blue arrows indicate the paths shaped by atmospheric evolution (e.g. atmospheric escape, atmospheric erosion, outgassing). Planets are divided into three broad categories: rocky/icy planets (mainly composed by Si, Mg, Fe, C, O), gas-rich planets (for which H and He represent a significant fraction of their mass) and transitional planets (encompassing the transition between the largest rocky/icy planets and the smallest gas-rich planets). The Solar System offers us examples of rocky/icy planets and gas-rich planets but not of transitional planets, for which we need to look to exoplanets. Figure credits: Diego Turrini and Mirko Riazzoli.

As shown in Figure 2-3, the planets falling below the critical mass range are labelled as *rocky/icy planets*, since they are expected to be gas-poor and mainly composed of rocks and ices. Planets above the critical mass range are labelled as *gas-rich planets*, as they are expected to have formed in the circumstellar discs and to have accreted a non-negligible fraction of their mass from the gaseous component of the discs. Planets falling into the critical mass range are instead labelled *transitional planets*, as depending on when they formed (i.e. before or after the dispersal of the circumstellar discs) they can either be massive super-Earths or sub-Neptunian gaseous planets. Each of these three classes is associated with a number of outstanding questions concerning the way they formed, how they evolved and their very physical nature (see §2.2).

The large observational sample of ARIEL will ensure that, for each of these three classes, ARIEL will observe a statistically significant population and will be able to address the very core of these questions.

The broad classes of planets identified in Figure 2-3 all expected to have very different formation, migration and evolution histories that will be imprinted on their atmospheric and bulk chemical signatures. Many theoretical studies have tried to understand and model the various processes controlling the formation and evolution of planetary atmospheres, with some success for the Solar System. However, such atmospheric evolution models need confirmation and tight calibrations from observations. ARIEL will focus especially – but not exclusively – on warm and hot planets, for which the atmospheric composition is more representative of the bulk one.

In Figure 2-4 we show the predicted bulk atmospheric compositions as a function of planetary temperature and mass (Forget & Leconte, 2014). ARIEL will focus on the central-right part of the diagram, providing the observational constraints for a large population of rocky and gaseous planets (hundreds) with a range of temperatures and stellar host. The statistical approach provided by ARIEL is *conditio sine qua non* to confirm or identify new transitions between different regimes, and explain the physical processes behind them. The ability to trace a wide range of astrochemical molecules is another essential feature of ARIEL, without which we would not be able to capture the diversity and the complexity of the exoplanets we will observe. Tracing a large number of molecules is important not only for rocky/icy planets but also for gas-rich planets. While the bulk of their atmospheres is composed of H and He, it is their metallicity (i.e. the abundance of heavier elements) that contains the story of their formation and evolution. As such, for gas-rich planets the relevant questions and transitions concern all the molecules and atoms other than hydrogen and helium (see §2.2).



trace a wide range of astrochemically important elements, from metals to refractories to volatiles, permits us to fully take advantage of such unique laboratory. Hot planets also allow us to investigate exotic chemical regimes (Si-rich and metal-rich atmospheres) that are impossible to observe in the Solar System and will offer us hints of the composition of the high-Z materials present in the interior of colder planets (see §2.2.2).

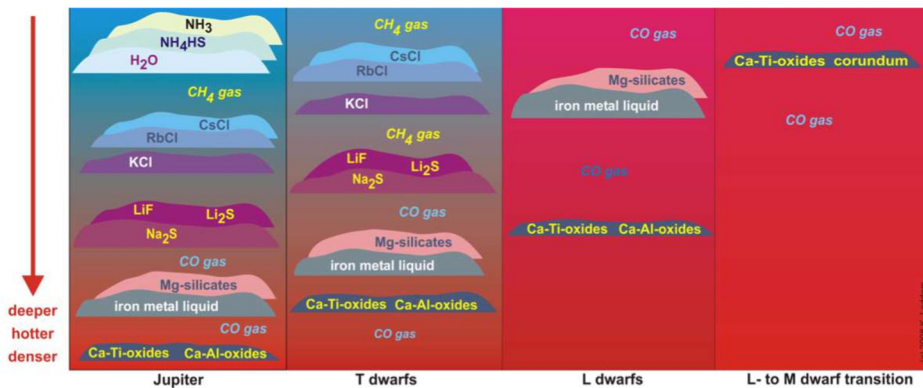


Figure 2-5: Cloud layers in atmospheres ranging from our Jupiter to the hottest brown dwarfs (Lodders & Fegley, 2006). Condensate clouds of various species form at specific points in the temperature - pressure profile. As atmospheres cool, these clouds sink deeper, falling below the observable gaseous layer.

2.1.2.1 Planetary migration: an ARIEL ally

The current sample of known extrasolar planets highlights how planetary migration is a widespread and important process in shaping the structure of planetary systems. About half the exoplanets discovered so far orbit their host star at semimajor axes inferior to 0.1 AU and, especially in the case of gas-rich planets (i.e. the hot-Jupiters and hot-Neptunes), which is a strong observational indication that they probably formed elsewhere – plausibly beyond the water ice condensation line – and migrated to their present position.

Migration can occur at different times in the life of a planetary system, can affect planets of very different masses and can have different causes (see Figure 2-6 and Baruteau et al. 2014; Davies et al. 2014; Turrini et al. 2015 and references therein). Due to its widespread prevalence and its capability to create “hot” planets, i.e. planets in orbits extremely close to their host stars with temperatures above 1000 K, planetary migration delivers planets that formed at different times, under different conditions and at different distances from their host stars to this optimal orbital region for transit spectroscopy, making the observational sample of ARIEL statistically complete from the point of view of the different formation and evolution tracks of the planetary bodies, as summarised in Figure 2-6.

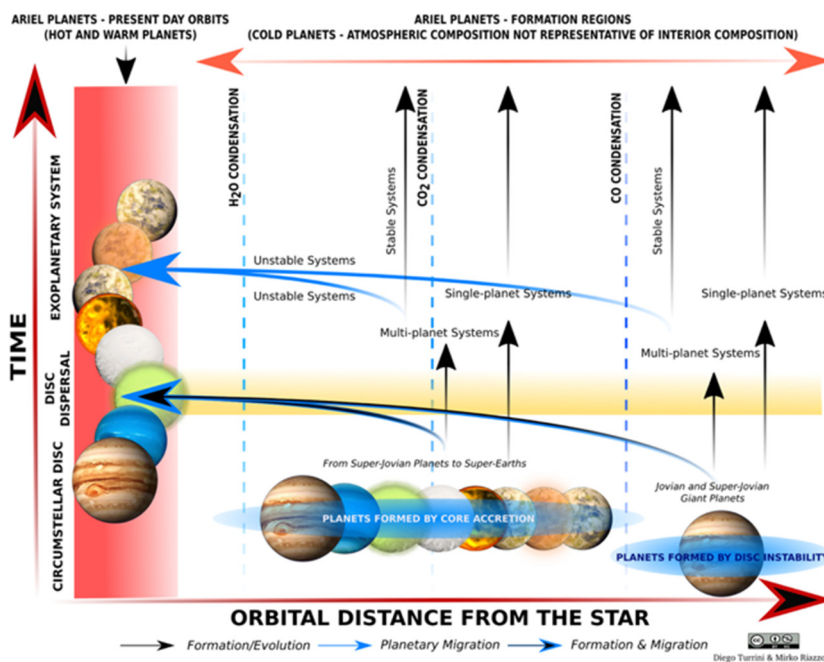


Figure 2-6: Giant planets, and also most of the smaller planets, form in the outer, colder regions of the circumstellar discs, where there is most of the gas, dust and ice. If they stayed there, we wouldn't be able to observe their atmospheres or we would get only very limited information about them. Luckily, migration delivers a good fraction of them closer to the star and makes them optimal targets for ARIEL for two main reasons: the chance they transit increases and the hot temperature makes the atmospheric signals more detectable on top of being more representative of the planet interior. Figure credits: Diego Turrini and Mirko Riazzoli.

### 2.1.3 Planet density: an inaccurate indicator of exoplanets’ nature

To date very little empirical correlation is apparent among the basic observable exoplanetary parameters. For planets transiting in front of their parent stars – of which some 2700 are known today – the simplest observables are the planetary radius and, when combined with radial velocity, the mass. Mass and radius allow the estimation of the planetary density. While the planetary density permits a very first distinction between primarily gaseous and rocky/icy planets, on its own it is an inaccurate and potentially misleading indicator of the exoplanet bulk composition. For instance, from Figure 2-7 left it is evident that gas giants can exist with a broad range of interior structures and core composition and/or are observed at different ages, therefore being more or less puffed-up (e.g. Guillot et al., 2005; Fortney et al., 2007; Vazan et al., 2016).

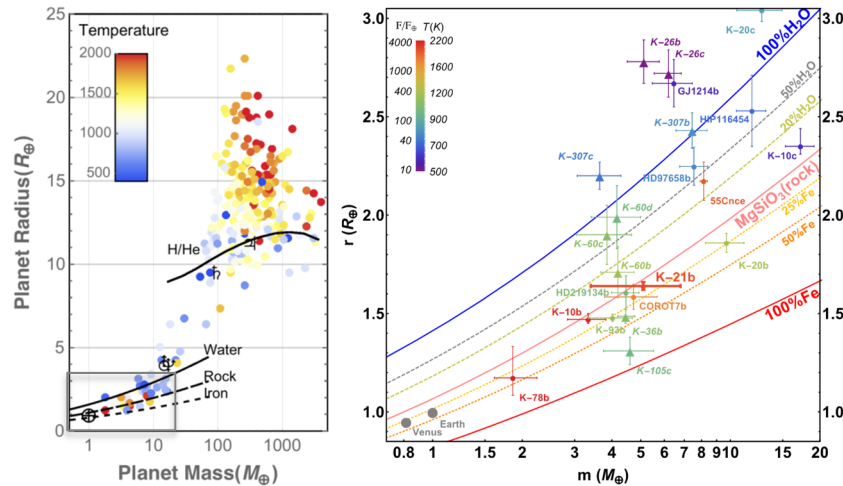
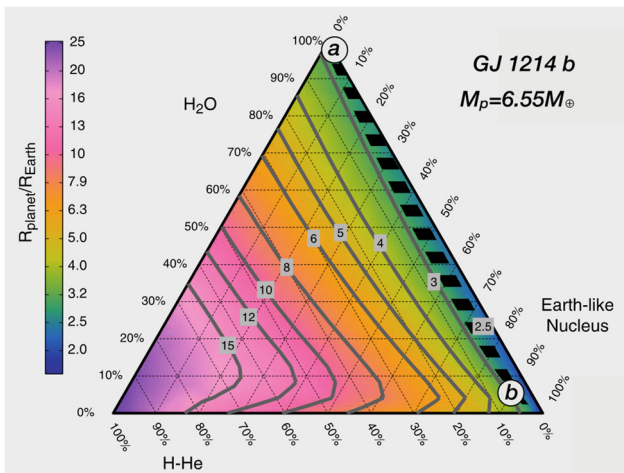


Figure 2-7: Top left: Masses and radii of known transiting exoplanets. Black lines show mass-radius relations for a variety of internal compositions: the models cannot fully capture the variety of cases and break the degeneracies in the interpretation of the bulk composition. Top right: zoom into the lower mass regime indicated as a grey rectangle on the left (Lopez et al., 2016). Coloured lines show mass-radius relations for a variety of internal compositions. Planets discussed in the text are labelled.



Left: Demonstration of the degeneracy left in the internal composition of a planet when only the mean density is known. This ternary diagram relates the composition in terms of Earth-like nucleus fraction, water+ices fraction, and H/He fraction to total mass, to the radius (color coded) for a specific planetary mass (here the one of GJ 1214b). Each vertex corresponds to 100%, and the opposite side to 0% of a particular component (Figure from Valencia et al. 2013).

Constant radius – or density, since the mass is fixed – curves are shown by contours. A perfect radius measurement forces the composition to follow one of these curves. The inferred composition is therefore not unique. In our example, the available Mass-Radius data constrain GJ 1214 b to the black dashed band on the right. So both an almost pure water composition (dot labelled a) and a

90% rocky core with a 10% envelop of mixed water and H/He (dot labelled b) are consistent with the present data. Only a further characterization of the gaseous envelope can remove this degeneracy.

Objects lighter than ten Earth masses (so called super-Earths, Figure 2-7 centre panel) are even more enigmatic – we cannot derive their properties based on mass and radius alone, as pointed out in many papers in the literature (e.g. Valencia et al., 2013; Adams et al., 2008; Grasset et al., 2009) and noticeable e.g. in Figure 2–7 right. Currently, we can only guess that the extraordinarily hot and rocky planets CoRoT-7b, Kepler-10b and Kepler-78b sport silicate compounds in the gaseous and liquid phases (Léger et al., 2011, Miguel et al., 2011). The “mega-Earth”, Kepler-10c (Dumusque et al., 2014), is twice the Earth’s size but is ~ 17 times heavier, making it among the densest planets currently known. The five inner planets orbiting Kepler-11 (Lissauer et al., 2011) show an extraordinary diversity, while being dynamically packed in orbits less than 0.45 AU in radius. Their masses range from ~2 to ~13 Earth masses and they cover a factor of six

in density. Kepler 11b and c are possibly super-Earths with H<sub>2</sub>O and/or H/He envelopes (Ikoma & Hori, 2012). Kepler 11d, e, f resemble mini-Neptunes. As explained in detail in §2.2, the characterisation of the atmospheres of these and other planets is essential to disentangle the degeneracies in the mass-radius relationship.

### 2.1.4 Current observations of exo-atmospheres: strengths & pitfalls

In the past decade, pioneering results have been obtained using transit spectroscopy with Hubble, Spitzer and ground-based facilities, enabling the detection of a few of the most abundant ionic, atomic (e.g. Charbonneau et al., 2002; Redfield et al., 2007) molecular species, condensates (Sing et al., 2016) and constraints to be placed on the planet’s thermal structure. Information on the stability of the atmospheres of transiting planets has been collected through UV observations with Hubble (e.g. Vidal-Madjar et al., 2003; Linsky et al., 2010; Fossati et al., 2010): hydrodynamic escape processes are likely to occur for most of the planets orbiting too close to their parent star. The infrared (IR) range, on the contrary, offers the possibility of probing the neutral atmospheres of exoplanets and exploring their thermal structure (e.g. Knutson et al., 2007; Majeau et al., 2012; Stevenson et al., 2014). In the IR the molecular bands are more intense and broader than in the visible (Tinetti, Encrenaz, Coustenis, 2013) and less perturbed by small particle clouds, and are hence easier to detect. On a large scale, the IR transit and eclipse spectra of hot-Jupiters seem to be dominated by the signature of water vapour (e.g. Barman 2007, Beaulieu et al. 2010; Birkby et al., 2013; Burrows et al. 2007, Charbonneau et al. 2008; Crouzet et al. 2012, 2014; Danielski et al. 2014; Deming et al. 2013; Grillmair et al. 2008; Kreidberg et al., 2014b, Line et al., 2016; McCullough et al. 2014; Swain et al. 2008, 2009; Tinetti et al. 2007, 2010). Other carbon-bearing molecules, such as CO (Snellen et al., 2010) and perhaps methane, are present (Swain et al. 2008). Similarly, the atmosphere of hot-Neptune HAT-P-11b appears to be water-rich (Fraine et al., 2014). The data available for other warm Neptunes, such as GJ 436b, GJ 3470b are suggestive of cloudy atmospheres and do not always allow a conclusive identification of their composition (e.g. Knutson et al. 2014; Morello et al., 2014b; Fukui et al. 2013). Multiple-band photometry and spectroscopy in the near-IR (1–5 μm) have been obtained for a number of young gaseous planets using ground-based dedicated instruments, such as VLT (SPHERE), Gemini (GPI), Subaru (SCEXAO). The comparison of the chemical composition of these young gaseous objects (e.g. Zurlo et al., 2016; Macintosh et al., 2015) with the composition of their migrated siblings probed through transit will help clarifying the role played by migration and by extreme irradiation on gaseous planets.

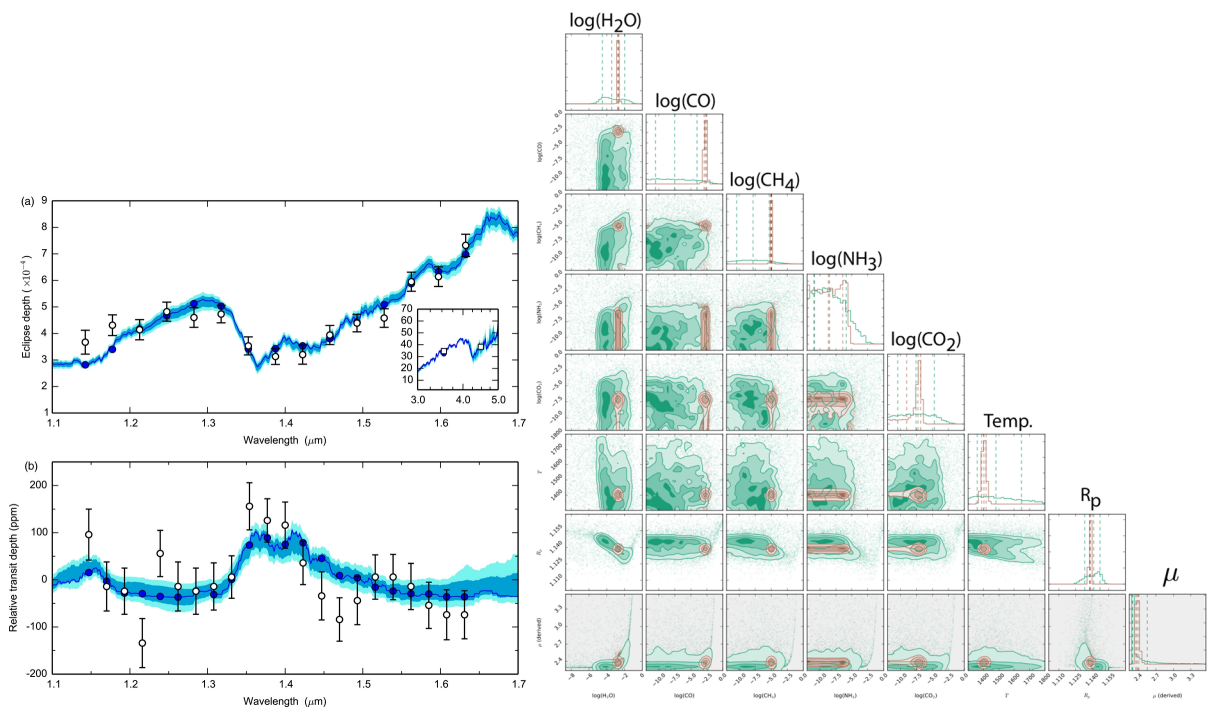


Figure 2-8: Left: transit and eclipse spectra of WASP43b as captured by the Hubble-WFC3 camera (Kreidberg et al., 2014b). Right: comparison between the information content of ARIEL (Brown) and WFC3 (green) spectra as obtained with the TauREx spectral retrieval model (Waldmann et al., 2015a). The broader wavelength range provided by ARIEL enables allows to constrain the molecular abundances and temperature with great precision, and with little or no

correlation among the parameters. The opposite is true for the WFC3, whose narrow spectral range does not permit to separate confidently the various atmospheric parameters.

Concerning smaller planets, the analysis of the transit spectra for the  $6.5 M_{\text{Earth}}$  super-Earth GJ 1214b has oscillated between a metal-rich or a cloudy atmosphere (e.g. [Bean et al. 2010](#); [Kreidberg et al., 2014](#)). An interesting case is 55 Cnc e, a very hot super-Earth orbiting around its star in less than one day. Most recent observations with Spitzer/Hubble suggest a very strong thermal gradient day-night and a volatile atmosphere around it ([Tsiaras et al., 2016](#); [Demory et al., 2016](#)). Further observations in a broader spectral range are needed to understand the history and composition of the planet ([Kite et al, 2016](#); [Hansen et al., 2015](#)).

Despite some early successes, current data are rather sparse – in particular, there is insufficient wavelength coverage and most observations were not made simultaneously. Because an absolute calibration at the level of 10-100 ppm is not guaranteed by current instruments, great caution is needed when one combines multiple datasets at different wavelengths which were not recorded simultaneously. The degeneracy of solutions embedded in the current transit observations ([Swain et al., 2009](#); [Madhusudhan and Seager, 2009](#); [Lee et al., 2012](#); [Line et al., 2013](#); [Waldmann et al., 2015a,b](#)) inhibits any reliable attempt to estimate the elemental abundances or any meaningful classification of the planets analysed. New and better data of uniform calibration and quality are essential for this purpose, and most importantly we need the data for a large population of objects. In other words, we need ARIEL. Figure 2-9 illustrates the capabilities of ARIEL for recording high quality, broad wavelength spectra for a range of planetary types. In the following sections, we explain how we are going to accomplish these objectives and we detail the specific questions ARIEL is going to address.

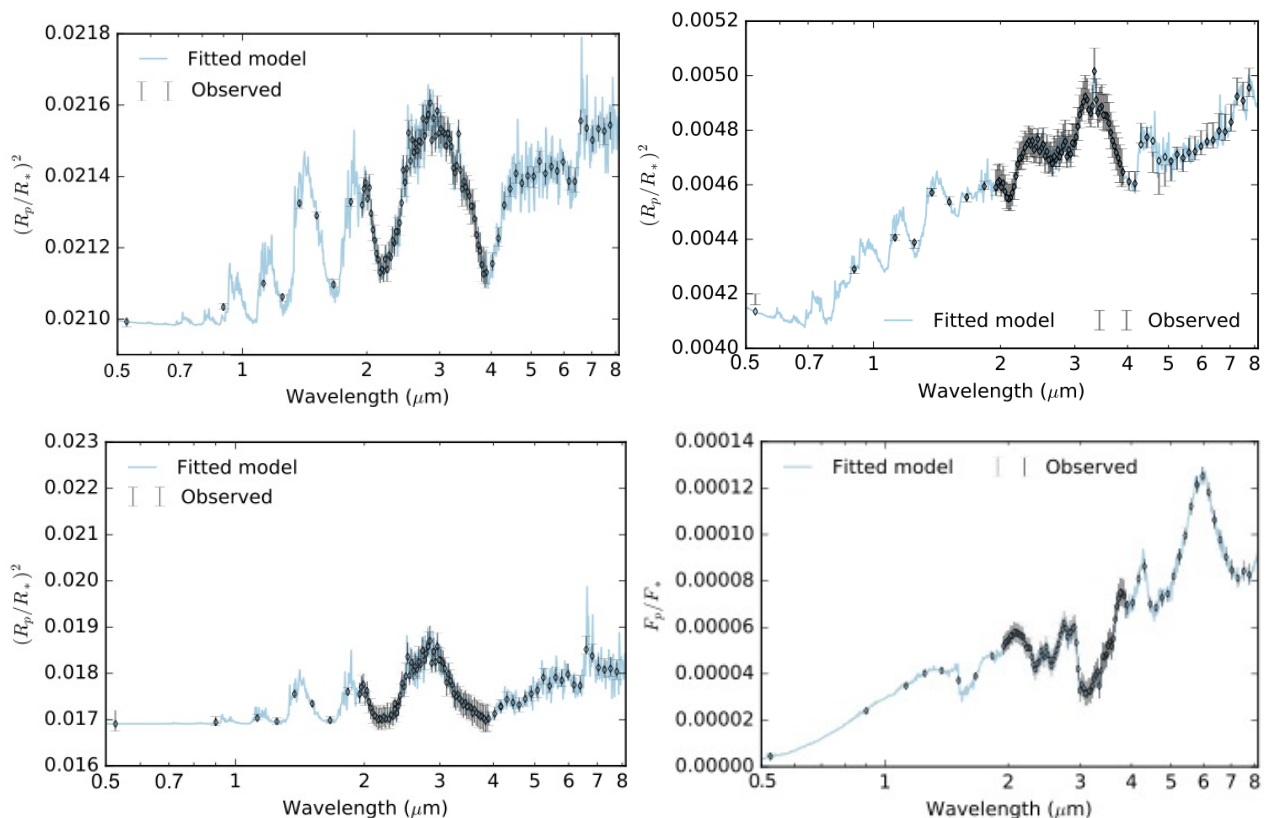


Figure 2-9: Simulated spectra of four existing planets with different sizes and temperatures as observed by ARIEL. The simulations were obtained with our instrument end-to-end simulator, ARIEL-Sim ([Sarkar et al, 2016](#)), see §3.2.1.1. Top: Transit spectrum of a hot-Jupiter similar to HD189733b, clouds are included in the simulation (left). Transit spectrum of a warm Neptune at 800K around a K-type star, mag. K= 7, similar to HAT-P-11b (right). Bottom: transit spectrum of a warm sub-Neptune, similar to GJ1214b, at 600 K around a M star, Mag K=9 (left). Eclipse spectrum of a hot super-Earth similar to 55-Cnc-e around a G-type star, Mag K =4. Note that the simulated spectra were generated assuming the current knowledge about these planetary types, which is in many cases negligible when it comes to atmospheric composition (right).

## 2.2 Key Science Questions Addressed by ARIEL

ARIEL will address the fundamental questions:

- *What are exoplanets made of?*
- *How do planets and planetary systems form?*
- *How do planets and their atmospheres evolve over time?*

through the direct measurement of the chemical composition and thermal properties of a large population of exoplanets. The diversity in compositions is expected to be linked to different formation, evolution scenarios. ARIEL will therefore observe spectroscopically hundreds of transiting planets of different sizes at different temperatures around a variety of stellar types to establish what these planets are made of.

ARIEL is going to address these fundamental questions, by enabling the advance in a number of key areas spelled out in the following sections.

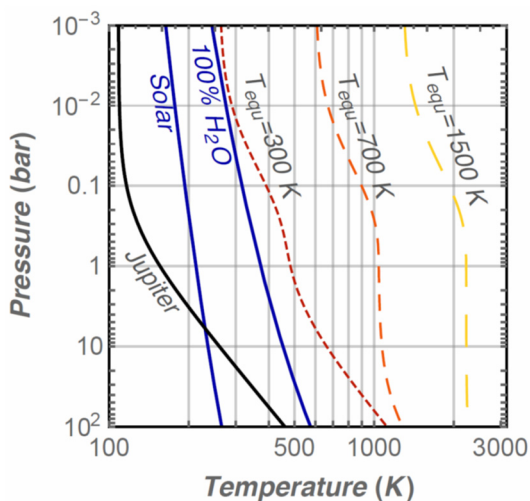
### 2.2.1 How ARIEL will place the Solar System into a broader context

The Solar System have been for decades our only example of a planetary system and its planets our only template of the different kinds of planetary bodies existing in our galaxy. The Solar System's planets, however, do not sample all possible outcomes of the planetary formation process. Moreover, when studying them we face the issue that the four giant planets are cold planets. Their low temperatures make so that their atmospheric composition, our window into their bulk composition, is extremely affected by condensation and removal processes. The atmospheres of hot Jupiters and Neptunes present a critical advantage compared to the planets of the Solar System: their high temperature. Unlike Jupiter, Saturn, Uranus and Neptune, there is no cold trap in their atmosphere for species such as  $\text{H}_2\text{O}$ ,  $\text{CH}_4$ ,  $\text{NH}_3$ ,  $\text{CO}_2$  etc., which condense at much colder temperatures. Observations of hot gaseous exoplanets can therefore provide a unique access to their elemental composition (especially C, O, N, S) and enable the understanding of the early stage of planetary and atmospheric formation during the nebular phase and the following few million years (see §2.2.2).

Even today, in the Solar System, linking the atmospheric abundances to the elemental bulk composition of our four gas-dominated planets still represents a challenge. Yet such information is so crucial to our understanding of the Solar System to justify in part the Juno and JUICE missions to Jupiter: measuring the atmospheric composition is our best opportunity to solve the conundrum.

- **Solar System difficulty 1 – Condensation:**

In the four Solar System major planets, the bulk abundance of the most common heavy element, oxygen, cannot be measured directly by spectroscopy from Earth because its main molecular carrier, water, condenses in the atmosphere and is removed from the observable region (see e.g. Taylor et al. 2004). This will not be true for our targets. As described in Figure 2-10, even for some of the coldest objects in our sample, temperatures in the atmosphere will be well in excess of the condensation temperature in a pure water atmosphere (the most conservative case). As most of the other main reservoirs of oxygen,



carbon, and nitrogen (e.g.  $\text{CO}$ ,  $\text{CH}_4$ ,  $\text{CO}_2$ ,  $\text{NH}_3$ ,  $\text{N}_2$ ) condense at even lower temperatures, the case is even stronger for these molecules. For some of the hottest objects, even more refractory elements (silicates, metals) can be detected, allowing us to constrain almost all of the major constituents of a potential core.

Figure 2-10: Atmospheric temperature profiles compared to the condensation curves for water (solid blue curves). The thermal profiles are computed using Guillot (2010) for a planet resembling Jupiter (solid black) and for higher irradiances (dashed curves; Equilibrium temperature of 300K, 700K and 1500K respectively from left to right). The right blue curve is the saturation vapor pressure curve, i.e. the temperature below which a pure water atmosphere would start to condense at a given pressure. This is the most conservative limit. The left blue curve represents the condensation temperature for water in an atmosphere with a solar

abundance. If an atmospheric profile stays on the right of these curves, condensation will never occur. Then, while Jupiter is too cold to keep a large amount of water vapour aloft, planets warmer than  $T_{eq} \sim 300K$  should not experience much condensation. As other species (e.g. CO, CH<sub>4</sub>, NH<sub>3</sub>, CO<sub>2</sub>) condense at even lower temperatures, the case is even more compelling for these species.

- **Solar System difficulty 2 – Chemical (dis)equilibrium:**

Because the main molecular carriers of the elements we want to constrain do not condense, as mentioned above, chemical disequilibrium is not necessarily a hindrance to the determination of the deep bulk elemental abundance of a planet. Indeed, when the most abundant molecules carrying a given element (for example, H<sub>2</sub>O, CO, CO<sub>2</sub> for oxygen) can be constrained, the abundance of the element deep in the interior can be determined. This remains true as long as the transport of chemical species is dominated by turbulence and advection (as opposed to molecular diffusion), which is the case within and below the probed atmospheric regions, and that no species is removed (e.g. by condensation and settling) during the transport. The wide spectral coverage of ARIEL will prove an important asset as it covers the most visible molecular features of the main species (H<sub>2</sub>O, CO, CO<sub>2</sub>, NH<sub>3</sub>, CH<sub>4</sub>, HCN, H<sub>2</sub>S, C<sub>2</sub>H<sub>2</sub>, PH<sub>3</sub>).

This approach could of course be more difficult for some elements forming relatively transparent molecular species, nitrogen in the form of N<sub>2</sub> for example. There, some chemical modeling will be needed. However, rather counter intuitively, thermochemistry at these warm to high temperatures is much better known and data-constrained than at the low temperatures encountered in Solar System giant planets. This is due to the huge databases used in industry to model combustion in engines which deal with the same type of pressure, temperature, and compositions (Bounaceur et al. 2007; Venot et al. 2012, 2015); these data are available to the scientific community through the KIDA database (Wakelam et al. 2012). In addition, measurements of the radiatively active species and of the thermal structure of the atmosphere by ARIEL will ensure that the results of such chemical models will be better constrained, and thus more reliable than at present.

In summary, because of the very fact that detected exoplanets in general, and ARIEL targets in particular, will be much warmer than the gaseous planets in the Solar System, most of the current hurdles in linking the atmospheric to the bulk composition will be effectively eliminated or mitigated.

- **There are only 8 planets in the Solar System...**

While the knowledge of the planets in our Solar System is getting more and more accurate due to ambitious exploration programs by ESA, NASA and other agencies, the statistics are too small to draw conclusions about the general properties of the planets and planetary systems in our Galaxy. A larger population of planets covering a broader parameter space in terms of size, mass, orbital characteristics, and stellar host is needed to progress in our understanding.

## 2.2.2 Formation-evolution of gas-rich planets & ARIEL

Gas-rich planets possess massive envelopes of hydrogen and helium captured from the nebular gas. The metallicity of these envelopes is determined by the heavy elements accreted by the planets through the gas and the solids and, as such, it records the formation history of the planets themselves. Different elements allow tracing different sources: metals and refractories are linked to the accreted rocks, volatiles to the ices and the most abundant elements C, O and N are linked to both the accreted solids and gas. The different formation and migration scenarios of gas-rich planets predict different relative contributions of these sources to the atmospheric composition and metallicity of the planets. In the following sections, we detail the ARIEL contribution to the understanding of formation and evolution processes for gas-rich planets.

### 2.2.2.1 How ARIEL observations will help overcome degeneracies in the study of the exoplanet interior

While mass and radius determination (and in the case of Solar System planets, gravitational moments) give constraints on the interior composition, they leave important degeneracies that can only be resolved by adding some independent constraints.

Even if mass and radius measurements were accurate enough to provide us with the mean density of a given planet at any arbitrary precision (a statement that could almost be considered true in the solar system), large degeneracies would still remain on the actual bulk composition of the interior (Table 2-1).

Degeneracies in the study of the exoplanet interior with only density constraints	Mitigation of the problem by ARIEL atmospheric observations
<p>Even without any uncertainty on the equation of state of the various materials potentially present, many different combinations of materials can yield the same mean density (Valencia et al. 2013; Baraffe et al. 2008).</p>	<p>By constraining the atmospheric composition, we will be able to constrain the elemental abundance in the deep gaseous envelope. Although this composition could still be different from that of the core, if it exists, this already reduces the uncertainty linked to the choice of the type of heavy elements to consider in modeling the interior (by fixing the C/O ratio for example).</p>
<p>Even at fixed composition, the distribution of the various materials inside the planet does impact the mean density. In other words, the amount of heavy elements needed to explain a given density will vary if these heavy elements are assumed to be segregated in a core or mixed into the gaseous envelope (Baraffe et al. 2008; Leconte and Chabrier 2012).</p> <p>All the heavy elements are often assumed to be gathered into a well defined core with a given composition (e.g. pure water, silicate, or iron).</p>	<p>Although atmospheric measurements will not give us the radial distribution of heavy elements directly, it could greatly illuminate this topic when compared to bulk internal enrichments inferred from the mass/radius data alone. Indeed, the presence or absence of a systematic bias between the enrichment values given by both methods would allow us to quantify the degree of compositional segregation and inform us on the strength of the mixing processes at play (Valencia et al. 2013).</p>
<p>Because thermal expansion is significant for many relevant materials, and especially for gases, the internal temperature of the object has a huge impact on its density (Guillot et al. 1996; Leconte and Chabrier 2012).</p> <p>The temperature today is inferred by relying on a model of the thermal evolution of the planet that itself assumes a given composition for the atmosphere (for the opacities) and that all the processes heating the interior be known (an assumption that we already know to be false because of the large unexplained radii measured for many transiting Hot Jupiters, the so-called radius anomaly; see e.g. Guillot 2008).</p>	<p>In the Solar System, the problem posed by the computation of the internal temperature is alleviated by the fact that the atmospheric temperature is measured and serves as an upper boundary condition that can be integrated downward to yield the whole thermal profile. Because spectroscopic measurements will be able to constrain the temperature profile (especially in eclipse) down to the bar level, we could ideally plan to apply the same approach to exoplanets. By providing the albedo, the thermal emission and the atmospheric composition (and thus opacity), ARIEL observations will strongly improve our modeling of the atmosphere and of the rate at which it allows the interior to cool down and contract (see Figure 2-11). It will thus provide the key information necessary to infer the thermal profile in the planet.</p>
<p>Therefore, at present, any composition inference based on the sole knowledge of the mass and radius relies on strong additional assumptions needed to break these degeneracies.</p>	<p>As it will constrain both the composition and the thermal structure of the atmosphere, ARIEL observations will help mitigate or remove some of the key assumptions that are necessary today to determine the bulk composition of a planet.</p>

Table 2-1: Degeneracies in the study of the exoplanet interior with only density constraints and mitigation of the problem by ARIEL atmospheric observations.

When considering the large number and the diversity of the planets that will be probed by ARIEL, such enhanced mass-radius-composition constraints will thus allow us to really start to address important questions: What are the main factors determining the total and relative elemental enrichments of a planet? Is enrichment determined by the stellar abundances or the formation location? Do planets have dense central cores?

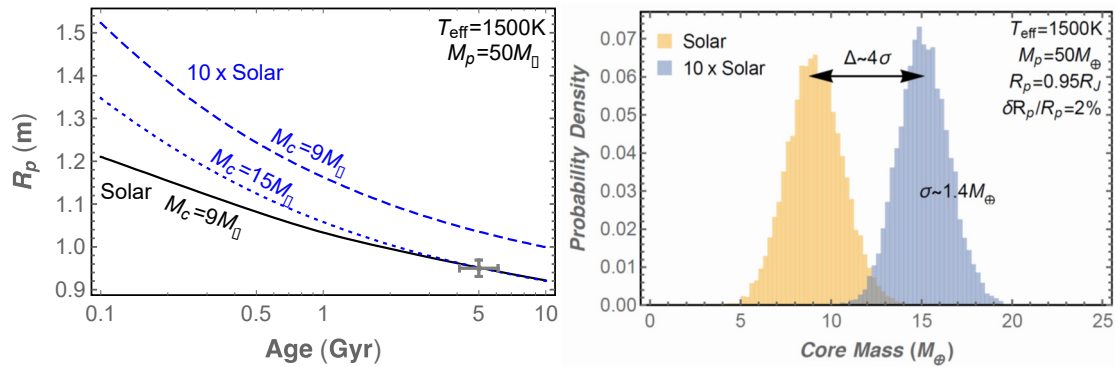


Figure 2-11: Benefits of knowing the atmospheric composition when inferring the core mass of a gaseous planet. Left: Radius evolution tracks for a half Saturn mass planet for two different atmospheric compositions (black: Solar; Blue: 10 times solar) illustrating the core inference process (models from [Leconte & Chabrier, 2013](#)). For the solar composition, a  $9 M_\oplus$  core is sufficient to explain the observed radius (grey cross). A super-solar atmosphere, being more opaque, slows down the cooling, hence the contraction, of the planet. A larger — here  $15 M_\oplus$  — core is thus needed to explain measured radius. Not knowing the composition can here lead to a 70% bias on the core mass inferred. Right: To see whether this effect is statistically significant when measurement uncertainties are taken into account, we repeated this process a large number of times, randomizing the measured radius ([Thorngren et al. 2016](#)). The radius uncertainty was taken to be equal to 2%, in line with the precisions envisioned for future missions ([Rauer et al. 2012](#)). For each atmospheric composition, a histogram shows the probability for the core to have a given mass. Assuming a given atmospheric composition (a given histogram), one would conclude that a 2% radius uncertainty entails 1 sigma =  $1.4 M_\oplus$  uncertainty on the core, but this is not accurate. The difference (or bias) on the average core mass inferred in the two atmospheric scenarios is 4 times larger. By constraining the atmospheric composition, ARIEL would thus lead to more accurate core mass predictions.

### 2.2.2.2 Gas-rich exoplanets: ARIEL ability to measure atmospheric chemistry

Among the different categories of exoplanets, the hot/warm gas-rich planets are the most interesting ones because the molecular abundances determined by observations are a direct reflection of their elemental abundances. In addition, they provide the highest quality observations. Indeed, unlike the giant planets of our own Solar System (Jupiter, Saturn...), condensation is likely to be less important in these very hot atmospheres, and there is therefore no cold trap for oxygen-, carbon- and nitrogen-bearing species (see Table 2-2). Key species such as  $\text{H}_2\text{O}$ ,  $\text{CH}_4$ ,  $\text{NH}_3$  do not condense and observations can provide a measure of the elemental composition. Table 2-2 summarises how ARIEL will test the validity of current theoretical predictions, which hypothesize classes of gaseous planets according to chemical and thermal properties.

The atmospheric temperatures found in short-period exoplanet atmospheres are very high and therefore one could think that the chemical composition of these atmospheres can be described by thermochemical equilibrium, as the high temperatures lead to very fast chemical kinetics. It is exactly what was assumed in the first models used to study these kind of planets (e.g. [Burrows et al. 1999](#); [Seager et al. 2000](#); [Sharp et al. 2007](#); [Barman 2007](#); [Burrows et al. 2007, 2008](#)), but it was quickly realised that interpreting observational data of hot-Jupiters was not so trivial. There are out-of-equilibrium processes (mixing and photodissociations) that can influence the chemical composition. Indeed, a strong vertical mixing induces the phenomenon of quenching. In the deep atmosphere, the temperature is high, the kinetics are fast, and the atmosphere is at thermochemical equilibrium. At lower pressures, temperature decreases, the kinetics slow down, and there is a level where the dynamical timescale becomes shorter than the chemical timescale. Here, kinetics are not sufficiently fast enough to maintain the atmosphere with a composition corresponding to the thermochemical equilibrium. Then, vertical transport brings the composition of this level (called quenching level) towards lower pressure levels. The chemical composition of the atmosphere above this quenching level no longer corresponds to the prediction of the thermochemical equilibrium.

To a fundamental level, the chemical composition of the atmosphere is determined by:

1. the elemental abundances (how much oxygen, how much carbon...) the planet formed with
2. the temperature of the atmosphere, which is of course dependent on the host star and internal heating and
3. physical processes in the atmosphere (mixing, photolysis, etc.).

Temp	Day-side	Night-side	Dynamics/ Chemistry	Cloud type	Observables by ARIEL
VERY HOT > 1500K	Equilibrium chemistry	Equilibrium chemistry	2D/3D models needed to represent chemistry & dynamics	Ca/Ti/V oxides  Corundum	Trace gases relative abundances (especially H <sub>2</sub> O, TO, VO, CO..)  Vertical & horizontal thermal structure through transits, eclipses & phase curves  Cloud detection through albedo and blue/red filters transit observations.  Cloud composition: detection TiO, VO, TiH.. gases  Inhomogeneities in the cloud decks through time-series
	Bulk composition is observable through atmosphere	Bulk composition is observable through atmosphere			
HOT ~750-1500K	Equilibrium chemistry	Non-equilibrium chemistry	2D/3D models needed to represent chemistry & dynamics	Mg-silicates  Fe  Na <sub>2</sub> S  LiCl  SiO <sub>2</sub>	Trace gases relative abundances (especially CH <sub>4</sub> , HCN, NH <sub>3</sub> )  Vertical & horizontal thermal structure through transits, eclipses & phase curves  Cloud detection through albedo and blue/red filters transit observations.  Cloud composition: detection FeH, SiO gases. Detection of alkali metals (Na, Li, K) mainly from ground.  Inhomogeneities in the cloud decks through time-series
	Bulk composition is observable through atmosphere	Bulk composition is partially observable through atmosphere	Equilibrium transition CO/CH <sub>4</sub>		
WARM ~350-750 K	Non-equilibrium chem. Negligible difference between day/night? Information on bulk composition at ~ T > 600K		1-D models represents well chemistry & dynamics ?  Equilibrium transition N <sub>2</sub> /NH <sub>3</sub>	KCl	Trace gases relative abundances (especially CH <sub>4</sub> , HCN, NH <sub>3</sub> )  Vertical thermal structure eclipses  Cloud detection through albedo and blue/red filters transit obs.  Inhomogeneities in the cloud decks through time-series
TEMPERATE & COLD <350K	Non-equilibrium chemistry No information on bulk composition Negligible difference between day/night if not tidally locked, otherwise difference is extreme More species are condensed out in clouds & interior		1-D models expected to represent well chemistry & dynamics.  Planets around cool-stars, might be tidally locked. 3D models are necessary.	H <sub>2</sub> O, CO <sub>2</sub> NH <sub>3</sub> , H <sub>2</sub> S CH <sub>4</sub> , C <sub>2</sub> H <sub>6</sub>	Solar System planets (not from ARIEL observations).  ARIEL observations only for most favourable gas-rich planets or rocky planets around very cool stars (e.g. TRAPPIST1 planets)

Table 2-2: Expected classes of gaseous planets according to chemistry and dynamical models (Venot et al., 2014, 2015; Lodders & Fogley, 2006; Agundez et al., 2012). The predicted transitions need to be confirmed or disproved by ARIEL observations.

For **warm planets** (see Table 2-2), with atmospheres unlikely to be described by chemical equilibrium, it is interesting to quantify the effect of the different parameters that are likely to influence the chemical composition. Venot et al. (2014) studied the atmospheric composition of a warm Neptune; GJ 3470b. They explored the parameter space for metallicity, temperature, eddy diffusion coefficient and stellar UV flux. They found that the value of the eddy diffusion coefficient and the intensity of stellar irradiation have a lower impact on the chemical composition, compared to the huge effect of metallicity and temperature. Change of several orders of magnitude in abundance could be observed for some species. For instance, Figure 2-12 shows that the abundances of the main reservoirs of carbon, CO and CH<sub>4</sub>, depend to a large extent on the metallicity and the temperature. These differences in chemical composition are visible in the synthetic spectra and, if present, will be easily observed by ARIEL.

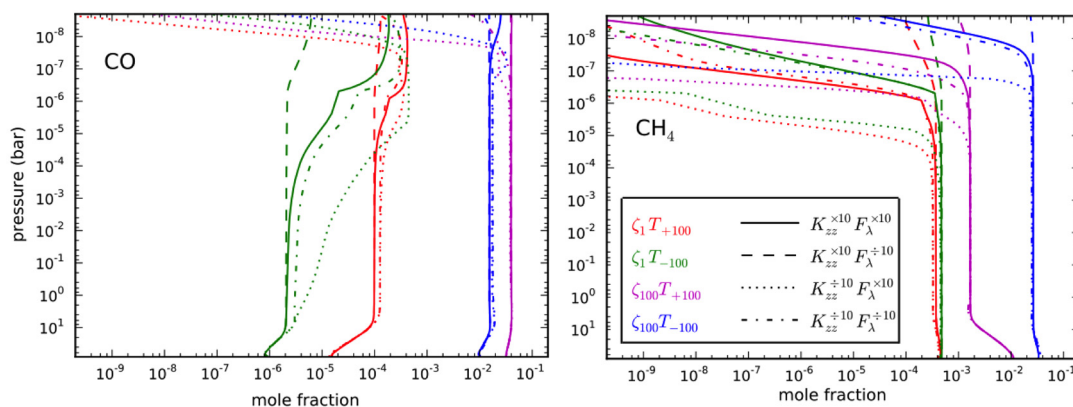


Figure 2-12: Vertical abundances profiles of CO (left) and CH<sub>4</sub> (right) as calculated through 16 models of GJ 3470b in which the space of parameters of metallicity ( $\zeta$ ), temperature ( $T$ ), eddy diffusion coefficient ( $K_{zz}$ ), and stellar UV flux ( $F_{\lambda}$ ) are explored. Each colour corresponds to a set of metallicity and temperature, and each line style to a set of eddy diffusion coefficient and stellar irradiation. From Venot et al. (2014).

The relative elemental abundances can also have a crucial effect on the atmospheric chemical composition of exoplanets. Venot et al. (2015) studied this effect as well as the consequences on the synthetic spectra. They found that for warm atmospheres, i.e. with a temperature around 500 K, changing the C/O ratio from solar (C/O = 0.54) to twice solar (C/O = 1.1) has almost no effect of the chemical composition, nor on the synthetic spectra

For **hot planets** (see Table 2-2), the effect of relative elemental abundances is very important (Venot et al., 2015). The increase of the C/O ratio leads to an important increase (by several orders of magnitude) of the abundance of hydrocarbon and other species (i.e. CH<sub>4</sub>, C<sub>2</sub>H<sub>2</sub>, HCN), accompanied with a decrease of the abundance of water (see Figure 2-12). These differences in chemical composition are visible in the synthetic spectra and, if present, will be captured by ARIEL (Figure 2-13).

**Non-Local Thermodynamic Equilibrium emissions** – Non-LTE emissions from CH<sub>4</sub> and other molecules have long been known in the upper atmospheres of the solar system gas giants (e.g. Kim et al. 2015). It provides for example insight into the emission level temperature, and is sensitive to both auroral and non-auroral conditions. The modelling of NLTE phenomena is relatively mature for the solar system gas giants. However, much work remains to be done to achieve a comparable degree of confidence in Non-LTE models for the high-temperature conditions of close-in gas exoplanets. CH<sub>4</sub> non-LTE detections have been reported on HD189733b (Swain et al. 2010; Waldmann et al., 2012), but such measurements from the ground are very challenging (Mandell et al., 2011). ARIEL's spectral coverage and resolving power are well suited to detect the Non-LTE emission from CH<sub>4</sub>, which is expected to peak at 2-5  $\mu$ m. Its detection will make it possible to test composition and temperature models of warm and hot Jupiter atmospheres.

### 2.2.2.3 Gas-rich exoplanets: ARIEL ability to measure atmospheric dynamics & cloud distribution

Chemistry and dynamics are often entangled. For instance, Agúndez et al. (2012, 2014) showed that for hot-Jupiters the molecules CO, H<sub>2</sub>O, and N<sub>2</sub> and H<sub>2</sub> show a uniform abundance with height and longitude, even including the contributions of horizontal or vertical mixing. For these molecules, it is therefore of no relevance whether horizontal or vertical quenching dominates. The vertical abundance profile of the other

major molecules CH<sub>4</sub>, NH<sub>3</sub>, CO<sub>2</sub>, and HCN shows, conversely, important differences when calculated with the horizontal and vertical mixing.

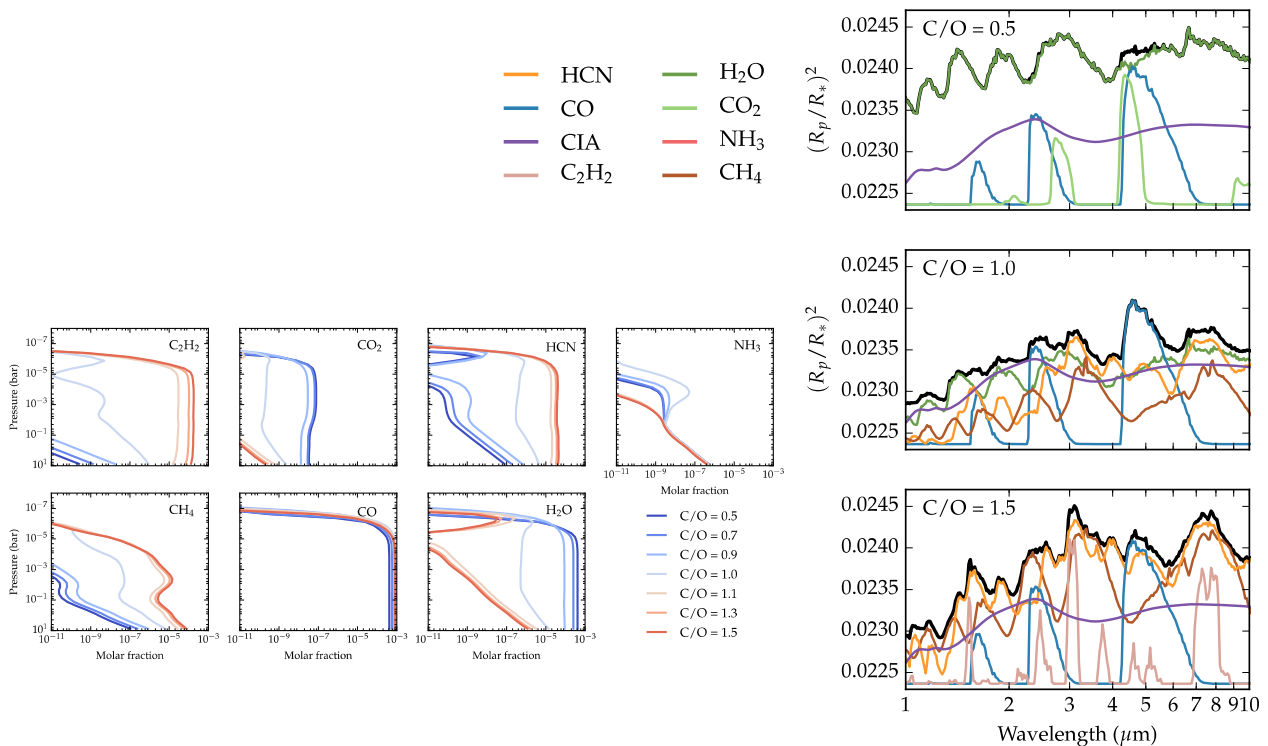


Figure 2-13: Left: Vertical abundance profiles for different molecules for a range of C/O. The different coloured lines show the molar fraction profiles at different C/O, as shown by the legend. Right: synthetic transit spectra and contribution of the various opacities for the atmospheric compositions shown on the left (Rocchetto et al., 2016).

Longitudinal variations in the thermal properties of the planet cause a variation in the brightness of the planet with orbital phase. This orbital modulation has been observed in the IR in transiting (e.g. Knutson et al., 2007) and non-transiting systems (Crossfield et al., 2010). In Stevenson et al. (2014) full orbit spectra have been obtained with Hubble/WFC3. These observations are key constraints to 2D and 3D global circulation models (e.g. Cho et al., 2008; Showman et al., 2013; Kataria et al., 2015). ARIEL phase-curve spectroscopic measurements of the dayside and terminator regions will provide a key observational test to constrain the range of models of the thermochemical, photochemical and transport processes shaping the composition and vertical structure of these atmospheres.

One of the great difficulties in studying extrasolar planets is that we cannot directly resolve the spatial variation of these bodies, as we do for planets in our solar system. However, the evolution of the overall brightness during ingress and egress provides information on the spatial distribution of the planet’s emission. Majeau et al. (2012) and De Wit et al (2012) derived the two-dimensional map of the hot-Jupiter HD189733b at 8 μm with Spitzer-IRAC (see Figure 2-19).

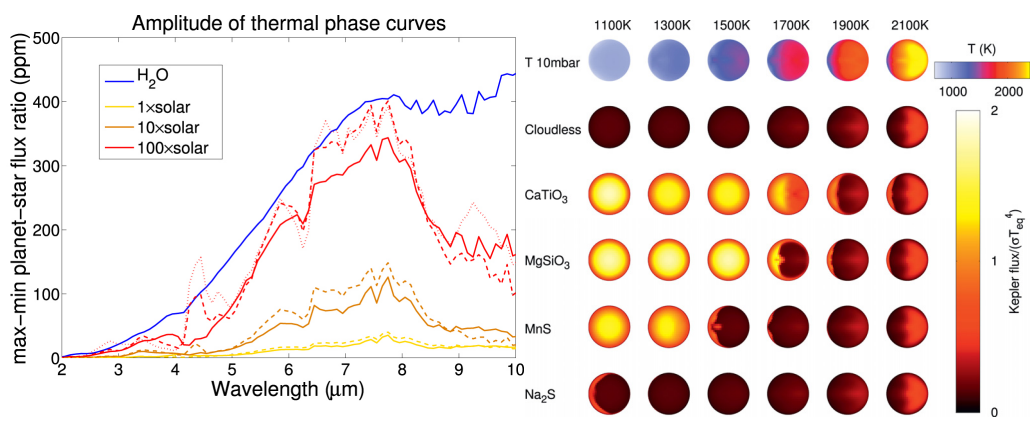


Figure 2-14: Left: Figure from Charnay et al. (2015). Amplitude of thermal phase curves of a warm sub-Neptune similar to GJ1214b without cloud (solid lines) and with cloud (dashed lines for radii of 0.5 μm and dotted line for radii

of  $0.1 \mu\text{m}$ ) for metallicity of 1, 10, 100 and a pure water atmosphere. Right: Figure from Parmentier et al (2016). Temperature and outgoing flux from the dayside of hot-Jupiters with different equilibrium temperatures. The first row shows the temperature at 10 mbar estimated by a global circulation model. The following rows show the total flux (emitted + reflected) from the dayside hemisphere in the spectral range observed by the Kepler spacecraft. The second row is a model without clouds, whereas in the subsequent rows one cloud species is condensing.

Clouds can significantly affect atmospheric opacities and reflectivity, and thus the atmospheric circulation and the thermal structure of irradiated planets. Detecting their presence and inhomogeneous spatial distribution is therefore paramount (e.g. Charnay et al. (2015), Parmentier et al., (2016), see Figure 2-14). As demonstrated for Kepler-7b (García Muñoz & Isaak, 2015), phase curves at visible wavelengths are partly dictated by reflected starlight, which encodes information on the cloud structure as well as the composition and particle size of the condensates. Disentangling the reflected starlight component from the planet thermal emission requires combined visible-infrared observations.

ARIEL will provide phase curves, 2D-IR maps recorded simultaneously at multiple wavelengths, for several gaseous planets, an unprecedented achievement outside the solar system. These curves and maps will allow one to determine horizontal and vertical, thermal/chemical gradients, cloud patchiness, exo-cartography.

#### 2.2.2.4 Gas-rich exoplanets: ARIEL ability to constrain exoplanet provenance & formation mechanisms

As the study of the formation and evolution of the Solar System and its different planetary bodies taught us, orbital parameters and mass and size are not enough to solve the puzzle of the origin of a planetary system and to constrain its past evolution. The orbital evolution of planets is randomly affected by planetary encounters and can be drastically altered by migration. Migration, in turn, can act either very early, due to the interaction between a planet and the circumstellar disk in which it is embedded in (e.g D'Angelo et al. 2011; Kley & Nelson 2012), or at a later time, as a result of planet-planet scattering in unstable multiplanet configurations (Weidenschilling & Marzari 1996; Chatterjee et al. 2008). Finally, the onset of the dynamical instability that will result in the planet-planet scattering event is affected by unknown or poorly constrained parameters, like the mass present in the form of solid bodies in the early life of the planetary system, and is therefore difficult to pinpoint in time (Tsiganis et al. 2005; Levison et al. 2011).

The experience derived from the study of the Solar System tells us that the additional information needed to solve the puzzle posed by the history of a planetary system and of its planets is compositional in nature (Helled & Lunine, (2014), Raymond et al. 2006; Turrini & Svetsov 2014). Migration and, more generally, the formation and dynamical history of a giant planet, affect the composition in different ways (Guillot & Gladman 2000; Matter et al. 2009; Turrini et al., 2015). Firstly, it affects the bulk elemental composition of the gaseous envelope by making it capture gas and solids from different regions of the circumstellar disk (therefore with different ratios between the condensate and gaseous phases for the most abundant elements like C and O (see Figure 2-15, Figure 2-16, Turrini et al., 2015, Venturini et al, 2016, Espinoza et al., 2017). Additionally, it affects the efficiency with which the long-range gravitational pull of the giant planets is able to accrete solid material from far away regions of the protoplanetary disk, enhancing the abundance of refractory elements and metals in the gaseous envelope (see Figure 2-16 right and Turrini et al., 2015).

ARIEL will be able to investigate the presence of high-Z materials (i.e. heavier than hydrogen and helium) in the atmospheres of hot planets, which are impossible to observe in the Solar System giant planets, as they have condensed out/sunk into their interior. To derive the elemental composition, we need to extract the relative abundances of the molecular species present in the atmosphere in great detail which can be done through spectral retrieval models applied to the spectra observed by ARIEL. Rocchetto et al. (2016) have demonstrated that transit spectra recorded over a sufficiently broad infrared wavelength range can be effectively used to distinguish scenarios where C/O is equal, larger or smaller than 1. In Figure 2-17 we show how C/O can be accurately recovered from simulated ARIEL spectra.

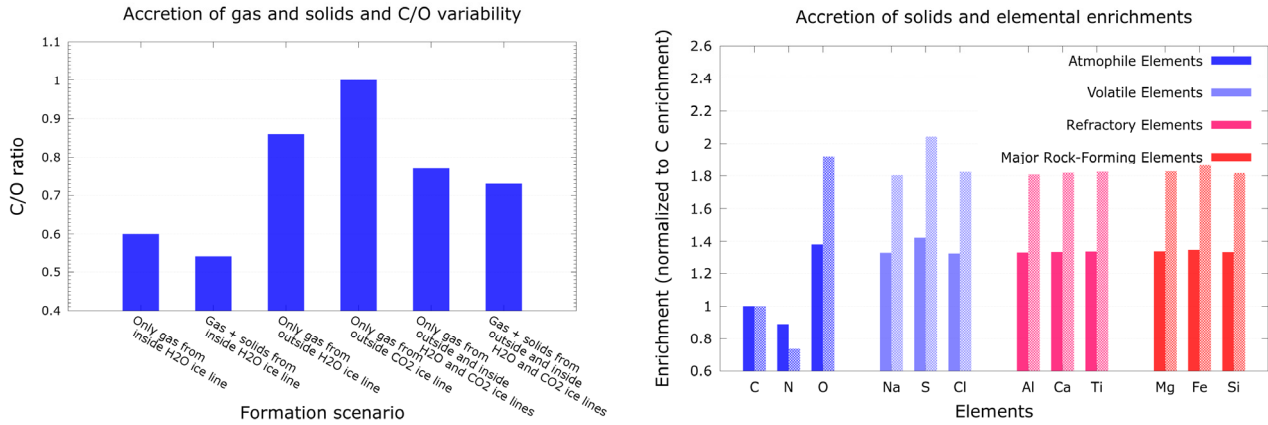


Figure 2-15: *Left: effects of the formation and migration history of a giant planet on its atmospheric C/O from the simulations of Turrini, et al. (2015). Right: two examples of enrichment patterns created by the accretion of solids through the four major cosmochemical groups for elements that have spectral features in the observing bands of ARIEL. The solid bars on the left of each pair of bars show the pattern created in a giant planet accreting solids mainly from beyond the water ice condensation line, while the criss-crossed bars on the right of each pair show the pattern created in a giant planet accreting solids also from inside the water ice condensation line. Rock-forming and refractory elements give us information on the rocky component of the solid material accreted. Volatile elements are delivered by both rock and ices: with the information provided by the previous two classes of elements, we can disentangle the contribution of rock from that of ices. Atmophile elements are contributed both by solids and by gas, the information provided by the other classes can help us disentangle the relative contributions of these two sources.*

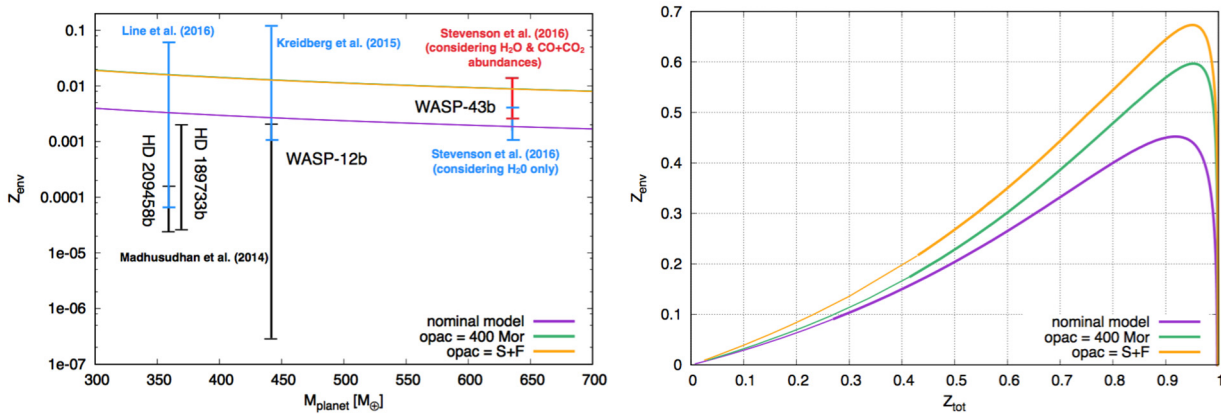


Figure 2-16: *Figure from Venturini et al., (2016) linking the bulk composition of the planets and the atmospheric enrichment, showcasing the need to use atmospheric measurements as guidance for determining the planetary composition and constraining formation models. Left:  $Z_{env}$  versus  $M_{planet}$ , and current measurements of hot Jupiters. Right: the relation between the metallicity of the gaseous envelope (including the atmosphere) and the total metallicity (including the mass of heavy elements in the core) as predicted by formation models.*

### 2.2.3 Formation-evolution of transitional planets & ARIEL

This class of planets is the one about which we know the least – as they are completely absent in the Solar System – and the one that challenges most what we think we know about planetary formation. Transitional planets encompass both large super-Earths and sub-Neptunes and one of the critical open questions, from a planetary formation point of view, is where exactly the transition between these two populations occurs. On one hand, according to our current theoretical framework, the formation of transitional planets should occur during the lifetime of circumstellar discs to allow for these bodies to capture the nebular gas and become the planetary cores of gas-rich planets. On the other hand, the formation of super-Earths could be an extreme end product of the same process governing the formation of rocky/icy planets (see next section) and, based on the chronological data from the case of the Solar System, should take place mostly after the dispersal of the gaseous component of the circumstellar disc.

Planetary bodies reaching the critical mass range before the dispersal of the nebular gas might give rise to the exoplanetary population of **sub-Neptunes (H/He rich formation scenario)**, while those that complete their accretion process after the dispersal of the disc might join the exoplanetary population of **super-Earths**

**(H/He poor formation scenario).** In such a scenario, the planetary radius can be an unreliable indication of the nature of the planetary body in question, as we have no reason to expect that the largest super-Earths cannot possess a greater radius than the least massive sub-Neptunes (see §2.2.3.1).

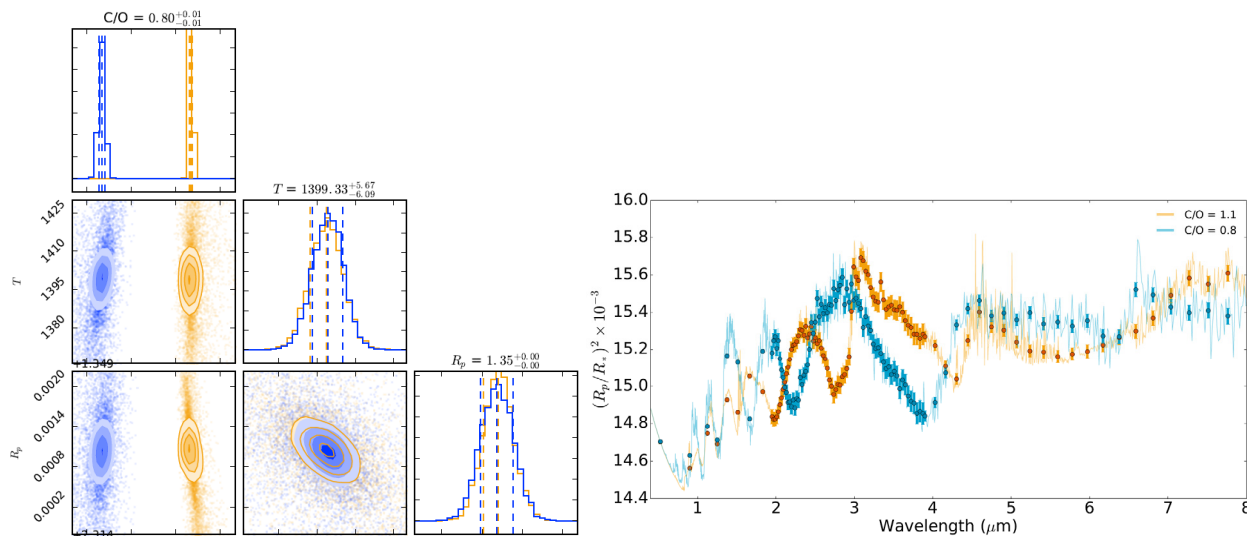


Figure 2-17: Right: Simulated transit spectra for an HD 209458b-like planet, with C/O of 1.1 and 0.8. as observed by ARIEL. The different spectral shapes are a result of the presence of different carbon and oxygen-bearing species for these two chemistries (Venot et al., 2015). Left: Retrievals of C/O, temperature and radius for two versions of an HD 209458b-like planet with different input C/O using spectral retrieval TauREx (Waldmann et al., 2015a). The C/O can be accurately recovered from the synthetic observed spectra.

Moreover, given that bodies in the critical mass range can already experience a significant migration due to their interaction with the disc also information provided by the planetary mass and density can be misleading: a large, ice-rich super-Earth that formed farther away than the water ice condensation line and a sub-Neptune with a rocky-metallic core that formed nearer to the host star could in principle have quite similar densities despite their extremely different natures. The most reliable measure of the nature of a critical-mass planet would therefore be supplied by the composition of its atmosphere.

This category of planets is therefore one for which the scientific observations of ARIEL can radically transform our understanding of planetary formation. Studying the transition between super-Earths and sub-Neptunes can be done to first order by searching, in the atmospheric signatures of the critical mass planets composing the observational sample of ARIEL, for the presence of hydrogen and helium. While super-Earths should possess secondary atmospheres generated by outgassing processes (therefore devoid of H and He), sub-Neptunes should possess primary atmospheres mainly composed by the gas captured from the circumstellar discs (therefore dominated by H and He), see Table 2-3.

### 2.2.3.1 Why mass-radius determination is not enough to constrain the transitional planets' composition

Today, the only constraint we have on the bulk composition of an exoplanet is from its average density. As pointed out by Adams et al. (2008) however, the average density is not unique within the range of compositions. Variations of a number of important planetary parameters produce planets with the same average densities but widely varying bulk compositions. A planet with a given mass and radius might have substantial water ice content (a so-called ocean planet), or alternatively a large rocky iron core and some H and/or He. Adams et al. (2008) conclude that H-rich thick atmospheres will confuse the interpretation of planets based on a measured mass and radius. They find that the identification of water worlds based on the mass-radius relationship alone is impossible unless a significant gas layer can be ruled out by other means. Transmission and emission spectroscopy through transit, as performed by ARIEL, is the only way to remove this degeneracy.

A thorough study of volatile-rich super-Earths/sub-Neptunes was published by Valencia et al. (2013). Figure 2-18 illustrates the degeneracy embedded in the measurement of the mass-radius to constrain the bulk composition of many of the exoplanets in the critical mass region discovered so far. They conclude that a

robust determination by transit spectroscopy of the composition of the upper atmosphere will help determine the extent of compositional segregation between the atmosphere and the envelope.

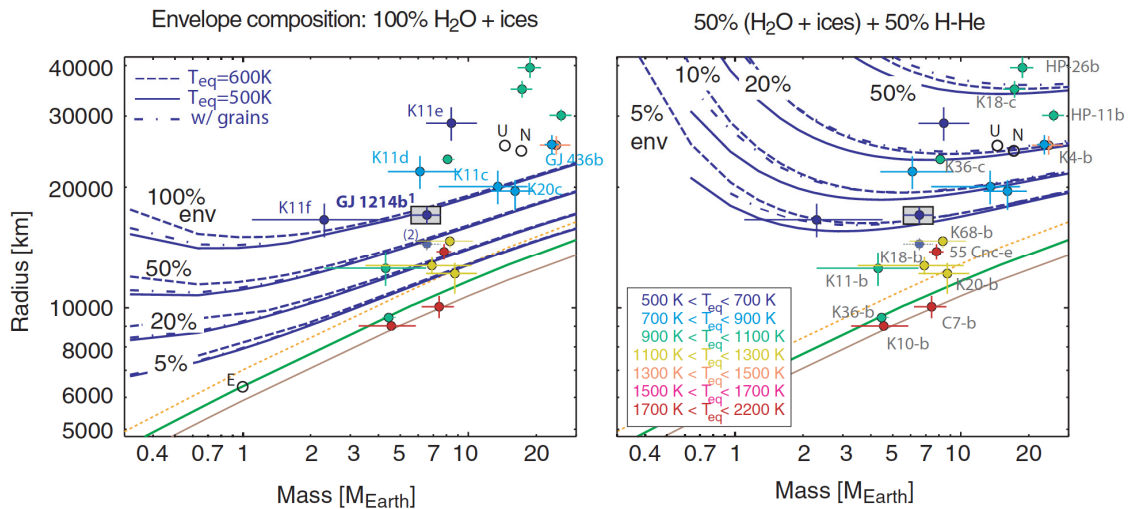
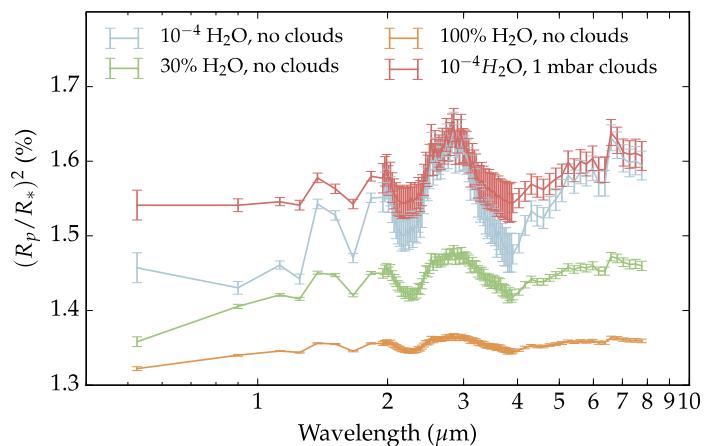


Figure 2-18: Demonstration of the degeneracy left in the internal composition of a planet when only the mean density is known. This ternary diagram relates the composition in terms of Earth-like nucleus fraction, water+ices fraction, and H/He fraction to total mass, to the radius (color coded) for a specific planetary mass (here the one of GJ 1214b). Each vertex corresponds to 100%, and the opposite side to 0% of a particular component (Figure from Valencia et al. 2013). Constant radius – or density, since the mass is fixed – curves are shown by contours. A perfect radius measurement forces the composition to follow one of these curves. The inferred composition is therefore not unique. In this example, the available Mass-Radius data constrain GJ 1214 b to the black dashed band on the right. Both an almost pure water composition (dot labelled a) and a 90% rocky core with a 10% envelop of mixed water and H/He (dot labelled b) are consistent with the present data. Only a further characterization of the gaseous envelope can remove this degeneracy.

### 2.2.3.2 How the atmospheric composition can solve the issue

A robust determination of the composition of the upper atmosphere of transitional planets will reveal the extent of compositional segregation between the atmosphere and the interior, removing the degeneracy originating from the uncertainty in the presence and mass of their (puffy?) atmospheres. Primordial (**primary atmosphere**) atmospheres are expected to be mainly made of hydrogen and helium, i.e. the gaseous composition of the protoplanetary nebula. If an atmosphere is made of heavier elements, then the atmosphere has probably evolved (**secondary atmosphere**). An easy way to distinguish between primordial (hydrogen-rich) and evolved atmospheres (metal-rich), is to examine the transit spectra of the planet: the main atmospheric component will influence the atmospheric scale height<sup>1</sup>, thus changing noticeably the amplitude of the spectral features (see Figure 2-19). The heavier is the main atmospheric component, the more compact is the atmosphere, the smaller is the signal detected. While clouds can mimic this effect to a degree, they mostly influence the short wavelengths (especially optical and NIR). See also Miller-Ricci, Fortney (2010).

Figure 2-19: Simulated ARIEL transit spectra for a hot super-Earth whose atmosphere shows different fractions of H/He and H<sub>2</sub>O. The heavier is the main atmospheric component (i.e. water dominated in this case), the more compact is the atmosphere, the smaller is the signal detected. While clouds can mimic this effect to a degree, they mostly influence the short wavelengths (especially VIS-NIR). The figure was produced using TauREx model (Waldmann et al., 2015a).



<sup>1</sup> The scale height  $H$  of an atmosphere is the altitude at which the atmospheric pressure decreases by  $1/e$ .  $H = \kappa / \mu g$ ; where:  $\kappa$  Boltzmann constant,  $T$  atmospheric temperature,  $g$  gravity acceleration,  $\mu$  atmospheric mean molecular weight. ARIEL can measure directly  $T$  through eclipse measurements,  $g$  is known through the radius and mass, so a measure of the scale height determine  $\mu$ , the molecular weight of the atmosphere.

As spectral signatures become compressed in heavier atmospheres, more observations need to be obtained to reach the same detection significances.

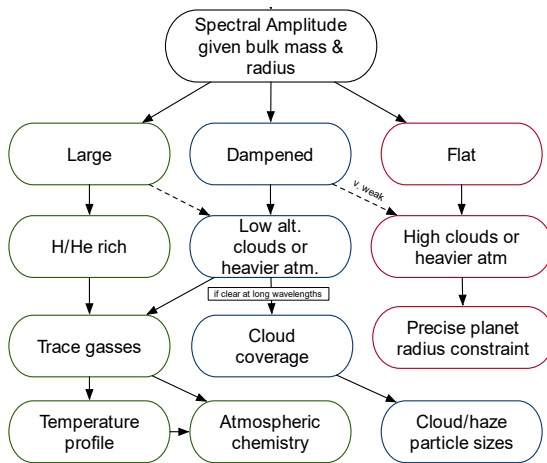


Table 2-3: Classification of transitional planets. Given their expected spectral amplitude (from bulk mass/radius) we can identify whether the planet is H/He rich (large spectral amplitude) has lower/mid-altitude cloud covers or heavier mean molecular weight atmosphere (dampened spectrum) or is devoid of features (heavy atmosphere or high altitude clouds). When H/He rich or dampened, we can infer the atmospheric trace gasses, temperature profiles and (if applicable) cloud distribution and particle sizes. ARIEL transit spectra will allow us to constrain the formation scenarios and structure of the interior of individual transitional planets.

### 2.2.4 Formation-evolution of rocky/icy planets & ARIEL

Several scenarios may occur for the formation and evolution of small planets – i.e. predominantly solid planets (Figure 2-2). To start with, these objects could have formed *in situ*, or have moved from their original location because of dynamical interaction with other bodies, or they could be remnant cores of more gaseous objects which have migrated in (Hansen et al, 2015). Having a lower mass, their atmospheres could have evolved quite dramatically from the initial composition, with lighter molecules, such as hydrogen, escaping more easily. Impacts with other bodies, such as asteroids or comets, or volcanic activity might also have altered significantly the composition of the primordial atmosphere. None of the terrestrial planets in our Solar System have primitive atmospheres of H and He: the atmospheres of the Earth and Venus are the result of partial degassing of their mantles. Isotope analyses demonstrate that these gases have been acquired with the solid material that built-up our planet. In fact, Earth’s gases (e.g. N, H, etc.) have a chondritic isotopic composition and not a solar composition; nevertheless, there is evidence for some solar gases (e.g. Ne, with solar isotopic composition) in the deep Earth’s mantle (Marty, 2012). All this is well explained in the generally accepted view that, within the lifetime of the gaseous proto-planetary disk, the planetary embryos that formed in the inner solar system had only (approximately) the mass of Mars (see Morbidelli et al. (2012), for a review). These embryos may have had thin primitive atmospheres and may even have absorbed some of these gases in their interiors. However, the terrestrial planets formed much later, after the removal of the gas from the protoplanetary disc, via mutual collisions among the embryos. During these high-energy impacts, the primitive atmospheres of the embryos got lost into space, while there was no more solar gas available to accrete. If super-Earths are analogous to solar system terrestrial planets in terms of formation process, but just more massive, they should have no H/He atmospheres either. ARIEL will be able to determine whether that is the case (see Table 2-3).

ARIEL Tier 1 observations not only will confirm the presence or absence of a substantial H/He atmosphere enveloping small planets (see §2.4.1 & §2.4.2), but ARIEL Tier 2 observations (see §2.4.3) can detect the composition of their atmospheres (SiO, H<sub>2</sub>O etc.), so we can test the validity of current theoretical predictions. More specifically:

Rocky/icy planets – science objectives	Contribution of ARIEL observations
<p><i>In current formation models, if the planet is formed close to the snow line, the water content of the planetesimals could be significantly large and tens to thousands of Earth oceans of water could be accreted (Elkins-Tanton, 2011).</i></p> <p><i>This suggests the existence of a vast population of planets with deep oceans (aqua-planets) or whose bulk composition is dominated by water (Ocean</i></p>	<p>ARIEL will test this scenario through transit and eclipse spectroscopy of candidate Ocean planets such as GJ1214b.</p>

<p>planets, <a href="#">Léger et al., (2004)</a>).</p>	
<p><i>If an object exhibits a radius that is bigger than that of a pure water world (water being the least dense, most abundant material except for H/He) of the same mass, this suggests that at least a few % of the total mass of the planet is made of low density species, most likely H/He. The fact that many objects less massive than Neptune are in this regime suggests that it is possible to accrete a large fraction of gas down to 2-3 <math>M_{Earth}</math>, the mass of Kepler-11 f.</i></p>	<p>ARIEL can test this hypothesis by probing the presence of H/He and H<sub>2</sub>O through primary transit spectroscopy (Figure 2-19).</p>
<p><i>An interesting case is 55 Cnc e (<a href="#">Tsiaras et al., 2016</a>; <a href="#">Demory et al., 2016</a>; <a href="#">Kite et al, 2016</a>; <a href="#">Hansen et al., 2015</a>). A hot world (~2000 K), of mass 8.6 <math>M_{\oplus}</math> and orbiting its host star every 18 hours. Current observations suggest the presence of a hydrogen-rich atmosphere (<a href="#">Tsiaras et al., 2016</a>) despite its proximity to the star. The hydrogen could be primordial (perhaps remnant of a giant planet, <a href="#">Hansen et al., 2015</a>) or produced through photolysis of outgassed chemical species from the interior. The large day-night temperature gradient probed through phase-curves (<a href="#">Demory et al., 2016</a>) is compatible with the presence of an atmosphere (<a href="#">Kite et al, 2016</a>). 55 Cnc e, bears evidence to the picture that indeed super-Earths are far more complex than simple mass/radius measurements allow us to constrain.</i></p>	<p>ARIEL will test these hypotheses by observing the atmospheres of planets like 55 Cnc e over a broad wavelength range. A robust determination of the composition of the upper atmosphere of super-Earths like 55 Cnc e by ARIEL will determine the extent of compositional segregation between the atmosphere and the interior.</p>
<p><i>A very thick atmosphere (several Earth masses) of heavy gas, such as carbon dioxide, ammonia, water vapour or nitrogen, is not realistic because it requires amounts of nitrogen, carbon, and oxygen with respect to silicon much higher than all the stellar ratios detected so far.</i></p>	<p>If ARIEL detects an atmosphere which is not made of hydrogen and helium, the planet is almost certainly from the terrestrial family, which means that the thickness of the atmosphere is small compared to the planetary radius. In that case, theoretical works provided by many authors in the last decade (<a href="#">Léger et al., 2004</a>; <a href="#">Valencia et al., 2006, 2007</a>; <a href="#">Adams &amp; Seager, 2008</a>; <a href="#">Grasset et al., 2009</a>) can be fully exploited to characterise the inner structure of the planet.</p>
<p><i>Among the most extreme examples portrayed in 2-4, “lava planets”, such as Corot-7b are so close to their host star that the temperatures reached on the dayside are sufficient to melt the surface itself. As a result, some elements, usually referred to as “refractory”, become more volatile and can form a thin silicate atmosphere (<a href="#">Léger et al., 2011</a>). Depending on the composition of the crust and interior, the most abundant species could be, Na, K, O<sub>2</sub>, O and SiO. In addition, silicate clouds could form.</i></p>	<p>ARIEL will test these hypotheses by observing the atmospheres of candidate “lava planets” similar to Corot-7b.</p>
<p><i>An important motivation for exoplanet characterisation is to understand the probability of occurrence of habitable worlds, i.e. suitable for surface liquid water.</i></p> <p><i>The recently discovered TRAPPIST1 planets (<a href="#">Gillon et al, 2017</a>) show that temperate rocky planets around</i></p>	<p>While ARIEL is not conceived to study habitable planets, transiting super-Earths in the temperate zone of late M and ultra-cool dwarfs might be within reach ARIEL capabilities, depending on the stellar brightness. For instance, simulations show that ARIEL can observe the most favourable TRAPPIST1 planets in Tier 2 mode starting from</p>

<i>very cool stars exist and are probably very numerous.</i>	30 transits. Nevertheless, ARIEL will make a major contribution to the topic of habitability resulting from its ability to detect the composition and structure of atmospheres of many small planets outside the habitable zone, providing a statically sound ground-truth of what a habitable planet does look like.
--	--

Table 2-4: Expected impact of ARIEL observations to the understanding of the atmospheric composition of rocky and icy planets.

## 2.2.5 Planets in rare and/or extreme conditions & ARIEL

As well as the population studies described in the previous paragraphs, ARIEL will observe a number of planets in extreme/odd conditions to test the physics in those extreme/unusual environments and get a glimpse of those exotic objects. We indicate here a few key examples:

- **Planets in high eccentric orbits** – In contrast to Solar System planets, a large fraction of exoplanets discovered today revolve around their parent stars in eccentric orbits. In some cases the eccentricity is extreme, e.g. 0.98 for HD80606b. From a climate/chemistry perspective these planets represent a very interesting challenge (e.g. Williams and Pollard 2002): for instance Laughlin et al. (2009) measured with Spitzer the thermal properties of HD80608b at periastron, finding that the planet temperature increased from 800 K to ~ 1500 K over a six-hour period. Maggio et al. (2015) observed with XMM the highly eccentric HD 17156b: its parent star showed enhanced chromospheric and coronal emission a few hours after the passage of the planet at the periastron suggesting a complex planet-star interaction. The origin of said “eccentric” planet is still being debated in the literature (e.g. Fabricky and Tremaine, 2007).

ARIEL will observe these and other similar planets to study the climate, and chemistry of high eccentric planets. By providing the elemental composition of high-eccentricity planets, ARIEL will be able to cast light on the provenance and history of those objects.

- **Circumbinary planets** – About twenty circumbinary planets, i.e. planets orbiting binary stars, including both S-orbit (planet orbiting just one of the 2 stars) or P-orbit (planet orbiting both stars at large distance) have been discovered. As in the case of eccentric planets, from a climate/chemistry perspective these circumbinary planets represent a very interesting challenge. ARIEL will observe transiting circumbinary planets to study the climate, and chemistry of these exotic bodies.
- **Transiting multi-planet systems** – Among the 3500 planets discovered so far, about 600 planets are part of a planetary system. Special examples are Kepler 11 (6 transiting planets with sizes between super-Earths and Neptunes, Lissauer et al. 2011), Kepler 9 (Holman et al. 2010), 55 Cnc (Fisher et al. 2008) and the most recent TRAPPIST1 (7 Earth-size planets transiting in the temperate zone of an ultra-cool dwarf, Gillon et al, 2017). Transiting multiplanet systems give us a unique opportunity to study not just a single object, but to enable comparative exoplanetology for planets within the same extrasolar system. ARIEL observations of those and other transiting planetary systems will reveal the intra-planetary-system diversity outside our solar system. Since the planets have likely experienced a very similar formation process, this body of work will present a unique probe into the physical processes that govern the composition and structure and their evolution.
- **Disintegrating planets and planetesimals** – The Kepler mission has reported the occurrence of a few transiting disintegrating planets (e.g. KIC 12557548b) and a postulated disintegrating planetesimal in orbit around the white dwarf WD 1145+017 (Vanderburg et al., 2015). These objects orbit their host stars in less than one day, and are suspected to carry dust tails with them. Characterizing the distribution of particle sizes will shed valuable light on the formation and evolution of the dust and, in turn, on the objects. Multi-wavelength photometry during transit (and slightly before/after) can put key constraints on the extinction cross sections of the dust particles and therefore on their sizes. So far, the observations from the UV to the IR (K’ band) have typically implied particle radii large enough ( $r \sim 0.5 \mu\text{m}$  or more) that they produce no chromatic extinction (Bochinski et al., 2015). For a given dust cloud, the cloud optical thickness depends strongly on the  $r/\lambda$  ratio. The fact that ARIEL will observe from 0.5 to 7.8  $\mu\text{m}$  means that the optical thickness of the dust cloud can change significantly over ARIEL’s range of

wavelengths. In other words, the same dust cloud that may appear optically thick at the shorter wavelengths would appear optically thin at the longer wavelengths. This information is pivotal to understanding the morphology of the dust cloud, the physical mechanisms that drive its variability, and in turn, to forming a more complete view of disintegrating planets and planetesimals.

- **Planets around flaring stars** – Venot et al (2016) investigated how the activity of a star can influence the chemical composition and resulting spectra of typical exoplanets. They focused on the effect of stellar flares (see 3.2.2.5 for a discussion about flaring stars), and found significant changes on the chemistry of the atmospheres of two typical planets around an active M star. These changes are visible in the transit spectra of these planets, and the resulting differences are observable with ARIEL observations (see also Miguel et al., 2015). ARIEL’s unique ability to measure a broad wavelength spectrum in one shot will enable the study of the atmospheres of planets around flaring stars with great accuracy and the testing/validation of theoretical predictions about planetary atmospheres in these extreme environments.

## 2.3 Extended use of ARIEL observations

ARIEL photometry (obtained through the FGS or by binning the AIRS spectra) will deliver high SNR signal as a consequence of targeting bright stars. In addition, this will be obtained with a cadence of up to 5 Hz, simultaneously at multiple wavelengths. High SNR and high cadence will produce transit light-curves of unprecedented precision allowing important additional (i.e. non-spectral) science at zero additional cost to the ARIEL core program.

- ARIEL will generally produce time-series of a few hours duration since it will observe any particular star only around the time of each transit. This will provide spectra for stellar oscillations with periods less than around an hour (i.e. frequencies greater than about 300  $\mu$ Hz). At these relatively high frequencies, stellar variability is dominated by p-mode oscillations and by granulation noise. P-mode oscillations provide constraints on a star’s mass, radius and internal structure (Matthews et al, 2004, Huber et al, 2013); information which is interesting in its own right but also necessary for accurate interpretation of the transits (e.g. as applied to *Kepler* data (Gilliland et al, 2010)). Models of granulation noise (Samadi et al, 2013a, 2013b; Cranmer et al 2014) will benefit from testing against the suite of noise time-series which ARIEL will provide across a range of masses, rotation rates and metallicities. This will lead to a better understanding of photosphere convection and turbulence.
- Moving to the “signal”, this can provide information about the planetary systems orbiting host stars since variations in the timing of transits are produced by perturbations from other bodies. The influence of other planets in a system has been clearly detected in *Kepler* data (e.g. see Fabrycky et al, 2012) but these transit time variations (TTVs) may also allow detection of moons (Sartoretti & Scheider, 1999; Kipping et al, 2012) and large Trojans (Ford & Holman, 2007).
- No exomoons or exo-trojans have yet been discovered but, because of its high cadence, high precision photometry in the IR – where no limb darkening or stellar variability affect the signal – ARIEL could be the first observatory to do so. Monte-Carlo simulation of ARIEL’s TTV sensitivity assuming that the transiter is a ten Earth-mass ice-giant orbiting at the right distance from its star to have an effective surface temperature of  $\sim 500$ K, show that the TTV signal produced by a five lunar-mass satellite orbiting at the maximum stable distance from the planet (i.e. 0.5 Hill radii, Domingos et al, 2006) is larger than the  $3\sigma$  timing uncertainty. Confirmation of the exomoon candidates will require additional transit duration variation (TDV) signal, also observable by ARIEL – along with analysis of dynamic stability (Sasaki et al, 2012) – to distinguish between signals produced by planets, moons and Trojans.

## 2.4 Strategy to achieve the science objectives

### 2.4.1 How do we observe exo-atmospheres?

For transiting planets, we have five complementary methods to probe their atmospheric composition and thermal structure, which are described briefly in the following paragraphs. ARIEL will use them all.

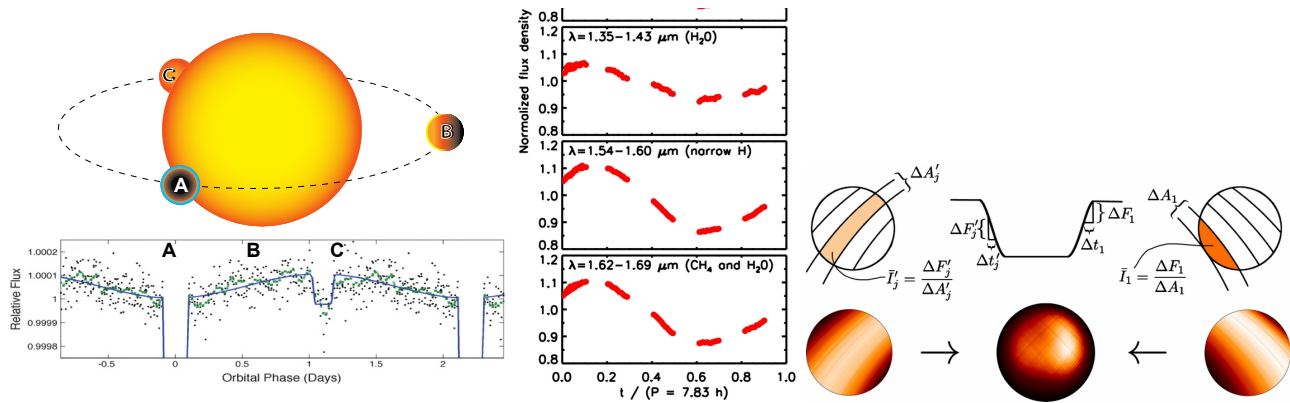


Figure 2-20: Methods adopted by ARIEL to probe the exoplanet composition and structure. *Left*: orbital lightcurve of the transiting exoplanet HAT-P-7b as observed by Kepler (Borucki et al., 2009). The transit and eclipse are visible. *Centre*: time series of brown-dwarf narrowband light curves observed with HST-WFC3 (Apai et al., 2013). The spectral bands have been selected to probe specific atmospheric depths and unhomogeneities in the cloud decks. *Right*: slice mapping with ingress and egress maps as well as a combined map of HD189733b at 8  $\mu\text{m}$ . These were achieved with Spitzer (Majeau et al., 2012, De Witt et al., 2012).

1. When a planet passes in front of its host star (**transit**), the star flux is reduced by a few percent, corresponding to the planet/star projected area ratio (transit depth, Figure 2-20). The planetary radius can be inferred from this measurement. If atomic or molecular species are present in the exoplanet's atmosphere, the inferred radius is larger at some specific (absorption) wavelengths corresponding to the spectral signatures of these species (Seager and Sasselov, 2000; Brown, 2001, Tinetti et al., 2007b).

The transit depth  $\Delta F(\lambda)$  as a function of wavelength ( $\lambda$ ) is given by:

$$\Delta F(\lambda) = \frac{2 \int_0^{z_{max}} (R_p + z)(1 - e^{-\tau(z,\lambda)}) dz}{R_*^2} \quad (1)$$

where  $z$  is the altitude above  $R_p$  and  $\tau$  the optical depth. Eq. (1) has a unique solution provided we know  $R_p$  accurately.  $R_p$  is the radius at which the planet becomes opaque at all  $\lambda$ . For a terrestrial planet,  $R_p$  usually coincides with the radius at the surface. For a gaseous planet,  $R_p$  may correspond to a pressure  $p_0 \sim 1\text{-}10$  bar.

2. A direct measurement of the planet's emission/reflection can be obtained through the observation of the **planetary eclipse**, by recording the difference between the combined star+planet signal, measured just before and after the eclipse, and the stellar flux alone, measured during the eclipse, Figure 2-20. Observations provide measurements of the flux emitted/reflected by the planet in units of the stellar flux (Charbonneau et al., 2005; Deming et al., 2005). The planet/star flux ratio is defined as:

$$\phi(\lambda) = (R_p/R_*)^2 F_p(\lambda)/F_*(\lambda) \quad (2)$$

3. In addition to transit and eclipse observations, monitoring the flux of the star+planet system over the orbital period (**phase curve**) allows the retrieval of information on the planet emission at different phase angles (Figure 2-20). Such observations can only be performed from space, as they typically span a time interval of more than a day (e.g. Stevenson et al., 2014; Borucki et al. 2009, Demory et al., 2016).

The combination of these three prime observational techniques utilized by ARIEL will provide us with information from different parts of the planet atmosphere; from the terminator region via transit spectroscopy, from the day-side hemisphere via eclipse spectroscopy, and from the unilluminated night-side hemisphere using phase variations.

4. In addition, eclipses can be used to spatially resolve the day-side hemisphere (**eclipse mapping**). During ingress and egress, the partial occultation effectively maps the photospheric emission region of the planet (Rauscher et al., 2007). Figure 2-20 illustrates eclipse mapping observations (Majeau et al., 2012; De Witt et al., 2012).
5. Finally, an important aspect of ARIEL is the repeated observations of a number of key planets in both transit and eclipse mode (**time series of narrow spectral bands**). This will allow the monitoring of

global meteorological variations in the planetary atmospheres, and to probe cloud distribution and patchiness (see e.g. Apai et al., 2013 for similar work on brown dwarfs, Figure 2-20).

## 2.4.2 ARIEL observational strategy: a 3-tier approach

The primary science objectives summarised in §2.2 and §2.3 call for atmospheric spectra or photometric light-curves of a large and diverse sample of known exoplanets covering a wide range of masses, densities, equilibrium temperatures, orbital properties and host-stars. Other science objectives require, by contrast, the very deep knowledge of a select sub-sample of objects. To maximize the science return of ARIEL and take full advantage of its unique characteristics, a three-tiered approach has been considered, where three different samples are observed at optimised spectral resolutions, wavelength intervals and signal-to-noise ratios. A summary of the survey tiers is given in Table 2-5. In the following subsections we report the expected performances of the ARIEL mission following the 3-tier strategy.

Tier name	Observational strategy	Science case
<b>Reconnaissance survey</b> (~30%)	Low Spectral Resolution observations of ~1000 planets in the VIS & IR, with SNR ~ 7	<ul style="list-style-type: none"> <li>• <i>What fraction of planets are covered by clouds?</i></li> <li>• <i>What fraction of small planets have still retained H/He?</i></li> <li>• <i>Classification through colour-colour diagrams?</i></li> <li>• <i>Constraining/removing degeneracies in the interpretation of mass-radius diagrams</i></li> <li>• <i>Albedo, bulk temperature &amp; energy balance for a subsample.</i></li> </ul>
<b>Deep survey</b> (~60%)	Higher Spectral Resolution observations of a sub-sample in the VIS-IR	<ul style="list-style-type: none"> <li>• <i>Main atmospheric component for small planets</i></li> <li>• <i>Chemical abundances of trace gases</i></li> <li>• <i>Atmospheric thermal structure (vertical/horizontal)</i></li> <li>• <i>Cloud characterization</i></li> <li>• <i>Elemental composition</i></li> </ul>
<b>Benchmark planets</b> (~10%)	Very best planets, re-observed multiple time with all techniques	<ul style="list-style-type: none"> <li>• <i>Very detailed knowledge of the planetary chemistry and dynamics</i></li> <li>• <i>Weather, spatial &amp; temporal variability</i></li> </ul>

Table 2-5: Summary of the survey tiers and the detailed science objectives they will address.

## 2.4.3 ARIEL Tier 1: exoplanet population analysis

ARIEL Tier 1 will analyse ~ 1000 exoplanets to address science questions where a large population of objects needs to be observed. For the majority of the targets observed by ARIEL, the necessary performance can be reached in 1 or 2 transits/eclipses (Figure 2-24). The ARIEL Tier 1 survey mode will also allow rapid, broad characterisation of planets so that decisions can be made about priorities for future observations with Tier 2 and Tier 3. Tier 1 science questions include:

- *What fraction of planets are covered by clouds?*

Tier 1 mode is particularly useful for discriminating between planets that are likely to have clear atmospheres, versus those that are so cloudy that no molecular absorption features are visible in transmission. Extremely cloudy planets may be identified simply from low-resolution observations over a broad wavelength range. This preliminary information will therefore allow us to take an informed decision about whether to continue the spectral characterization of the planet at higher spectral resolution, and therefore include or not the planet in the Tier 2 sample.

In addition, it may be possible to discriminate between broad cloud types simply using photometric indices. This will also be useful for planning follow-up observations, and additionally, if borne out by full retrieval analyses of ARIEL spectroscopic data, will increase the pool of cloudy planets to compare and contrast.

Examples of how such indices could work are given in Figure 2-21. We assume that the photometric observation mode for ARIEL will utilise the three FGS photometry channels, and that the FGS prism and the two main spectroscopic channels will each be binned up to a single point, resulting in a total of six photometric points. Useful indices for cloud diagnostics are the relative slopes between these six points. Below are two examples that show clear differences in these indices for cases where cloud is either absent,

deep or has low optical depth, against opaque, high grey clouds and opaque, high Rayleigh scattering clouds. In addition, it may also be possible to discriminate between vertically extended and vertically confined clouds, although this is more ambiguous (Barstow et al., 2017).

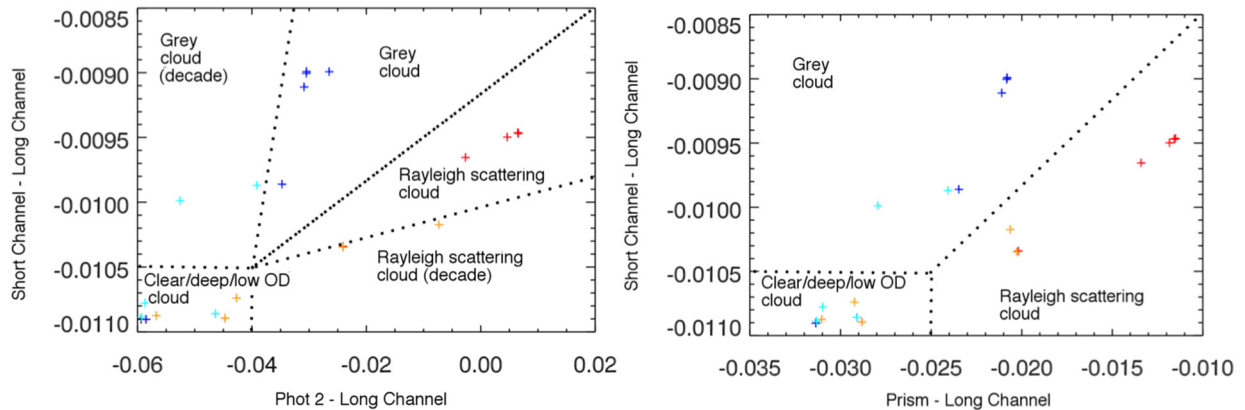


Figure 2-21: Preliminary cloud diagnostics using ARIEL Tier 1 type data (Barstow et al., 2017). Plots are the result of an approximately solar composition model run for a planet with the bulk properties of HD 189733b. The channels shown are FGS 1 (FGS photometry channel from 0.8-1 micron), Prism (FGS prism between 1.25 and 2 microns) and the short and long spectroscopic channels. Colours are: black (clear atmosphere); red (Rayleigh scattering cloud, extended); orange (Rayleigh scattering cloud, confined); blue (grey cloud, extended); turquoise (grey cloud, confined). For the confined clouds, high cloud will have a lower optical depth than deeper cloud for the same specific density as the atmospheric density is reduced, so some high confined cloud models appear to show little evidence of strong cloud scattering. For the extended cloud models, cloud top altitude increases from the bottom left to the top right of the plots.

- What fraction of small planets have still retained molecular hydrogen?  
See §2.2.2 for a detailed description of the science case and Figure 2-19 in particular.
- Constraining/removing degeneracies in the interpretation of mass-radius diagrams  
See §2.2.3 for a detailed description of the science case.
- Potential classification through colour-colour diagrams or colour-magnitude diagrams

Colour-colour or colour-magnitude diagrams are a traditional way of comparing and categorising luminous objects in astronomy. Similarly to the Hertzsprung-Russell diagram, which led to a breakthrough in understanding stellar formation and evolution, the compilation of similar diagrams for exoplanets might lead to similar developments (Triaud et al., 2014, Figure 2-22, Figure 2-23).

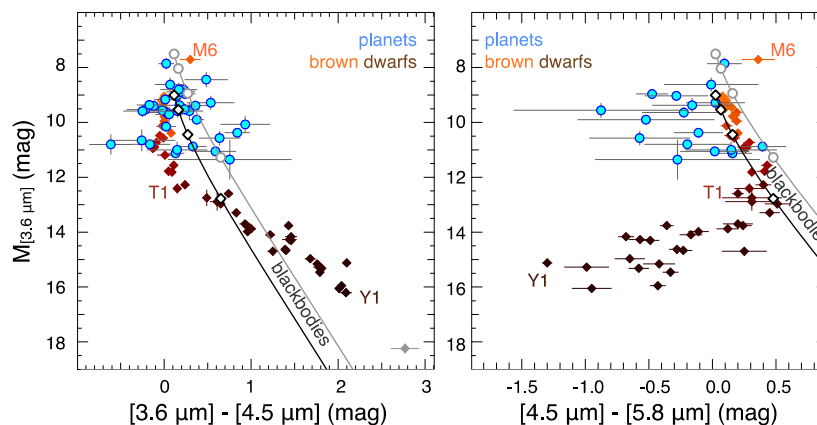


Figure 2-22: Mid-infrared colour-magnitude diagrams, using Spitzer’s IRAC photometric system. The dayside emission of transiting exoplanets are represented as blue dots, while the coloured diamonds show ultra-cool dwarfs from spectral type M6 to Y1. The two lines show the locus of blackbodies with 1  $R_{jup}$  (black) and 2  $R_{jup}$  (grey). Planets do not follow this: they are not blackbodies. The systematic bias from the blackbody, on the right panel, indicates the presence of water in the population of planets. Whereas individual measurements were unable to extract this information, taken as a group, there is a significant detection. Adapted from Triaud et al. 2014.

It is worth noting that many planetary scientists are sceptical about the usefulness of such diagrams to understand and classify planets, as they consider them too simple to capture the complexity and diversity of

planets. However, as pointed out in §2.1.1, a large number of objects needs to be analysed to fully appreciate the underlying properties of the planetary population, a requirement which cannot be fulfilled today. Increasing by two orders of magnitude the number of planets characterised and multiplying the number of colour-filters available in the 0.5-8  $\mu\text{m}$  wavelength range compared to current observations, ARIEL Tier 1 observations will provide, among other results, the ultimate test of whether an equivalent H-R diagram for planets does exist or not.

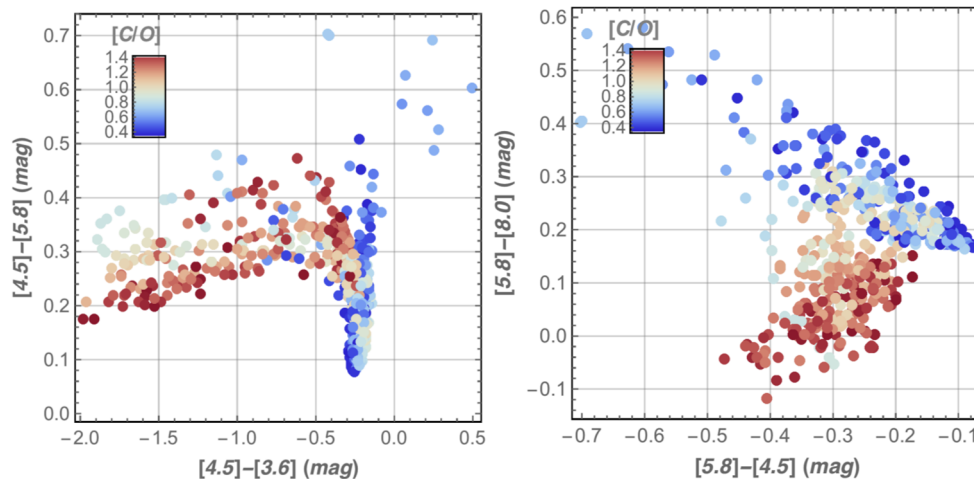


Figure 2-23: Simulated mid-infrared colour-colour diagrams as will be obtained by ARIEL in the tier 1 survey. For each planet in our randomly generated sample, we determine the closest model spectrum from the grid made by [Mollière et al. \(2015\)](#). Then the colours in the various photometric bands are determined using the standard Spitzer/IRAC filter characteristics. To remain within the boundaries of the parameter space covered by the [Mollière et al. \(2015\)](#) grid, each planet in the sample has been randomly assigned a temperature between 1000 and 2500 K, a metallicity between -0.5 and 2 dex, and a C/O ratio between 0.35 and 1.4. The colour coding shows the C/O ratio used for each planet. This shows that a population of planets with a low C/O ratio (blue) occupies, on average, a relatively distinct area of the diagram compared to high C/O ratio planets (red). Although we adopted IRAC bands for comparison, ARIEL will actually observe the entire spectrum and perform an optimal spectral binning afterward, therefore the bands containing more information can be determined a-posteriori during the analysis (through principal component analysis, for example).

- Albedo, bulk temperature & energy balance

Eclipse measurements of VIS and IR broadbands provide the bulk temperature and albedo of the planet, thereby allowing estimation of the planetary energy balance and whether the planet has an internal heat source or not.

To generate an indicative core mission sample observable by ARIEL in 2026 during its four year mission, a list of targets with different stellar types (F, G, K, M) and planetary parameters (size: Jupiters, Neptunes, sub-Neptunes, super-Earths, Earth-size; different temperatures) has been created ([Zingales et al, 2017](#)). This list was compiled using the statistics provided by the NASA Kepler mission combined with the number/types of stars in the Solar neighbourhood ([Fressin et al, 2013](#)). The required number of transits/eclipses to achieve the SNR/R reported in Table 2-5 has been calculated using the ESA Rad Model ([Puig et al., 2014](#)) and the end-to-end instrument simulator ExoSim ([Sarkar et al, 2016](#)). Figure 2-24 shows the complete set of planet candidates observable by ARIEL Tier 1 in this indicative sample. The final list of Tier 1 targets will include an optimal sub-sample of  $\sim 1000$  planets which can be observed during the four year mission out of the  $\sim 9500$  available (see e.g. Figure 2-33). Different colours in Figure 2-24 top panel indicate the number of transits/eclipses needed to reach Tier 1 performances (mostly one).

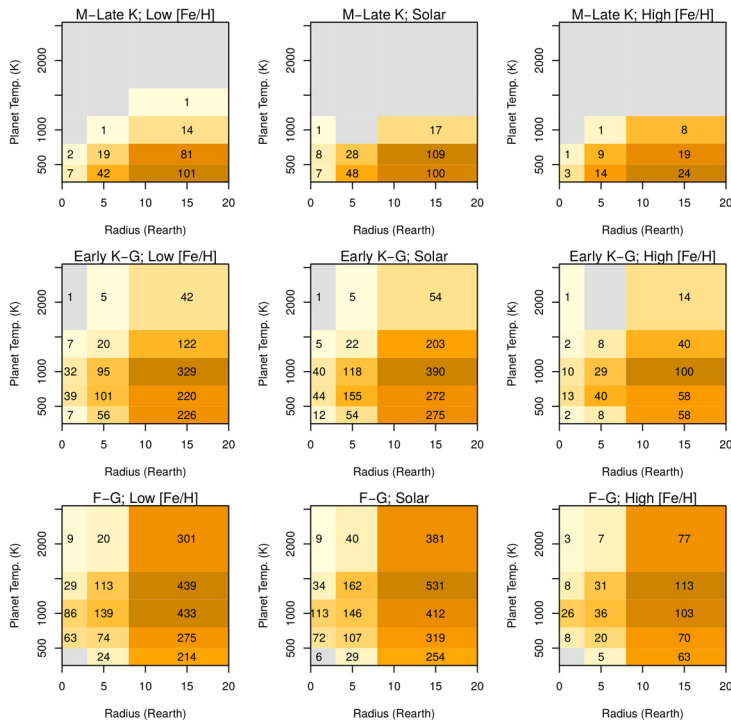
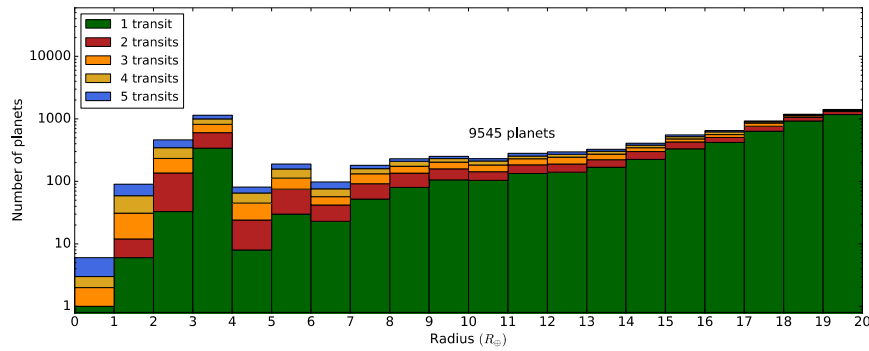


Figure 2-24: *Top*: planet candidates observable by ARIEL in the Survey modality (Tier 1) with a small number of transits/eclipses (mostly 1) divided in size bins. About ~1000 including planets of various sizes and temperatures can be observed in ~30% of the mission life-time (see Fig. 2-33). From Zingales et al. (2017). *Left*: spectral types and metallicity of the stars hosting the planet candidates observable by ARIEL in Tier 1 modality (Pillitteri & Micela (2017)).

### 2.4.4 ARIEL Tier 2: single planets & population analysis

We used the TauREx and NEMESIS spectral retrieval models to investigate the impact of wavelength coverage, SNR and spectral resolution on the retrievability of individual model parameters from transit and eclipse spectra as observed by ARIEL. Model parameters include the planetary temperature, molecular abundances and cloud parameters.

The Non-linear optimal Estimator for MultivariateE spectral analysis (NEMESIS) (Irwin et al. 2008) uses a combination of the correlated-k forward model with an optimal estimation retrieval scheme (Rodgers 2000). It has been used to successfully investigate planetary atmospheres in our own Solar System and beyond (Lee et al., 2012; Barstow et al., 2014a,b). Here simulated spectra are generated using an input atmospheric model, and random noise of the appropriate magnitude added. These are then used as inputs for the NEMESIS optimal estimation retrieval scheme and the retrieved atmospheric state compared with the input.

Tau-REx (Tau Retrieval for Exoplanets), as developed by Waldmann et al. (2015a,b), is a line-by-line radiative transfer and fully Bayesian retrieval framework. It contains 1) the optimised use of molecular line-lists from the ExoMol project (Yurchenko and Tennyson, 2013); 2) an unbiased atmospheric composition prior selection, through custom built pattern recognition software; 3) the use of two independent algorithms to fully sample the Bayesian likelihood space: nested sampling as well as a more classical Markov Chain Monte Carlo approach; 4) iterative Bayesian parameter and model selection using the full Bayesian Evidence as well as the Savage-Dickey Ratio for nested models

We report in Figure 2-25 and Figure 2-26 the results obtained in the case of a hot Jupiter and warm-Neptune respectively. These simulations confirm that Tier 2 and Tier 3 ARIEL data would provide very accurate results and would fulfil the science objectives as stated in sec. 2-3. For the majority of the targets observed

by ARIEL, these performances can be reached between 1 and 10 transits/eclipses (Figure 2-27). We have also run some blind tests, where forward models of cloudy planets generated by NEMESIS were combined to a noise model generated by the ARIEL instrument simulator (§3.2.1.1) and then they were analysed with TauREx. TauREx and NEMESIS have been cross-validated with CHIMERA (Line et al., 2016).

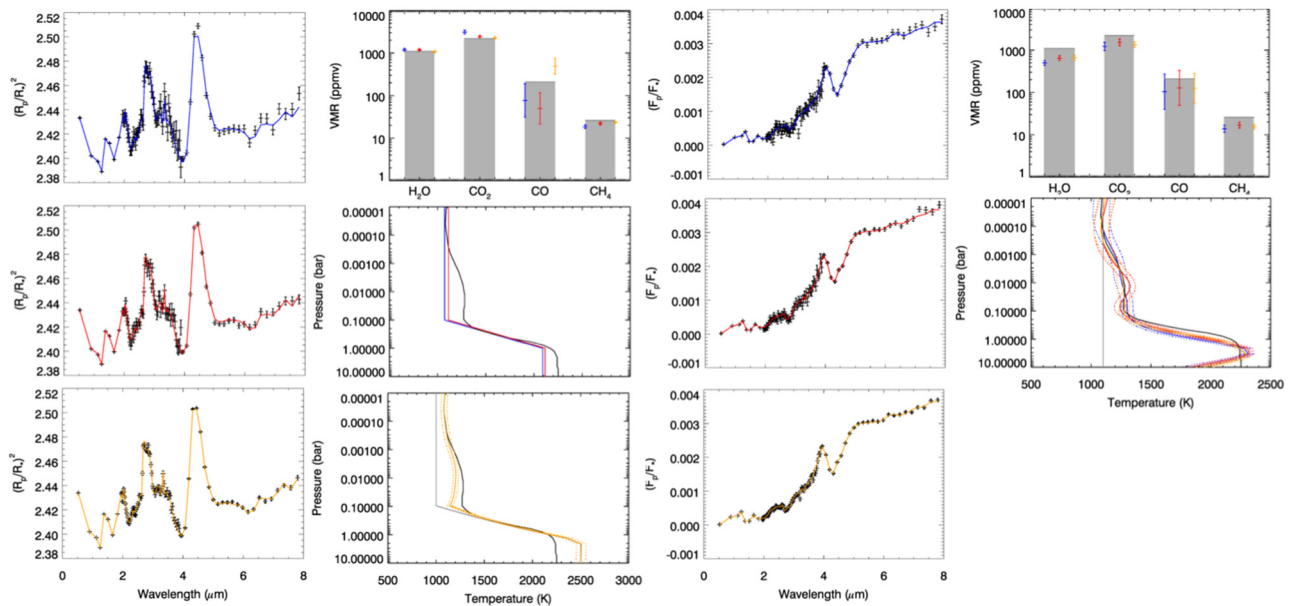


Figure 2-25: NEMESIS Retrieved results for signal-to-noise ratios of 7 (blue), 10 (red) and 20 (orange) for hot Jupiter HD 189733b in transit (2 panels on the left) and eclipse (2 panels on the right). Spectral fits are shown in the left-hand column, with retrieved molecular species and temperature profiles on the right. Grey bars indicate the input values for molecular abundances. A parameterized temperature profile, with variable deep and upper atmosphere temperatures, fixed knee pressures (at 0.1 and 1 bar) and an adiabat calculated in between, is retrieved for SNRs of 7 and 10, but for SNR 20 a continuous temperature profile is retrieved with a pressure correlation length of 1.5. In the upper atmosphere, the correct shape of the temperature profile can be recovered. NEMESIS retrievals of H<sub>2</sub>O, CO<sub>2</sub>, CO and CH<sub>4</sub> abundances and the temperature-pressure profile from synthetic secondary transit spectra of cloudy hot Jupiter HD 189733b. Colours correspond to SNR=7 (blue), SNR=10 (red) and SNR=20 (orange). In secondary transit, especially in the presence of cloud, there is some degeneracy between absolute abundances of molecular species and temperature structure; however, the abundance ratios between species can be reliably retrieved.

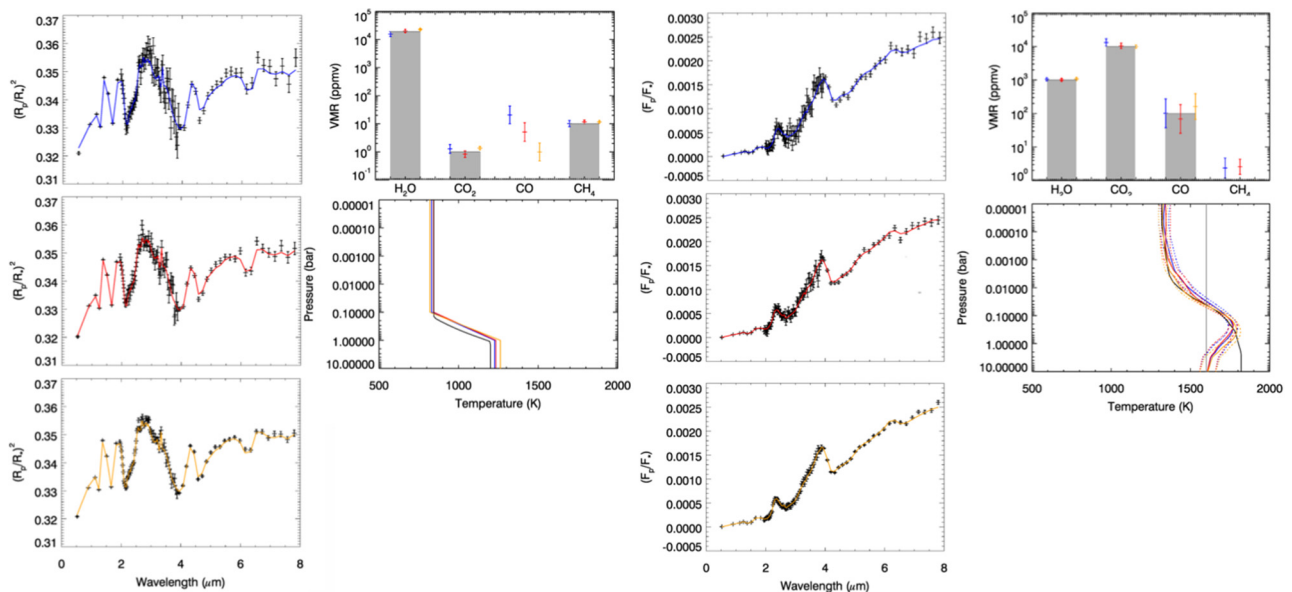


Figure 2-26: Same as Figure 2-25 but for planet HAT-P-11b.

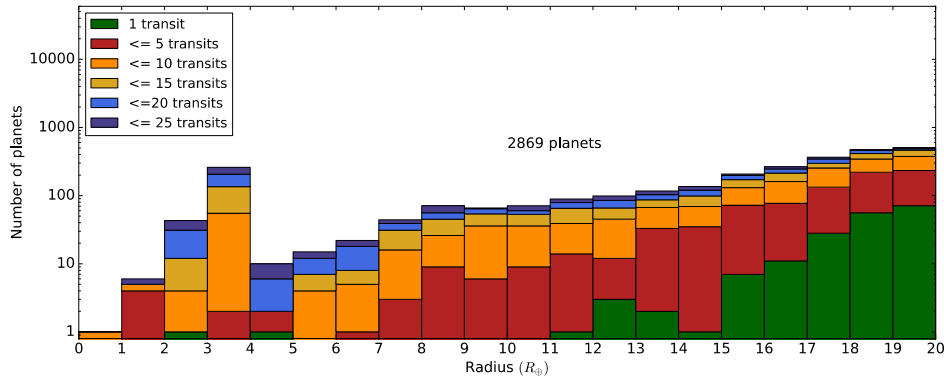


Figure 2-27: Number of planets observable by ARIEL in the Deep modality (Tier 2) with a small/moderate number of transits/eclipses, divided in size bins (left) and equilibrium temperature bins (right). From Zingales et al., (2017).

### 2.4.4.1 Phase-curves

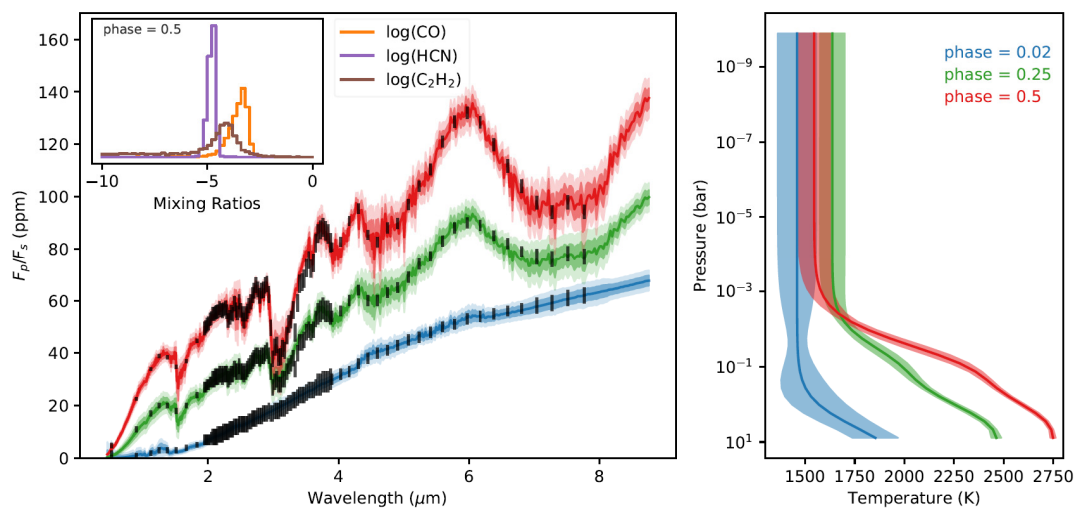


Figure 2-28: Simulated data for phase angles 0.1, 0.25 and 0.5 for super-Earth 55 Cnc e as observed by ARIEL. Phase 0.5 is considered the eclipse spectrum whereas phase 0.0 denotes mid-transit. *Left*: Black error-bars show the simulated spectrum at these angles and blue shaded areas the one sigma confidence interval of the retrieved emission model. The inset graphs show the marginalised posterior distributions of CO, HCN and C<sub>2</sub>H<sub>2</sub>. *Right*: retrieved temperature-pressure profiles at the various phases. These are snap-shots of an animation available at: <http://bit.ly/2kGL4Wz> (fig. credit Ingo Waldmann).

As described in 2.2.1.4, ARIEL phase-curves spectra will provide key observational constraints on the range of transport processes shaping the composition and vertical/horizontal structure of these atmospheres. We show here ARIEL performances in the case of phase-curves spectra for a hot super-Earth (Figure 2-28). Figure 2-29 shows the results of the TauREx spectral retrieval, demonstrating ARIEL’s capability to deliver very accurate chemical abundances and vertical thermal profiles as a function of the orbital phases for a hot super-Earth (55 Cnc e).

## 2.4.5 ARIEL Tier 3: very detailed study of select planets

Missions flying earlier than ARIEL or ground-based surveys, as well as ARIEL in its Tier 1, will likely identify "oddballs" that can have an impact on our general perspective of exoplanets. As a dedicated mission, ARIEL has the capability and the time for a detailed study of these identified interesting objects (Benchmark planets).

ARIEL Tier 3 observations will focus in particular on the study of the variability through time of the exoplanet atmospheres (weather). “Weather planets” are selected from the very best targets, i.e. planets for which the maximum ARIEL spectral resolving power and SNR > 7 can be reached in one observation. Repetition through time of the same observations will cast light on the temporal variability of the exo-atmospheres due to variations in the cloud coverage (see Figure 2-21) or patterns in the global circulation (see Figure 2-30). Concerning the latter, a robust feature of tidally-synchronized, close-in planets –

especially hot-Jupiters – is the variability of their atmospheres. The variability is exhibited as quasi-periodicity (Figure 2-30 left) and multiple equilibria (Figure 2-30 right, J. Cho priv. comm). ARIEL Tier 3 observations will identify variations in the thermal vertical and horizontal structure through time and provide critical insight into the complex circulation patterns of these exotic atmospheres. These results will be used also to quantify for the first time the error introduced when we obtain only disc and time integrated spectra. By combining all the observations obtained through time for a Benchmark planet, unprecedented SNR will be achieved, enabling an extremely detailed study of the atmospheric chemistry and dynamics.

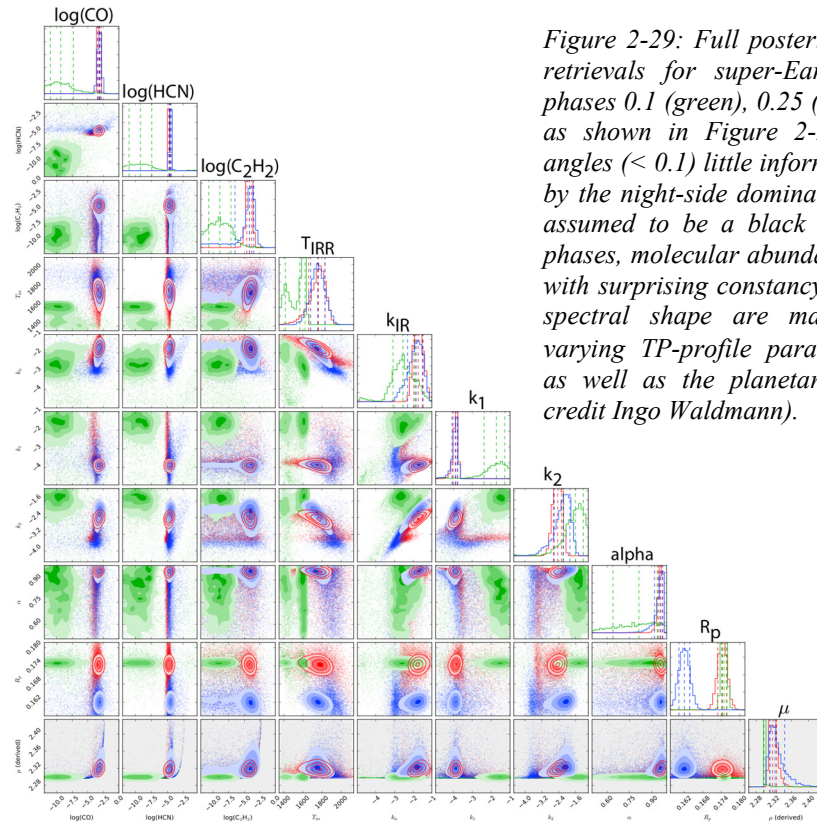


Figure 2-29: Full posterior distributions of retrievals for super-Earth 55 Cnc e at phases 0.1 (green), 0.25 (blue) and 0.5 (red) as shown in Figure 2-28. At low phase angles ( $< 0.1$ ) little information is contained by the night-side dominated spectrum (here assumed to be a black body). For higher phases, molecular abundances are retrieved with surprising constancy. Variations in the spectral shape are mainly captured by varying TP-profile parameters ( $k_1, k_2, k_{irr}, \alpha$ ) as well as the planetary radius  $R_p$ , (fig. credit Ingo Waldmann).

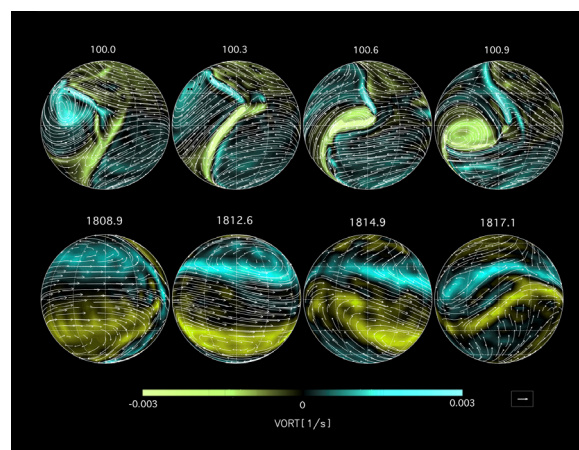
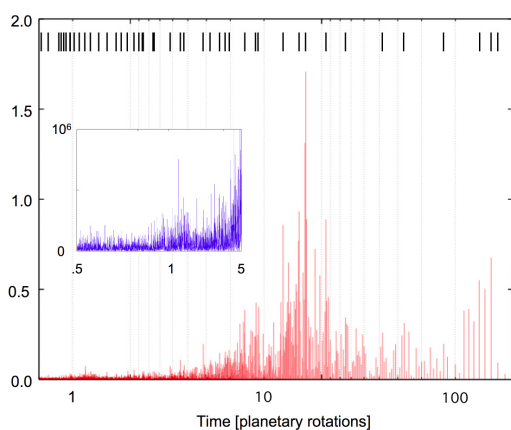


Figure 2-30: Left: Power spectrum of the quasi-periodic disk-integrated radiation flux centred on east terminator time series; the high-frequency part of the spectrum is shown in the inset. Strong peaks are demarcated at the top. The strongest peaks are in the 10-20 day periods, with the strongest at  $\sim 17$  day period, in this case. Right: Multiple equilibria of hot-Jupiter atmospheres: two circulation states are exhibited from a single simulation. The top row shows a state characterized by cyclogenesis (formation of cyclonic storms), alternating in the northern and southern hemispheres. The Bottom row shows a state characterized by a translating dipole-pair, which is nearly phase-locked. Transitions between the two states, as well as a small number of others, are seen in long-duration simulations (fig. credit, James Cho).

### 2.4.6 Targets available for ARIEL today

ARIEL will study a large population of planets, already discovered by other facilities. In particular, it will focus on hundreds of warm/hot gaseous objects (Jupiters, Saturns, Neptunes) and of super-Earths/sub-Neptunes around bright stars of all types. There are > 200 currently known planets complying with these requirements

The current 200 known targets have been discovered mainly close to the ecliptic plane because provided by ground-based surveys, as shown in Figure 2-31, illustrating also the sky visibility for ARIEL. K2, Cheops and NGTS are expected to complete the search for planets around bright sources closer to the ecliptic plane. TESS and PLATO will extend the planet search closer to the ecliptic poles, which are where ARIEL has continuous coverage.

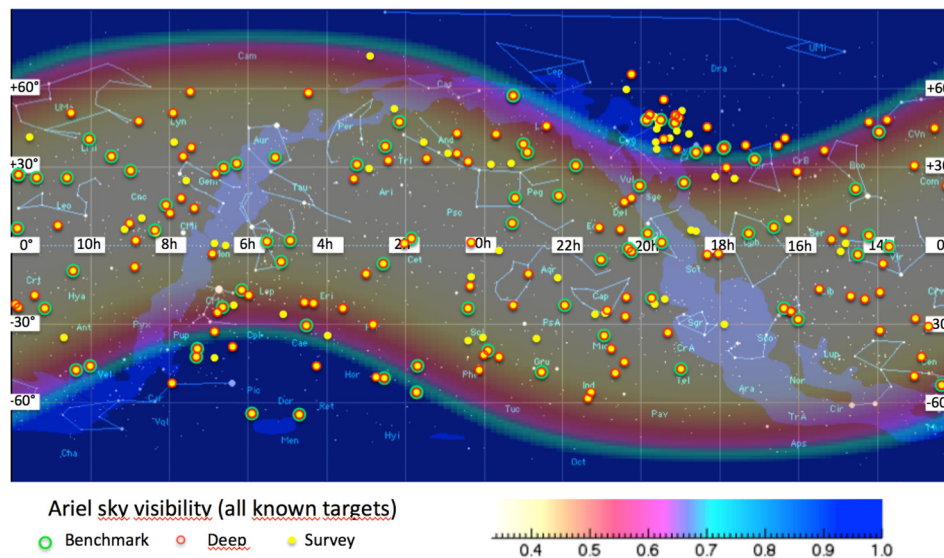


Figure 2-31: A plot illustrating the fraction of the year for which a given location in the sky (in equatorial coordinates) is visible to ARIEL, as seen from a representative operational orbit of ARIEL around L2. Orange and green targets are the currently known best targets in terms of stellar brightness and planetary parameters (green are the very best, including e.g. 55 Cnc e, HD 189733b, HD 209 458 b, GJ 436 b etc.), yellow targets are currently known transiting planets observable by ARIEL.

### 2.4.7 The ARIEL Mission Reference Sample in 2026

An optimal sample of exoplanets – including both the already known exoplanets and the "expected" ones yet to be discovered – observable by ARIEL was estimated – the Mission Reference Sample (MRS). The current ARIEL design enables the observation of ~1000 planets during the mission lifetime which exceeds the mission requirements. It is clear that this nominal list of planets will change over the years depending on the new exoplanet discoveries. In Figure 2-33 we show a possible mission scenario where the ~ 1000 ARIEL planets are grouped according to their size, density, temperature and stellar type.

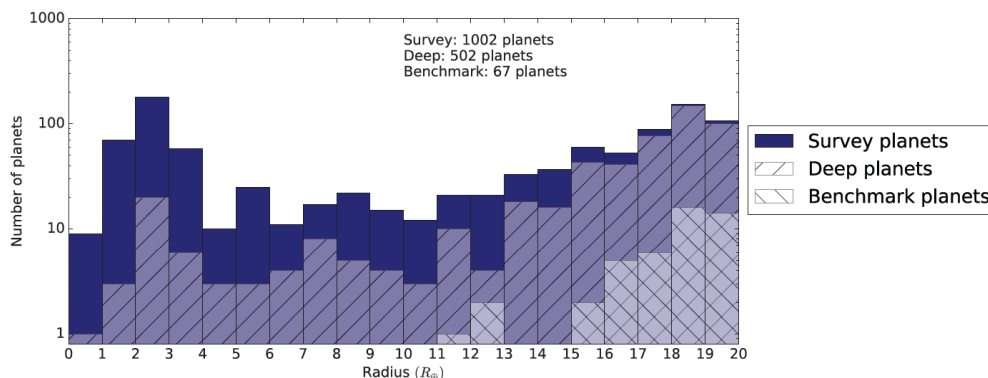


Figure 2-32: Overview of the ARIEL MRS. The graph shows how the ARIEL 3 Tiers, i.e. Reconnaissance Survey, Deep Survey and Benchmark planets are nested (Zingales et al., 2017).

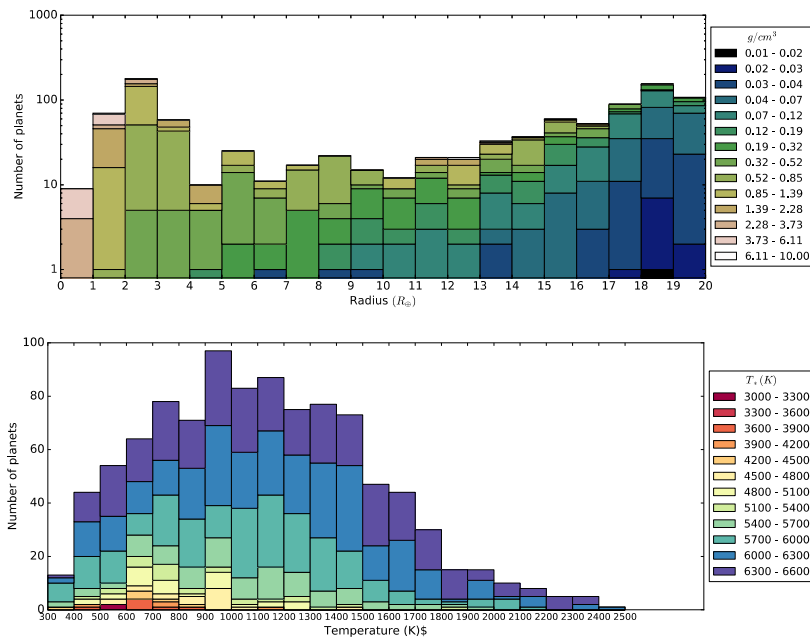


Figure 2-33: Tier 1 planets plotted as a function of size versus planetary density (top) and planetary versus stellar temperature (bottom) (Zingales et al., 2017).

Several surveys both from ground and from space will provide targets with the necessary characteristics to meet the objectives of the mission (i.e. 500-1000 planets observed). Table 2-6 summarises the most important surveys from which we expect a significant contribution to the final core sample. The list is not exhaustive.

Even without future planned and approved space missions such as CHEOPS, TESS and PLATO, there is expected to be a catalogue of >2000 possible targets to choose from available. When these missions are included as well the potential list could number >8000.

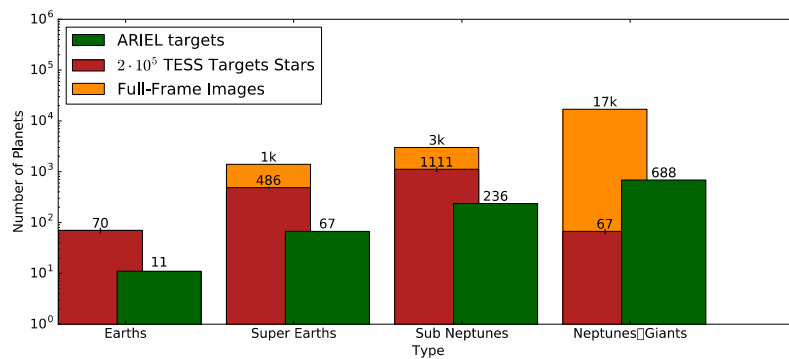


Figure 2-34: Comparison between the TESS targets (red and yellow bars, Sullivan et al., 2015) and ARIEL target sample (green bars). TESS will be an important mission that will be probably providing many of the targets for the ARIEL space mission.

Transit from ground	Survey/Facility	Jupiters	Neptunes	Super Earths
<b>Past / Ongoing</b>	HATNet/HATSouth (Bakos et al., 2004) WASP/SuperWASP (Pollacco et al., 2006; Maxted priv. comm.) MEarth (Nutzman et al., 2008) TRAPPIST (Gillon et al., 2016) APACHE (Sozzetti et al., 2013)	~300	~50	~30

	XO (McCullough et al. 2005) TrES (Alonso et al., 2004)			
<b>Future</b>	NGTS (Chazelas et al., 2012)	100	25	25
<b>Space Transit &amp; astrometry</b>	<b>Survey/Facility</b>	<b>Jupiters</b>	<b>Neptunes</b>	<b>Super Earths</b>
<b>Past / Ongoing</b>	CoRot (Auvergne et al. 2009, Fridlund et al. 2006)	25	3	1
	Kepler (Borucki et al. 2010)	200	50	10
	K2 (Howell et al. 2014)	500	100	100
<b>Future</b>	GAIA (Perryman et al. 2014; Sozzetti priv. comm.)	15	0	0
	PLATO (Rauer et al., 2014; Pagano priv. comm.)	1000	1200	1300
	CHEOPS (Fortier et al., 2014, Pagano priv. comm.)	80	10	5
	TESS (Ricker et al. 2014, Sullivan et al. 2015)	1000+	1800+	500+
<b>Radial velocity</b>	<b>Survey/Facility</b>	<b>Jupiters</b>	<b>Neptunes</b>	<b>Super Earths</b>
<b>Past / Ongoing</b> (mainly follow-up)	HARPS/HARPS-N (Pepe et al., 2000) CORALIE (Queloz et al. 2000) CARMENES (Quirrenbach et al., 2016) AAPS (Tinney et al. 2001)	>100s	>50s	>10s
<b>Future</b> (mainly follow-up)	ESPRESSO (Pepe et al., 2010) GIANO (Oliva et al., 2004) SPIROU (Artigau et al. 2011)	>100s	>50s	>10s

Table 2-6: Summary of the main surveys/projects that will provide targets for ARIEL in the next ten years (Micela et al., 2015). The columns on stars and expected planets refer specifically to the observations relevant for ARIEL. J=Jupiters, N=Neptunes, SN=sub-Neptunes, SE= Super-Earths.

## 2.5 Uniqueness of ARIEL & Synergies with other facilities

Future general purpose facilities with large collecting areas (James Webb Space Telescope, ESO-Extremely Large Telescope, etc.) will allow the acquisition of better exoplanet spectra compared to those currently available, especially for fainter targets. Tens of planets will probably be observed with JWST and E-ELT in great detail, but to address the questions of formation and evolution of exoplanets we need to be able to observe a sample that is one or two order of magnitude larger, i.e. we need a dedicated mission like ARIEL.

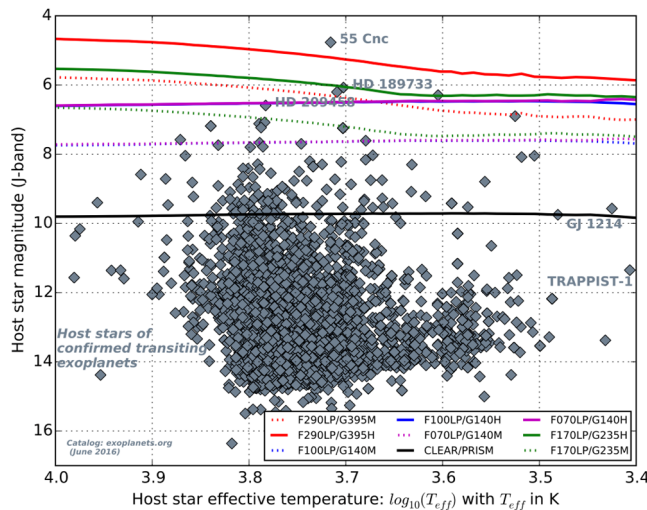
ARIEL	Other instrument
Complementary spectral range Large sample	JWST-MIRI
Focus on much brighter sources Large sample	JWST-NIRSPEC
Broader, simultaneous spectral range, lower resolution Large sample	E-ELT
<ul style="list-style-type: none"> <li>IR rather than VIS</li> <li>Transmission/emission rather than reflection</li> <li>Planets close to the stars rather than large separation</li> </ul>	WFIRST
Spectroscopy, IR	Cheops

Table 2-2-7: Synoptic view of ARIEL unique capabilities compared to other future facilities with some exoplanet capabilities.

### 2.5.1 Complementarity ARIEL-JWST

JWST will be the most powerful space observatory for transiting planets in the coming decade, and the only one able to study the climate of temperate terrestrial planets. JWST will likely obtain high-quality transmission and emission spectra of a variety of exoplanet atmospheres over a wavelength range of 1–11  $\mu\text{m}$ . However, a few key points make this great observatory unsuitable for the science case addressed by ARIEL, as detailed here:

1. Obtaining JWST spectra over 1–11  $\mu\text{m}$ , will typically require observations of four separate transit (or eclipse) events using four instrument modes for planets with bright host stars (Greene et al., 2016; Cowan et al., 2015; Beichman et al., 2014).



Faint targets can be observed in 2 passes, provided they do not saturate NIRSpec near 1–2  $\mu\text{m}$  (see Figure 2-35).

Figure 2-35: J-band limiting magnitudes for the different NIRSpec modes as a function of host star temperature<sup>2</sup>. The colored dashed lines are for the high resolution gratings, the coloured solid lines for the medium resolution gratings, and the solid black line for the prism. Sources below the lines can be observed in the full wavelength range of the given mode as specified in the table above. Labeled planets are known optimal targets for ARIEL. Figure on the right zooms into the region covered by NIRSpec gratings and where ARIEL has optimal performances.

2. A first cut, notional observing program for the JWST is encompassed in the Science Observations Design Reference Mission (SODRM – <http://www.stsci.edu/jwst/science/sodrm/jwst/science/sodrm/>): this consists of a number of observing programs built around seven science themes designed to allow the mission team test the observation planning tools. The allocation to exoplanet science is 16.1%. This includes also direct imaging observations.
3. Cowan et al. (2015) anticipating that actually 25% of JWST time will be devoted to transiting planets (based on the community interest) and multiplying this by the 70% duty cycle of the observatory and a 5 year mission, estimate 320 days devoted to the observation of transiting exoplanets. They provide in Table 2-8 possible science portfolios for transiting exoplanets and the time required to complete the observations. If the focus is on hot-Jupiters, up to 150 planets could be observed by JWST. They conclude that a dedicated mission is needed to performance an atmospheric survey in order to compliant the detailed characterisation of the most challenging targets that will be conducted with JWST.

JWST TRANSITING PLANET OBSERVING PORTFOLIOS

Portfolio Name	Number of Targets	Duration per Target	Total Time
Atmospheric Structure	150	2 days	300 days
Atmospheric Mapping	25	12 days	300 days
Temperate Terrestrials	3	100 days	300 days

NOTE.—Endmember portfolios for transiting planet science with JWST. Linear combinations of these are possible, and probably more scientifically productive: e.g.,  $70 \times 2 = 140$  days of structure,  $5 \times 12 = 60$  days of mapping, and 1 terrestrial (100 days) also adds up to 300 days.

Table 2-8: from Cowan et al. (2015).

4. JWST will simply have insufficient time to study the hundreds – thousands of planets discovered by current and future missions and ground-based surveys. Additionally, these observations will be heterogeneous both in terms of spectral coverage and observing mode. The best way to capitalise on

<sup>2</sup> <http://www.cosmos.esa.int/web/jwst-nirspec/exoplanets>

these discoveries is ARIEL, designed to perform a large survey of the brightest transiting planets in its 4-year mission.

5. Having a large collecting area, i.e. more photons, is certainly positive, but the lesson learnt from Spitzer and Hubble is that other aspects are also critical, especially the instrument stability and the knowledge of the instrument systematics. Kepler has been an incontestable success because it was built from start to achieve the 100 to 10 ppm photometric precision needed to discover Earth-size planets. We do not know at this time exactly how JWST data will be impacted by systematic noise, but one can assume that the noise is consistent with the best performance of HST or Spitzer as appropriate for each wavelength range. We show in Figure 2-36 the comparison between JWST and ARIEL performances in the case of a hot-Jupiter. As shown from the posteriors of the molecular abundances and other atmospheric parameters, in this case the retrieved information is very similar for ARIEL and JWST.
6. Instruments are most of the time not calibrated at the level needed to combine multiple observations. The ability to observe simultaneously a broad wavelength range, and the use of frequent observations to external calibrators will solve these issues in the case of ARIEL.
7. Another critical point is the stellar activity (see §3.2.2), which often interferes with the possibility of combining measurements at different wavelengths, if recorded at different times. [Barstow et al. \(2015\)](#) find that stellar activity could be the limiting factor for accurate retrievals of JWST observations of active stars. While simultaneous photometric observations by other observatories at relatively short wavelengths would be needed to correct this effect in the case of JWST, the ARIEL mission has been designed to be self-sufficient in its ability to correct for the effects of stellar activity. This is possible thanks to the instantaneous, broad-wavelength coverage and the strong chromatic dependence of light modulations caused by stellar variations. This is a unique capability of ARIEL, unmatched by present and future space and ground observatories.
8. In the first months of observations, ARIEL will re-observe some of the targets studied by JWST for calibration purposes. In general, the knowledge acquired through JWST observations will be fed into the ARIEL observational planning: e.g. whether duplicating some of the observations by JWST is desirable to study e.g. weather variability or to record a missing data set.

## 2.5.2 Complementarity ARIEL-E-ELT

ARIEL and E-ELT are expected to be operational in the same time-frame, i.e. 2025+. ARIEL and E-ELT observations will be highly complementary and mutually beneficial. Ground-based observations of exoplanet atmospheres have many challenges and limitations: large parts of the electromagnetic spectrum are blocked from view due to absorption and scattering in the Earth's atmosphere. In addition, the thermal background from the sky and telescope are strongly variable, making high-precision ground-based transit or eclipse spectroscopy practically impossible from the ground at wavelengths longer than 5  $\mu\text{m}$ . However, the E-ELT will be very valuable in specific ways. One particularly successful observing strategy makes use of spectroscopy at a very high dispersion of  $R \sim 100,000$  using the METIS instrument ([Brandl et al, 2016](#)). At this resolution, molecular bands in exoplanet spectra are resolved into hundreds to thousands of individual lines, whose signals can be combined to secure a molecular detection. Only astrophysical information over small wavelength scales is preserved, hence the line-contrast is being measured with respect to a local pseudo-continuum. This technique has been used very successfully using the VLT, for both exoplanet transmission spectroscopy ([Snellen et al, 2010](#)) and emission spectroscopy ([Brogi et al, 2012](#)), and will be more effective on the next-generation of extra-large telescopes.

E-ELT observations will be highly complementary to ARIEL. The ARIEL spectra, which will be obtained over a large instantaneous wavelength range, are crucial for measuring the most important planetary atmosphere parameters – the temperature-pressure profile, the cloud coverage and the key molecular abundances. With these parameters determined by ARIEL, i.e. the local pseudo-continuum, high-resolution E-ELT observations, providing planet differential transmission and day-side spectra at specific wavelengths, can then be calibrated and used to target other, specific aspects of the planetary atmospheres. For the best observable targets, the E-ELT can provide information on the rotation of the planet and high-altitude wind speeds using the absorption line profiles ([Snellen et al., 2010; 2014](#)).

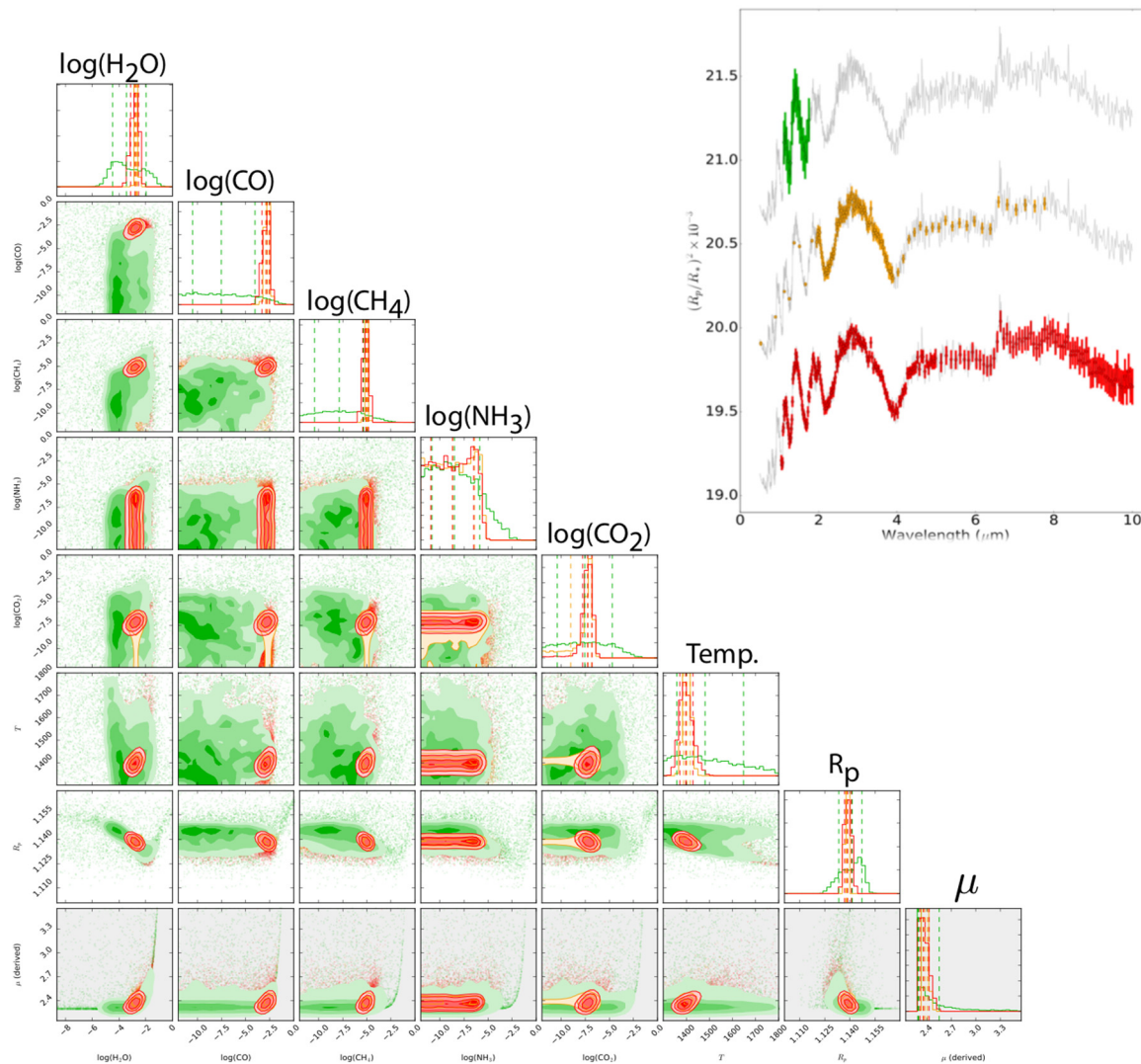


Figure 2-36: Posterior distributions of various atmospheric trace gases, temperature and top cloud pressure obtained with TauREx by retrieving the simulated spectra shown on the right, as observed by HST/WFC (green), JWST (red) and ARIEL (orange). Dashed lines in the histogram plots show the 1 sigma confidence intervals. The gases and atmospheric parameters retrieved include H<sub>2</sub>O, CO<sub>2</sub>, CO, CH<sub>4</sub> and NH<sub>3</sub>, temperature, radius and derived mean molecular weight. There is still considerable degeneracy for retrievals from WFC3 spectra, but ARIEL and JWST data are expected to be very constraining. The information content for JWST and ARIEL in the case of bright sources is comparable, indicating that ARIEL will be able to characterize atmospheres to a similar degree of accuracy.

## 2.6 Conclusions

We have presented in this chapter a brief overview of the science objectives for the ARIEL mission.

In order for the ARIEL mission to address the fundamental questions of “what are exoplanets made of” and “how do planetary systems form and evolve” we propose to investigate the atmospheres of many hundreds of diverse planets by transit spectroscopy. By observing a large number (~1000) of transiting planets from a range of different classes of object we will gain a statistical understanding of their nature.

We will focus on warm and hot planets to take advantage of their well-mixed atmospheres which should show minimal condensation and sequestration of high-Z materials and thus reveal their bulk and elemental composition (especially C, O, N, S, Si). Observations of these warm/hot exoplanets will allow the understanding of the early stages of planetary and atmospheric formation during the nebular phase and the following few million years. ARIEL will thus provide a truly representative picture of the chemical nature of the exoplanets and relate this directly to the type and chemical environment of the host stars.

### 3 Scientific Requirements

In chapter 2 we presented the Science Objectives of the ARIEL mission. Here we detail the Science Requirements which need to be met by the ARIEL mission to enable those objectives. These include the spectral coverage and resolution, the signal to noise ratios, the photometric stability and the data needed to be able to deal with astrophysical noise sources such as stellar variability, activity and flaring.

#### 3.1 Required wavelength coverage, spectral resolution and S/N

To maximise the scientific impact achievable by ARIEL, we need to access all the molecular species expected to play a key role in the physics and chemistry of planetary atmospheres. It is also essential that we can observe warm and hot planets at different temperatures (mainly from ~500 K to 3000 K, Figure 3-1) to probe the differences in composition potentially linked to formation and evolution scenarios.

Broad, simultaneous wavelength coverage is therefore required to:

- Measure both albedo and thermal emission to determine the planetary energy budget (Figure 3-1).
- Classify the variety of planets at different temperatures.
- Detect the variety of chemical components present in warm & hot exoplanet atmospheres
- Guarantee redundancy (i.e. molecules detected in multiple bands of the spectrum) to secure the reliability of the detection – especially when multiple species overlap in a spectral range (Figure 3-3).
- Enable an optimal retrieval of the chemical abundances and thermal profile (§2.2.3.2).
- Detect clouds and constrain their spatial distribution and temporal variability (see §2.4.3).
- Correct for stellar variability (see §3.2.2)

This means covering the largest wavelength range feasible given the temperature limits. Table 3-1 summarises the choices made for ARIEL in terms of wavelength bands, Resolving power (R) and required signal to noise (SNR) to maximise the scientific return.

Wavelength range	Required R & SNR			Scientific motivation
	Tier 1	Tier 2	Tier 3	
<b>VISPhot</b> 0.5 – 0.55 $\mu\text{m}$	Integrated band SNR $\geq 200$ on the Stellar SNR SNR $\geq 7$ on the exoplanet (goal)			<ul style="list-style-type: none"> <li>• Correction stellar activity (optimised early stars)</li> <li>• Measurement of planetary albedo</li> <li>• Detection of Rayleigh scattering/clouds</li> </ul>
<b>FGS1</b> 0.8 – 1.0 $\mu\text{m}$	Integrated band SNR $\geq 200$ on the Stellar SNR SNR $\geq 7$ on the exoplanet (goal)			<ul style="list-style-type: none"> <li>• Correction stellar activity (optimised late stars)</li> <li>• Measurement of planetary albedo</li> <li>• Detection of clouds</li> </ul>
<b>FGS2</b> 1.05 – 1.2 $\mu\text{m}$	Integrated band SNR $\geq 200$ on the Stellar SNR SNR $\geq 7$ on the exoplanet (goal)			<ul style="list-style-type: none"> <li>• Correction stellar activity (optimised late stars)</li> <li>• Detection of clouds</li> </ul>
<b>NIRSpec</b> 1.25 – 1.95 $\mu\text{m}$	R: 10 averaged bands for 1.25 – 7.8 $\mu\text{m}$ SNR $\geq 7$	R $\geq 10$ SNR $\geq 7$	R $\geq 10$ SNR $\geq 7$	<ul style="list-style-type: none"> <li>• Correction stellar activity (optimised late stars)</li> <li>• Detection of clouds</li> <li>• Detection of molecules (esp. TiO, VO, metal hydrides)</li> <li>• Measurement of planet temperature (optimised hot)</li> <li>• Retrieval of molecular abundances</li> <li>• Retrieval of vertical and horizontal thermal structure</li> <li>• Detection time variability (weather/cloud distribution)</li> </ul>
<b>AIRS</b> (Channels 0 & 1) 1.95 – 7.8 $\mu\text{m}$		R $\geq 50$ for $\lambda < 3.9\mu\text{m}$ ; R $\geq 15$ for $\lambda > 3.9\mu\text{m}$ SNR $\geq 7$	R $\geq 100$ for $(\lambda < 3.9\mu\text{m})$ ; R $\geq 30$ for $(\lambda > 3.9\mu\text{m})$ SNR $\geq 7$	<ul style="list-style-type: none"> <li>• Detection of atmospheric chemical components</li> <li>• Measurement of planet temps. (optimised warm-hot)</li> <li>• Retrieval of molecular abundances</li> <li>• Retrieval of vertical and horizontal thermal structure</li> <li>• Detection time variability (weather/cloud distribution)</li> </ul>

Table 3-1: Summary of the ARIEL spectral coverage (left column) and resolving power as designed (central column, see §4.7& §4.9). The key scientific motivations are listed in the right column.

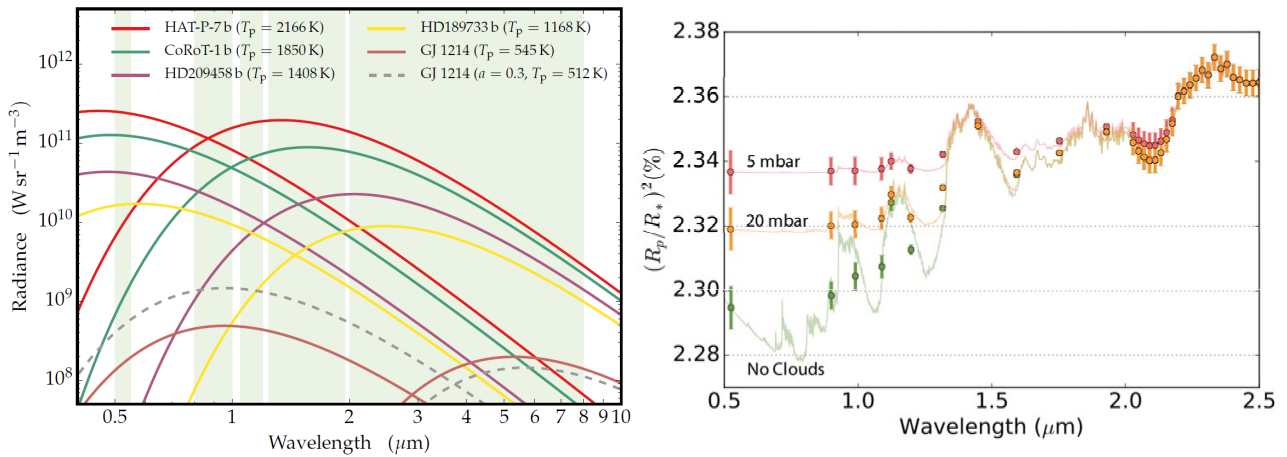


Figure 3-1: Left: Reflected and thermal components for very hot (HAT-P-7b and CoRoT-1b), hot (HD209458b and HD189733b) and warm objects (GJ 436b and GJ 1214b). Calculations are made for a very low value of the albedo  $a = 0.1$ , and for  $a=0.3$  in the case of GJ1214b. The green area indicates the spectral window covered by the ARIEL, as indicated in Table 3-1. Right: Cloud signature in the 0.5-2.5  $\mu\text{m}$  range: through the spectral coverage provided by ARIEL, clouds can be well detected and characterised (particle-size, distribution, etc.).

Some spectral regions are more critical than others (see also e.g. Tinetti et al., 2013; Encrenaz et al., 2015):

- (i) For hot and warm planets, the wavelength coverage 1.25 – 7.8  $\mu\text{m}$  is critical for ARIEL, as it guarantees that ALL the key chemical species (shown in Figure 3-3) can be detected.
- (ii) Redundancy (i.e. molecules detected in multiple bands of the spectrum) significantly improves the reliability of the detection, especially when multiple chemical species overlap in a particular spectral range.
- (iii) Redundancy in molecular detection is also necessary to allow the retrieval of the vertical thermal structure and molecular abundances (Barstow et al., 2014).
- (iv) The moderate resolving power of ARIEL will permit the detection of most molecules at warm and hot temperature given the spectral broadening (Tinetti et al., 2013).
- (v) Two photometric bands in the visible and one in the NIR are sufficient to measure the planetary albedo (see Figure 3-1), and to correct for stellar variability (see §3.2.2).
- (vi) The spectrograph in the NIR and VIS/NIR photometers enable to detect and differentiate between of Rayleigh scattering as opposed to clouds/hazes (see Figure 3-1 right).

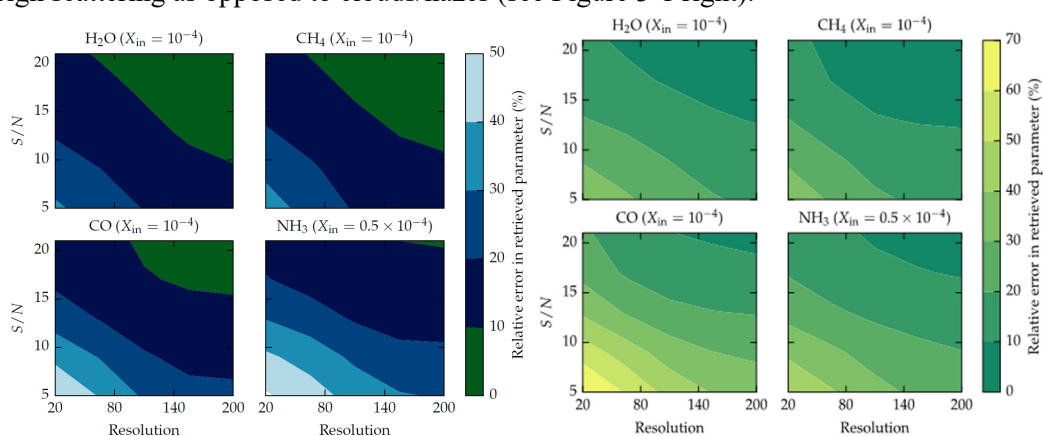


Figure 3-2: Left: Spectral retrieval of cloudy hot-Jupiter atmospheres observed with transit spectroscopy. The error in the estimation of the molecular abundances is provided as a function of the spectral resolution & SNR obtainable with ARIEL (plots obtained with TauREx model, Rocchetto priv. comm). Right: Spectral retrieval of cloudy warm Neptune atmospheres observed with transit spectroscopy. The error in the estimation of the molecular abundances is provided as a function of the spectral resolution & SNR.

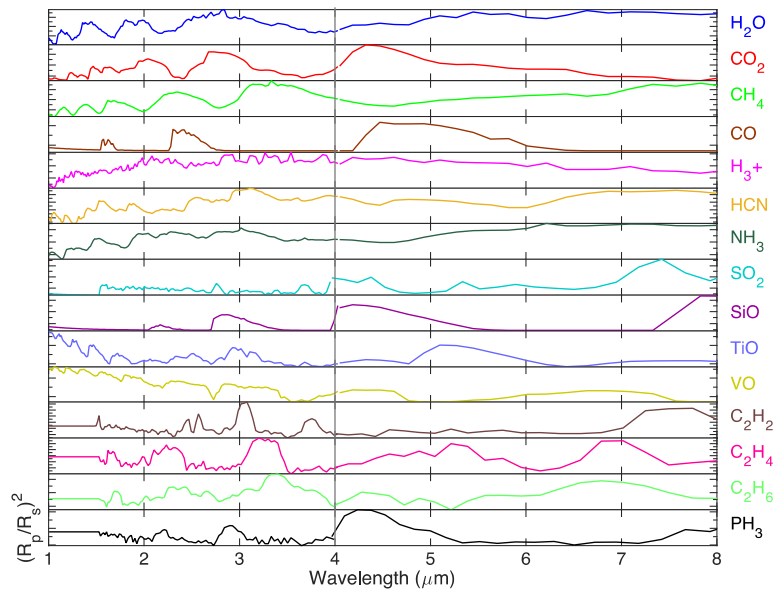


Figure 3-3: Molecular signatures in the 1-18  $\mu\text{m}$  range at the required spectral resolving power of ARIEL ( $R=100$  for 1.95 – 3.9 $\mu\text{m}$  and  $R=30$  for >3.9  $\mu\text{m}$ ).

## 3.2 Dealing with Systematic and Astrophysical Noise

### 3.2.1 ARIEL performance requirements

ARIEL’s top-level requirement is that the photometric stability over the frequency band of interest shall not add significantly to the photometric noise from the astrophysical scene (star, planet and zodiacal light). The frequency band over which the requirement applies is between  $2.8 \times 10^{-5}$  Hz and 3.7 mHz, or ~5 minutes to 10 hours (Puig et al., 2015; Eccleston et al., 2105; Pascale et al., 2015; Waldmann and Pascale, 2015). This implies having the capability to remove any residual systematics and to co-add the elementary observations from many repeat visits to a given target. The photometric stability budget is described in §4.10 using the tools described by Pascale et al. (2015), Waldmann and Pascale (2015) and Puig et al. (2015). To achieve the required performance, particular attention is required to:

- the design of the spacecraft, payload & instruments
- the calibration strategy to characterise all possible systematic variations in performance
- the data processing pipeline(s).

The top level science requirements for ARIEL on sensitivity are to meet a signal to noise ratio (SNR) of 7 for the resolutions defined in Table 3-1 for each of the Survey tiers. A derived requirement from this has been formulated by the SST and ESA using the ESA Radiometric Model to specify parameters X and Nmin such that the system level noise (after post-processing) shall be lower than X times the astronomical noise floor (defined by the RSS of stellar target and zodiacal background shot noises) plus an absolute noise floor Nmin:

$$Noise_{TOTAL} \leq \sqrt{((N_0 + zodi) \times (1 + X)) + N_{min}}$$

Where  $N_0$  is the flux of the target star being observed. The parameter X covers all noise sources which are related to the target brightness (such as jitter noise) and parameter Nmin covers all other source (such as detector dark current and read noise). The required values of X and Nmin are shown in Figure 3-5. These parameters give an equivalent photometric stability in the target frequency band of between 10 and 50 ppm for all the ARIEL required targets depending on the source brightness.

In deriving the noise performance requirements, a sensitivity study has been completed that shows that the mission science goals are very robust against the noise parameters assumed. The minimum required noise performance (which is exceeded by the design) allows the mission science to be achieved with up to 1000 planets being observed within the baseline mission lifetime to the required SNR. Increases in the noise levels lead only to a gradual degradation of the number of targets that can be successfully observed in each of the 3 tiers during the mission life.

3.2.1.1 The ARIEL end-to-end instrument simulator: ARIEL-Sim

In order to simulate the performance of the ARIEL system, the ExoSim tool (Sarkar et al., 2016) has been used. ExoSim is a generic, numerical end-to-end simulator of transit spectroscopy intended as open-access software. It permits the simulation of a time-resolved spectroscopic observation in either primary transit or secondary eclipse. The observational parameters can be adjusted, and the telescope and instrument parameters changed in a simple manner to simulate a variety of existing or proposed instruments. ExoSim is a tool to explore a variety of signal and noise issues that occur in transit spectroscopy observations, including the effects of the instrument systematics, correlated noise sources, and stellar variability. The simulations are fast, which allows ExoSim to be used for Monte Carlo simulations of such observations. A specific instance “ARIEL-Sim” has been created with the baseline instrument parameters of the payload and spacecraft performance detailed in §4, §5 (Sarkar et al., 2017).

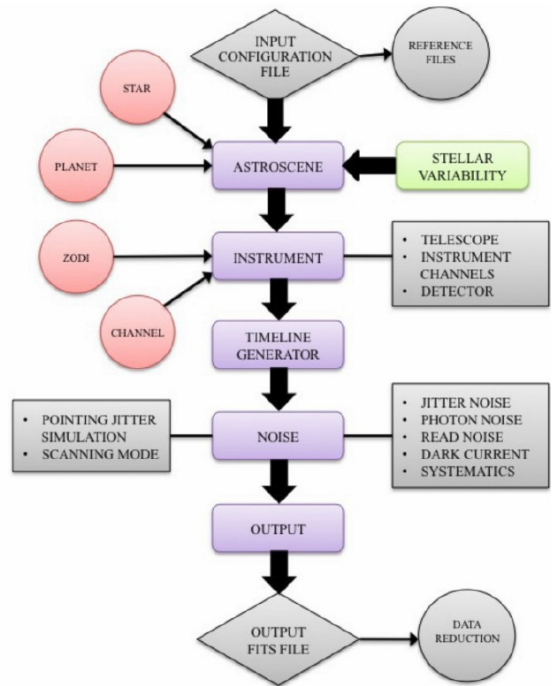
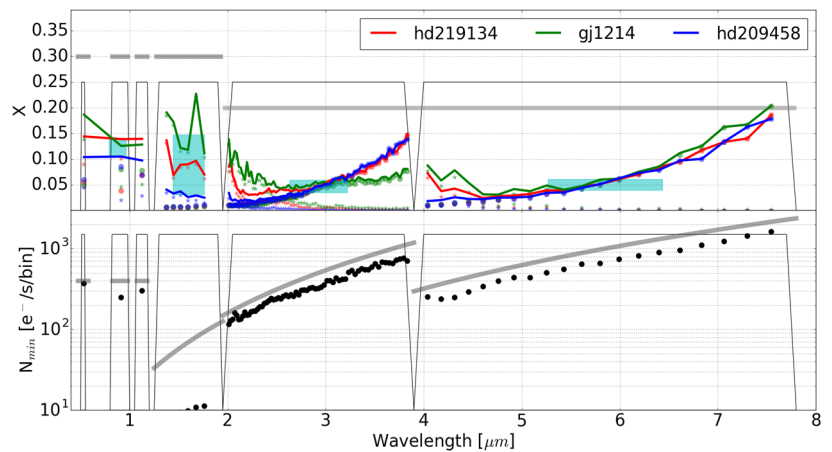


Figure 3-4: ExoSim Model Architecture

The simulator has been validated against both existing published transit data (Berta et al., 2012, Kreidberg et al., 2014), and the combination of simulator and ARIEL specific instrument parameters has been validated against the independent (static) Radiometric Model prepared by ESA (Puig et al., 2015). The simulations include a representative pointing jitter timeline (supplied by the ESA industrial study teams) and all other noise sources identified in §4.10. A basic data reduction pipeline (not using optimal data extraction and noise decorrelation techniques at this stage) is used to post-process the output data in the same way as the real science data will be handled.

Figure 3-5: Performance of ARIEL for the brightest, bright and faintest targets compared to noise requirements from the Mission Requirements Document. The requirements are shown by the bold grey lines, the thin grey lines denote the channels and the red, green and blue are the different targets. The noise requirements are expressed as the achieved Variance on the signal ( $Var(s)$ ) must be less a factor of  $(1+X)$  above the target star signal ( $N_0$ ) with an absolute variance floor of  $N_{min}$ . Hence the noise requirement is that  $Var(s) = (1+X)N_0 + N_{min}$  where  $X$  and  $N_{min}$  are given in the plots above for each channel. These noise requirements are shown to be equivalent to a photometric stability requirement of 10 – 100ppm for the range of target brightnesses covered by ARIEL.



3.2.1.2 Postprocessing analysis techniques

Within the ARIEL consortium, we have developed field-leading time series decorrelation techniques based on non-parametric machine learning (Waldmann 2012, 2014 Waldmann et al. 2013, Morello et al. 2014,2015,2016; Morello 2015) which recently won the Spitzer time-series data challenge (Ignals et al 2016) and enabled the first detection of a super-Earth’s atmosphere with Hubble-WFC3. These techniques are highly complementary to traditional de-trending and post-processing as they de-trend the data from systematic (e.g. instrument) noise on a purely statistical basis. Hence, we can well address any residual systematic noise that has not been captured by more traditional, parametric data de-trending routines.

### 3.2.2 Correcting for stellar activity

The differential spectroscopy measurement strategy of ARIEL (before/during/after the transit) may be affected by changes in the host star spectrum on the timescale of the transit. Changes in the host star spectrum are caused by magnetic activity (flares, co-rotating active regions and spots) and convective turbulence (granulation, pulsations). Results from the Kepler mission (Basri et al. 2013) indicate that most G dwarfs have photometric dispersions less than 50 ppm over a period of 6 hours, while most late-K and M dwarfs vary at a level of some 500 ppm. Note that Kepler operates in the visible where stellar photometric variability is few times higher than in the “sweet spot” of ARIEL – the NIR and MIR – because of the contrast between surface inhomogeneities and the stellar photosphere.

The ARIEL mission has been designed to be self-sufficient in its ability to correct for the effects of stellar activity. This is possible thanks to the instantaneous, broad-wavelength coverage and the strong chromatic dependence of light modulations caused by stellar variations. This is a unique capability of ARIEL, unmatched by present and future space and ground observatories.

The impact of stellar variations on the ARIEL data has been carefully evaluated in parallel by many teams part of the ARIEL consortium working on stars (Herrero et al., 2015; Micela, 2015; Scandariato et al., 2015) and more specifically through ARIEL-Sim (Sarkar et al., 2016). We have explored several possible approaches to evaluate the effect of oscillations and stellar activity and developed methodologies to prove the performance of ARIEL data in reaching the required precision. We describe here these methodologies.

#### 3.2.2.1 ARIEL-Sim simulations of impact of stellar variability on ARIEL observations

We have simulated two sources of stellar variability:

- a) convection-driven variability arising from pulsations and granulations
- b) star spot activity.

These simulations have been coupled with the end-to-end simulator, ARIEL-Sim incorporating the ARIEL instrument model, to obtain estimates of the impact of these sources of variability on ARIEL observations

#### ★ Pulsations and granulations

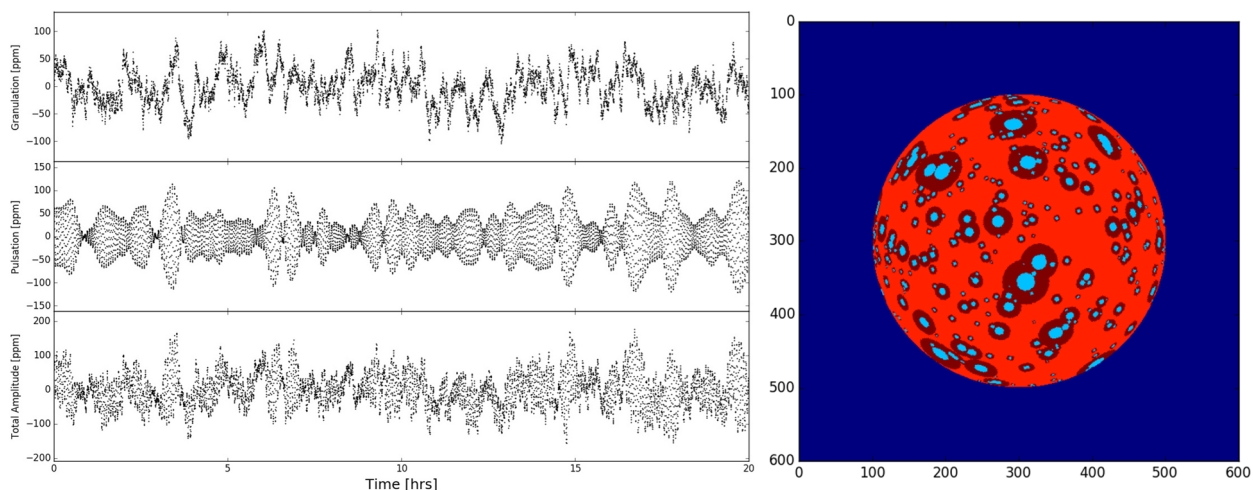


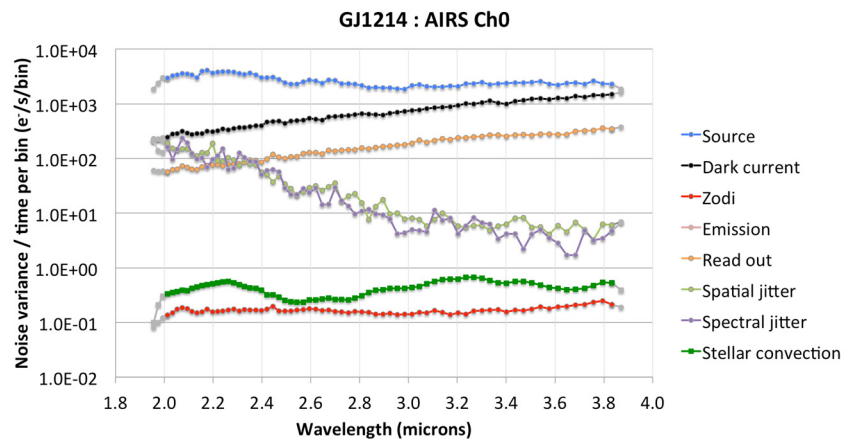
Figure 3-6: Left: Time series showing the effect of simulated granulation and pulsations on the bolometric luminosity of a star of spectral type M2V. The plot has a timebase of 20 hours, sampled every 10 seconds. Right: ARIEL-Sim star spot simulator – example of an extreme case: a star with 10% spot (the Sun is below 1%). Cold spots are shown in light blue. Hot faculae are in brown surrounding each spot. The temperature contrast with the photosphere is higher for spots than faculae.

Convection in the outer layer of stars induces stochastic pulsations and the emergence of granulation on the stellar surface. Both of these phenomena cause local temperature fluctuations and yield a stellar effective temperature that varies over time. Figure 3-6 shows time series from the convection model simulating pulsations and granulations. For oscillations, the timescales and amplitudes of optical and infrared variability

were calculated based on University of Leuven’s simulations using the BiSON solar data from [Broomhall et al. \(2009\)](#) where amplitudes and frequencies were rescaled using the scaling relations from [Kjeldsen and Bedding \(2011\)](#). The peak-to-peak variation due to oscillations was computed on a 10 hour basis. The Marcs model atmosphere parameters for the different spectral types were chosen following [Habets & Heintze \(1981\)](#) and [Pickles \(1998\)](#). For granulation, the variability for solar type stars was simulated using different red noise components due to active regions and background granulation ([Palle et al., 1995](#)). The scaling from the optical to the infrared was done using SEDs from Marcs models ([Gustafsson et al., 2008](#)).

Timelines from these models were incorporated into the ARIEL ExoSim model and the noise resulting on the out-of-transit timelines obtained for each spectral bin and channel. An example is shown in Figure 3-7, which shows the noise budget for M-dwarf GJ1214 (faintest required target) in AIRS channel 0, where the stellar convection noise can be compared to the contribution of other noise sources. We find that noise from granulations and pulsations is insignificant when compared to the photon noise and most other noise sources.

Figure 3-7: AIRS Ch0 noise budget for GJ1214 showing the noise from granulations and pulsations (shown in green) in relation to other noise sources. The photon noise limit arising from the source is shown in blue. The noise from granulations and pulsations is not significant when compared to the photon noise and most other noise sources.



★ Star spots

A star spot model has been developed which is now fully integrated with ARIEL-Sim (Figure 3-5 right). The spot model can simulate different star classes, with spots and faculae of different sizes, temperatures and spatial distributions. The star and planet are selected in ARIEL-Sim with parameters obtained through the Open Exoplanet Catalogue ([Rein, 2012](#)). The size distribution of spots is determined by a log-normal law ([Solanki and Unruh, 2003](#)), and a chosen hemispheric spot coverage can be applied. The transit of a planet across the spotted star can be simulated at multiple wavelengths and the resulting light curves from the ARIEL instrument model recovered, and used to obtain a reconstructed planet spectrum with the effects of spots in each channel. Spots may affect transit depths and the reconstructed spectrum in a number of ways:

- Unocculted spots may increase the transit depth, with the bias being wavelength dependent.
- Occulted spots may reduce the transit depth obtained through curve fitting, with the amplitude on the light curve being wavelength dependent.
- Spots with molecular absorption features can contaminate the planet spectrum.

The situation is simpler for eclipses, where the planetary emission follows directly from the depth measurement. In this case, only activity-induced variations on the timescale of the duration of the occultation need to be corrected to ensure that the proper stellar flux baseline is used.

Star spot simulations using the ARIEL-Sim was used to explore the effects of spots on transit spectra. As a first study, we performed a Monte Carlo simulation to assess the degree of distortion in the recovered spectrum, and how this may vary between observations. We show the results of the spot simulator and we describe in the various decorrelation methodologies to mitigate the effects of spots.

★ Star spots: ARIEL-Sim Monte Carlo simulation

We present here the case of a potentially problematic planet-star system, i.e. the super-Earth GJ1214 b which orbit an M-dwarf star. The star in ARIEL-Sim was simulated with 10% hemispheric spot coverage, which is an extreme case (the Sun is below 1%). The faculae:spot area ratio was set to 6. The star temperature was 3026K, with spot and faculae contrasts set at -337K and 66K respectively. A Monte Carlo simulation was performed with 200 realizations in each case. The spots were distributed using a random uniform

distribution, so that spot positions on the stellar hemisphere changed with each realization. The planet spectrum was reconstructed for each channel within each realization. An example result is shown in Figure 3-8 left for AIRS Ch1. We see that in this wavelength range, the uncertainty on the spectrum caused by spots is much less than that due to photon noise.

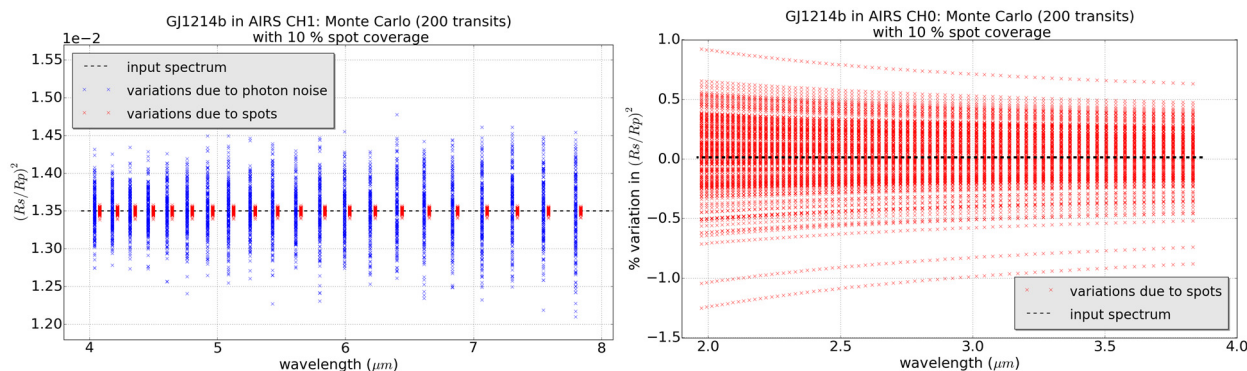


Figure 3-8: Left: AIRS Ch1 Monte Carlo simulation. Blue crosses show recovered transit depths from 200 simulations of GJ1214b with photon noise only. Red crosses (offset for clarity) are the transit depths from 200 realization with spots alone, where the spatial distribution of spots is randomly varied between realizations. Right: Monte Carlo simulation in ARIEL-Sim for AIRS Ch0 with 200 realizations showing the distribution in wavelength dependent bias due to spots. The bias can be above or below the true spectrum depending on the effect of the spots in any particular case.

Figure 3-8 right shows the results of the Monte Carlo simulation in AIRS Ch0. The 200 extracted planet spectra are shown as a percent variation from the input (or ‘true’) planet spectrum – in this case a flat spectrum. The combination of spot crossings and un-occulted spots produces a wavelength dependent bias, rather than a random noise, therefore this effect on the spectrum can be decorrelated by monitoring the spot variations in the visible/NIR channels, as demonstrated by Micela 2015, Herrero et al., 2015 and other methods described in the following sections.

### 3.2.2.2 Methods to correct the effect of star spots on transit spectra

We have developed two different methods based on models to correct for effects occurring during transits.

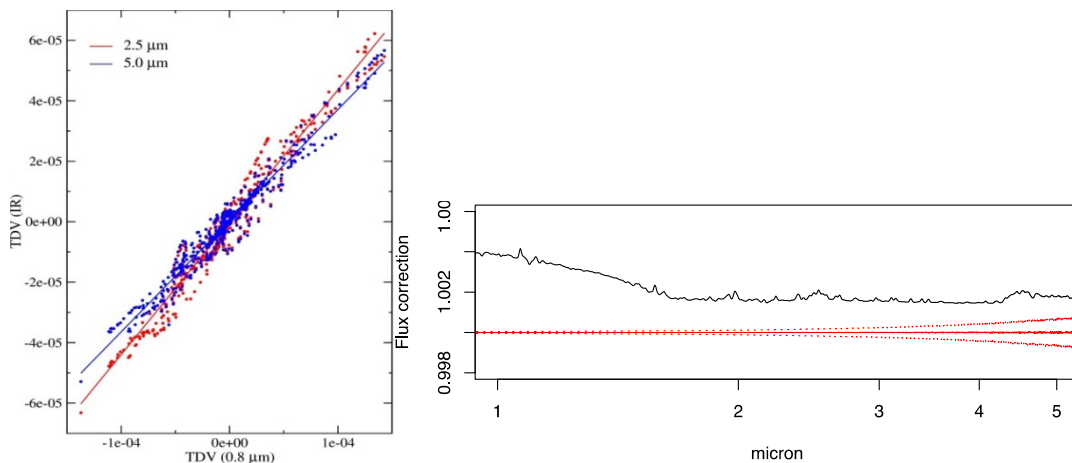


Figure 3-9: Left: (method 1) Correlation of activity-induced transit depth variations (TDV) in the visible (0.8  $\mu\text{m}$ ) and the IR (2.5 and 5.0  $\mu\text{m}$ ) for a star with  $T_{\text{eff}}$  5200. [Ballerini et al, 2012](#) calculate the relation between depths in optical and IR with a very similar approach. Right: (method 2) Spectrum distortion without corrections (solid black line), residual distortion after correction (median and 25 -75% percentiles of simulations).

**Method 1** – A realistic stellar simulator has been developed that produces time series data with the same properties as the measurements from ARIEL. The simulator considers surface inhomogeneities in the form of (dark) starspots and (bright) faculae, takes into account limb darkening (or brightening in the case of faculae), and includes time-variable effects such as differential rotation and active region evolution. We have generated series of transits at wavelengths 0.8, 2.5, and 5.0  $\mu\text{m}$ , measured the transit depths and calculated the variations of those depths with time. There is a well-defined correlation between activity-induced transit depth variations in the visible (0.8  $\mu\text{m}$ ) and the IR (2.5 and 5.0  $\mu\text{m}$ ). An illustration of the correlation

between visible and IR transit depth variations (TDV) can be seen in Figure 3-9 left. In practice, the correction of ARIEL data for stellar activity using, for example, a series of measurements in the visible and an IR band can be done using the following expression:

$$d_{IR}^{corr} = d_{IR} + a_0 + a_1 \cdot (d_{VIS} - \langle d_{VIS} \rangle),$$

where  $d$  stands for the transit depth, and  $a_0$  and  $a_1$  are the coefficients of a linear fit that can be determined from simulations. A number of combinations of stellar photospheres and active region parameters (size and location of spots, temperature contrast) were considered to obtain a statistical view of the method (Herrero et al. 2015). In all the explored cases, the procedure provides a correction of the transit data down to 10 ppm, and thus is fully compliant with ARIEL noise requirements.

**Method 2** – A complementary method has been developed to reconstruct the spectral energy distribution of the target stars in the IR using the visible spectrum (0.55-1  $\mu\text{m}$ ) as an instantaneous calibrator. Having a sufficient number of spectra of a given stars observed at different levels of activity, it is possible to calibrate the method for each star. The approach, based on Principal Component Analysis, has been developed on a grid (in spot temperature and filling factor) of models of active stars and has been tested through simulations including the photon noise. In all cases the first two components are retained: the first component is related to the slope of the spectrum while higher order components are related to features of the spectrum. The method has been validated through extensive simulations with a variety of star-spot combinations. Figure 3-9 right shows e.g. the stellar spectrum distortion, with and without correction, for a  $T_{\text{eff}}=5200$  K star, and a stellar SNR=500. In this case also the correction is fully compliant with ARIEL requirements (Micela 2015).

**Blind decorrelation correction** – A further approach has focused on statistical methods to de-correlate astrophysical noise from the desired science signal. Given single time series on an active star with various modes of pulsation obtained by the Kepler space telescope, Waldmann (2012) showed that a randomly chosen pulsation mode of the star could be isolated and the remaining autocorrelative noise of the star suppressed, resulting in a strong reduction of the stellar noise component. Similar concepts apply to periodic exoplanetary lightcurves observed over multiple transits and/or wavelengths. The results were repeated for a sample of Kepler stellar light curves, spanning from M to G types. In all cases a correction of the order of 10-100 ppm in the visible wavelengths depending on the frequency of the sampling (i.e. 10 hours continuous observations every day or 10 hours once a week), was obtained.

### 3.2.2.3 Flares

Flares show up as stochastic stellar variations on short time scales on all solar type stars (A to BDs). They are rare events, more prominent in the bluest bands than in the red and in infrared, since their emission is due to material heated by magnetic reconnection (up to ten(s) thousand degrees). The recent Balona (2015) paper analyses the flare properties along the HR diagram making usage of the short (1min) cadence Kepler data of 4758 stars from A to M types spanning a few months. These data have a cadence sufficient to resolve even relatively short flares and a photometric precision of 0.1 ppt (part per thousand). Their results indicated that only 209 stars show flares for a total of 3140 flares. This number indicate that flaring stars are rare, with a maximum of ~10% among the K-M stars (see Table 3-2 from Balona, 2015). Furthermore, the average number of flares for each flaring star (~15) indicates that flaring/non-flaring stars belong to different classes, and that it is very unlikely that a star in the non-flaring class shows a flare. Flaring stars are more common among fast rotators and therefore among active young stars. Most of those will not be observed by ARIEL.

Type	No stars in the sample	No flaring stars	Fraction(%)
<b>K-M</b>	561	57	10.16
<b>G</b>	2018	99	4.91
<b>F</b>	1617	41	2.54
<b>A</b>	424	10	2.36

Table 3-2: Fraction of flaring stars in SC Kepler data (from Balona 2015)

The first step will be, therefore, the identification of planets around flaring stars and either eliminate them from the sample, or actually target them for specific science cases (Venot et al, 2016). However even if after the cleaning of the sample, some flares will occur, it will be possible to recognize a typical flare from the shape of light curve with the photometric channels from the FGS. The typical sudden rise and slow decay signature of a flare over one/several hours allows to disentangle it from a transit signature. The hot color of

the flare emission will also allow to use the two optical channels to recognize the flare in the light curves and discard the data if necessary.

If some low intensity flares remain undetected in the optical channels, the contamination of the NIR-MIR spectra will be very limited. In fact, a recent detailed study of three M dwarf flare stars (Tofflemire et al. 2012) and M dwarf stars from SDSS and 2MASS surveys, Davenport et al. (2012) did a multi-wavelength characterization of flares in low-mass stars. Using their results, it is possible to obtain the relation between the flare intensity in the u-band and in the IR. The flare intensity reduces towards the longer wavelengths nearly following a power-law, and it depends on the sub-spectral type. In Table 3-3  $\Delta m_u$  and  $\Delta m_v$  are the expected magnitude changes in the U and V band, respectively, and produce effects in K band at levels as indicated (courtesy of J. Zoreck, IAP), while Figure 3-10 left from Davenport et al. (2012) gives the probability to detect a flare for stars from M0 to M6 as a function of the band.

$\Delta m_k$ [mag]	M0		M3	
	$\Delta m_u$	$\Delta m_v$	$\Delta m_u$	$\Delta m_v$
<b>0.01</b>	2.05	0.21	3.20	0.53
<b>0.001</b>	0.48	0.02	1.15	0.07
<b>0.0001</b>	0.15	0.002	0.25	0.007

Table 3-3: expected variation in K band for a given variation in V-band. The reported case is relative to a very intense flare. A flare on a M0 star with an amplitude in U of  $\Delta u=2.05$ , has an amplitude of  $\Delta v=0.21$  in V and of  $\Delta m_k=0.01$  in K band. Such a strong flare will be easily detected.

Globally the flare effect in the NIR is therefore very small, as illustrated from the case of AD Leo (a very active M-star) reported in Figure 3-10 right (from Davenport et al. 2012). In Table 3-3 we give example of intense flares for M0 and M3 stars. Earlier spectral type stars will have flares of significantly lower intensity.

To summarize, stars with intense flaring are uncommon and might not make it to the final ARIEL sample. Isolated flares would be immediately identified with the FGS and the flare effect in the IR is very small.

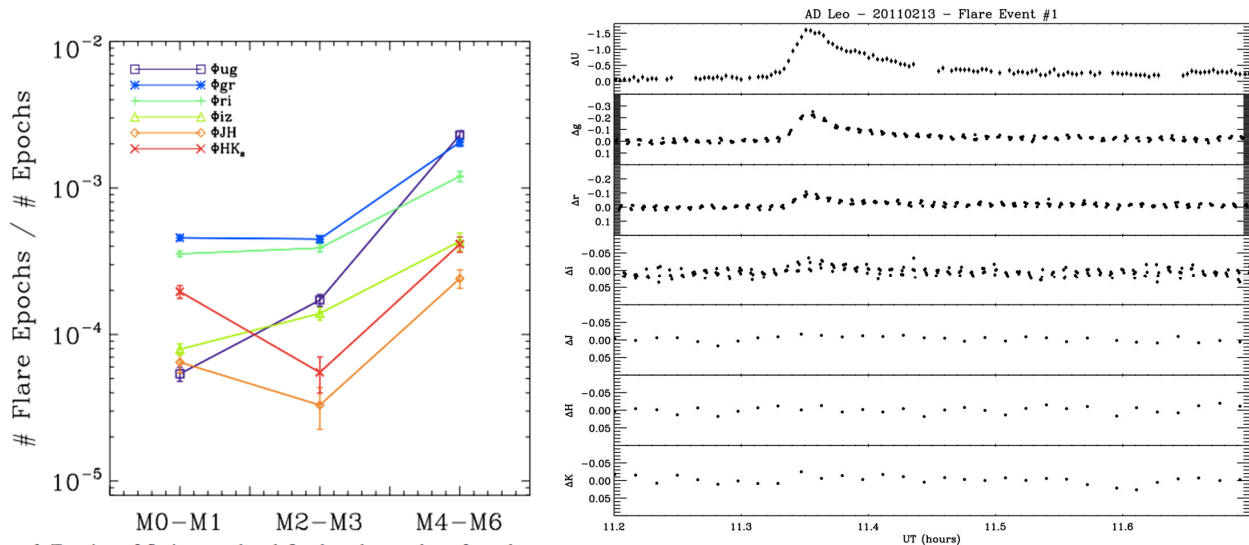


Figure 3-10: Left: Probability (# Flare Epochs/ #Epochs) to detect a flare for stars from M0 to M6 as a function of the band. Right: Multi-wavelength observations of a bright flare in AD Leo. The entire time span is 30 minutes. The variation in the U band is of the order of 1.5 magnitude (at peak) while the upper limit in K is less than 0.02 mag.

### 3.3 Conclusions

The combination of a stable platform, operating in a stable thermal environment and with a highly integrated payload and systems design, will ensure the very high level of photometric stability required to record exoplanet atmospheric signals, i.e. 10-50 ppm relative to the star (post-processing). The broad, instantaneous wavelength range covered by ARIEL will allow to detect many molecular species, probe the thermal structure, identify/characterize clouds and monitor/correct the stellar activity. Finally, requiring an agile, highly stable platform in orbit around L2, from which the complete sky is accessible within a year, will enable the observation of hundreds of planets during the mission lifetime.

### 3.4 Key Questions and Answers about ARIEL

#### 1. *Why do we need another exoplanet mission? [after Corot, Kepler, TESS, Cheops, PLATO]*

NASA Kepler, K2, TESS and ESA Cheops & PLATO are all missions performing photometric observations in the visible wavelengths to detect new transiting exoplanets or measure the radii of the planets discovered through radial velocity. Thanks to those missions, thousands of transiting exoplanets will be discovered in the next decade, especially the ones orbiting bright stars. The next logical step to take is IR spectroscopy to reveal the composition of those planets (see ESA-EPRAT report, MS1<sup>3</sup>).

None of the above mentioned missions will do spectroscopic characterization of exoplanets in the VIS and IR, like ARIEL. ARIEL will be the first dedicated mission, worldwide, to measure the chemical composition and thermal structures of hundreds of exoplanets, enabling planetary science beyond the boundaries of the Solar System.

#### 2. *Why do we need to observe hundreds of planets? [as opposed to a few tens with general purpose instruments]*

Work in exoplanet spectroscopy, has thus far been very piecemeal with one or perhaps a few spectra over a narrow wavelength range being studied at any one time. This approach is inadequate to provide answers to the key questions of exoplanetary science spelled out in the previous sections. A statistically significant number of planets (approximately two orders of magnitude larger than the sample observed with future general purpose facilities) needs to be observed systematically in order to fully test models and understand which are the relevant physical parameters. This requires observations of a large sample of objects, generally on long timescales, which can only be done with a dedicated instrument like ARIEL, rather than with multi-purpose telescopes not optimised for the specific application. ARIEL will enable a paradigm shift: by identifying the main constituents of hundreds of exoplanets in various mass/temperature regimes, we would be looking no longer at individual cases but at populations. Such a universal view is critical to understand the processes of planet formation and evolution and how they behave in various environments.

#### 3. *Why space? [as opposed to ground facilities]*

Broad, instantaneous wavelength coverage is necessary to detect as many molecular species as possible, to probe the thermal structure of the planetary atmospheres and to correct for the contaminating effects of the stellar photosphere. From the ground, the possibility to access the 2 to 8  $\mu\text{m}$  spectral region is seriously hampered by the telluric contamination. Also, at hot temperature the molecular bands are broadened, requiring only modest spectral resolving power to be detected, easily obtainable by a relatively small telescope in space (see Figure 2-36 and Figure 3-3).

Finally, to observe hundreds of planets an agile, highly stable platform from space is required. For an ARIEL-like mission, the complete sky is accessible within a year, with a source at the ecliptic observable for  $\sim 40\%$  of the mission lifetime (see §2.4.6). This is not achievable from the ground.

#### 4. *Is a 1-m class telescope too small for exoplanet spectroscopy? [as opposed to 6.5 m telescope in space or 30 m on the ground?] Why a dedicated mission (in an epoch of JWST and ELT)?*

No. If we assume the observations to be dominated by the stellar photon noise, the planetary SNR goes linearly with telescope diameter ( $D$ ). For instance, if we observed with a 6.5 m telescope a target star with Mag K = 11, we would obtain the same planetary SNR with a 1 m telescope by observing a target star which is  $\sim 2$  Mag brighter. By focusing on bright targets, we can obtain excellent SNR with a reasonable integration time (see §2.5 and Figures 2-24 and 2-26). While spectroscopic characterisation of exoplanetary atmospheres with ARIEL is perforce restricted to targets bright enough to permit acquisition of the necessary high signal-to-noise data, among the current crop of transiting exoplanets some  $\sim 200$  targets are brighter than Mag K=12.5, yet the surface of this vast treasure trove has been barely scratched. By 2026, this number is expected to be at least 10-20 times higher thanks to ground based surveys, K2, TESS (launching 2017), Cheops (launching 2018), PLATO (launching 2024) etc. (see Table 2-6).

Notice also that a large space telescope incurs additional observational overheads due to the time taken to move and repoint agilely from one target to another in the sky. A 1m class telescope from space would trade a lower spectral resolution over a broad, simultaneous wavelength coverage with extremely high spectral resolution over a narrow

<sup>3</sup> <http://sci.esa.int/jump.cfm?oid=47855>

spectral range obtainable with a ~30m from the ground. The higher SNR from the ground would be hampered by the telluric contamination. The two configurations are thus highly complementary: to get the full picture we need a dedicated telescope from space; to address very focused questions for a more limited number of planets, a large telescope from the ground is optimal.

#### **5. Why will ARIEL target mainly warm & hot planets? [as opposed to focusing e.g. only on habitable zone]**

Hot planets offer the unique opportunity to have access to the bulk and elemental composition, as there is no cold trap in their atmospheres for species such as H<sub>2</sub>O, NH<sub>3</sub>, CH<sub>4</sub>, SiO, CO<sub>2</sub>, CO and, depending on the temperature, metallic compounds e.g. TiO, VO, CrH. The knowledge of hot planets is therefore imperative to understand the big picture before we focus on colder regimes. Additionally, a large fraction of the currently available/expected to be discovered planets will orbit very close to their star and therefore will be hot. Having a short orbital period, these are the best targets for transit and eclipse spectroscopy measurements.

A long term scientific objective is to characterize the whole range of exoplanets, including, of course, potentially habitable ones. ARIEL would act as a pathfinder for future, even more ambitious campaigns.

#### **6. Why are gaseous planets also important? [not just rocky]**

While the search for habitable planets naturally focuses on terrestrial bodies, in the struggle to understand how planetary systems form and under which conditions they can produce habitable environments giant planets occupy a special place. From the study of the Solar System we know that the delivery of water and all the elements necessary for pre-biotic chemistry and the appearance of life on Earth, be it primordial or late, is associated with the formation and dynamical evolution of the giant planets. Contrary to what the present orderly nature of the Solar System would suggest, some scenarios actually link the formation of the terrestrial planets and their initial water budget to extensive migration events of the giant planets at the very beginning of the life of the Solar System. Understanding how and where giant planets form and when and why they migrate is therefore the key to unveiling what set of conditions and processes resulted in the Earth and us.

#### **7. Why the transit method? [as opposed to direct imaging]**

In parallel with transit studies, in the next decade, direct imaging is expected to provide insight into hot, young planets at large separations from their parent stars, i.e. gaseous planets newly formed in the outer regions of their planetary disc and not (yet?) migrated in. The first spectra of hot, young super-Jupiters at large separation from their host stars, were observed in the past years (e.g. [Bonney et al., 2013](#); [Konopacky et al., 2013](#)). Spectroscopy in the wavelength range of YJHK-band has started with dedicated instruments on VLT (SPHERE), Gemini (GPI), Subaru (SCEXAO). The comparison of the chemical composition of these young gaseous objects (e.g. [Zurlo et al., 2016](#); [Macintosh et al., 2015](#)) to the composition of their migrated siblings probed through transit, will be of great help to understand the role played by migration and by extreme irradiation on gaseous planets.

Scientifically, the advantage of transiting planets is that the planetary size and the mass are known. Direct imaging observations suffer from the lack of knowledge of the planetary radius and often the mass. When the mass and the radius are not known, model estimates need to be invoked, increasing the source of degeneracy. Observationally, the transit and eclipse spectroscopy methods allow us to measure atmospheric signals from the planet at levels of at least 10<sup>-4</sup> relative to the star. No angular resolution is needed, as the signals from the star and from the planet are differentiated using knowledge of the planetary ephemerides.

Finally, a space mission for direct imaging would be technically far more challenging than a transit one and certainly far more expensive: the telescope must be much higher performance and cannot be a light bucket as is sufficient for ARIEL. In the longer term though, such a mission would open up the spectroscopic exploration of planets at larger separation from the stars, a domain that is impracticable with transits. NASA WFIRST will include a spectrograph with a resolution of 70 in the range 400-1000nm. A coronagraph is under study to allow to operate at a contrast of 1 part per billion and an inner working angle of 0.2 arcsec. It is expected to characterise over a dozen of the known radial velocity planets and to detect at least a dozen new planets with direct imaging.

#### **8. Isn't stellar activity a critical hurdle for exoplanet spectroscopy?**

Not if we can monitor VIS and IR wavelength simultaneously. See §3.2.2 for further discussion.

### **9. Can clouds prevent the detection of molecules? What if all planets are cloudy?**

Clouds modify the albedo, contribute to the greenhouse effect, and sequester the chemical species which condense out. Clouds therefore have a critical impact on the atmospheric energy budget and compositional balance. If present, clouds will be revealed by ARIEL through transit and eclipse spectroscopy and photometry. Clouds show, in fact, distinctive spectroscopic signatures depending on their particle size, shape and distribution (see Figure 2-21). Current observations in the VIS and NIR with Hubble and MOST have suggested their presence in some of the atmospheres analysed (e.g. [Kreidberg et al., 2014](#); [Knutson et al., 2014](#); [Sing et al., 2016](#)). We do not know, though, how they are spatially distributed and whether they are a transient phenomenon or not. Further observations over a broad spectral window and through time are needed to start answering these questions (see e.g. most recent work done for brown dwarfs by [Apai et al., 2013](#)). This is an additional reason to justify a dedicated mission, as repeated observations through time and phase-curves for a large number of planets can be done only through a dedicated telescope from space.

Additionally, ARIEL Tier 1 mode is particularly useful for discriminating between planets that are likely to have clear atmospheres, versus those that are so cloudy that no molecular absorption features are visible in transmission. This preliminary information will therefore allow us to take an informed decision about whether to continue the spectral characterization of the planet at higher spectral resolution, and therefore include or not the planet in the Tier 2 sample.

### **10. Why are ESA and Europe well positioned to build the ARIEL mission?**

Europe has invested serious resources to be at the forefront of exoplanet detection (RV & transit surveys from the ground, Corot, Cheops and PLATO). The next obvious step to be taken in the exoplanet roadmap, is a dedicated mission for IR spectroscopy of the planets detected through the space and ground facilities (see ESA EPRAT report). If selected, ARIEL will continue to keep Europe at the forefront of exoplanetary science.

Our proposal will build upon the leading role of the scientists and institutes who are part of this consortium in building PI instruments for ESA's previous very successful IR and sub-millimetre astronomical missions: the LWS for the Infrared Space Observatory (ISO), SPIRE for the Herschel Space Observatory, MIRI for the forthcoming JWST and the Planck thermal system, as well as Solar System space instruments on Venus Express, Mars Express, JUICE, Cassini, Rosetta etc.

ARIEL will provide a large number of spectra to be analysed and interpreted. Many teams in our consortium, are building the necessary model infrastructure to interpret exoplanet spectra, predict atmospheric dynamics, chemistry, formation and structure of the interior – e.g. ERC-funded programs: *E3ARTHS* and *WHIPLASH* (chemistry & dynamics of exoplanetary atmospheres); *MoltenEarths* (interior of super-Earths); *ExoLights* (data analysis & retrieval of exoplanet spectra); *SPECULOOS* (discovery & characterization of habitable planets around very cool stars), *AEROSOL*; *ExoMol* and ANR-funded *e-PYTHEAS* (molecular database for exoplanets) –. Therefore, we are in an excellent position to lead the characterisation of the variety of exoplanets observed by ARIEL.

### **11. What is the ARIEL data policy?**

It is recognized that ARIEL data and science will be of interest to a large community of 'external' exoplanetary scientists, and there is a strong wish to embrace them. The intention is to provide publically available high quality data products in a timely manner and to have a continuous dialogue with the wider community, optimising the mission planning and target list and hence ultimately maximising the science that can be achieved by ARIEL.

During the science demonstration phase the data will be released as soon (1 month TBC) as practical after observing, and a public workshop will be organized in connection to the data (levels 1 and 2) release. Datasets up to and including level 2 products for Tier 1 targets will be released quarterly with the objective to achieve this 1 month after the end of each calendar quarter. Datasets up to and including level 2 products for Tier 2 and Tier 3 targets will be released similarly, after each semester where the required signal-to-noise (SNR) and spectral resolution for a particular target requiring multiple observations has been achieved.

# 4 Payload

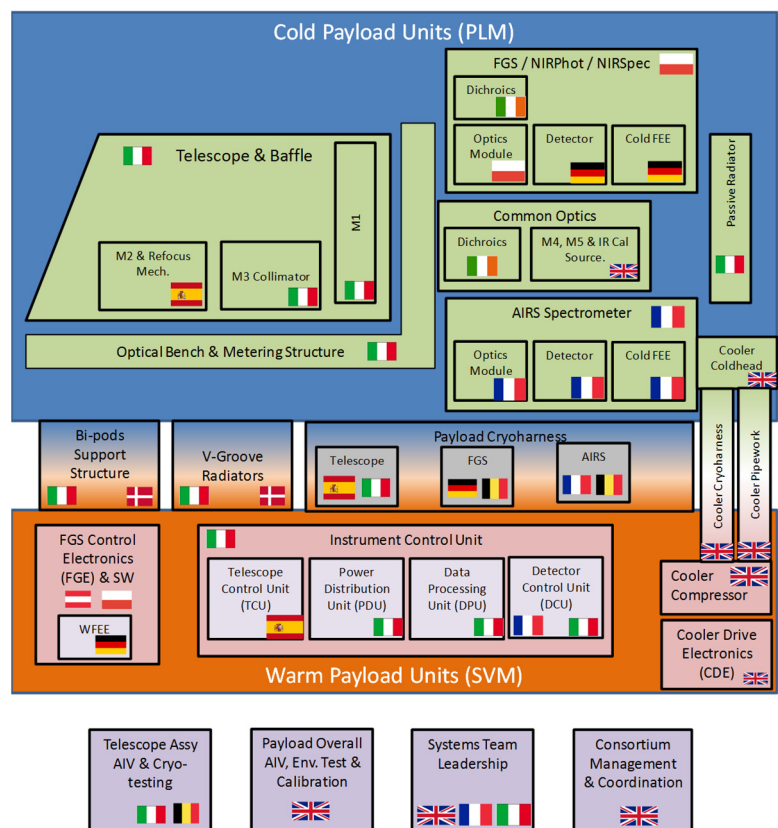
The payload for ARIEL consists of a 1m-class telescope feeding three low and medium resolution spectrometer channels covering the wavelengths from 1.2 to 7.8 microns, and a three photometric channels (two of which also acts as a Fine Guidance Sensor) with bands between 0.5 and 1.2 microns. The entire payload is provided by a consortium of European countries as an integrated and verified unit in order to maximise the stability and optimise the performance of the system.

## 4.1 Payload Architecture

The baseline architecture for the ARIEL payload is illustrated in Figure 4-1 below. This diagram also shows the nationalities of the members of the payload consortium who are taking responsibility for each element.

The baseline architecture splits the payload into two major sections, the cold payload module (PLM) and the items of the payload that mount within the spacecraft service module (SVM). The major items are:

- Cold PLM:
  - Telescope system, incorporating M1, M2 & M3 mirrors, a re-focusing mechanism on the M2 mirror (M2M), the telescope structure and baffles.
  - An optical bench / metering structure onto which the telescope and instruments are mounted.
  - A set of common optics including fold mirrors, dichroics, formatting optics, and a common calibration source.
  - The ARIEL IR Spectrometer (AIRS) instrument.
  - The Fine Guidance Sensor / Visible Photometer / Near-IR Spectrometer (FGS / VISPhot / NIRSpec) instrument.
  - Thermal hardware including: active cooler coldhead, passive radiator for cooling of FGS detectors and all cFEE & the V-grooves and support structure to isolate the PLM from the warmer SVM.
- Warm SVM mounted units:
  - Instrument Control Unit (ICU) housing the AIRS detector control unit (DCU), the central data processing unit (DPU), a power supply unit (PSU) and the telescope control unit (TCU).
  - FGS Control Unit (FCU) electronics incorporating the FGS / VISPhot / NIRSpec wFEE and the processing electronics and SW for determining the pointing from the FGS data.
  - Active cooler system consisting of the Cooler Drive Electronics (CDE), the Cooler Compressors and the Cooler gas handling panel.
  - The cryoharnesses that connect the warm SVM units to the PLM with good electrical properties and low thermal conductance.



Extensive details of the design of the ARIEL payload are contained in Eccleston et al., 2017.

Figure 4-1: ARIEL Payload architecture and responsibilities

## 4.2 Payload Module Structural Design and Analysis

The main mechanical units composing the PLM are the V-Grooves, the bipods and supporting struts, the Telescope Assembly (optical bench, mirrors, struts and baffle) and the Instrument Enclosure (AIRS & FGS optical modules, common optics, radiator). The overall PLM mechanical design is shown in Figure 4-3.

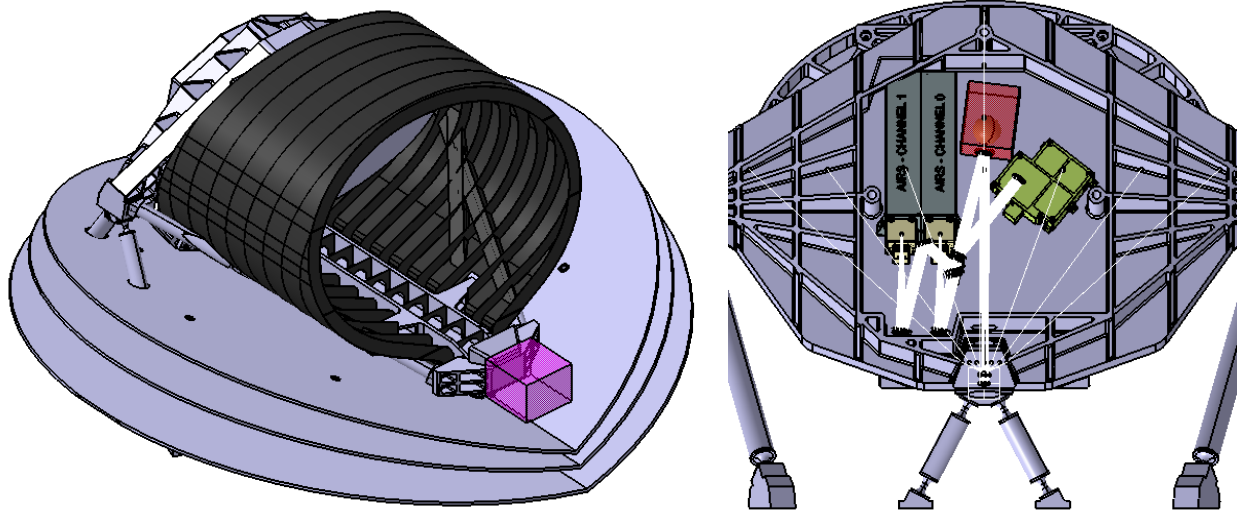


Figure 4-3: ARIEL PLM mechanical design

### 4.2.1 Common Optical Bench Design

The Optical Bench (Figure 4-3, right) is a key mechanical component as it forms the main structure of the PLM: the telescope M1 is mounted to its front surface and telescope support beam projects from its bottom edge forward to support the M2 near the front bi-pod. On the other side the Instrument enclosure has been incorporated into the bench design, increasing the bench thickness and thus stiffening the structure. The design of this platform, and the units mounted on it, will be as isothermal as possible except for the components that need thermal decoupling. The bench, the telescope mirrors, the modules and the common optics supports are to be manufactured predominantly with the same aluminium alloy in order to minimize possible optical effects that occur during thermo-elastic contraction.

### 4.2.2 Support Bi-pods Design and Sizing

The PLM is supported by three bipods mounted onto the PLM/SVM interface panel as shown in Figure 4-3. Bipods preliminary thermo-mechanical configuration is based on the Planck design. They are hollow cylinders, made of GFRP (a trade-off with CFRP and other materials will be conducted in phase B), a low conductive material with good structural properties. To prevent radiative transfer up the inside of the struts and to increase their mechanical stiffness the inner volume of the cylinders is filled with low thermally conductive rigid foam.

The final shape and dimensions of the bi-pods and flexures have been defined via the telescope sub-system study and have been confirmed to be adequate by the system level structural model (first mode analysis shown in Figure 4-2, full details in [Hunt et al., 2017](#)).

### 4.2.3 V-Groove Radiation Shields

The V-Grooves (VGs) are high efficiency, passive radiant coolers, providing the first stage of the PLM cooling system. The Planck mission has demonstrated their efficiency as passive cooling systems. Parasitic

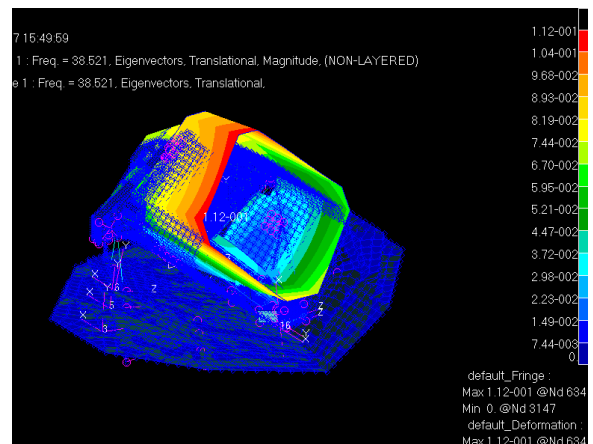


Figure 4-2: PLM first mode (38.5 Hz) shape showing compliance to Ariane 6-2 requirements. This is a lateral mode, the PLM as a rigid body moving predominantly in the plane of the primary mirror and parallel to the SVM interface plane.

heat from warmer SVM is intercepted by the VGs and radiated to space after multiple reflections between the adjacent shields. To achieve this, VGs surfaces have a very low emittance coating; only the upper surface of the last VG (VG3), exposed to the sky, is coated with a high emissivity to maximize the radiative coupling, and so heat rejection, to deep space. The VG's are a simple honeycomb structure of Aluminium alloy, thermally attached to the three bipods and are separately mechanically supported by eight GFRP struts.

### 4.3 Payload Module Thermal Design and Analysis

#### 4.3.1 Thermal Architecture

The spacecraft thermal design (Figure 4-4) is based on a cold Payload Module (PLM) sitting on the top of a warm Service Module (SVM). The mission thermal control is accomplished by a combination of passive and active cooling systems. The SVM is thermally controlled in the 270K-290K range for nominal operations of all the S/C subsystem units. The function of the thermal system of the PLM is to shield the scientific instrumentation from the environment and the S/C and to provide the required cooling and thermal stability.

Passive cooling is achieved by a high efficiency thermal shielding system (the V-Grooves) based on a multiple radiators configuration that, in the L2 environment, can provide stable temperature stages down to the 50 – 60 K range as demonstrated on Planck. At 1.5 million km from the Earth in the anti-Sun direction, the L2 orbit allows to maintain the same spacecraft attitude relative to the Sun-Earth system, while scanning the whole sky during the mission duration. By limiting the allowed Solar Aspect Angle (SAA) range to  $\pm 5^\circ$  around the S/C X-axis and to  $\pm 25^\circ$  around the Y-axis, ARIEL will operate in a very stable thermal environment, always preventing the Sun/Earth/Moon illumination of the coldest section of the PLM.

There will be active cooling provided for the AIRS detectors using a Neon JT cooler – see section 4.4. All of the detectors will be located on dedicated isolated thermal control stages to enable active control and stabilisation of their temperatures to accuracies of  $\pm 50\text{mK}$ .

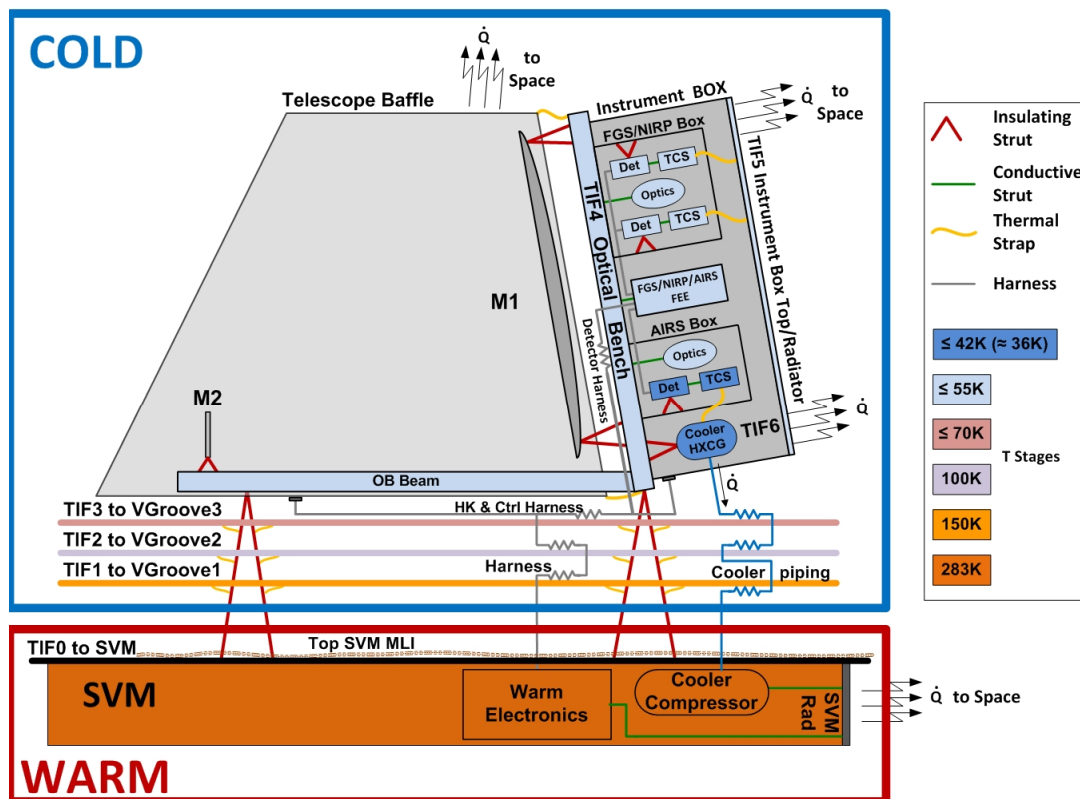


Figure 4-4: PLM Thermal Architecture Scheme

#### 4.3.2 Thermal Analysis Results and Margin Analysis

Figure 4-6 shows the solved steady-state temperatures of the cold and hot cases for the nominal conditions, with the S/C orbiting at the Earth-Sun L2 point. The cold and hot cases assume different fixed boundary

temperatures and attitudes. The temperatures of all passively and actively cooled units are fully compliant to the requirements including margins. The mirror temperatures in the hot case are shown in Figure 4-5 demonstrating minimal thermal gradients (hence minimal thermo-elastic deformation of the mirror surface). Full details are contained in [Morgante et al., 2017](#).

### 4.3.3 Transient Thermal Analyses

In order to size the active control systems on the thermal control stages and to inform the performance stability modelling, transient analyses have been carried out where the SVM interface temperature is changed by 10K (the maximum allowable fluctuation) and the effect on the temperatures on the PLM is modelled. The results show (without stabilisation) maximum temperature changes of the detectors of 9mK over a 10-hour observation period, with the M1 mirror temperature changing by only 2mK. These compare to required temperature stabilities of  $\pm 50\text{mK}$  for the detectors (in order to have stable dark current and gain) and  $\pm 1\text{K}$  for the telescope mirrors (in order to have stable background) which are derived from the photometric stability requirements.

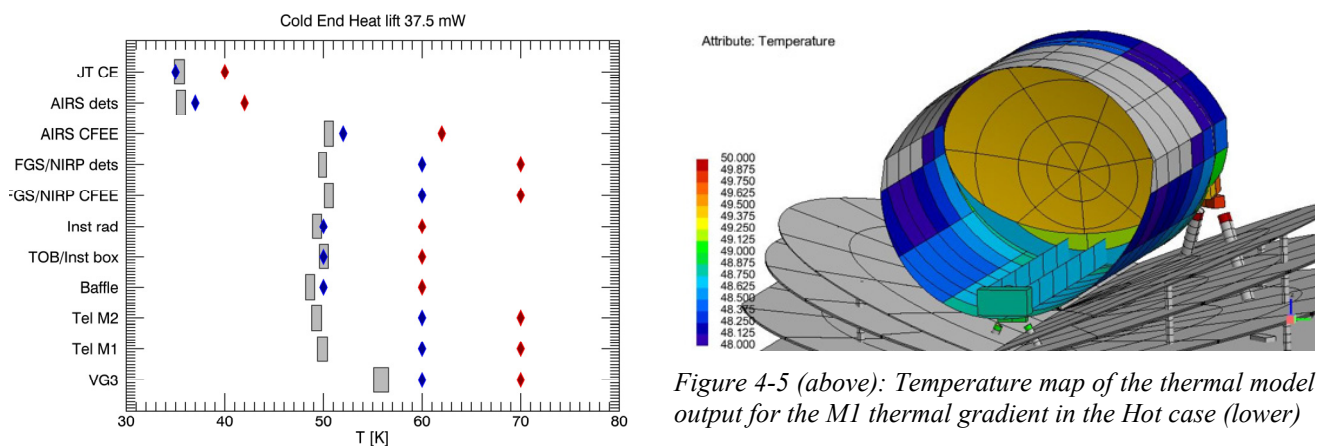


Figure 4-5 (above): Temperature map of the thermal model output for the M1 thermal gradient in the Hot case (lower)

Figure 4-6 (above left): Thermal model results compared to requirements and margins for each key system component. The red diamonds show the raw maximum temperature requirements, the blue diamonds show the temperature requirements including margin which is required by ESA to be held in a phase A on each temperature requirement, the grey bars show the temperature range given as output of the thermal model (the delta between the hot and cold cases).

## 4.4 The ARIEL Active Cooler System

The baseline active cooling system for ARIEL is a closed cycle Joule-Thomson (JT) system with Neon as the working fluid. It is based on the successful 4K-JT cooler for the Planck spacecraft and draws from developments for the 2K cooler for the Athena mission. Key to success is the high reliability and lifetime of the cooler mechanisms, which stems from the philosophy of non-lubricated, non-contacting moving parts, enabled by a flexure bearing suspension system operating in the infinite fatigue strength regime; there have been no failures of the compressors of this design of cooler with over 111.5 years operation in space on 24 different cooler system as of May 2016 ([Ross, R., 2016](#)).

The baseline JT cooler system comprises two reciprocating linear motor compression stages, based on the RAL 2K-JT cooler mechanism (shown in Figure 4-7, lower left), to perform an expansion of the gas across a JT orifice to produce the cooling. Neon is selected as the working fluid because its boiling point (27.05K at 1atm) is well matched to the temperature requirements for ARIEL. Although oversized for this application, they offer significant margin on cooling power, whilst still satisfying the available mass and power budgets for ARIEL, and give maximum flexibility in future phases. The baseline performance predictions and mass and power resource needs are summarised in Figure 4-7, upper left for operation at 28K.

The system makes use of the V-Groove radiators as pre-cooling stages. Counter-flow heat exchangers are also implemented to utilise the cold return gas in order to minimise the loads on the radiators. An ancillary panel carries gas handling and measuring equipment as well as filters and a reactive getter to ensure cleanliness. The cooler is controlled by a set of drive electronics which provide the electrical input power for the compressors, perform all controlling functions such as active vibration cancellation and return the cooler housekeeping data.

ARIEL two-stage Ne JT cooler performance estimates (@ 28K)	
Parameter	Baseline Est.
cooling power at 28K	50 mW
heat rejected at 180K	100 mW
heat rejected at 70K	300 mW
total input power	61 W

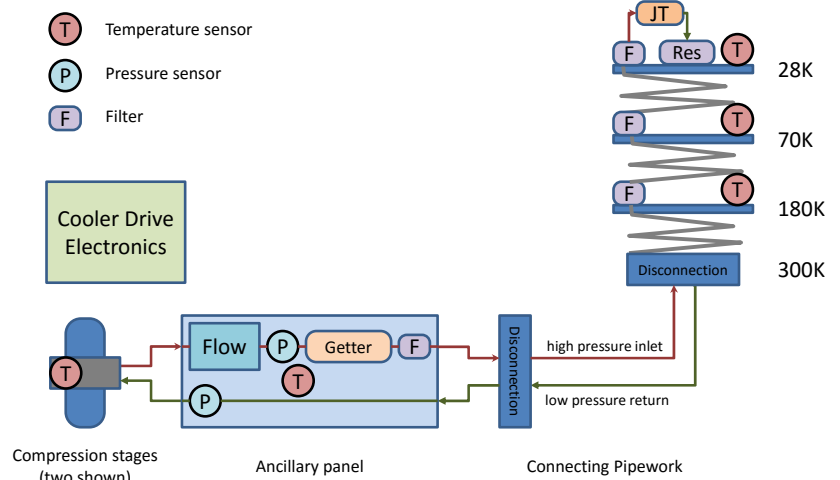


Figure 4-7: (Upper left) Cooler system parameter sizing; (Lower left) 2K cooler motor mechanism (mass is 820g); (Right) JT Cooler Schematic.

## 4.5 The ARIEL Telescope Design

### 4.5.1 Optical Design

The telescope is a Cassegrain design (parabolic primary M1 and hyperbolic secondary M2) with a third parabolic mirror M3 used to recollimate the beam. A fourth flat mirror M4 directs the collimated beam onto the optical bench. The telescope optical design is described in more detail in Middleton et al. (2017). Figure 4-8 shows the telescope optical layout also including the first common optics mirror, M5.

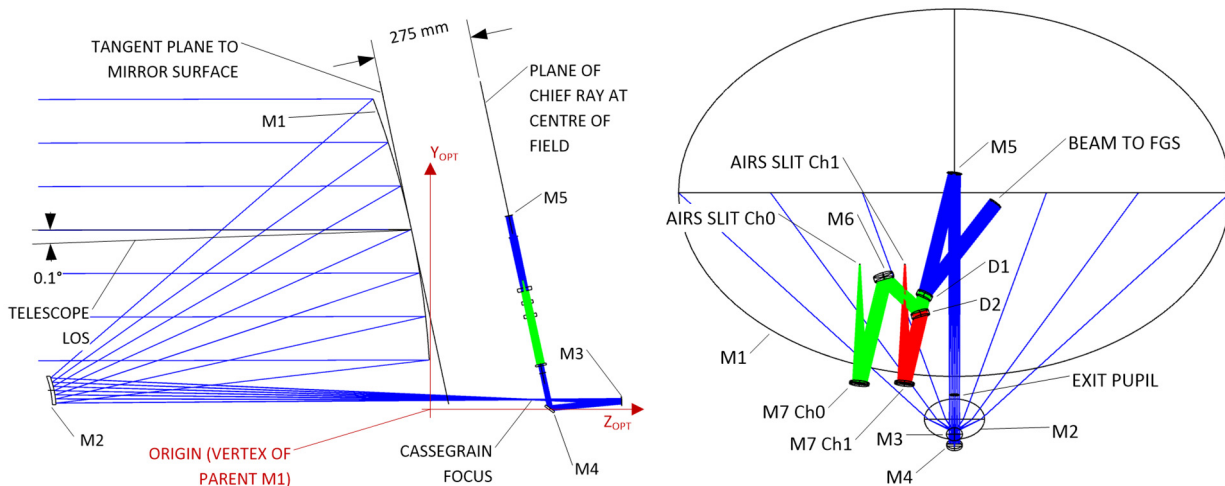


Figure 4-8: Scale drawings of the telescope and common optics. (Left): view in  $Y_{OPT}$ - $Z_{OPT}$  plane. The  $0.1^\circ$  offset is exaggerated for clarity. (Right) view in  $X_{OPT}$ - $Y_{OPT}$  plane.

The aperture stop, located at the primary mirror M1, defines the elliptical entrance pupil, of size 1100 mm x 730 mm. The entrance baffle, a cylinder extending the length of the optical bench, limits M1's view of the sky. In combination with placing the stop at the first optical surface (M1), this provides the first line of defence to block out-of-field light. An additional baffle is positioned over the 'top' of M2 (as viewed in Figure 4-8 left) to block any direct view of the sky from M2 past the end of the entrance baffle. The Cassegrain focus after M2 provides the possibility of inserting a field stop to aid stray-light rejection. After the Cassegrain focus, the beam is recollimated by M3. The baseline design results in a recollimated beam of size 20 mm x 13.3 mm, which is directed onto mirror M4, used to direct the beam onto the optical bench. The telescope is required to be diffraction limited at 3  $\mu$ m, which equates to an rms Wave Front Error (WFE)

of about 200 nm. This is expected to be dominated by M1 surface error as shown in the WFE budget developed in phase A and contained in Eccleston et al., 2017.

M2 has a refocus mechanism with three degrees of freedom as a baseline (focus and tip/tilt). The purpose is to correct for one-off movements due to launch loads and cool-down and potentially to make occasional adjustments (for example to compensate for any long term drifts in structural stability). The optimum setting is determined by ground analysis of FGS image vignettes and AIRS spectral data during commissioning.

The first line of defence for stray-light control is the cylindrical baffle at M1, which limits M1’s view of the sky. There is a Cassegrain focus after M2 and this allows a field stop to be included in the system. The field stop also serves to block any unwanted views that downstream mirrors may have of either M1 or M2. There is an accessible image of the aperture stop in the collimated space after M4 and this allows the placement of Lyot stop at this location. A slit will be included at the entrance to the AIRS spectrometer, forming a further field stop to limit stray light particularly from field stars. There is also an additional field stop at the intermediate focus of the FGS telescope to limit straylight impact in this instrument.

### 4.5.2 Preliminary Mechanical & Thermal Design and Modelling

A detailed trade-off of the material to be used for the telescope mirrors and structures has been carried out during the assessment phase. This trade is documented in detail in Da Deppo et al., 2017. The conclusion is that for the consortium provision of the telescope the optimum solution is a telescope with mirror and structures made from Aluminium 6061 T651 alloy.

The ARIEL Telescope is composed by three mirrors: M1 is elliptical with major axis 1.1m x 0.73m and M2 and M3 of smaller diameter (respectively about 110 mm and 30 mm), there is also a 30 mm diameter plane mirror (M4) for folding the beam exiting M3. All mirrors are made of Al6061, an alloy that, together with optical quality specifications, ensures a very good thermal uniformity. M1 is supported directly from the Optical Bench via a 9-point whiffletree structure that connects to the optical bench by 3 triangular mountings. The telescope mechanical configuration is shown in Figure 4-10.

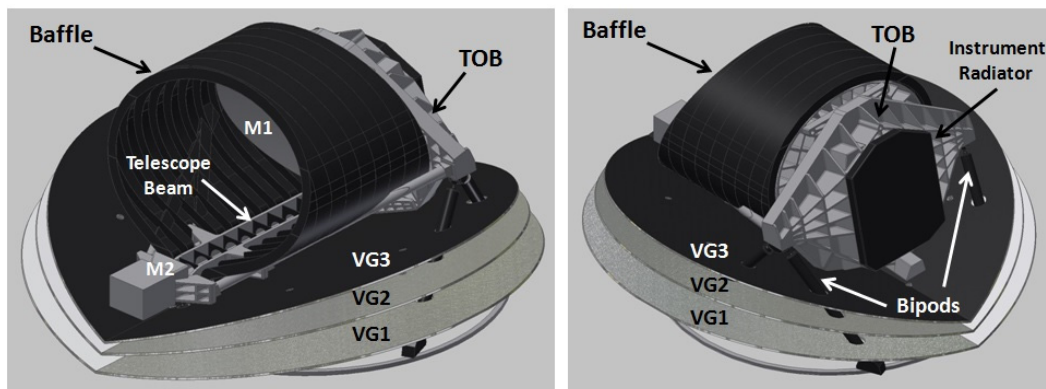


Figure 4-10: ARIEL telescope mechanical configuration.

The design has undergone mechanical and thermo-elastic analysis to assess strength & stiffness and the ability of the design to maintain optical alignment of the telescope throughout the operational temperature ranges. An example output of the thermo-elastic analysis is shown in Figure 4-9, with the detailed analysis being used as input to the overall WFE budget for the optical system. The WFE budget in Eccleston et al., 2017 demonstrates that under conservative modelling assumptions for the thermo-elastic deformations, the telescope assembly will deliver the required optical quality.

### 4.5.3 Pathfinder Telescope Mirror

The viability of Aluminium as the baseline material

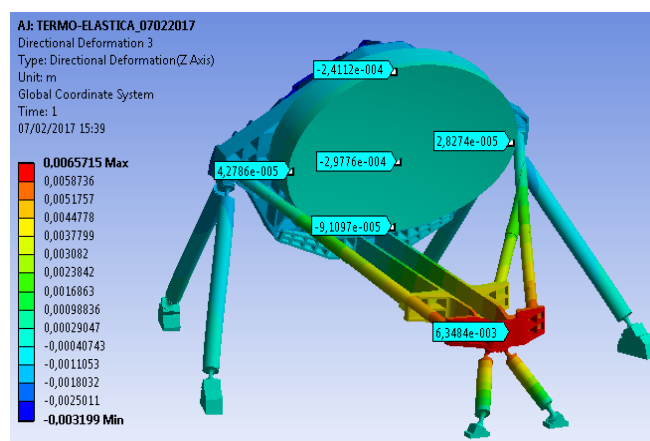


Figure 4-9: Directional deformation -  $Z_{A\_TEL}$  axis from the thermo-elastic deformation in the hot operational case

for the telescope mirrors has been assessed during the phase A by producing a Pathfinder Telescope Mirror (PTM) from the baseline material. The PTM mirror after milling and diamond turning is shown in Figure 4-11. Figure 4-12 shows the surface error on the diamond turned surface with respect to the theoretical surface. In addition to the work on the main PTM mirror, trials have been undertaken during phase A to demonstrate the surface roughness that is achievable on the Al6061-T651 and to develop the polishing processes foreseen. The final roughness polishing was also trialled, demonstrating the capability to achieve a surface roughness below 10 nm rms as shown in Figure 4-12.

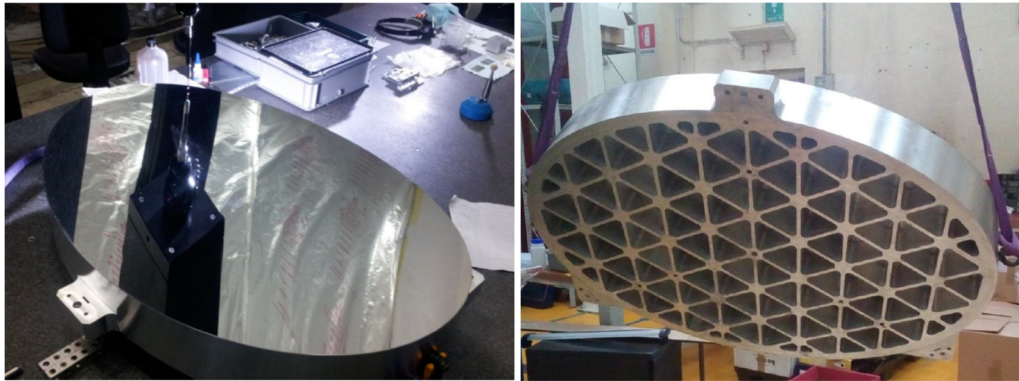


Figure 4-11: PTM mirror after milling and diamond turning processes completed including undergoing CMM measurement of surface form (left)

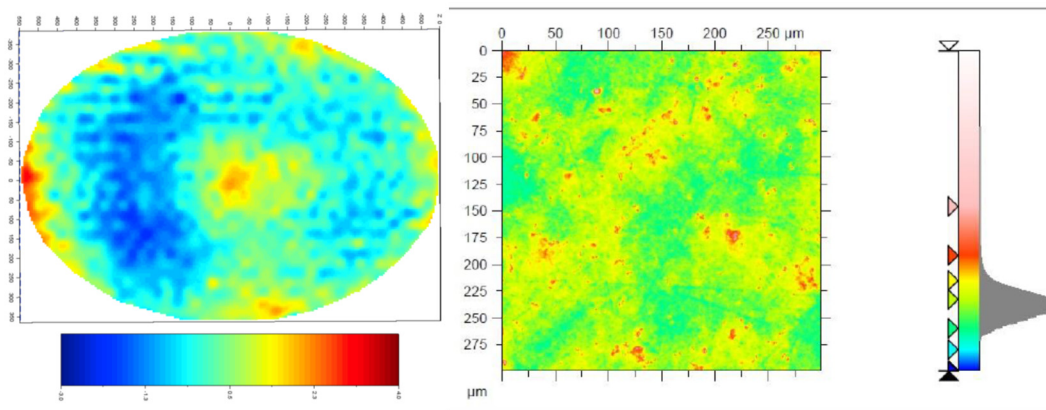


Figure 4-12: (Left) Deviation from theoretical surface of the PTM after diamond turning (large scale astigmatism removed as this can be corrected in iterative diamond turning process) showing 0.8  $\mu\text{m}$  rms shape accuracy with 5.3  $\mu\text{m}$  P-V. (Right) Surface roughness measurements polishing run on 150mm diameter Al6061-T651 sample, results shown for a 300 x 300 microns region demonstrating 9.1 nm rms roughness.

### 4.5.4 M2 Mirror (M2M) Mechanism

The mechanism which is necessary to ensure that the telescope is in best focus and meets it’s WFE requirements when in operations is located on the M2 mirror. This mechanism builds on the heritage from other similar M2 mechanisms which has been developed at Sener, ES. Specifically, it builds on the design heritage from the Gaia and Euclid M2 mechanisms.

During the phase A study an initial assessment of the possible requirements on the M2 mechanism has been made. In phase B1 there is a development plan in place to review the requirements and conduct the necessary delta-qualification for components in order to demonstrate TRL 6 by mission adoption.

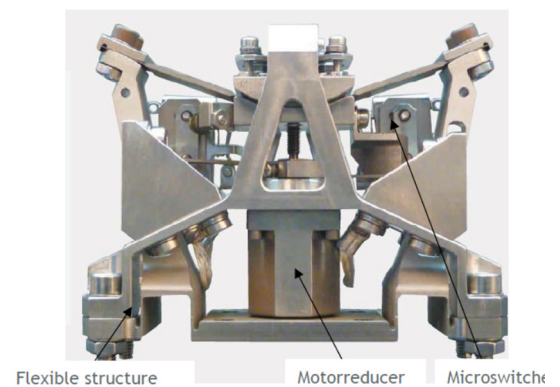


Figure 4-13: Actuator used in Gaia and Euclid M2M which would be re-used for ARIEL M2M

## 4.6 Common Optics, Dichroics and In-Flight Calibration Unit

The function of the common optics is to split light into three channels (FGS; AIRS Ch0 and AIRS Ch1); deliver the collimated beam to the FGS; deliver focussed beams, of the correct f/number, at the AIRS input slits; and to provide an input position for the in-flight calibration system. The common optics positions can be seen in Figure 4-8.

The splitting of the channels by wavelength is done by dichroic mirrors. Details of the dichroic designs obtained from vendors are given in [Ray et al., 2017](#) and used in calculation of the overall throughput performance as shown in §4.11.3.

An on-board calibration unit (OBCU) is placed in the common optics. When the calibrator is operated, it provides a uniform illumination sources on all focal planes. This will be used during commissioning and calibration to monitor variations in QE, as an alternative to diffuse astronomical sources, and to transfer over time the calibration obtained on the ground. During science operation, the focal plane flat field calibration can be monitored in a similar way if necessary.

The OBCU makes use of a thermal source and 4 light emitting diodes (LED) feeding a 40mm diameter integrating sphere with its output port behind M5. Light is injected through a 1 mm diameter hole in the M5 mirror, which in the collimated beam results in less than 0.4% loss of throughput. A thermal source emitting a graybody spectrum is used for the spectroscopic channels. JWST-MIRI and NIRSpec use tungsten filament sources for the same purposes in a temperature range from 500 K (on JWST MIRI ([Wright et al, 2015](#))) to 1600 K (JWST NIRSpec ([Bagnasco et al., 2007](#))).

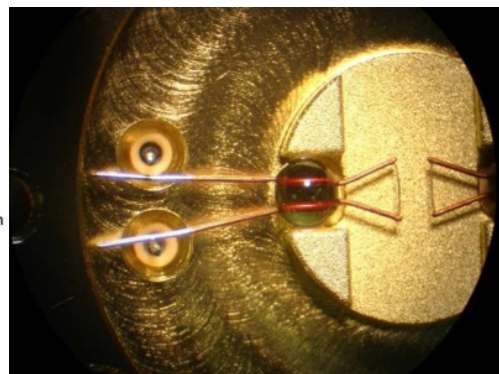
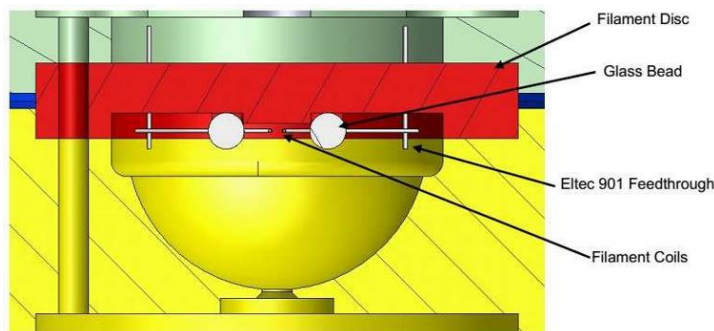


Figure 4-14: The two filaments are shown at the centre of the assembly. The glass beads which achieve mechanical bonding of the filaments are also visible. A microscope picture of the filaments is shown on the right.

## 4.7 The ARIEL InfraRed Spectrometer (AIRS) Design

### 4.7.1 Functional Design and Architecture

AIRS is the ARIEL scientific instrument providing spectroscopy in 2-IR channels (called Channel 0, CH0, for the [1.95-3.90]  $\mu\text{m}$  band and Channel 1, CH1, for the [3.90-7.80]  $\mu\text{m}$  band). It is located at the intermediate focal plane of the telescope and common optical system. AIRS instrument is composed of three main architectural blocks.

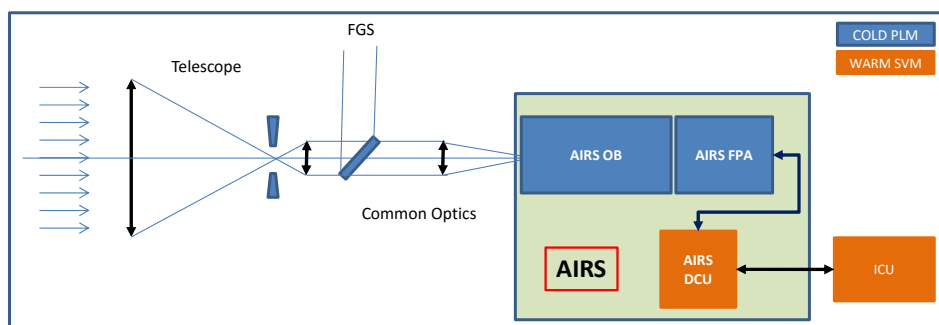


Figure 4-15: Architectural block diagram of the ARIEL Infra-Red Spectrometer.

- The **AIRS Optical Bench** is the main structural element of the AIRS, providing the mechanical and thermal interfaces to the optical bench, structural support of the optical elements, interfaces to the focal plane assemblies and provides light-tightness and baffling to limit straylight.
- The **AIRS Focal Plane assemblies** of Channel CH0 and Channel CH1 are composed of a thermal-mechanical structure interfacing with the AIRS-OB and containing the detector Sensor Chip Assembly for each channel and its Cold Front end electronics with the associated harness.
- The **AIRS Detector Control Unit (AIRS-DCU)** is a Warm Front End Electronics unit located on the warm part of the SVM, which interfaces internally to the FPA CFEE and the detector in order to control the detection process, and externally to the ICU to transfer the Science Data Packet.

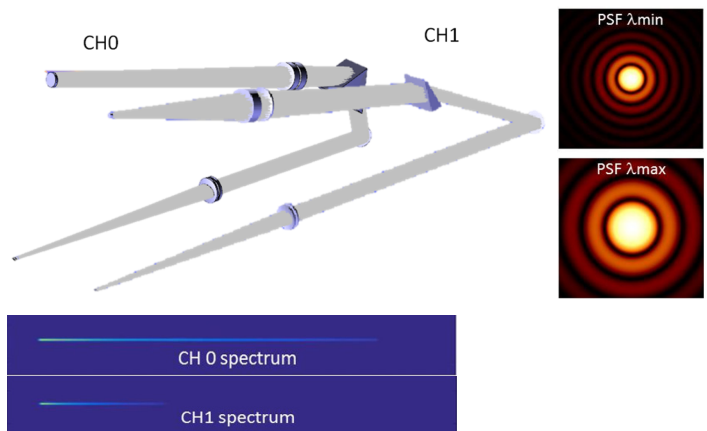


Figure 4-16: Detailed optimized folded Zemax implementation of Channel 0 and Channel 1 spectrometer. The windows on the detector needed for the spectra are 270 x 64 pixels in Ch0 and 100 x 64 pixels in Ch1 where the spatial direct size is set by the need to monitor the background and dark current of the detector. The PSFs are shown for Ch0 for a region of 18 x 18 pixels.

AIRS-OB and AIRS-FPA 1 & 2 are located on the cold section of the PLM, while the AIRS-DCU is located in the warm part of the SVM.

### 4.7.2 Optical Design

Following a detailed trade-off analysis a prism system was selected as the baseline design for AIRS. The main advantage of this design is to limit the dilution of Flux by circularizing the PSF of the elliptical telescope making best use of prism anamorphosis. The implementation is made at operational temperature of 55 K and the indexes of refraction are defined at this temperature. The selected material for the prisms is CaF<sub>2</sub>, which has heritage from previous IR space missions.

The detailed Zemax model introduces doublets systems for the Camera (CaF<sub>2</sub>/Sapphire) and the Collimator (CaF<sub>2</sub>/ZnSe) in order to control the chromatic aberrations. With this correction the system is diffraction limited over the useful wavelength ranges. A fold mirror is inserted on the optical path following between the collimator and the prism in order to allow having both channel entrance planes and exit plane (detector plane) collocated and to optimize the location of the exit focal plane above the entrance slit. This solution improves the volume implementation of the overall instrument.

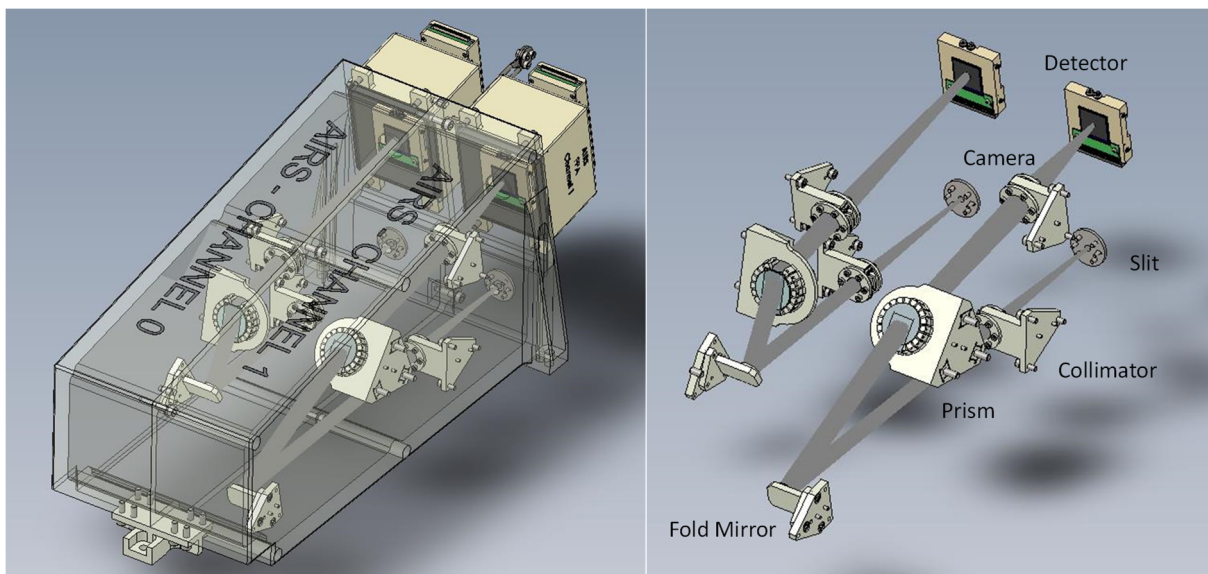


Figure 4-17: Implementation of AIRS optical design into the allocated volume. The size of the AIRS OB volume is 482 x 206 x 184 mm; the optical interface is at the two input slits 40mm above the mounting plane and separated by 90mm.

### 4.7.3 Mechanical and Thermal Design

The approach for the mechanical design at that stage is to have two independent spectrometer half-boxes, each containing one channel, that are ultimately assembled together. The folding of the two channels in the volume is described in Figure 4-17. The AIRS Optical unit has a predicted mass of 9.62 kg (including contingency). The thermal interfaces are through the mounting plane for the passively cooled optical bench and optics, and on the rear of the detector modules for the attachment by thermal straps to the Cooler Coldhead heat exchanger which cools the two actively cooled detectors.

### 4.7.4 Detector and Signal Chain System

The AIRS detection chain is defined as the functional sub-assembly of the AIRS that is necessary to detect the AIRS spectrometer images and to pre-process scientific data to fit with the telemetry allocation. The AIRS detection chain electrical system encompasses the detector array assemblies, the Cold Front End Electronics (CFEE) and the Detector Control Unit (DCU) which is the warm front end electronics.

#### 4.7.4.1 Baseline Detectors: Teledyne HIRG

The 2 AIRS Focal Plane Assemblies (FPA) are thermal mechanical boxes containing for each channel:

- Sensor Chip Assembly (SCA) with the detector and associated Read Out Integrated Circuit, and the thermal control (2 temperature probes + 2 heaters per SCA). The SCA is thermally decoupled from the mechanical structure and regulated through a thermal control at 42 K $\pm$ 0.05K.
- Cold Front End Electronics (CFEE), linked to the Detector ROIC with a dedicated harness, and conductively cooled to 55 K through the AIRS-Optical Bench.

The baseline detector for CH1 is Teledyne Imaging Sensors (TIS) HIRG with 10.5 $\mu$ m cut-off developed in the frame of the NEOCam program. [McMurty et al., 2013](#) provides a detailed summary of this devices performance. Currently tested devices for CH1 have a cut-off wavelength between 9.3 and 10.6  $\mu$ m. When operated at a temperature of 42K (Figure 4-19) the device has an operability of 94%, with a dark current of 16 e/s for 90% of detectors pixels. The Quantum Efficiency without AR coating is measured in excess of 60%. The baseline CH0 detector is a standard HIRG product with cut-off at 5.3  $\mu$ m.

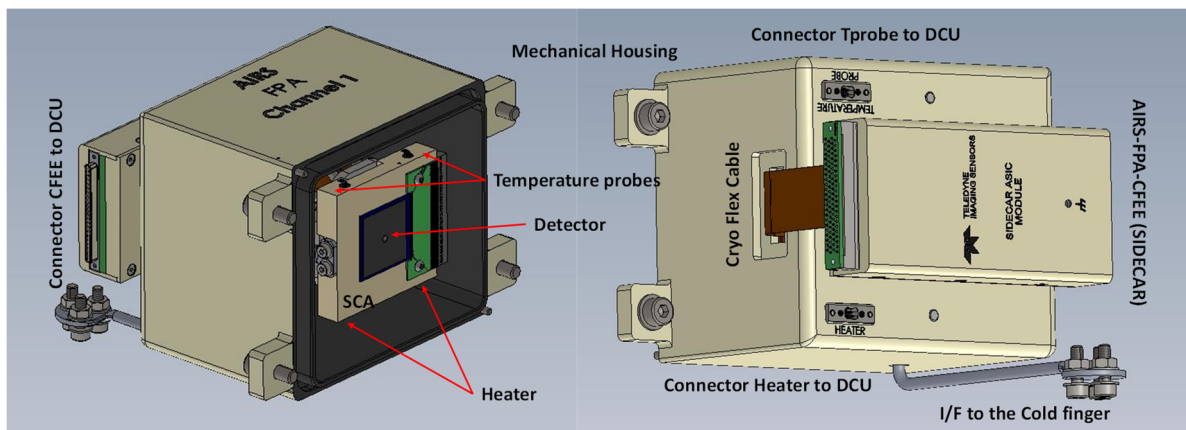


Figure 4-18: Design of the AIRS Focal Plane Assembly with the detailed units (one FPA per channel).

The baseline device technology readiness is estimated to be at level 9 for Chanel 0 and 6 for Channel 1, while the control-electronics SIDE CAR ASIC and ROIC being at TRL 9, as these are effectively the same technology used on NIRSpec on JWST and on Euclid. For ARIEL, the cut-off wavelength of the photosensitive layer can be adapted by modifying the stoichiometry of the Hg<sub>1-x</sub>Cd<sub>x</sub>Te Cadmium X proportion during the epitaxy layer growth.

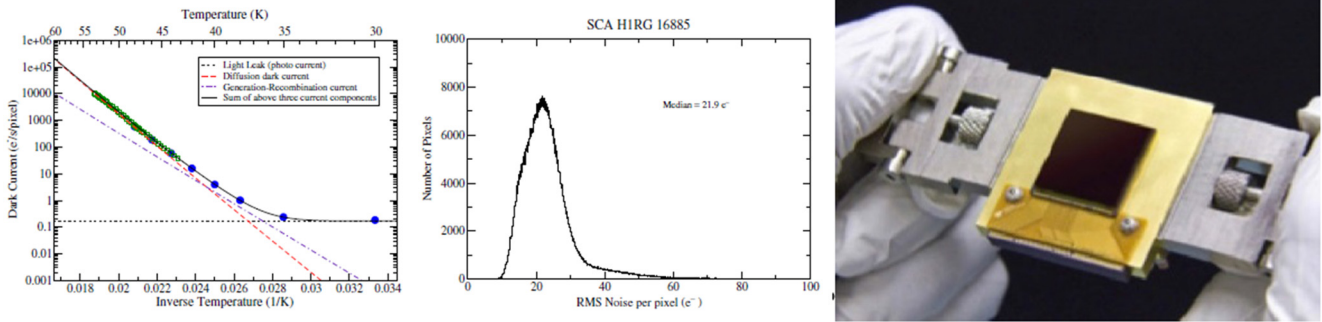


Figure 4-19: Dark current (left), Readout noise (Fowler-1) (central) for Teledyne MCT detector selected for ARIEL baseline (from McMurty et al., 2013). Device is presented on the right panel.

4.7.4.2 Option European detector developments

There are specific efforts underway within Europe (CEA / LETI under CNES funding) to develop a detector (640x512 or 320x256, 15um pixels) with cut-off at 8.2um @45K, with both source follower per unit cell (SFD) and Charge Trans Impedance Amplifier (CTIA) based Read-Out Integrated Circuits (ROIC) aimed at meeting the requirements for ARIEL IR Spectrograph within Europe. The objective of the study is to demonstrate maturity and performance of such a detector in terms of Quantum efficiency, Read out noise and low dark current with n/p technology.

First result (shown in Figure 4-20) indicate that the technology would have a dark current dominated by diffusion regime down to operational temperature, allowing these detectors to meet the dark current requirements of ARIEL.

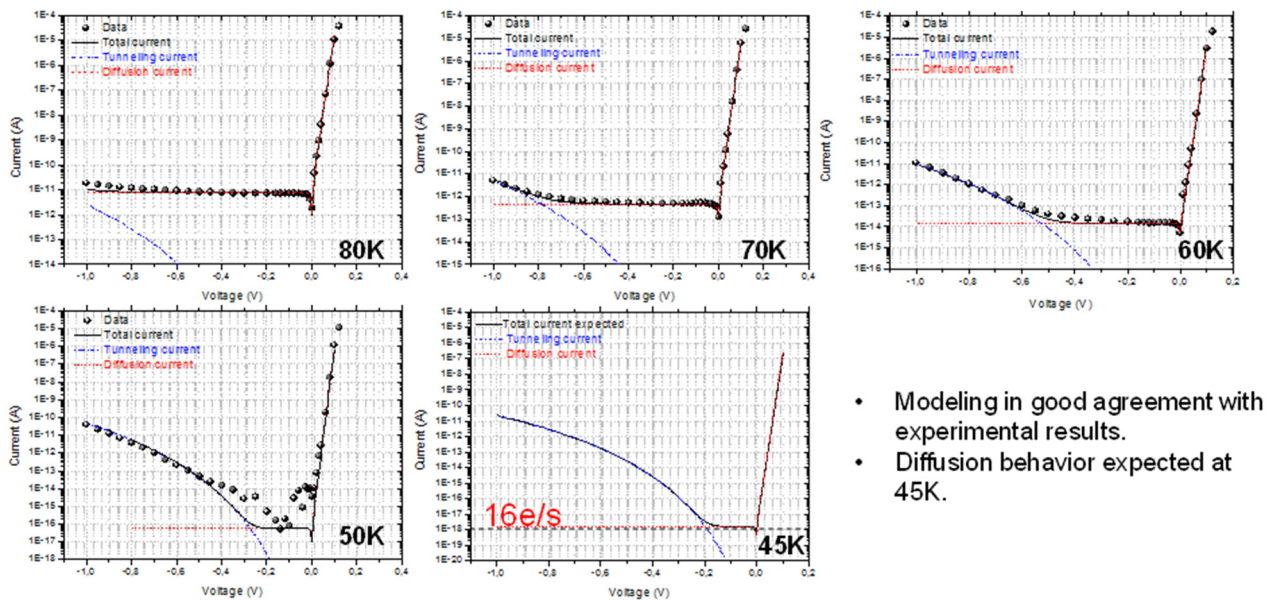


Figure 4-20: Dark current on CEA-LETI 8.2 μm cut-off n/p diodes measured by Tip Auto tests at wafer level indicating that diffusion is the main contributor to dark current at operating temperature over a 200 mV polarization plateau.

4.7.4.3 Cold and Warm Detector Electronics

The main functions of the cold front-end electronics (CFEE) are data digitalization, control signals, biasing, commands and housekeeping. In case of a European detector for AIRS then a coupled CFEE will be required. Developments of prototype CFEE ASIC modules have been performed in 2012-2014 in, Norway, Belgium and the Netherlands. The next stage of development of such an ASIC module should start soon under the frame of an ESA TRP ITT.

## 4.8 Instrument Control Unit

### 4.8.1 Architecture & Functionality

The ARIEL ICU (for more details refer to [Focardi et al., 2017](#)) implements the commanding and control of the AIRS Spectrometer and is interfaced on one side with the instrument and on the other side with the S/C SVM Data Management System (DMS) and Power Conditioning and Distribution Unit (PCDU). The baseline ICU architecture includes 5 (active or switched-on at the same time) units as shown in Figure 4-21:

- 1 PSU - Power Supply Unit (nominal and redundant boards)
- 1 DPU - Data Processing Unit (nominal and redundant boards)
- 2 DCU - Detector Control Unit (only nominal boards)
- 1 TCU - Telescope Control Unit (nominal and redundant boards)

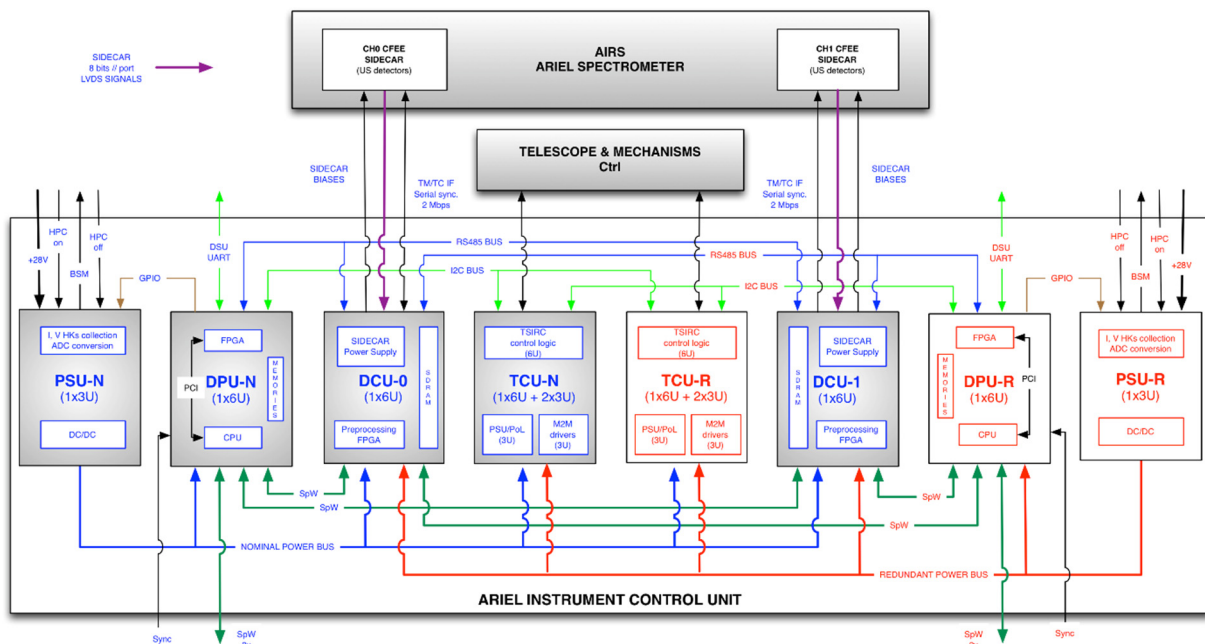


Figure 4-21: ARIEL ICU baseline solution block diagram and electrical I/F

It is desirable to minimise the level of on-board data processing taking place – the more processing is possible to be done on the ground gives the maximum flexibility in the algorithms and the chance to improve the processing during the mission to allow the science team the optimum chance to extract the best SNR from the available data. The baseline design has the capability to implement all the potentially necessary processing such as flat-fielding, ramp fitting, glitch detection etc, with flexibility to select the algorithm.

### 4.8.2 Telescope Control Unit

The Telescope Control Unit acts as an ICU slave subsystem and accomplishes the following tasks: drives the M2 refocusing mechanism, drives the on board calibration lamps, monitors the thermal state of the PLM elements, controls temperature of the detectors and the M1 mirror.

The Telescope Control Unit (housed with the ICU) will be composed of three separated boards (N&R). As seen in Figure 4-22, a 6U PCB (TSIRC) will hosts the PLM thermal monitoring and control HW,

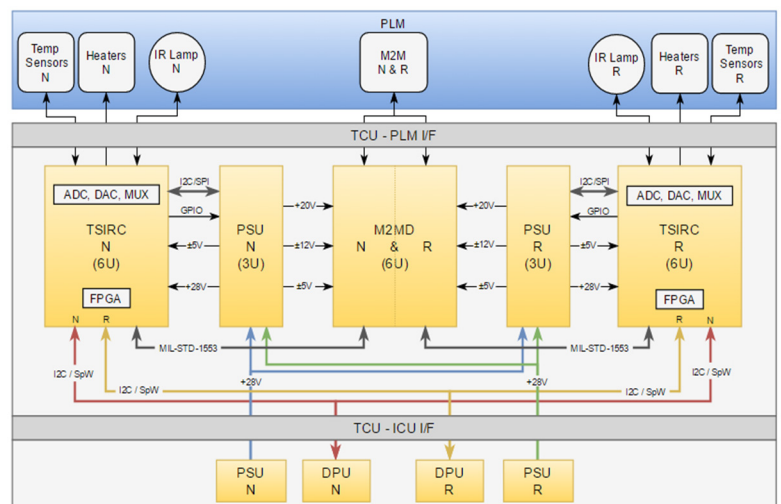


Figure 4-22: TCU block diagram and electrical I/F

the IR calibration lamp driver and their multiplexing stages. For the driver electronics of M2 mechanism, it is foreseen an upgraded version of Euclid's M2M, with the same driver, which will require a separated 6U board for both nominal and redundant systems.

## 4.9 The Fine Guidance System (FGS), Visible Photometer (VISPho) and Near-IR Spectrometer (NIRSpec) Design

### 4.9.1 Functional Design and Architecture

The Fine Guidance System (FGS) main task is to ensure the centering, focusing and guiding of the satellite, but it will also provide high precision astrometry and photometry of the target in the visible and additionally a low resolution near-IR spectrometer. The term “FGS instrument” will be used to refer to this combined functionality of both guidance and science channels. The FGS function uses star light coming through the optical path of the telescope to determine the changes in the line of sight of the ARIEL payload. The attitude measurement is then fused with the rate information from the star tracker, and used as input for the control loop stabilizing the spacecraft through the high performance gyros.

To meet the goals for guiding and science, four spectral bands are defined: FGS-1 (0.8-1.0  $\mu\text{m}$ ), FGS-2 (1.0-1.2  $\mu\text{m}$ ), VISPho (0.50-0.55  $\mu\text{m}$ ) and NIRSpec (1.25-1.95  $\mu\text{m}$  spectrometer with  $R>10$ ). The two FGS channels (FGS-1 and FGS-2) deliver redundant guiding information to the S/C by providing the centroid position of the target star at 10 Hz. Data from FGS-1 and FGS-2 will also be used for photometric analysis. The spectral bands are selected using a series of dichroic mirrors as shown in Figure 4-23 (left).

### 4.9.2 Optical Design and Performance

The FGS optical module interfaces to the collimated beam fed by the telescope and common optics. It then includes an off-axis Gregorian mirror telescope before inputting to the dichroics system to divide the field of field into the four separate channels. Figure 4-23 (right) presents the baseline optical design solution.

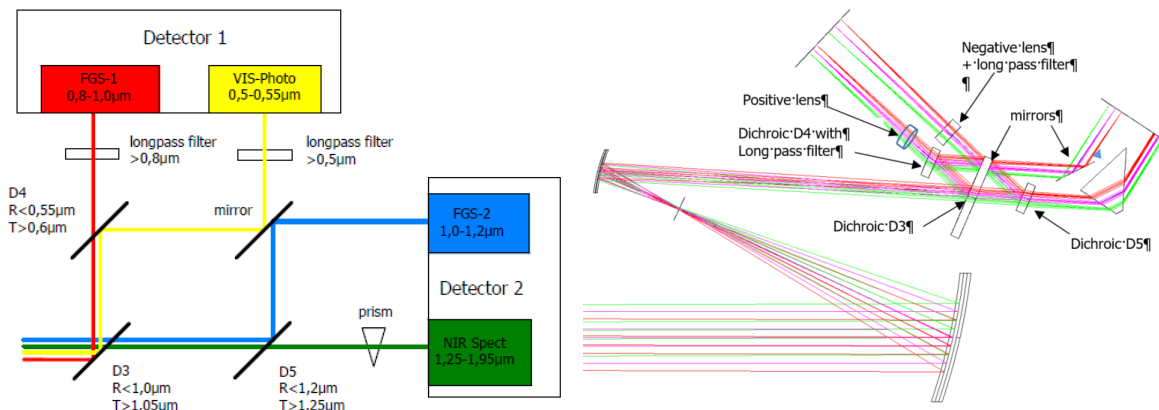


Figure 4-23: Left: Dichroic schematic showing how channels are split. Right: Baseline optical layout for FGS.

To obtain a final prediction of the optical performance of the FGS the two sources of aberration have to be taken into account: the optical system of the FGS and (substantially more influential) the main ARIEL Telescope assembly. The Telescope Assembly WFE was implemented in the Zemax model using Zernike polynomials based on the scaling up of the STREGO primary mirror WFE (a 235mm Aluminium mirror produced by the same provider as intended for the ARIEL M1) to match the allowable WFE for the ARIEL M1; the details of this analysis are presented in [Pascale et al., 2017](#). Results of the optical analysis are presented below with the PSFs as seen on a 6 x 6 pixel region of the detector for three wavelengths 0.55  $\mu\text{m}$  (VISPho), 1.0  $\mu\text{m}$  (FGS-1 / FGS-2 boundary) and 1.95  $\mu\text{m}$  (NIRSpec longest wavelength). As can be seen from these plots, the PSF remains coherent in all cases and will allow centroiding of the position of the star (see the central plot for the wavelength of FGS-1/2). These simulations are then used in the evaluation of the pointing system performance shown in section 4.9.6.

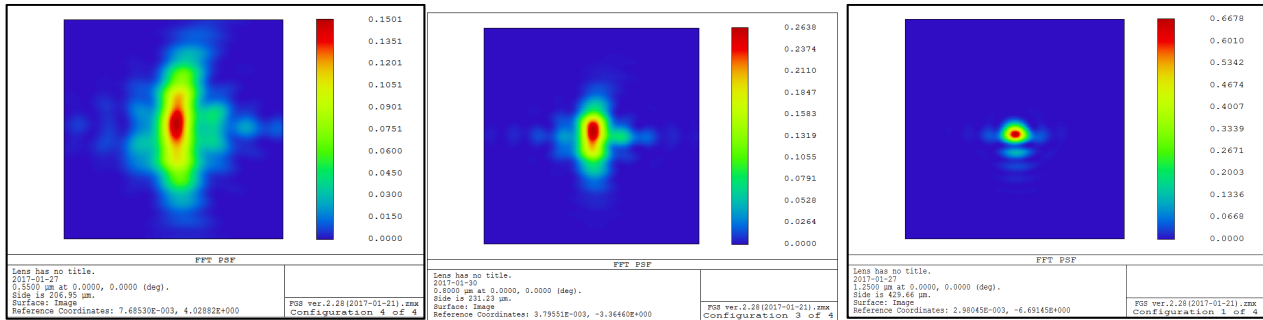


Figure 4-24: PSF plots for a 6x6 pixel region for the end-to-end optical performance of VISPhot (right) at  $\lambda=0.55 \mu\text{m}$ , FGS-1/2 (centre) at  $\lambda=1.0 \mu\text{m}$  and NIRSpec (right) at  $\lambda=1.95 \mu\text{m}$  including telescope assembly WFE

### 4.9.3 Mechanical Design

Based on the optical design, mechanical dimensions of the dichroic beam splitters, the telescope mirrors and the MCT detector with accompanying electronics, the design of the FGS cold unit is shown in Figure 4-25.

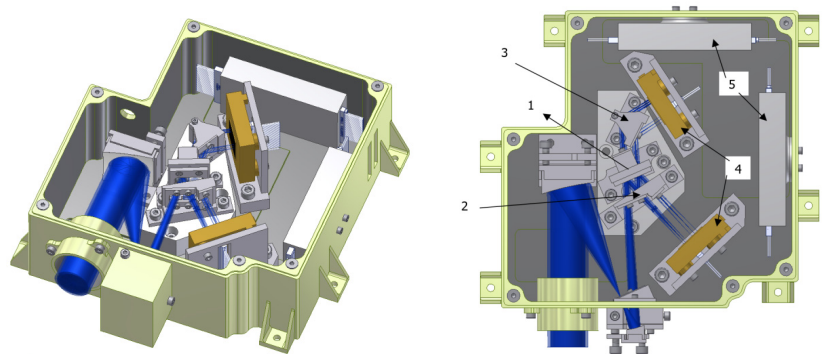


Figure 4-25: FGS Optical Module mechanical design. Labels on the right image are: 1 – Plate containing dichroic D3 and two mirrors; 2 – Holder for D4 and optical path compensation lens; 3 – Holder for fold mirror and NIRSpec prism; 4 – HIRG detectors; 5 – SIDECAR ASICs in close proximity.

The mirrors of the Gregorian off axis telescope are fixed in mounts which give the possibility to align the optical axis of the FGS telescope to the instrument telescope. The distance between mirrors is adjusted by the mount of the first mirror. At the entrance of the FGS telescope the set of baffles are placed to control straylight at the interface. The three holders of the dichroics are mounted on a single baseplate.

### 4.9.4 Detector System

The baseline detector for the FGS (for both channels) is a HIRG detector from Teledyne. These detectors have demonstrated performance that meets and exceeds the required capabilities in terms of wavelength coverage, QE, read noise, dark current and linear well capacity, while also meeting the necessary engineering constraints in terms of operating temperature, power consumption and packaging. They have high heritage and good performance in this wavelength range (as noted in section 4.7.4.1 and demonstrated in [Crouzet et al., 2015](#)). These detectors would also use the SIDECAR ASIC as the CFEE, with the interface and driving of the cold electronics coming from the FGS Control Unit (FCU).

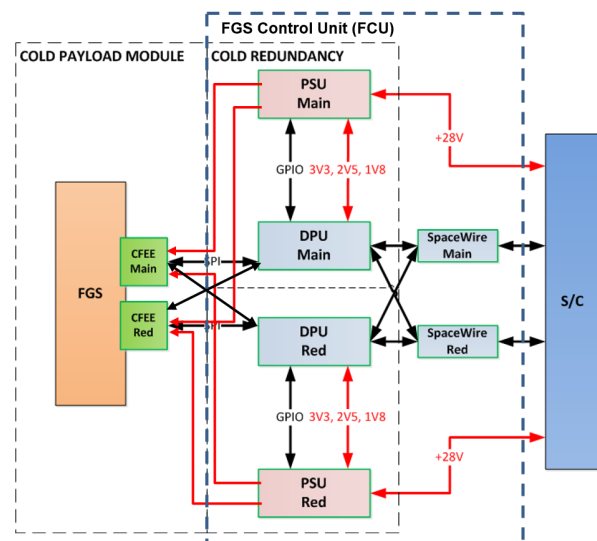


Figure 4-26: Scheme of the FGS control unit

### 4.9.5 FGS Control Unit (FCU)

The FGS has its own control electronics (the FCU) in the SVM to carry out all necessary communication, control and data processing tasks. It will drive and read the FGS detector electronics, establish a control loop with the spacecraft computer and deliver scientific data products from the FGS channels to the S/C mass memory. The FCU will consist of a mechanical chassis holding a number of electronics boards providing

the functions as shown in Figure 4-26. The detector control units will share a common design with those that drive the SIDECAR ASIC for AIRS which are contained in the ICU – see section 4.8.

Based on the heritage designs from Solar Orbiter STIX and the JUICE SWI from which the FCU draws heritage, the mass is estimated to be 5.5kg and the nominal operating power consumption is 12.6 W.

### 4.9.6 Centroiding and Guidance Software

The FGS will have to carry out and support a number of different tasks through its application software. There will be functions to control the FGS subsystems, process the detector data and communicate with the spacecraft. The FGS application software will offer its functionality in the form of service commands and reports. The software includes FDIR functionality and offers several modes of operation to support maintenance and calibration activities.

The main requirement of the FGS is the centroiding performance of 10 milli-arcsec at 10 Hz. For the best support of the operating modes, several centroiding and data extraction algorithms will be implemented, fully configurable by parameter and command. In the warm FGS control electronics the data will be processed in real-time. Output data products are reformatted images, centroid coordinates, dimensions and errors in both axes, photometry, glitch count and housekeeping.

Figure 4-27 presents the results from a centroiding study demonstrating that the precision requirement can be met for the whole range of target brightnesses for ARIEL. A sample of 864 simulated images was used as input for the centroiding algorithm under test.

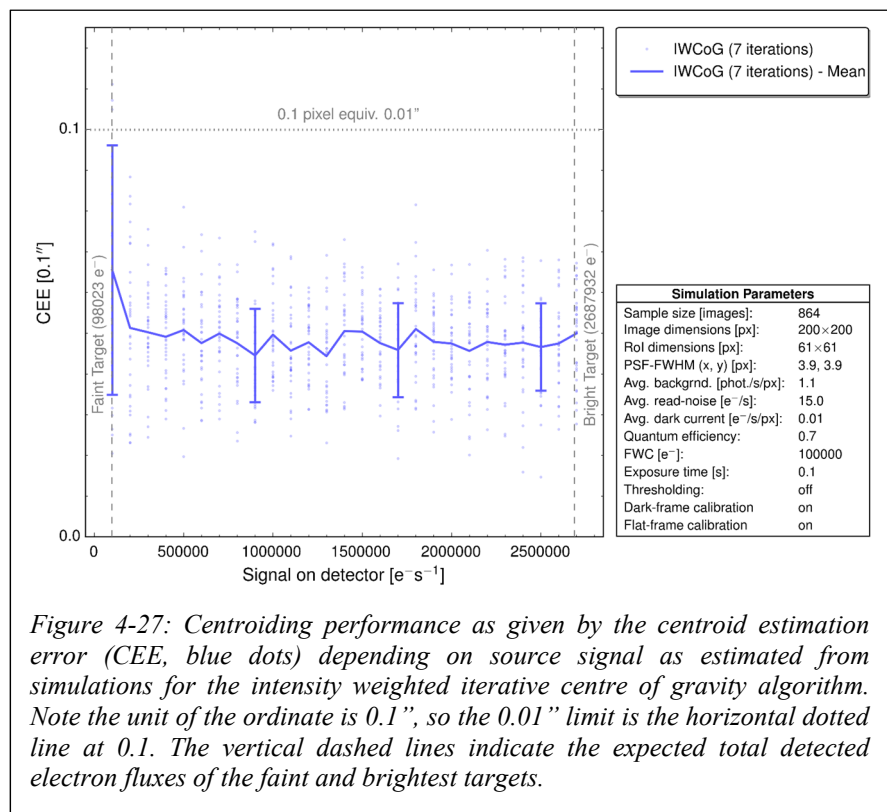


Figure 4-27: Centroiding performance as given by the centroid estimation error (CEE, blue dots) depending on source signal as estimated from simulations for the intensity weighted iterative centre of gravity algorithm. Note the unit of the ordinate is 0.1", so the 0.01" limit is the horizontal dotted line at 0.1. The vertical dashed lines indicate the expected total detected electron fluxes of the faintest and brightest targets.

### 4.10 The Payload Noise Budget and Performance Simulation

Transit spectroscopy and multi-band photometry has been so far conducted using general-purpose, space-based instruments. Some success has been obtained using ground-based instrumentation as well. These measurements however suffer from a high level of systematic error due issues such as pointing jitter, thermal and opto-mechanical stability, wavelength and photometric calibration, and detector stability.

Key aspects which allow ARIEL to obtain its stable performance are:

- 1) Simultaneous observations of the same transit event by all photometric and spectroscopic channels;
- 2) Thermally and photometrically stable conditions due to continuous observation of the transit event.
- 3) Design which is resilient to major sources of systematics or make possible post processing removal.

This is summarised in Table 4-1 below, which lists the most important sources of noise and systematics identified, along with the approach used to mitigate their impact on the observation, and on the overall photometric stability.

We demonstrate how the ARIEL design is capable of achieving its photometric stability requirements using comprehensive time domain simulations. We use the end-to-end ExoSim simulator to comprehensively model the ARIEL performance. The simulator implements a detailed instrument model and generates

photometric and spectroscopic light-curves similar to those ARIEL will provide during science operations. The details of the ARIEL ExoSim tool are provided in [Sarkar et al., 2017](#) & [Papageorgiou et al., 2017](#).

Type of uncertainty	Source	Mitigation Strategy
<b>Detector noise</b>	Dark current noise	Choice of low-noise detectors and optimisation of observing strategy for each target brightness
	Readout noise	
	Gain stability	Calibration, post-processing data analysis, choice of stable detectors.
	Persistence	Post-processing decorrelation. Continuously staring at a target for the whole duration of the observation.
<b>Thermal noise</b>	Emission from telescope, common optics and all optical elements	Negligible due to surface emissivity properties and in-flight temperatures of the payload.
	Temperature fluctuations in time	Negligible impact by design
<b>Astrophysical noise</b>	Photon noise from the target	Fundamental noise limit, choice of aperture size.
	Photon noise arising from local zodiacal light	Negligible over ARIEL band
	Stellar variability with time	Multi-wavelength stellar monitoring, post-processing decorrelation
	Contamination of signal by background sources within slit	Combination of target selection, spatial filtering of resolved PSFs and scheduling as detailed in <a href="#">Nascimbeni et al., 2017</a> .
<b>Pointing jitter</b>	RPE and PDE effects on the position, Spectral Energy Distribution, and detector intra/inter pixel response	Small RPE and PDE, Nyquist sampling, post-processing decorrelation
	Slit losses	Spectrometer input slit sufficiently large to minimise

Table 4-1: Summary of noise sources and systematic errors

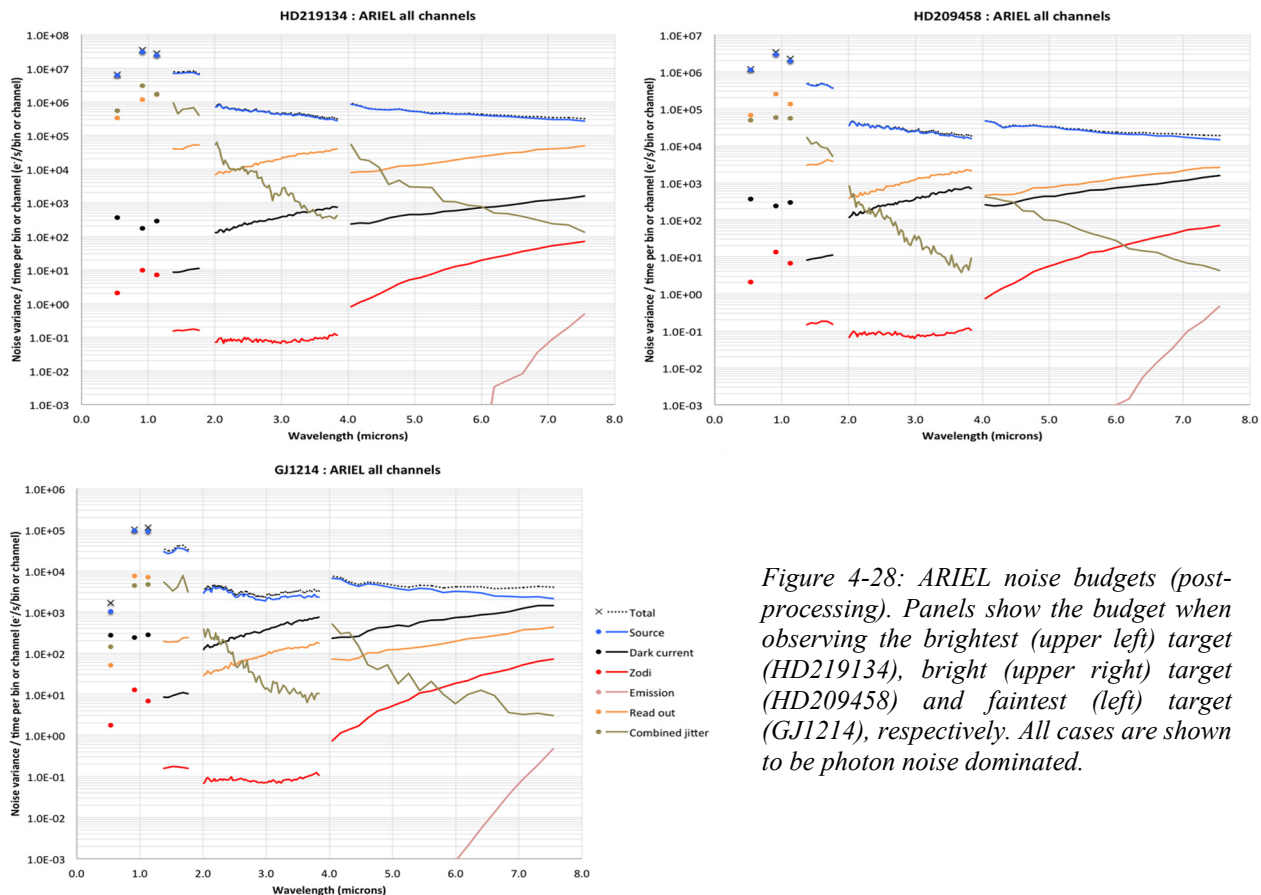


Figure 4-28: ARIEL noise budgets (post-processing). Panels show the budget when observing the brightest (upper left) target (HD219134), bright (upper right) target (HD209458) and faintest (left) target (GJ1214), respectively. All cases are shown to be photon noise dominated.

The overall noise performance is shown in Figure 4-28 which gives the current best estimate of the complete instrument noise performance from ExoSim for the sizing stars identified in the ARIEL Mission Requirements Document (HD219134, HD209458 & GJ1214). All cases are photon noise limited by the target star. The following general observations on the noise performance can be made:

- Pointing jitter is the second most dominant noise component in NIRSpec the blue end AIRS.
- Detector dark currents used are 1, 30 and 50 e/s in VNIR, and AIRS CH0 and CH1, respectively. Their associated Poisson noise is important when observing faint targets (VISPhot and AIRS). It should be noted that the baselined Teledyne detectors have significantly lower dark current than this.
- Detector readout noise variances presented are based on a simple CDS and are the second most important noise component at the red-end of AIRS for bright targets and for some of the photometers. This is an overly pessimistic assumption when observing fainter targets as the detector will be read up-the-ramp with slope fitting. This largely negates readout noise in these cases.

All other noise sources are negligible.

## 4.11 Payload Budgets

### 4.11.1 Power and Data Rate Budgets

The power and data rate budgets for the ARIEL payload are reported in detail in Eccleston et al., 2017. The power budget is shown in Table 4-2 for the science operational mode.

The data rate budget from the payload for all science data and payload housekeeping is estimated to be 25.0 Gbits / day, made up of 5.7 Gbits/day from the FGS, 13.3 Gbits/day from AIRS, 0.2 Gbits/day for housekeeping and a 30% data volume margin.

### 4.11.2 Payload Mass Budget

The PLM mass budget is shown in Table 4-3. Note that further mass optimisation is to be carried out on the telescope structure; further optimisation and investigation into more aggressive light weighting will be carried out in phase B. Mass maturity margin of 20% is applied across the board except for the instrument optical modules where 25% is used in case of further design developments, and the optical bench carries reduced margin (5%) as current design considered highly conservative.

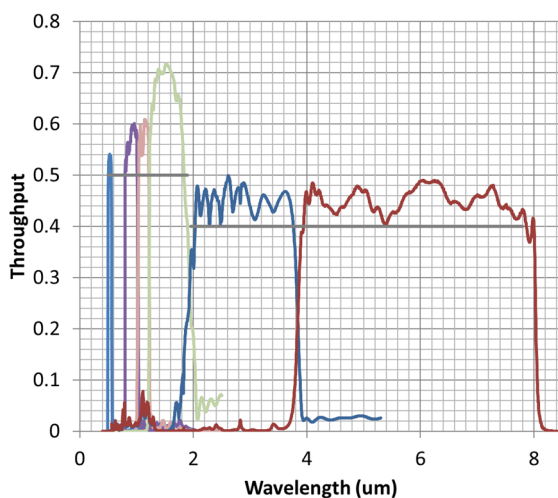


Figure 4-29: End-to-end throughput for the AIRS and FGS channels (each shown in a different colour). The requirement from the MRD is the grey lines.

Item	CBE (W)	Nom. (W)
Instrument Control Unit	35.4	42.5
FGS Control Unit	10.2	12.6
Active Cooler System	61.0	73.2
<b>Total ARIEL Payload</b>	<b>106.9</b>	<b>128.3</b>

Table 4-2: ARIEL Payload Power Budget

Item	CBE Mass (kg)	Nominal Mass (kg)
<b>Telescope Subsystem</b>	<b>263.3</b>	<b>300.0</b>
Optical Bench	106.6	111.9
Telescope Beam	29.2	35.0
Telescope Baffle	12.0	14.4
TA Heaters, Harness	6.0	7.2
M1	85.0	102.0
M1 Supports	16.9	20.2
M2	1.5	1.8
M2 Refocus Mechanism	5.0	6.0
M3	0.2	0.2
M3 Mounting	1.0	1.2
<b>Instrument Subsystems</b>	<b>25.3</b>	<b>30.5</b>
FGS	1.6	2.0
AIRS	7.7	9.3
Common Optics	2.0	2.4
Instrument Radiator	6.0	7.2
JT Cooler Cold Head	1.5	1.8
Payload Cryo Harnesses	6.5	7.8
<b>Thermal Shield Assy</b>	<b>69.3</b>	<b>83.2</b>
PLM Support Struts	16.0	19.2
V-grooves	53.3	64.0
<b>PLM Total:</b>	<b>357.9</b>	<b>413.6</b>
<b>SVM Components</b>		
Instrument Control Unit	10.5	12.7
FGS Electronics	5.5	6.6
Cooler Compressors	8.0	9.6
Cooler Drive Electronics	8.0	9.6
<b>SVM Total:</b>	<b>32.0</b>	<b>38.5</b>
<b>Grand Payload Total:</b>	<b>389.9</b>	<b>452.1</b>

Table 4-3: ARIEL Payload Mass Budget Estimates

### 4.11.3 Throughput Budget

A throughput budget is maintained to inform the performance modelling (§4.10) and confirm compliance requirement. The prediction (Figure 4-29) accounts for all foreseen efficiency losses.

## 5 Mission Design

This Chapter presents the ARIEL mission analysis (section 5.1) and the two S/C designs coming from the parallel industrial studies (sections 5.2 and 5.3), followed by a description of the S/C development plan (section 5.4) and an evaluation of the technology readiness (section 5.5).

Note that the two S/C designs from the industrial contractors include some general design features that are common to both of them. These are explained in the following subsections, but the details specific to each contractor are not elaborated upon.

As a support to the reader throughout this Chapter:

- The spacecraft axes are illustrated in Figure 5-1.
- The main structural elements that comprise the ARIEL spacecraft are illustrated in Figure 5-2.

Both of these figures use the baselined payload Consortium PLM on top of an illustrative SVM based on the ESA internal CDF study performed at the beginning of the Phase A. They are meant as illustrations only and do not reflect the true S/C as designed by the two industrial contractors (see section 5.2 for accurate views of the S/C as designed by industry).

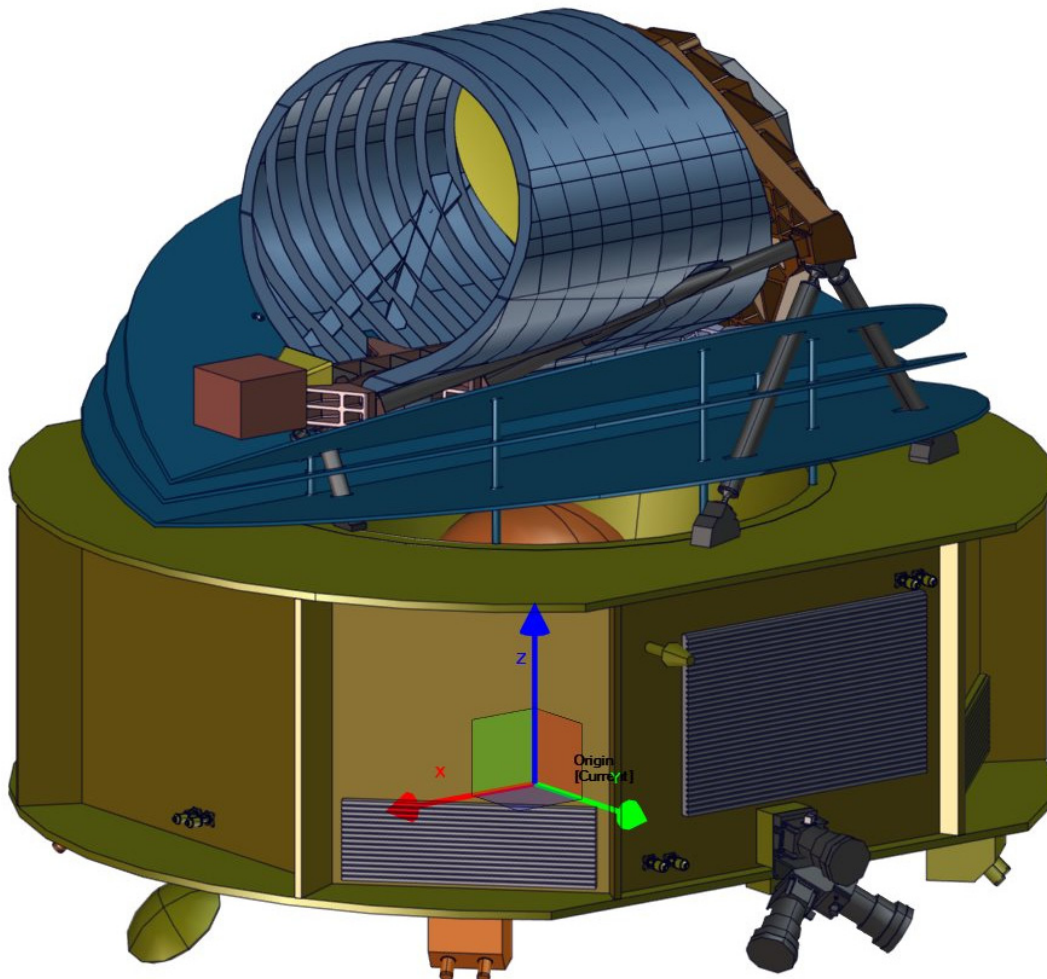


*Figure 5-1: Illustration of the ARIEL S/C and its reference frame. The origin is at the geometrical centre of the separation plane between the LV adapter and the S/C (in the middle of the SVM bottom panel). The  $Z_{\text{ARIEL}}$  axis is coincident with the LV longitudinal axis (perpendicular to the separation plane or SVM bottom panel). The  $(X_{\text{ARIEL}}, Y_{\text{ARIEL}})$  axes define the separation plane.  $X_{\text{ARIEL}}$  is parallel to the telescope pointing axis in this plane.  $Y_{\text{ARIEL}}$  completes the right-handed orthonormal triad. During nominal science operations, the Sun always remains underneath the SVM in the  $-Z_{\text{ARIEL}}$  hemisphere, to ensure the PLM is constantly obscured and can be passively cooled.*

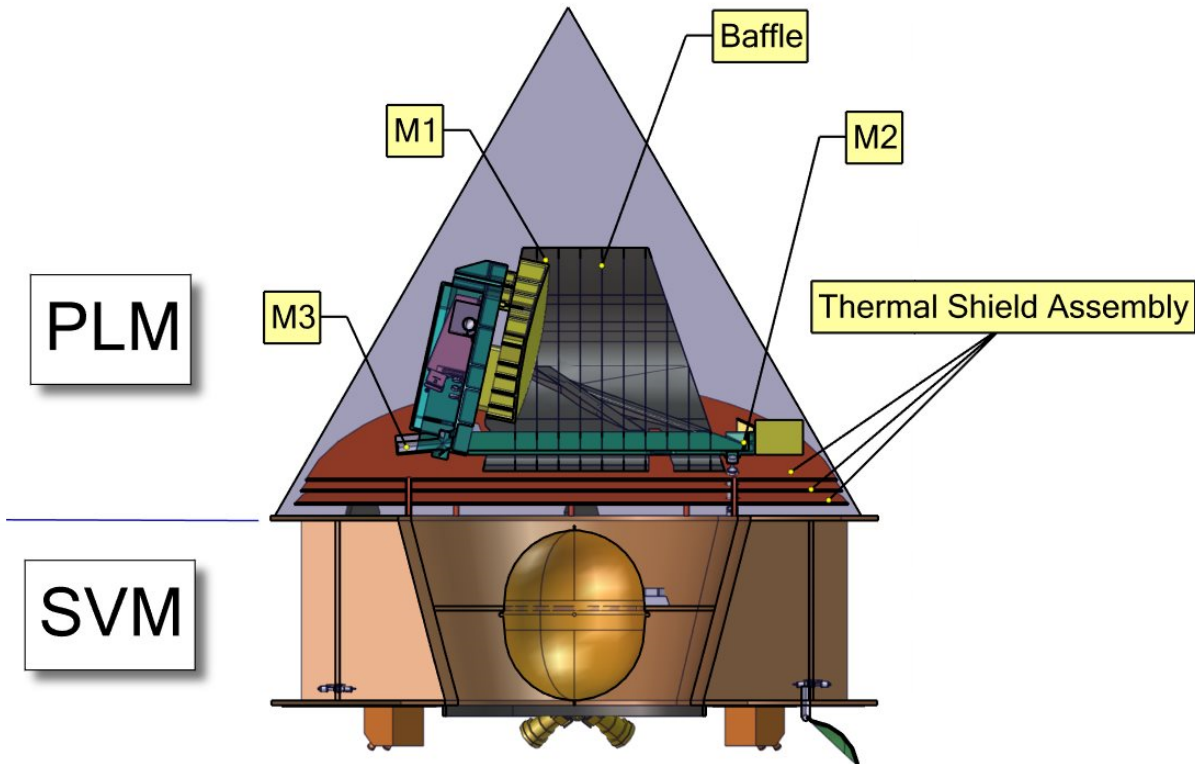


Figure 5-2: Cross-section in the XZ plane of ARIEL showing the main structural elements that compose the S/C and the PLM cut angle of  $\pm 25^\circ$  (with an additional  $\pm 5^\circ$  for margin) around  $Y_{\text{ARIEL}}$ . Combined with the capability to perform a  $360^\circ$  rotation around the  $Z_{\text{ARIEL}}$  axis, this gives access to  $\geq 30\%$  of the sky at any given time (and the full sky in 3 months).

## 5.1 Mission Analysis

The ARIEL nominal science operations orbit is an eclipse-free (Earth and Moon) large amplitude orbit around the Sun-Earth L2 point (see Figure 5-3). This orbit is key to meeting two of the most important science requirements: it offers a very stable thermal environment (constant view to the Sun on one side and to cold space on the other side, and no eclipses), combined with a very large instantaneous field of regard. In addition this orbit also enables a simple design of the communications and power subsystems (stable distances to the Earth and Sun and stable Sun-S/C-Earth angle), along with a benign radiation environment compared to Earth orbits that cross the radiation belts.

The baseline launch strategy consists of an Ariane 62 launch from Kourou (Ariane 64 also possible). Two transfer options to the orbit around L2 are possible:

- A direct injection into the L2 transfer orbit (as Herschel/Planck).
- An injection into a low inclination circular parking Low Earth Orbit (LEO) followed by a final burn (after  $\sim 1$  orbital period) by the Launch Vehicle (LV) upper stage to propel the S/C towards L2 (similar to Gaia).

Both options are feasible and have different benefits, and as a result are both kept as possibilities. The circular parking orbit option has benefits with respect to the thermal design of the PLM, as the time during which the Sun is above the PLM is shorter than for the direct injection option during the launch ascent phase. The PLM thermal design is optimised for the nominal cryogenic conditions, therefore any PLM sun illumination phase should be minimised to avoid any risk of damage (e.g. to over-heating structural/thermal elements or payload detectors etc.) and ensure all elements and materials stay within their qualified temperature range. In addition this option provides a more robust launch window. On the other hand, it requires the Station Navale Ariane (SNA), a mobile tracking station located in the Caribbean sea to cover the LV visibility (standard practice but slightly higher launch cost). It also has an implication on the battery sizing to cover the one eclipse that occurs in the circular parking orbit, and has a slightly lower performance (lower mass injected to orbit around L2).

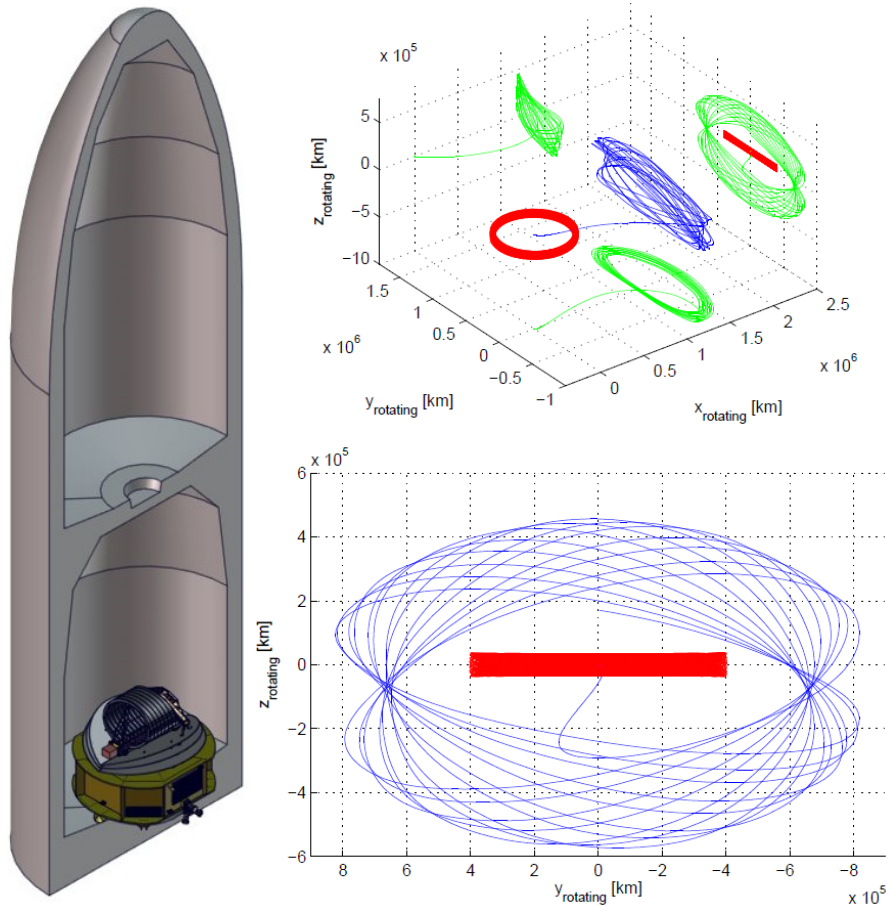


Figure 5-3: (Left) Illustration of the ARIEL S/C in the lower position inside the A62 dual launch fairing. (Right) Example of the ARIEL quasi-halo orbit around L2 and how eclipses are avoided. Blue shows the 3D trajectory, while green shows the projections in the rotating frame. Red indicates the Moon and its projection in the YZ plane of the rotating frame.

Since Ariane 6 is anticipated to provide a much larger performance to L2 than required ( $\sim 3.5$  t anticipated for A62, even more for A64, versus  $< 1.3$  t needed for ARIEL, see section 5.3.1), additional dual launch scenarios are kept as options. These would reduce the ARIEL launch cost and make better use of the A6 performance. With ARIEL positioned under the dual launch adapter (assuming an equivalent SYLDA type adapter will be available for Ariane 6), a  $\sim 1$  t to 2 t passenger (even more for A64) could be accommodated in the upper position. This would also have the advantage of protecting the ARIEL PLM from direct Sun illumination during LEOP (as discussed in the previous paragraph). The same two possible injection orbits (low inclination circular parking LEO or transfer to L2) could be offered to such a passenger.

Near daily launch windows exist with a duration of  $\sim 1$  to 2 hrs, as depicted in Figure 5-4.

The transfer and insertion into the orbit around L2 is designed to be propellant free, however three opportunities at day 2, 5 and 10 after launch are available for Transfer Correction Manoeuvres (TCM) to correct for launcher dispersion and perigee velocity errors.

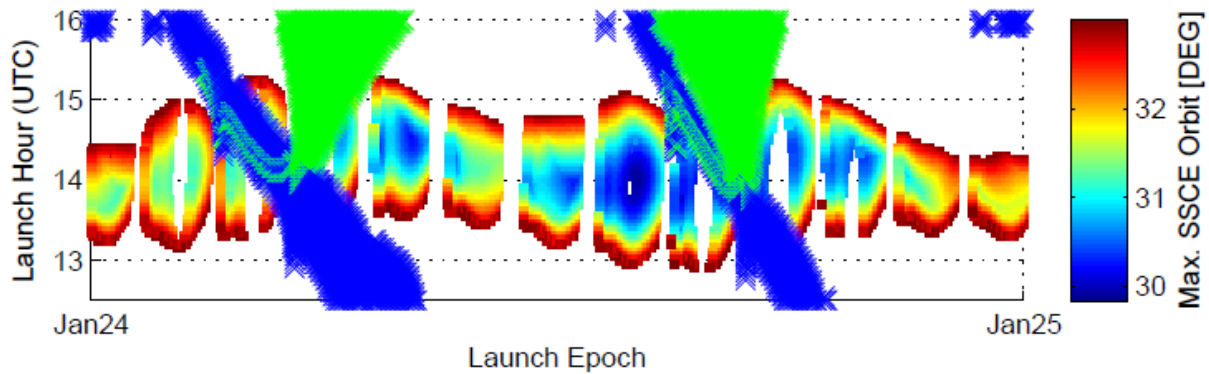


Figure 5-4: Example launch windows in 2024-2025 with the circular parking orbit scenario. The colour scale indicates the resulting Sun-S/C-Earth angle in orbit around L2 as a function of launch time. Eclipses during the transfer to the orbit around L2 are taken out with a green “x” and eclipses during the nominal operations phase are taken out with a blue “x”. Similar results are valid for any launch year.

The orbit is around L2 designed to be biased after TCM#2, meaning TCM#3 and monthly orbit maintenance manoeuvres will only be required in the  $-Z_{\text{ARIEL}}$  direction (i.e. the Sun direction). This avoids having to thrust in the  $+Z_{\text{ARIEL}}$  hemisphere and therefore deletes any risk of contamination of the payload by the plume of the thrusters. The only penalty of orbit biasing is a small increase of  $\Delta V$  for the subsequent orbit maintenance manoeuvres, meaning a little extra propellant in the mass budget. TCM#1 and #2 are not biased though, so thrust in the anti-Sun direction could be required until day 5 after launch. This can be done either by rotating the S/C  $180^\circ$  and using the  $-Z_{\text{ARIEL}}$  thrusters (with additional Sun illumination of the PLM to survive), or by using additional thrusters in the  $+Z_{\text{ARIEL}}$  hemisphere, sufficiently canted away from the  $+Z_{\text{ARIEL}}$  axis to minimise any risk of payload contamination.

After launch, 3 months are allocated to the S/C commissioning phase, followed by another 3 months for the payload verification and science demonstration phase. The remaining 3.5 years are dedicated to the nominal science operations phase, while the mission is sized for an additional 2 years goal extension, with small impacts on units degradation over lifetime, radiation dose and consumables (mainly Solar cells and propellant).

During the nominal science operations phase, the S/C is designed to have an observation efficiency  $\geq 85\%$ . Very few events impact this efficiency (eventual safe modes, monthly station keeping manoeuvres, reaction wheels off-loading and slews between targets), while the rest of the time the S/C is available for science observations (including calibration observations). Ground contacts do not degrade the observation efficiency as parallel telemetry downlink and science observations are possible thanks to the accommodation of the antenna on a 2 DoF mechanism. This simplifies the ground contact schedule, while at the same time avoiding any interference with the time critical observations of exoplanet transits/eclipses.

At end of life, de-commissioning is performed with a de-orbiting manoeuvre to ensure the S/C does not return to Earth and contaminate the protected LEO and GEO regions. This is a probabilistic analysis resulting in a likelihood  $> 99\%$  that the S/C does not return to Earth within the next 100 years.

## 5.2 Spacecraft Design

### 5.2.1 Structures, configuration and thermal

The spacecraft is designed in a modular way, with the SVM upper panel acting as a clear physical separation between the SVM and PLM (see Figure 5-5). This will simplify the procurement and Assembly, Integration and Verification (AIV) approach by allowing both modules to be procured and tested in parallel and independently.

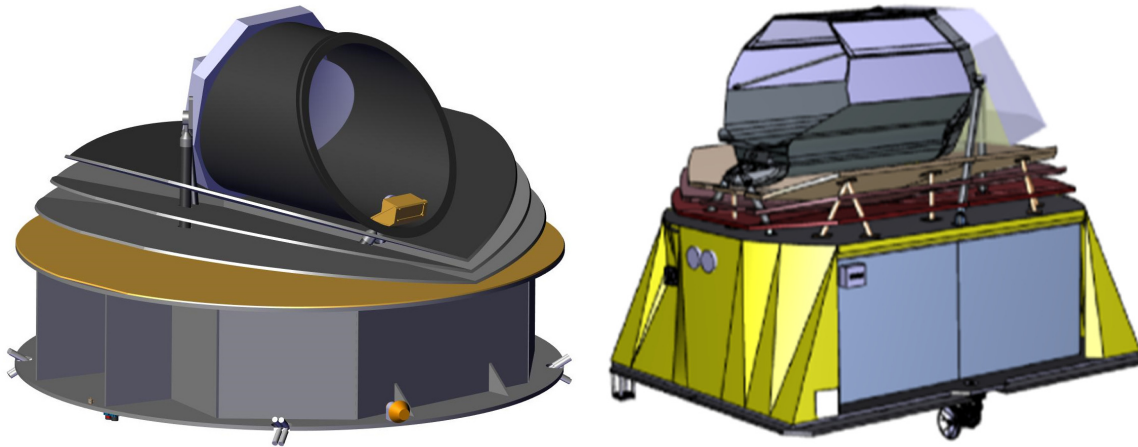


Figure 5-5: Industrial S/C designs (courtesy of TAS and ADS) with alternative PLM designs compared to the Consortium baseline PLM.

The PLM is composed of the thermal shield assembly (a set of 3 shields in a V-groove configuration that minimises the radiative heat transfer from the SVM to the PLM) and the optical bench, carrying both the telescope and the instrument boxes. The optical bench is supported on the SVM through 3 GFRP bi-pods. These are designed to carry the PLM during launch, transferring the loads down to the stiff SVM structure, while minimising the conductive heat transfer from the SVM to the PLM during nominal science operations thanks to a very low thermal conductivity. In addition, these bi-pods are thermally anchored to each thermal shield, to intercept as much heat as possible coming from the SVM before it reaches the PLM. Further details of the baseline PLM from the payload Consortium can be found in Chapter 4.

Note that as a risk mitigation measure, alternative telescopes and PLM designs have been investigated by industry during the Phase A using qualified / flight proven telescope ceramic materials (see Figure 5-6). This also included a thermo-elastic analysis of the full optical bench including the back-up ceramic telescope and the baseline Aluminium instrument bench to ensure that these materials and their interfaces can be properly designed to work together as a full system despite the differences in CTE. These alternative industrial PLM designs ensure that at least one feasible solution is in place in case the development activity on the Aluminium telescope by the payload Consortium is not successful. These alternative designs will be kept in place and further analysed during the next Phase B1 until the Aluminium telescope development activity (see section 4.5.3 and 5.5.2) is successfully completed.

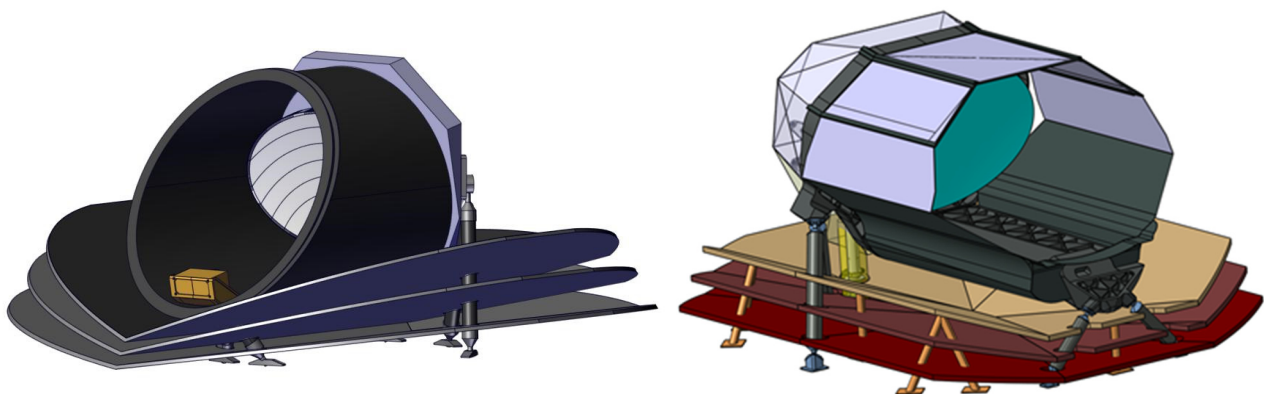


Figure 5-6: Alternative industrial PLM designs (courtesy of TAS and ADS).

The SVM structural design differs in shape and size between the two industrial contractors, but uses a common and standard approach, based on a central cylinder or cone, side walls and shear panels, and bottom and top panels (see Figure 5-7). The central cylinder/cone is the main structural elements that carries the launch loads and interfaces with the LV adapter at its bottom end, while holding the propellant tank(s) inside. All other S/C units are accommodated on the side walls. The SVM also carries the warm payload elements (cryo-cooler, ICU and FCU). The SVM is thermally controlled at  $\sim 20^{\circ}\text{C}$  for nominal operations of all the

S/C subsystem units. This is achieved through dedicated heaters where required and radiator areas are available on the  $\pm Y_{\text{ARIEL}}$  walls SVM that are constantly looking towards the cold sky.

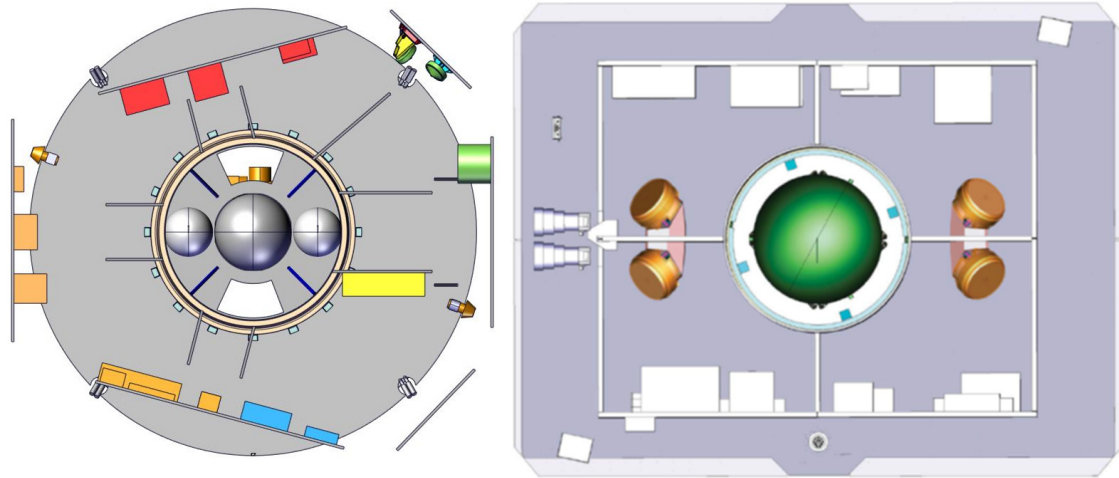


Figure 5-7: Inside view of industrial SVM designs (courtesy of TAS and ADS).

The overall configuration of the S/C is driven by the thermal requirements and the accessible sky requirements. The SVM upper panel shape and size drives the design of the PLM thermal shield assembly following the required cut angles shown in Figure 5-2, while it also acts as Sun shield (or V-groove #0) for the PLM.

## 5.2.2 Attitude and Orbit Control Subsystem

Note that all pointing errors detailed in this section are half cone angles expressed with a 99.7% confidence level.

The Attitude and Orbit Control Subsystem (AOCS) provides control of the S/C attitude and of the telescope and instrument Line of Sight (LoS). The AOCS requirements are split into 2 main pointing modes: a coarse pointing mode and a fine pointing mode.

The coarse pointing mode is achieved by only using the AOCS units accommodated in the SVM, with the star tracker as the main sensor and the reaction wheels as the sole actuators (i.e. without the FGS in the control loop). This mode is used to slew between target stars. The resulting coarse Absolute Performance Error (APE) of 8'' across the LoS of the FGS channels is included in the sizing of the FGS Field of View (FoV). As such, this mode ensures the FGS can acquire the target star within its FoV, to then successfully transition to the fine pointing mode. The main terms that are included in this coarse APE are the star tracker measurement noise, the AOCS control loop error, and the alignment error between the star tracker and the FGS LoS. This last error includes static biases (e.g. from assembly and alignment plus launch and 0g effects) that can be calibrated out in the commissioning phase once a target is found in the FGS FoV, but also dynamic errors linked to thermo-elastic effects (although with a long time constant) between the star tracker accommodated in the warm SVM and the FGS located in the cryogenic PLM.

The fine pointing mode is the precise pointing mode that will be used during observations of all science targets. It is achieved with the FGS in the control loop to provide fine pointing knowledge around the 2 axes across the LoS of the instruments, hybridised with the star trackers for a coarse determination of the attitude around the 3<sup>rd</sup> roll axis (pointing errors around the roll axis of the telescope/instruments are less constrained since ARIEL is observing a single target at a time in the centre of the FoV). A fine gyroscope can also be included in the design to further improve the pointing knowledge from the FGS. The main fine pointing requirements achieved by the system across the instruments LoS are:

- Fine APE  $\leq 1''$
- Relative Performance Error (RPE)  $\leq 200$  mas up to 90 s
- Performance Drift Error (PDE)  $\leq 100$  mas up to 10 hrs for integrations of 90 s

These requirements are applicable when observing bright targets. This is because the brighter the target is, the larger the photometric variation induced by a pointing variation is. As a corollary, for fainter targets,

these pointing requirements are more relaxed. This benefits the AOCS subsystem, since the FGS centroiding error increases with a lower input flux. The requirements given above are to be achieved with a specification on the FGS measurement error  $\leq 20$  mas at 10 Hz.

Similarly to the coarse APE and the sizing of the FGS FoV, the fine APE is taken into account in the sizing of the entrance slits of both AIRS channels.

The RPE contains all the high frequency jitter terms. Most of this jitter is un-resolved, because the detector read out rates are slower than most sources of high frequency jitter (FGS error at 10 Hz, reaction wheel and cryo-cooler micro-vibrations in the 10s to 100s Hz range). This jitter induces a small blur of the large system PSF (driven by the telescope diffraction limit requirement at 3 micron), but does not result in photometric variations in the frequency range of the science observations.

The PDE is the most important pointing requirement, as it translates directly into photometric variations that add to the instrument noise budget. As the PSF drifts on the focal plane detectors, the number of photons incident on the individual pixels will vary. This photometric variation (including allowance of the errors in the detector flat-fielding and a representative timeline of pointing error) is taken into account in the instrument noise and photometric stability budget as reported in section 4.10. Since the PDE applies to very low frequencies (minutes to hours), it is more easily met than the RPE. The main phenomena that translate into attitude drifts in this frequency range are thermo-elastic errors due to changes in attitude of the S/C between targets (and therefore changes in attitude with respect to the Sun leading to different thermal loads on the S/C) and the Solar Radiation Pressure (SRP). In the case of ARIEL the SRP is more than one order of magnitude lower than that of typical astrophysics missions with telescopes that are accommodated vertically (e.g. Herschel or Euclid). This is because the horizontal accommodation of the PLM on the SVM allows for a well-balanced S/C which minimises the torque that originates from the misalignment between the centre of gravity of the S/C and the centre of pressure of the SRP. Any drifts occurring from thermo-elastic effects and the SRP are in any case seen by the FGS as it is operating at a much higher frequency, and are therefore corrected by the AOCS subsystem.

While these fine pointing requirements impose the need for the FGS as a fine sensor in addition to the star trackers, they can still be met with reaction wheels as the sole actuators (i.e. no need for a fine pointing actuation system). To achieve this, the reaction wheels need to be operated in a narrow angular speed range, away from any peak vibration mode and away from any possible amplification frequency of the S/C structure. This derives into the need to very frequently off-load the reaction wheel momentum to ensure they remain within this narrow operating range, as the angular speed will continuously be evolving as the wheels are constantly gaining momentum to counteract the SRP. This off-loading is performed with the propulsion subsystem and can be done as frequently as between every target observation, in parallel to the slew to the next science target. The detailed fine tuning of this concept with the exact angular speed range will however need to occur late in the development process, as the flight models of the wheels are available and their actual micro-vibration profile is measured as well as the S/C structure transfer function.

Similarly, the micro-vibrations from the cryo-cooler must be controlled to ensure they do not excite any structural mode of the S/C and are sufficiently damped. With the capability to fine tune and adjust the exact operating frequency of the cooler compressors within a band of a few Hertz and the possibility of active vibration control by automatic drive waveform modification, this enables the cryo-cooler to comply with the pointing budgets allocations.

Based on this, all the fine pointing requirements have been demonstrated to be met. The only exception is the RPE which becomes marginal when also taking into the reaction wheel spikes (more accurately referred to as friction torque variations) when observing bright targets (faint targets are fine with the more relaxed RPE requirement). Such spikes have been measured on past missions and this is considered as a complex phenomenon that is due to multi-body interactions of the different balls and the distribution of lubricant within the bearing. Several mitigation measures are possible:

- Screen the reaction wheels and select those with low (or no) spikes (at the cost of procuring and testing more wheels).
- Discard the observations when large spikes occur, with a very low impact on the observation efficiency (expected loss of time at the level of  $\sim 1\%$ ), or alternatively accept a small degradation in performance for these short durations.

- Add a fine steering tip/tilt mechanism in the optical path to correct for these spikes (technology development on-going).
- Add an internal control loop on the wheel tachometer to correct for these spikes (some technology development needed).

Additionally, to further consolidate the pointing budgets, the industrial contractors are considering the possibility to mount the reaction wheels on dampers. This would add robustness to the design by further damping the high frequency micro-vibrations that will only be well characterised and fine-tuned late in the development phase. The same concept could also be implemented on the cryo-cooler.

### 5.2.3 Propulsion

The propulsion system is a simple mono-propellant system (hydrazine) that is based around standard qualified off-the-shelf components (typically 1 to 20 N thrusters). Note that both industrial contractors have traded-off the simplicity and cost of the system (number and size of thrusters) with the optimisation of the manoeuvres (minimum thrust time and propellant needed with cosine losses) resulting in different solutions.

All thrusters are redundant, and provide control of the S/C around the 3 rotational degrees of freedom for reaction wheels off-loading and safe modes, as well as thrust at least along the  $-Z_{\text{ARIEL}}$  axis for orbital correction manoeuvres. Thrust in the two other directions can be done with additional thrusters or using the same ones after slewing the S/C in the right attitude.

### 5.2.4 SVM Electrical Architecture

The power subsystem uses standard qualified off-the-shelf components. Solar cells are accommodated on the bottom floor of the SVM which provides sufficient area to cover the needs of the mission without requiring deployable Solar arrays. The required packaging ratio of the cells leave sufficient areas for all the other units accommodated under the SVM (e.g. antennas and mechanisms, Sun sensors etc.). Since the orbit is eclipse-free, batteries are only necessary during the launch phase and possibly for the TCM#1 and #2 manoeuvres (in case thrust for these manoeuvres is required in the Sun direction and no thruster is accommodated along the  $+Z_{\text{ARIEL}}$  direction, necessitating a  $180^\circ$  rotation of the S/C).

The communication subsystem uses X-band only, with at least 2 Low Gain Antennas (LGA) distributed around the S/C to provide a full  $4\pi$  steradian sky view to allow for S/C recovery in case of a safe mode or loss of attitude. These antennas provide only a low bit rate and can therefore only be used for such recovery cases and for uplink telecommands. For science data downlink, a high bit rate is achieved with a Medium Gain Antenna (MGA) located on the bottom of the SVM. It is accommodated on a 2 DoF mechanism to ensure that ground contact can be achieved whatever the attitude of the S/C. This enables parallel data downlink and science observations to optimise the observation efficiency budget. More importantly, it relieves any constraint on the observation plan (as the transit/eclipse observations are time critical) while allowing for fixed pre-planned ground contact times and durations in order to simplify the MOC schedule and keep the operations cost low. Any of the 3 ESA 35 m antennas (Cebreros, Malargue and New Norcia) is suitable, selection will be made closer to the launch date when the antennas' usage are better known. 14 hrs of ground contact are planned every week, split in 3 passes of  $\sim 4$  hrs to 6 hrs. Each ground contact includes 15 min at its beginning and end for ranging and Doppler activities, in parallel to the full contact time for telemetry.

Memory is sized to enable continuous science operations without any loss of science data in the case of 1 missed ground contact, while the S/C is sized to survive autonomously at least if 2 successive ground contacts missed.

## 5.3 Spacecraft Budgets

### 5.3.1 Mass Budget

The ARIEL industrial mass budgets are presented in Table 5-1. Note that the PLM mass refers to the industrial alternative designs. The baseline PLM mass budget from the payload Consortium with the heavier Aluminium telescope and optical bench is presented in Table 4-3, however the SVM structural designs with the mass budgets presented here have been sized to support this heavier Consortium PLM.

		<i>ADS</i>	<i>TAS</i>
<b>PLM</b>	Telescope structure, optics and baffles	126	100
	Thermal shield assembly (V-grooves and struts + others (e.g. harness, mounts etc.))	130	138
	Payload	51	70
<b>Total PLM</b>		<b>307</b>	<b>307</b>
<b>SVM</b>	Warm instrument units and cryocooler	41	41
	Structure and thermal control	222	211
	Communications	37	39
	CDMS	37	44
	AOCS	30	54
	Propulsion	58	46
	Electrical power	72	39
	Harness	61	30
<b>Total SVM</b>		<b>558</b>	<b>504</b>
<b>S/C total dry</b>		<b>866</b>	<b>812</b>
20% system margin		173	162
<b>S/C total dry with margin</b>		<b>1039</b>	<b>974</b>
Propellant		107	138
<b>Wet mass</b>		<b>1146</b>	<b>1112</b>

Table 5-1: ARIEL S/C mass budgets from the two industrial designs (in kg), including their alternative PLMs.

For both designs, the resulting dry mass is about ~ 1 t (wet mass < 1.2 t). This is to be compared to the ~ 3.5 t expected performance of A62 for injection towards L2.

With the heavier Aluminium baseline PLM from the payload Consortium (mass budget given in Table 4-3), the spacecraft wet mass remains < 1.3 t for both industrial Contractors.

### 5.3.2 Power Budget

The ARIEL industrial study power budgets are presented in Table 5-2. The budgets are shown for two of the main mission modes:

- Commissioning and decontamination. This mode occurs during the first 3 months of the mission after launch, with the SVM going through its commissioning phase and the payload (optics and detectors at least, possibly the baffle as well) is kept warm in decontamination mode while the rest of the cryo-structure is left to passively cooling down until it reaches its operational temperatures.
- Science and communications. This is the main mode used during observations in the nominal science operations phase, and allows for parallel communications with ground thanks to the antenna mechanism to optimise the observation efficiency.

Note that the exact definition of each mode varies between each contractor and therefore the budgets are not directly comparable (different units used at different times, e.g. AOCS actuators versus propulsion system, various payload units on or off during the SVM commissioning phase etc.).

	Commissioning and decontamination		Science and communications	
	ADS	TAS	ADS	TAS
Payload	0	72	117	140
Thermal control	365	290	12	120
TT&C	112	112	112	147
Data handling	61	53	103	73
AOCS + propulsion	38	151	38	138
Electrical power	46	20	45	20
<b>Total power without margins</b>	<b>633</b>	<b>698</b>	<b>434</b>	<b>670</b>
Unit uncertainty margins	93	38	59	35
30% system margin + losses	228	221	155	211
<b>Total power with margins</b>	<b>943</b>	<b>957</b>	<b>641</b>	<b>916</b>

Table 5-2: ARIEL S/C power budgets from the two industrial design for two different modes (in W).

Overall, these budgets indicate that the power needs of the S/C are rather modest (under 1 kW).

## 5.4 Spacecraft and Payload AIV and Development Plans

The spacecraft development plan is based on a standard Proto Flight Model (PFM) approach, although with some adaptations due to the specifics of the ARIEL mission: optics in cryogenic conditions, and a clear SVM / PLM separation (both physically and in terms of responsibility between ESA / industry and the payload Consortium / Member States). This implies that all final qualification tests are conducted on a S/C PFM. Such an approach carries an acceptable amount of risk and avoids having to produce and pay for two full S/C models in parallel (one for testing / qualification and one for launch). To consider environmental tests only at final S/C FM level would further decrease the cost but would increase the risks to a level that is no longer acceptable (i.e. large cost impact if a test fails so late in the development phase and results in the need for re-design and re-qualification).

The PFM model is typically supported by additional models earlier in the development plan. The following models are baselined:

- an Avionics Model (AVM) to verify the electrical and electronics interfaces
- a Structural Thermal Model (STM) to re-risk the structural and thermal design with a focus on environmental testing
- a Performance Verification Model (PVM) of the PLM only under the responsibility of the Consortium.

Some major payload design aspects will also be de-risked earlier (starting in Phase B1) in the program using development models where possible within the programmatic constraints. Details on the planned models and the test philosophy of the PLM are illustrated in Figure 5-8 and detailed in [Bishop et al., 2017](#).

The AVM will integrate Engineering Models (EMs) of the payload elements (e.g. M2 mechanism electronics, Instrument and FGS Control Units, cryo-cooler drive electronics) that will be delivered to the S/C prime and assembled with the SVM AVM model. This model typically enables to check all the functional and electrical (power, data and communications) interfaces between all units, to verify the functionality of the avionics including the on-board software and the AOCS closed control loop (which will require a simulator of the FGS output), plus some EMC and RF tests etc.

The STM allows to qualify the spacecraft structure and demonstrate the thermal performance of the design. The SVM and PLM can each have a separate STM model that will be developed and tested in parallel. Mating these models into a single S/C STM is potentially not required due to the clear mechanical and thermal interface and different temperature conditions experienced by both modules. The only exceptions to this are:

- A cryo-cooler development model is included in the PLM STM with dedicated GSE to support it, as it is nominally integrated within the SVM.
- The verification of the micro-vibrations impact on the instrument LoS (as part of the structural tests) can only be fully demonstrated if the reaction wheels and the cryo-cooler (which are in the SVM) are tested

with the PLM model, including the structural load path between these units (so part of the SVM structural model is potentially needed).

Based on heritage and fidelity of the structural and thermal analysis tools, the SVM STM could also potentially be considered unnecessary, leaving the full qualification of the SVM structural and thermal design only to the PFM with an acceptable risk.

Similarly, the PLM STM can also be adapted. In particular, the optics (within the telescope and instruments) are not required to be representative in terms of optical performance and can be simple mirror dummies, as only structural and thermal performance is tested here, not optical performance. The primary mirror M1 though could benefit from re-using the M1 pathfinder development model (which is a spherical approximation of the real M1 aspheric mirror) and its focus / radius of curvature measured in cryogenic conditions on the STM telescope assembly (before full integration of all other PLM units), which will help determine the alignment and shimming procedures for the PVM and PFM models.

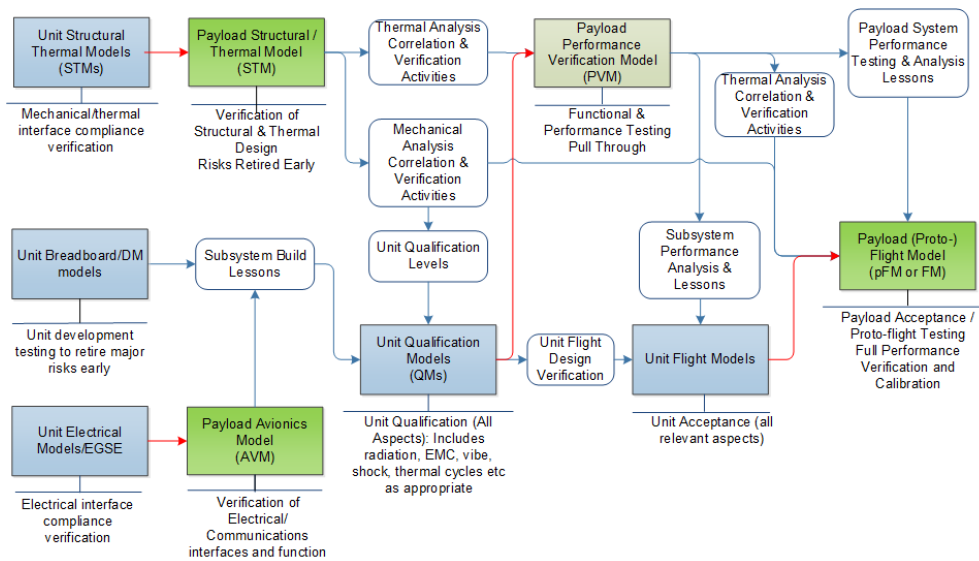


Figure 5-8: Verification flow for the ARIEL Payload programme. Blue boxes represent instrument / subsystem level AIV activities, green boxes are PLM level AIV activities (only the bright green items are delivered to ESA / S/C level AIV), red lines represent hardware deliveries, blue lines are information or specification flows that feed into the activities.

In addition to the AVM and STM, an additional PVM is baselined by the Consortium early in the development process, so as not to leave the full performance testing of the payload (including optics and detectors) in cryogenic conditions too late in the development process. This model will be stand-alone, i.e. will not require any other S/C or SVM units and models to mate and interface with, and as such does not require to interface with the industrial contracts and be delivered to the S/C prime. It may include flight spares for the telescope mirrors and engineering models of the detector (functionally representative in terms of performance, but not flight grade) and will enable performance validation of the payload in cryogenic conditions (although some simplifications might also be possible, e.g. depending on the need or not for straylight verification, the mirrors’ roughness could be relaxed if not affecting the PSF quality, enabling a faster development/polishing time at a reduced cost), and more importantly validation of all payload performance software models based on correlation between test data and analysis results. If enhanced with some SVM elements, it could also be used to validate the micro-vibrations impact on the instrument LoS (as opposed to the STM test described above).

The PLM performance verification and ground calibration will be carried out in a dedicated test facility at STFC – RAL Space. This will provide a low temperature environment allowing simulation of the thermal environment of the PLM. A dedicated set of OGSE with an ultra-high stability source (from heritage of the calibration of space-based EO radiometer instruments to mK level) will be used to verify the payload system overall photometric stability. Further details can be found in [Bowles et al., 2017](#).

The final model is the PFM. It will be built from the SVM and PLM PFM models that will then be assembled together. The FM units of all payload units (telescope, instrument, cryo-cooler etc.) will be included, aligned and functionally tested in operating conditions at PLM PFM level only. Therefore, no cryogenic or optical test is needed at full S/C PFM level.

## 5.5 Technology Readiness

### 5.5.1 ESA Developments

A number of ESA Technology Development Activities (TDAs) are running for ARIEL. They all relate to payload developments, as no need for any new technology has been identified on the SVM. Some of these are developments that are required in the baseline design, while others are only back-ups or nice-to-have for enhanced performance. The objective of these activities is to ensure that all elements of the ARIEL design have reached a  $TRL \geq 6$  by mission adoption at the end of the Phase B1 study (Q4/2018). These TDAs are:

- Cryogenic re-focussing M2 mechanism (required mechanism for ARIEL, but the baseline solution is under the responsibility of the payload Consortium and covered by their own development activity). This activity aims at qualifying, under cryogenic conditions, a re-focussing mechanism ( $\geq 3$  DoF) that will be put behind M2. This activity has now passed Preliminary Design Review (PDR) and is awaiting confirmation of the final requirements imposed on this mechanism coming out of this Phase A study to continue towards Critical Design Review (CDR), followed by manufacturing and testing.
- Performance verification of a Ne JT cooler at  $\leq 30$  K (required cooler for ARIEL). This activity aims at verifying the performance of the European JT cooler (evolution from the Planck cooler) with Ne instead of He as the working fluid. The ITT has been issued and negotiations held, KO is imminent.
- Development of low noise HgCdTe detectors (back-up for ARIEL). Several activities exist on this topic, covering detectors with different cut-off wavelengths to cover all the channels of ARIEL (from VNIR to AIRS#1). These activities would provide European alternatives to the baseline American detectors. The activities covering the VNIR channels were originally initiated for the M2 Euclid mission and are now well advanced with detectors showing sufficient performance for ARIEL, while the activity aimed at AIRS#1 has just been kicked-off during the Phase A of ARIEL.
- Cryogenic fine steering tip/tilt mechanism (optional for ARIEL). This activity was originally initiated for the M3 candidate mission EChO and was successfully completed. A follow-up activity has been initiated to modify and adapt this mechanism to the new needs of ARIEL, in particular to enable correcting for the reaction wheel spikes discussed in section 5.2.2. This activity has now passed PDR.

### 5.5.2 Payload Consortium Development Status and Plans

The development status of all baseline technologies for the payload is assessed to be  $TRL \geq 6$  at the time of writing with the following exceptions:

- the dichroic D1 (cutting at  $1.95\mu$ ) which is currently  $TRL=4$  and subject to a develop testing activity at University of Reading which is on-going;
- the 1m class primary mirror made in Aluminium 6061-T651 which is currently  $TRL=4$ . This is being developed and demonstrated to higher  $TRL$  by the PTM mirror program discussed in §4.5.3;
- the M2M refocus mechanism which is currently  $TRL=4-5$ . A development activity by Sener (Spain) to develop the Gaia and Euclid M2M mechanisms into one fully suitable for the ARIEL requirement is planned for phase B1;
- the Visible / NIR LED sources for in-flight calibration which are  $TRL=5$  and will undergo a radiation qualification test in phase B1; and
- the Neon JT cooler as a system which is currently  $TRL=4-5$  and subject to a TRP development activity funded by ESA which will kick-off in April 2017 to complete at the end of phase B1.

It should be noted that the AIRS Ch1 baseline detector from Teledyne from the NEOCam developments is assessed as  $TRL=6$  by the manufacturer, but verification of this by testing by the ARIEL team will be needed in phase B1. There are development plans in place (which have been reviewed and agreed with ESA) for phase B1 for all of these items. The optional European detectors for the AIRS and FGS systems (and the associated European CFEE) are assessed to have a  $TRL=4-5$  currently. There are funded plans in place for the testing of sample AIRS detectors (through CNES) and FGS detectors (through ESA as noted above) during the phase B1.

In summary, the phase A study has identified no technologies that can not be developed to the required  $TRL6$  by the mission adoption. Plans have been put in place by ESA and the payload consortium to enable the necessary development activities to take place in a timely fashion following mission selection.

# 6 Mission Operations and Ground Segment

## 6.1 Overview

### 6.1.1 Overview of the operational centres

The ARIEL Ground Segment (GS) provides the means and resources with which to manage and control the mission via telecommands, to receive and process the telemetry from the satellite, and to produce, disseminate and archive the generated products.

Responsibility for and provision of the ARIEL GS is split between ESA and a nationally-funded Instrument Operations and Science Data Centre (IOSDC).

ESA will be responsible for the following GS elements:

- The Mission Operations Centre (MOC)
- The ESA tracking station network (ground stations)
- The Science Operations Centre (SOC)

A schematic view of the operational interfaces for the ARIEL mission is presented in Figure 6-1. Full details of the operational interfaces and plans are contained in Kohley et al, 2017. The ground stations together with the MOC build the Operations Ground Segment (OGS), while the SOC and the IOSDC comprise the Science Ground Segment (SGS). The responsibility for the SGS tasks and activities are distributed and shared between SOC and IOSDC.

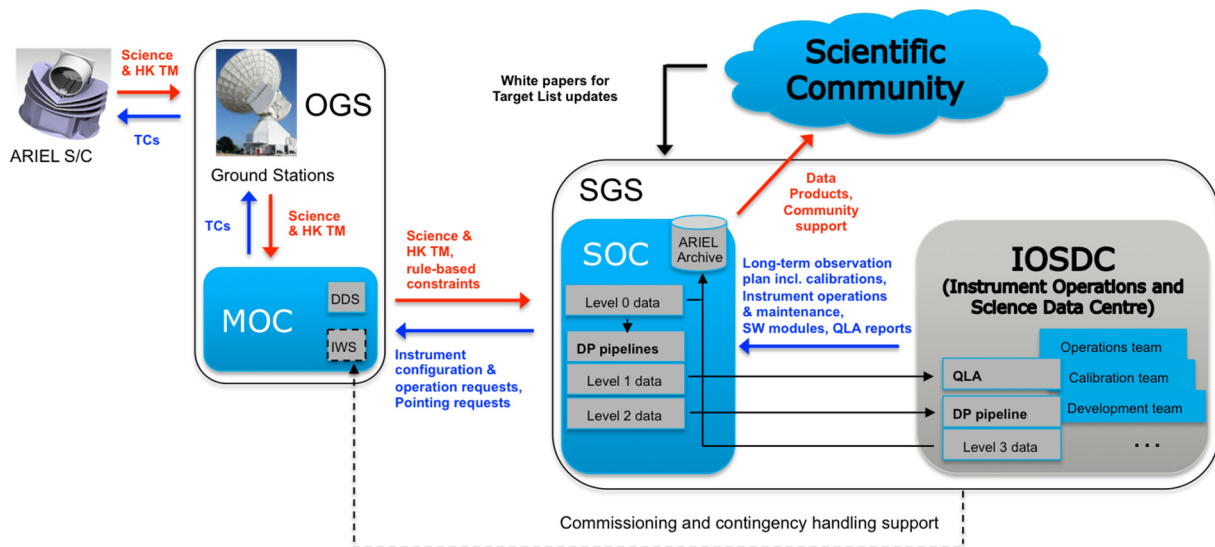


Figure 6-1: ARIEL Ground Segment interfaces and data flow. SOC is the nominal point of contact to MOC during in-orbit operations, exceptions include the commissioning phase and the case of contingency handling, where a direct link between IOSDC and MOC can be established through the instrument workstation (IWS).

The following is a list of the key tasks that will be performed during ARIEL operations:

- Science planning (target selection and long term planning)
- Mission operations planning
- Production and execution of operations requests (including spacecraft and instrument sequences)
- Ground control and monitoring at MOC (including spacecraft health and orbit maintenance)
- Contingency isolation, management and recovery
- Instrument operations and calibration
- Mission (including science) data processing, population of archive, provision of data products
- Ground infrastructure operations and management
- Spacecraft and ground segment performance analysis and tuning

- Science data archive and community support

### 6.1.2 Mission Operations Centre

The ground segment and operations infrastructure for the Mission Operations Centre (MOC) of the ARIEL mission will be set up by ESA at the European Space Operations Centre (ESOC) in Darmstadt, Germany. The ARIEL MOC will be based on extensions of the existing ground segment infrastructure, customised to meet the mission specific requirements thereby maximising the sharing and reuse of facilities and tools made available from other Science Observatory missions. ESOC will prepare the ground segment including all facilities, hardware, software, documentation, the respective testing, validation and training of staff required to conduct the mission operations.

The MOC will be responsible for all operations of the ARIEL spacecraft and instruments during all mission phases covering both nominal and contingency operations.

Prime responsibilities include:

- Operations preparation: development of operations procedures and training of operations team.
- Spacecraft platform and payload monitoring and control.
  - Maintaining the health and safety of both platform and payload and intervention in case of anomalies.
  - Planning, generation and upload of all spacecraft and instrument commands. Science observation commanding inputs are provided by SOC.
  - Spacecraft maintenance and engineering support, e.g. on-board software maintenance.
  - Off line performance analysis.
- Flight dynamics support, including determination and control of the satellite's orbit and attitude.
- Planning, scheduling and execution of the ground station contacts,
- Receipt of all telemetry including science data.
- Distribution of all relevant data (Science, housekeeping and auxiliary data) to the SOC and archiving of all housekeeping data.

Links between MOC and SOC are foreseen using standard internet capability without the need for dedicated links.

### 6.1.3 Ground Stations

The MOC performs all communications with the satellite through the ground station network.

The 35m ground stations of the ESA ESTRACK network comprising New Norcia, Cebreros and Malargüe antennas will be used for communication and precise orbit determination. Additional coverage will be provided during LEOP from the small New Norcia (NNO-2) antenna to support first acquisition. No additional external ground stations are currently foreseen for LEOP and/or commissioning.

All communications and tracking with ARIEL will be done at X-Band using existing capability in the ground segment. No ground station upgrades are currently needed to support the ARIEL mission.

### 6.1.4 Science Operations Centre

The Science Operations Centre (SOC) of the ARIEL mission will be set up by ESA at the European Space Astronomy Centre (ESAC) near Madrid, Spain, which also hosts the archives of all ESA science missions. The SOC will design, develop and operate the ESA-funded part of the ARIEL science ground segment throughout all mission phases. Required science operations system functionalities at the SOC include:

- Centralised scheduling system as interface to MOC to produce instrument commanding and pointing requests and involvement in mission planning activities.
- Reception of science, housekeeping and auxiliary data from MOC.
- Operation of a data processing system to process science data products up to Level 2, Fine-Guide-Sensor (FGS) and other ancillary data, and data distribution to the IOSDC.

- Operation of quality control system dedicated to instrument & FGS data quality analysis and mission planning feedback.
- Operational support, i.e. for instrument operations, performance checks, Quick- Look, trend analysis and observations tracking.
- Development, operation and maintenance of the ARIEL archive comprising mission data base and science data archive.
- User Support (in collaboration with the IOSDC), i.e. documentation, HelpDesk, workshops.

### 6.1.5 Instrument Operations and Science Data Centre

The nationally-funded Instrument Operations and Science Data Centre (IOSDC) is a subset of the PI Consortium team with specific responsibility for instrument operations and fulfilling the PI / Consortium contribution to the ARIEL Ground Segment. The IOSDC will follow a distributed structure across multiple institutes, chaired and supervised by the IOSDC Manager, who also acts as the single point interface between IOSDC and ESA (SOC). Internally the IOSDC will be organized into a set of teams with their respective team leaders: the management team, operations team, software and data processing team, observations team, editorial team, instrument team, and calibration team. The IOSDC Manager, together with the Management Team, will be co-located at the ARIEL Instrument AIV integration and test facility. The IOSDC main responsibilities can be summarised as follows:

- Preparation and maintenance of the long term scientific mission planning.
- Instrument operations and calibration, and payload expertise to support anomaly resolutions.
- Provision of an Instrument Workstation at MOC for commissioning and contingency support.
- Provision of on-board software and instrument command and telemetry definition (updates).
- Development and operation of a Quick-Look (performance health monitoring) and trend analysis system.
- Development and maintenance of the data processing pipelines and associated quality control tools, and delivery to SOC for operation.
- Operation of a data processing system to generate Level 3 science data and calibration products for ingestion into the ARIEL archive.

## 6.2 Mission operations

Support is provided by ESOC from the start of the mission definition phase through preparation and implementation.

The ARIEL mission is planned with a short 2 day LEOP, followed by a 90day Commissioning Phase. The orbit transfer to the operational orbit around L2 occurs within this Commissioning Phase. Flight operations teams will be optimised throughout this period to ensure full MOC team and ground station coverage during the critical early stages of the mission reducing to smaller teams and day passes during the later commissioning phases. After the IOCR the mission transitions into the Performance Verification Phase where ground station pass durations and shift sizes are gradually further reduced in working hours, ground station passes, and team configurations to those planned for routine science operations at the beginning of the science demonstration phase.

For routine operations the ARIEL mission is foreseen to be operated in a highly automated way. The ARIEL mission on board capability is foreseen to handle simplified commanding for execution of slews between observations based on requested target position, reaction wheel momentum management will be controlled on board and all operations executed on board from preloaded mission timelines. This approach reduces the need for ground based definition of the slew profiles and momentum management. The mission timelines are uplinked on a periodic basis (e.g. weekly) and the shortened pass durations (~14 hours per week) are primarily used for downlink of the science data and collection of tracking data needed for orbit determination. The orbit control is anticipated to be of a predictive nature allowing the mission to apply rule-based planning for engineering windows for platform operations, allowing the remaining science planning to

be done on a long term basis by the SOC. It has been assumed that based on the moveable antenna the ground station passes can be scheduled independent of the science observations.

In the event of ground anomalies ARIEL is foreseen to continue nominal operations without the loss of Science data for a period of 5 days and in all post LEOP mission phases the spacecraft will be able to survive without ground contact for 7 days.

## 6.3 Science operations, calibration and data handling/archiving

### 6.3.1 Mission planning

The scientific mission planning consists in generating a long-term observation plan of the ARIEL surveys including the needed calibration observations (on sky and internal), based on the list of targets observations and mission constraints (S/C attitude constraints, data rates, straylight from bright out-of-field sources such as planets, etc.). As stated in Section 6.2, the rule-based input of MOC constraints and independency of ground station booking leads to a highly simplified and optimized mission planning cycle.

To achieve the high scheduling efficiency, an optimisation process based on a figure-of-merit for maximizing the scientific return as integral part of a long-term planning tool will be used ([Garcia-Piquer et al. 2014, 2015, 2017](#); [Morales et al. 2015](#)). This tool will be developed and maintained by the IOSDC. Two independent initial versions based on artificial intelligence and a system of priorities already exist and have been used to show the feasibility and performance of the ARIEL surveys under the current Mission Reference Sample (existing and simulated exoplanet targets). The independent simulations of the mission planning demonstrate that about 950 exoplanets could be observed, including ~375 Tier 2 and 66 Tier 3 targets in the MRS, dedicating a total of 90-92% of the mission life time spent observing science targets (see [Morales et al. 2017](#) for details). This efficiency is extremely satisfactory and well above the requirements of 85%.

The Consortium/IOSDC is in charge of running the scientific mission planning activity under the guidance of the Science Team, chaired by the ESA Project Scientist. The long-term observation plan will be produced and could be revised on a monthly basis (to account for missed observations or new targets being added to the target list) always covering until end of mission and within a mission planning working group under participation of IOSDC, SOC and MOC. After final approval by the Project Scientist, it serves as input to the observation scheduling and product generation under responsibility of SOC. These pointing and instrument operations requests are sent to from SOC to MOC for uplink to the spacecraft.

### 6.3.2 Instrument operations and calibration

Due to the survey nature of the ARIEL mission and the concise suite of science instruments, the complexity of instrument operations is inherently low with operations modes mainly conditioned by the target brightness. Most calibration observations will be on-sky and use the same instrument operations modes as used for the science target observations. Some internal calibrations may require dedicated modes.

The generation of the instrument configuration files and operations requests for target observations and calibration is under the responsibility of the IOSDC and goes along with the long-term mission planning exercise. The IOSDC will also maintain the On-board Software (OSW), which will be stored and version controlled with any updates by SOC before uplink through MOC to the spacecraft.

To support the commissioning phase and contingency cases, and Instrument Workstation (IWS) will be developed and operated by the IOSDC as direct interface to the MOC data distribution system. The IWS is based on the Electrical Ground Support Equipment (EGSE) already used during instrument on-ground tests and together with the training and continuity of expertise of instrument teams support the concept of “smooth transition” from development to operations. From start of PV phase SOC will execute the interface to MOC.

To provide feedback on the quality of the received science data and the payload/instrument health, a Quick-Look Analysis (QLA) will be performed on the data received after each ground station pass. The QLA tools are developed and operated by the IOSDC, again based on ground test tools. SOC will operate a subset of the QLA functionality based on meta-data information for fast feedback on the observation success and survey execution. Another aspect is the pointing reconstruction, also under responsibility of SOC based on information and products from MOC, which is further used for calibration in the data processing.

### 6.3.2.1 Ground Calibration:

Calibration activities start with the on-ground testing to obtain instrument calibration data for the bootstrapping of the calibration products in the data processing. A central and critical part in this context is the detector system performance.

The ground test and calibration campaign will be the responsibility of the payload consortium and is described in [Pearson et al., 2017](#). It is desirable to implement as many tests as possible at the lower levels (Component and Unit Level) to avoid complication further down the signal chain at instrument (subsystem) or payload module level. The test plan will follow the methodology given below and shown in Figure 5-8 and will follow the development schedule outlined in section 7.3:

- **Component Level Test:** Low level testing of components such as Detector SCA, CFEE, Dichroics, mechanism actuators, etc.
- **Unit Level (parts of a subsystem) Test:** Unit level tests are those carried out on individual components of the system without inter-dependencies / influences from other components. This would include the FGS and AIRS detector systems, the FGS Beam splitter assembly, Cooler compressor, etc.
- **Subsystem Level Test:** This is the Instrument Level Testing (ILT) and would include the entire AIRS instrument, FGS instrument (including FCE), the Telescope Assembly (including the Bipods and the V-grooves), Instrument Control Unit (ICU) and the Cooler system.
- **Payload Module Level Test:** This level comprises the integrated instruments and telescope assembly and includes payload functional, environmental and performance tests, EGSE integration testing and Ground Segment End-to-end testing.

### 6.3.2.2 Flight Calibration

Regular in-orbit calibration is required to establish, track and update calibration parameters, either if the required accuracy can only be obtained in orbit or due to environment changes, e.g temperature and radiation effects. The on-sky and internal calibrations are absorbed in the long-term observation plan.

The internal calibrator is described in section 4.6 and will be used for monitoring trends in the detector systems, particularly for the flat-fielding of the detector systems. On-sky calibrations as described in detail in [Pearson et al., 2017](#) will be made using pre-selected highly stable target stars (for first selection of possible stars see [Petrálie & Micela, 2017](#)) with similar flux to the bright targets of ARIEL.

## 6.3.3 Data level products

ARIEL data level products represent natural breakpoints in the data flow through the data processing pipeline that starts with the consolidated raw telemetry received from the spacecraft through MOC and ends in a single, fully-calibrated exoplanet spectrum for each of the targets observed. The data level products for ARIEL are defined below. The definition has been derived for data from the main science instrument, AIRS, but it is applicable up to Level 2 also for the photometry channels, the low-resolution spectrometer channel and the FGS data.

Level 0	<i>Raw telemetry</i> (sent from MOC to SOC)
Level 1	<i>Raw Spectral cubes of frames</i> (unpacked, uncompressed, meta-data enriched raw data): Formatted cubes of raw spectral detector images (ADU) of all frames for each observation.
Level 2	<i>Extracted target spectra (star+planet)</i> : Level 1 data converted to physical units as a function of time with all instrument signatures removed using the appropriate calibrations, e.g de-trended, flat-fielded, de-glitched, scattered light corrected, etc.
Level 3	<i>Individual spectra for each selected planet</i> (Final core science product): Stacking of Level 2 products and extraction of planet spectrum.

Level 1 is defined for two purposes, first it serves as input to the QLA and secondly it provides a valuable product for the scientific community user who prefers to process and calibrate the raw data with external tools and methods than those implemented in the pipeline processing.

The Level 2 science data products already are most important to the exoplanet community to derive their science, not necessarily following the ARIEL consortium selected procedure and tools to extract the final planet spectra (e.g. the Level 3 product).

### 6.3.4 Science data processing

All processing levels are processed sequentially, not concurrently accessing the same data sets: Level 0 to Level 1, Level 1 to Level 2 and Level 2 to Level 3. An overview of the data processing pipeline and levels is shown in Figure 6-2.

Up to Level 2 is processed at SOC using the data processing pipelines and calibration products provided by the IOSDC. The pipelines are delivered in form of Virtual Machines (VMs) and are configured to run autonomously at SOC. Foreseen processing steps up to Level 2 are considered standard and of low complexity for the baseline detector systems and expected science image data: de-compression, bias correction, flat fielding, non-linearity correction, de-glitching, etc. The quality control will be part of the science data processing: IOSDC will be responsible for the definition of the metrics, i.e. the products and meta-data that shall be generated for quality checks, and will deliver the software modules necessary for quality control to SOC for operations.

The Level 2 to Level 3 processing fetches the level 2 data from the archive and will require sophisticated procedures and manual intervention in order to extract the planet spectra. This task is fully under Consortium/IOSDC responsibility. The finalised Level 3 products are written back to the archive.

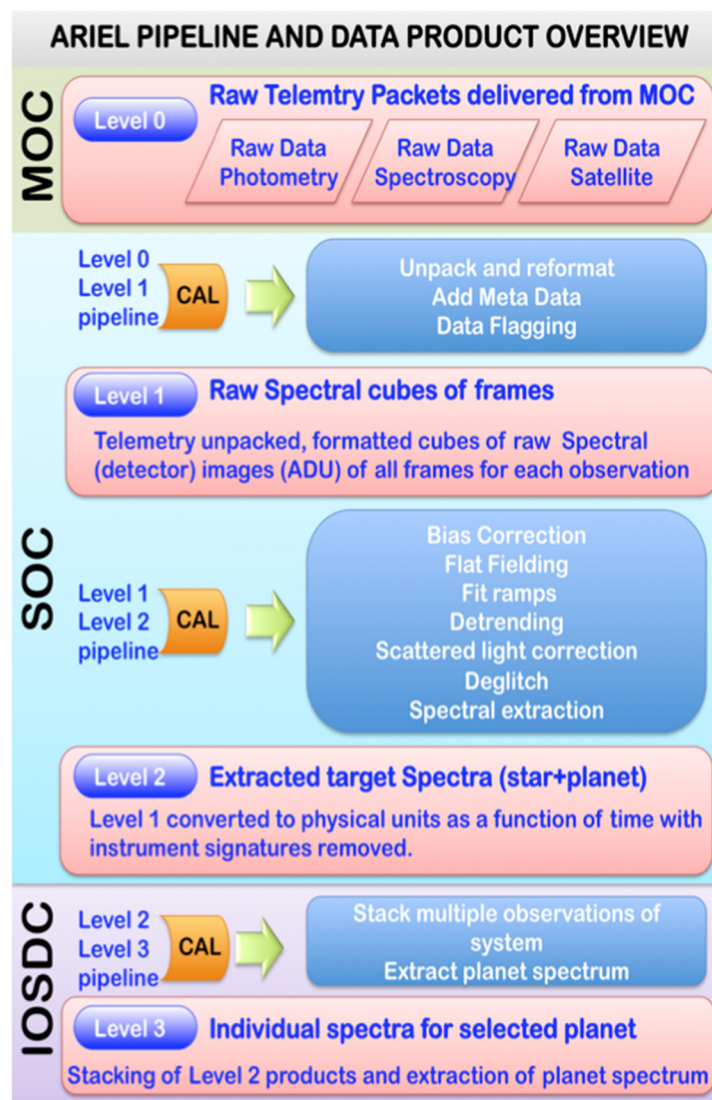


Figure 6-2: Overview of the ARIEL data processing pipeline and data processing levels.

While clearly the data processing rate needs to be significantly faster than the raw data generation rate, there is no time-criticality associated to the availability of certain products from the pipeline processing for any of the data processing levels, nor for QLA. Re-processing of the data is foreseen when new calibration data becomes available or new insights into processing steps require modifications to the pipeline modules. Cadence is currently foreseen to be approximately once per year.

The data rate (science, HK and ancillary) is about 25 Gbit/day and the total data volume including all processed data levels over the nominal mission lifetime is estimated to around 8 TB.

### **6.3.5 ARIEL archive and scientific community support**

ARIEL has a single archive serving the purpose of mission database and science data archive, which after completion of the post-operations phase becomes the legacy archive. SOC will also store for long-term preservation MOC database information such as TC history, housekeeping, ancillary data, etc., in so far the information is of relevance for the data processing or calibration. Together with the raw and processed science data the versioned data processing pipelines together with their source code and the calibration data will be stored and based on the agreed data releases made publicly available to the scientific community.

The archive serves as central interface and data repository for the data processing including calibration processing, Quick-Look Analysis, any off-line data analysis, and data dissemination of the final science data products to the general scientific community through the science data archive.

The archive will be developed, operated and maintained by ESA at ESAC, which hosts all science data archives of ESA science missions. The archive interfaces are foreseen to support International Virtual Observatory Alliance (IVOA) protocols for meta-data access, queries and distributed data storage.

With help from the IOSDC, SOC will support the scientific community user in access and exploitation of the ARIEL science data, activities that include:

- Helpdesk
- Documentation: ARIEL users handbook, data processing guides, archive guide, etc.
- Science community support activities, including data processing workshops and support to science conferences
- ARIEL web portal, ARIEL newsletter/announcements

Another planned activity will be the web publishing of the long-term observation plan and current mission status and target observation to aid follow-up and parallel observations of ARIEL targets.

## 7 Management

### 7.1 Project management

#### 7.1.1 Overview

The science and project management will follow the current practices of ESA science missions. Following the selection of ARIEL as the sole M4 mission by SPC, ESA the two parallel industrial contractors for the Definition Phase (B1), for a typical duration of 18 months. This phase will build upon the results of the Assessment Phase (0/A) study both at S/C level and at payload level. Phase B1 will be concluded by a System Requirements Review (SRR), after which ARIEL will go through the process of mission adoption and SPC approval. By the time of the SRR, all science requirements should be frozen, the subsystem level requirements documents (for both the Payload and the Spacecraft) should be available and the overall technical and programmatic feasibility of the mission should be confirmed with a design supported by detailed analyses. In parallel, all Technology Development Activities (TDAs) required will have been issued and completed by the SRR, so that all S/C and payload units have a TRL  $\geq 6$  before mission adoption.

Following mission adoption, ARIEL will move into the Implementation Phase (B2/C/D/E1). A Prime industrial contractor will be selected an ITT. The final industrial organisation will be completed in Phase B2, mostly through a process of competitive selection and by taking into account geographical distribution requirements in place at the time. At the start of this phase, a project team will be established in the Project Department of the Science Directorate (SCI-P). This team will be led by the Project Manager (PM), who will have overall responsibility to ESA for implementing the ARIEL mission. The PM will be supported by the Project Scientist (PS) who will have responsibility for science-related aspects of the mission.

Over the course of the implementation phase, the project team will conduct a Preliminary Design Review (PDR), a Critical Design Review (CDR) and finally a Flight Acceptance Review (FAR).

Responsibility for the ARIEL mission will transfer from the PM to the Mission Manager, located at ESAC, following the successful commissioning of the satellite and scientific payload. The task of the PS will continue throughout the operations and post-operations phases.

#### 7.1.2 Management of operations

ESA will be responsible for the launch, checkout and operation of the ARIEL spacecraft. ESA will establish a mission operations centre (MOC), to be located at ESOC, and a science operations centre (SOC) that will be located at ESAC.

Definition of the MOC will commence at the beginning of the definition phase, under the responsibility of a Ground Segment Manager located at ESOC who will report to the Project Manager. The responsibility for the MOC will transfer from the Ground Segment Manager to the ARIEL Spacecraft Operations Manager (SOM, located at ESOC), following the successful commissioning of the satellite and scientific payload.

Definition of the SOC will commence at the same point in time, and will be under the responsibility of a SOC Development Manager in the Operations Development Division at ESAC. The SOC Development Manager will work closely with the PS, but will formally report to the Project Manager.

Management of the Science Ground Segment will be transferred from the Operations Development Division to the Operations Division following successful commissioning of the satellite and scientific payload. As described in Chapter 6 the mission operations will be under the overall control of the ARIEL SOC at ESAC in close collaboration with the IOSDC provided by the payload consortium.

### 7.2 Procurement philosophy

ESA will have overall responsibility for the following items:

- The overall design of the mission and spacecraft (Industrial contract)
- Provision of the spacecraft service module, to include integration of the SVM and PLM together modules (Industrial contract)

- Launch (Arianespace)
- Mission and science operations (ESOC and ESAC)
- Data acquisition and distribution (ESOC and ESAC)

The payload consortium team will have responsibility for the following items:

- The cold payload module (PLM) including:
  - An Optical Bench including support structures for the telescope mirrors and baffles;
  - The ARIEL telescope assembly including all mirrors and structures plus the M2M mechanism;
  - The AIRS optical module including detectors and cold Front End Electronics;
  - The FGS optical module including detectors and cold Front End Electronics;
  - The common optics, including the dichroics to separate the light for the various channels and the on-board calibration system;
  - PLM support structure (isolating bipods);
  - Thermal control system (V-Grooves, instrument radiators, thermal straps, active cooler HX)
- The warm payload units located in the SVM
  - The Instrument Control Unit (ICU) including the AIRS Warm Front End Electronics, Data Processing Unit and Power distribution, plus hosting the Telescope Control Unit (TCU) for control of the telescope mechanism, calibration source and thermal control;
  - The Active Cooling System (ACS) including the Ne JT cooler with associated Cooler Drive Electronics (including JT-pipes interconnecting the warm units and the PLM)
  - The Fine Guidance System Control Unit (FCU) electronics providing detector control, readout and centroiding to provide the input necessary for the AOCS system.
- The cryo-harnesses that connect between the warm SVM upper panel and the cold PLM units.
- Elements of science ground segment:
  - Provision of the Instrument Operations and Science Data Centre (IOSDC; note: instrument operations will be performed by MOC);
  - Payload-specific software, modules and processing blocks for processing up to Level 2 data;
  - Long-term mission planning tool;
  - Calibration and instrument-monitoring;
  - Support to the MOC and SOC (contingencies, expert advice, payload monitoring).

Figure 4-1 summarises the hardware activities of the consortium, including the representatives from different countries. The telescope assembly and the scientific instruments will be delivered by the consortium funded by the national agencies and institutes.

The procurement approach has a significant influence on the development and AIV plan and therefore on cost, schedule and risk. An early start to the development programmes is required to demonstrate the key performances of critical technologies (e.g. Aluminium telescope / detectors / cooler) early in the programme.

The baseline for the ARIEL consortium is fully European mission, with some key technologies potentially procured from US suppliers where this is determined to be optimal for mission science return. However, the possibility of external collaboration remains open.

A proposal, CASE (Contribution to ARIEL Spectroscopy of Exoplanets), has been made to NASA under the 2016 Astrophysics call for Missions of Opportunity for US participation in ARIEL. The proposal is to supply the Sensor Chip Assemblies (SCAs) and Cold Front End Electronics (CFEE) for both of the detectors within the FGS. If both ARIEL is selected as M4 and the CASE proposal is approved by NASA then during phase B1 the implementation of the US contribution into the consortium will be negotiated and agreed both by the consortium and the CASE team, and through the official ESA / NASA channels before adoption.

### 7.3 ARIEL schedule

The key dates for the ARIEL project top level schedule are shown in Table 7-1 below. The required launch date for M4 is in 2026. With the kick-off of the Implementation Phase in Q2 2019, this leaves ~7 years for the complete development, manufacturing, assembly, integration, testing and launch campaign.

The critical path contains the manufacturing, testing and assembly of the telescope, followed by the pFM AIV for the PLM, the FM AIV of the complete spacecraft, and finally the launch campaign. The payload FM will be delivered to the spacecraft in Q3 2024.

Milestone	Schedule
MAR	Q4 2018
Phase B2/C/D Kick-off	Q2 2019
SRR	Q4 2019
PDR	Q3 2020
CDR	Q2 2022
FAR	Q3 2025
Launch (L)	2026
LEOP	L + few hours
Start of Satellite & Payload Commissioning	L + few days
Start of nominal in-orbit science operation phase	L + < 6 months
End of nominal in-orbit science operation phase	L + 4 years

Table 7-1: Key Schedule Dates for ARIEL M4 Mission

## 7.4 Science Management

In this section we outline the current assumptions for science management responsibilities for the ARIEL mission. These will form the basis of the ‘Science Management Plan’ (SMP) that will be written in the next stage of the study. The SMP will be the top-level science management document for the mission, and will require approval by the Science Programme Committee (SPC).

### 7.4.1 Project Scientist

At the start of the implementation phase ESA will appoint a Project Scientist (PS). The task of the ARIEL PS shall be to ensure the maximum science return from the mission within all applicable constraints during all mission phases. The PS shall act as the interface between internal ESA teams and contractors on science matters, and between internal and external (ARIEL) teams, including the payload consortium, and the wider scientific community.

The PS shall prepare and monitor the scientific requirements and priorities of the mission, acting in close coordination with the ARIEL Science Team (AST – see Sec. 7.4.2). In particular, the PS will be formally responsible for the ‘Design Reference Mission’ (DRM) document for ARIEL that will detail the target list (aka the ‘core sample’) that meet all science requirements (see Sec. 7.4.3).

The PS will also approve all observing schedules to be uplinked to the spacecraft for execution, and will be responsible for the handling of, in coordination with the AST and with support from the SOC as required, inputs to the DRM and all data rights issues associated with ARIEL mission data.

### 7.4.2 Science Team

The ARIEL Science Team (AST) will comprise the instrument consortium PI and scientists who are both internal and external to the instrument consortium, as well as the PS. The AST will be chaired by the PS.

The AST will support the PS in the preparation and execution of the scientific operation of the mission, and will advise on all aspects of the mission that have an impact on scientific performance. The AST will be responsible for the final selection of the ARIEL targets and relative survey Tiers, as documented in the DRM. Members of the AST will be requested to undertake ARIEL-specific tasks related to all mission phases, and may also be invited to participate in major project reviews.

### 7.4.3 Target List

ARIEL is a survey mission with the primary objective to observe a diverse sample of known, transiting exoplanets as described in Chapters 2 and 3 and documented in the DRM. The choice of targets shall meet the science requirements that govern the core sample (see Chapter 3), and will be made before launch by the AST. Inputs will be solicited from the wider community (e.g. through whitepapers, meetings, and other

mechanisms) that will be kept informed about the status of the target list, as will the ESA Advisory Bodies whose feedback will be solicited.

By the time of launch it will have evolved into a description of the final nominal pre-launch ARIEL target list documented in the DRM, however, it can – and should – evolve during the mission if there are sound scientific reasons, such as e.g. including previously unknown particularly interesting targets and actual mission in-flight performance.

#### **7.4.4 Data Rights and Proprietary Periods**

ARIEL is an ESA mission with Consortium lead that will characterise a large diverse sample of known transiting exoplanets. It is recognized that ARIEL data and science will be of interest to a large community of ‘external’ exoplanetary scientists, and there is a strong wish to embrace them. The intention is to provide high quality data products in a timely manner and to have a continuous dialogue with the wider community, ultimately maximising the science that can be achieved by the mission.

The last step (see Sec. 6.2.x) before commencing the ‘routine science phase’ (RSP) of the mission will be the ‘science demonstration phase’ (SDP). The data from the approximately 1-month duration of the SDP will be released as soon (1-month TBC) as practical after observing, and a public workshop will be organized in connection to the data (levels 1 and 2) release.

In the RSP the ARIEL observing strategy (see §2.4.2) will be to observe the targets in three ‘Tiers’ labelled ‘survey’ (Tier 1), ‘deep survey’ (Tier 2), and ‘benchmark’ (Tier 3), respectively. The data will be pipeline processed to different levels of data products (see §6.3.3) labelled ‘raw telemetry’ (level 0), ‘raw spectral frame cubes’ (level 1), ‘target (star + planet) spectra’ (level 2), and ‘individual planet spectra’ (level 3), respectively.

Datasets up to and including level 2 products for Tier 1 targets will be released quarterly, the objective is to achieve this 1 month after the end of each calendar quarter, e.g. 1 May for Q1 etc. Early in the mission this delay may need to be longer, if this is the case this interval will be reduced to 1 month as soon as possible as the mission progresses and a more complete understanding of the instrument characteristics, calibration needs and data processing/correction or systematics is gained.

Datasets up to and including level 2 products for Tier 2 and Tier 3 targets will be released similarly, after each semester where the required signal-to-noise (SNR) and spectral resolution for a particular target requiring multiple observations has been achieved. Early in the mission this delay may need to be longer, if the calibration needs and data processing/correction or systematics is not fully gained.

Release of associated ancillary data, pipeline input files, and similar will be performed in connection with the above-mentioned releases.

In addition, level 3 products will be produced and publicly released. These are not pipeline products but involve manual processing, and require a good understanding of ARIEL data, their instrumental signatures, and possible peculiarities that will only be obtained once in orbit. It is in the interest of the ARIEL consortium to have level 3 data processed, published and released soon and frequently. It is foreseen to provide level 3 products at least on an annual basis, and sooner/more frequently when the knowledge to produce them is firmly in hand.

## 8 Communications and Outreach

A mission to characterize the atmospheres of diverse worlds beyond our Solar System provides an excellent opportunity to harness curiosity, imagination and philosophical reflection in people of all ages. The discovery of more than 3500 exoplanets in the last 20 years is possibly one of the most exciting developments of modern astronomy. These discoveries resonate with the public, who have already shown very strong curiosity and interest in the exploration of the disparate worlds in our own Solar System, as well as the exotic worlds that are starting to be revealed around other stars. Closer to home, our own planet's atmosphere is so familiar that it is often taken for granted, but gives us constant reminders of the profound influence it has on our environment and very existence. The atmosphere provides the air we breathe; its presence is felt through the winds that drive it, and the colours of our sky – whether blue during the day or orange/red at sunset and sunrise – show the direct fingerprints of the Earth's atmosphere on the light arriving from the Sun.

ARIEL's communication and outreach activities will reach out to a wide audience that includes the public at large, as well as focused groups such as school students, amateur astronomers, politicians and artists. ESA will be responsible for planning and coordinating education, outreach and press release activities relating to the ARIEL mission, with the support of the Instrument Consortium. The plan will be developed and executed by ESA and the Instrument Consortium, with guidance from the ARIEL Science Team. ESA will coordinate the implementation of all education and outreach activities within the data rights framework of the mission. For the purpose of public relations activities, the Instrument Consortium will provide ESA with unlimited access to all processed and analysed data, including data still within its proprietary period. Due credit will be given regarding scientific and technical results as applicable. Details of the communications, outreach and education activity plan will evolve with the mission, with an outline for responsibilities of the different ARIEL stakeholders detailed in the science management plan. In this chapter we describe some of the initiatives that are already under consideration, with activities intended to be Member State-wide where possible.

The Instrument Consortium will work closely with space outreach and educational networks, including Europlanet, Space Awareness, Ecsite, European Schoolnet, Hands-on Universe, the Galileo Teacher Training Programme, ESA's own European Space Education Resource Offices, as well as national and more local networks, to achieve a wide engagement across Member States. All ARIEL team members will have access to communication training, ensuring that they are equipped with the skills to engage effectively with different audiences, including the public, schools, educators, media and policy makers. An open approach will be adopted: except where commercial confidentiality is at stake, the Instrument Consortium teams will welcome media professionals into their institutions, laboratories and workshops during all phases of the mission. Broadcasters will be invited to follow the mission with a view to producing bespoke programmes and documentaries that cover scientific and engineering aspects of ARIEL from cradle to grave. These activities will build on the strong record that many ARIEL Instrument Consortium scientists have with TV and radio interviews, including with leading European broadcasters such as the BBC and Euronews. Social media channels, including Twitter, Facebook and Instagram will provide up-to-the minute engagement with all aspects of the mission, with the opportunity for different instruments or exoplanet targets to have their own, individual feeds and "voices". This will complement the rapid dissemination of mission news and updates through existing ESA channels, allowing interested parties to stay informed about mission progress and performance during flight, as well as to engage with the stories and experiences of the people behind the mission. Online outlets such as YouTube and blogs will be used to post updates and interviews with ARIEL scientists and engineers to illustrate the wide range of tasks that technical professionals engage in over the course of a space mission. Short, "Day in the life of..."-type films and vodcasts, targeted at school and university students, will highlight the very wide ranges of challenges that careers in science and engineering have to offer. Live webinars and chats will provide opportunities for the public and schools to interact directly with members of the ARIEL team.

The excitement generated by the ARIEL mission and its discoveries will provide a topical platform around which to develop educational materials, helping to raise the profile of both the ARIEL mission and ESA in general within schools. Many of the core concepts behind ARIEL's science objectives and technological challenges are covered in school syllabi at different levels e.g. conditions for life, or power generation. Curriculum-linked resources will be developed covering a broad range of scientific and technical topics, such

as the study of exoplanets and their formation, exoplanet discovery techniques, spectroscopic signatures of atoms and molecules, and orbital mechanics. Materials will be disseminated to school students Europe-wide through educational partner networks, and will be supported by Continued Professional Development courses to enable school teachers to use the science and engineering challenges of ARIEL to enliven and illustrate classroom lessons and activities.

ARIEL offers many enquiry-based learning opportunities for school students. Involving students in state-of-the-art research from an early age eliminates the idea that science is ‘only for scientists’ and empowers young people to explore STEM subjects. ARIEL will build on pilot programmes, already underway with secondary school groups in the UK, to produce original, publishable scientific research associated with the characterisation of exoplanetary atmospheres, under the supervision of young PhD students and Post-Docs. Initial projects have focused on compiling data points for molecules of interest for modelling the atmospheres of cool stars and exoplanets (e.g. acetylene, titanium oxide, methane). ARIEL’s Instrument Consortium will support the roll-out of these projects through ESA member states.

Schools will be actively engaged in the selection of the ARIEL core sample. A competition will be run across ESA member states to choose a School’s Target Exoplanet. Supporting material detailing potential ARIEL candidate targets will be developed to enable students to make a scientifically-informed vote. Students will be able to follow observations of the chosen planet via a dedicated website, and participate in the analysis and interpretation of the data.

The public will also be invited to participate in the science exploitation of the ARIEL mission through access to ARIEL data sets for analysis and interpretation, taking advantage of the networks and platforms developed by very successful citizen science programmes such as Zooniverse’s Planet Hunters project, which uses Kepler data, and Backyard Worlds: Planet 9 ([Zooniverse website, 2017](#)).

Amateur astronomers play a crucial role, both in cascading the outreach efforts of professional scientists by providing a link with the broader general public, and by providing valuable scientific input. ARIEL scientists will work to engage the amateur astronomer community, organising workshops and encouraging the community to undertake a programme of observations to support ARIEL in particular (including transits and stellar variability), and the science of exoplanets, in general. Some robotic telescope networks ([LCOGT website, 2017](#)) have spectrographs installed that are available to amateur astronomers and school groups. Since most of the targets of ARIEL are relatively bright stars, follow-up observations will be feasible, profitable and exciting to both the highly experienced and relatively novice amateur astronomers and schools.

The payload Consortium will execute an active programme to brief and inform policy makers at national and European levels on scientific and technological developments of ARIEL. One-on-one meetings, seminars for politicians and stakeholders, exhibitions at venues such as the European Parliament, and public events that will involve political figures as keynote speakers will be organized to keep policy makers abreast of developments which, although in the “blue-skies” field of space exploration, create indirect economic benefits to society.

The fascinating and exotic new worlds that will be revealed by ARIEL will need visual support to capture the imagination of the public. ARIEL scientists will work together with ESA to produce images, animations, and 3-D simulations suitable for a wide range of online and broadcast media formats. Artistic and musical collaborations will be fostered to spread the impact of the mission through artworks, compositions, writing and performance inspired by the ARIEL mission and its findings. This continues and expands the tradition of the “Space Art” movement that was initiated in Europe a century ago (most notably by L. Rudaux, ([IAAA website, 2013](#))), and the multiple artistic and musical tributes to Rosetta ([Rosetta Art Tribute website, 2016](#)). Cultural and visual arts programmes will be developed at school level also, facilitating cross-curriculum discussion and interpretation of the scientific, historical and philosophical contexts of ARIEL.

## 9 References

All ESA documents, ARIEL Science Study Team technical notes and Consortium technical notes that are referred to in the text can be found at <http://ariel-spacemission.eu/publications/YBTechNotes> or directly from ESA on request.

### 9.1 References for Sections 2 & 3 – Science Case and Requirements

- Adams E.R., Seager, S., ApJ **673** 1160 (2008)
- Agúndez, M., et al., A&A **548** A73 (2012)
- Agúndez, M., et al., A&A **564** A73 (2014)
- Apai, D., et al., ApJ **768** 121 (2013)
- Ballerini, P., et al., A&A **539** 140 (2012)
- Bakos G. A., et al., PASP **114** 974 (2002)
- Barman, T. S., ApJ **661** L191 (2007)
- Barstow, J.K., et al., MNRAS **430** 1188 (2013)
- Barstow, J.K., et al., MNRAS **434** 2616 (2013a)
- Barstow, J.K., et al., Exp. Astron. **40** 545 (2015)
- Barstow, J. K. et al., MNRAS **448** 2546 (2015)
- Barstow, J.K., et al. ApJ **834** 50 (2017)
- Barstow et al., ARIEL-UCL-SCI-TN-002, 2017
- Baruteau C., et al. Protostars and Planets VI, University of Arizona Press, p.667 (2014)
- Basri, G., et al., AJ **141** 20 (2011)
- Batalha, N., Proc. NAS **111**12647 (2014)
- Bean, J. L., et al., Nature **468** 669 (2010)
- Beaulieu, J.-P., et al. MNRAS **409** 963 (2010)
- Beaulieu J.-P., et al. ApJ **731**, 16 (2011).
- Beichman, C., et al. PASP **126** 1134 (2014)
- Berta, Z. et al. ApJ **747** 35 (2012)
- Bethe, H.A., Physical Review **55** 434 (1939)
- Birkby, J.L., et al. MNRAS **436**, L35 (2013)
- Bodenheimer, P., et al., ApJ, **548**, 466, (2001)
- Bounaceur, R., et al., Int. J. Vehicle Design, **44** 124 (2017)
- Borucki, W.J., et al., Science, **325**, 709 (2009)
- Brandl, B., et al., Proc. SPIE **9908**-74 (2016)
- Brewer, J.M., et al., AJ (2016) arXiv:1612.04372
- Broeg et al., EPJWC **47** 03005 (2013)
- Brown, T.M., ApJ **553** 1006 (2001)
- Burrows, A., et al, ApJ **661**, 502 (2007)
- Broomhall, A. et al., MNRAS **396** L100 (2009)
- Cassan, A., et al., Nature **481**, 167 (2012)
- Charbonneau, D., et al., ApJ **568**, 377 (2002)
- Charbonneau, D., et al, ApJ **626**, 529 (2005)
- Charbonneau, D., et al. ApJ **686**,1341 (2008)
- Charnay, B. et al., ApJL, **813** L1 (2015)
- Chatterjee, S., et al., ApJ **686** 580 (2008)
- Chazelas, B., et al. SPIE **8444** 10 (2012)
- Cho, J.Y.-K., et al. ApJ **675** 817 (2008)
- Crossfield, et al., ApJ **723** 1436 (2010)
- Crossfield, I. J. M., ApJS **226** 7 (2016)
- Crouzet, N., et al. ApJ **761** 7 (2012)
- Crouzet, N., et al., ApJ **795** 166 (2014)
- D’Angelo, G., et al. Vol. 2011, pp. 319 U. of Arizona Press (2011)
- Danielski, C., et al. ApJ **785** 35 (2014)
- Davenport et al., ApJ **748** 58 (2012)
- Davies M. B., et al., Protostars and Planets VI, University of Arizona Press, p.787 (2014)
- Deming, D., et al. Nature **434** 740 (2005)
- Deming, D., et al. ApJ **774** 95 (2013)
- Demory, B. O., et al. ApJ **776**, L25 (2013)
- Demory, B.O., et al., Nature **532** 207 (2016)
- De Wit, J. et al., A&A **548** 128 (2012)
- De Wit, J., et al., Nature **537** 69 (2016)
- Dumusque, X., et al., ApJ **789**, 154 (2014)
- Eccleston P., et al, Proc. SPIE **9904**-33 (2016)
- Eddington, A.S., MNRAS **84** 308 (1924)
- Elkins-Tanton, Astrophysics and Space Science, **332**, 359 (2011)
- Encrenaz, T., et al. Exp. Astron. **40** 523 (2015)
- Espinoza, N., Fortney, J., Miguel, et al. ApJL (arXiv:1611.08616)
- Fabricky, D., Tremaine, S., ApJ **669** 1298 (2007)

- Fisher D.A. et al., *ApJ* **675**, 790 (2008)
- Forget, F., Leconte, J., *Phil. Trans. Royal Society* **372**, #20130084 (2014)
- Fortney, J., et al., *ApJ* **659** 166 (2007)
- Fraine, J., et al., *Nature* **513**, 526 (2014)
- Fukui, A., et al., *ApJ* **770** 95 (2013)
- Garcia-Munoz, A., Isaak, K., *PNAS* **112** 13461 (2015)
- Garcia-Piquer, A., et al., *Exp. Astron.* **40** 671 (2015)
- Gillon M., et al., *Nature* **533** 221 (2016)
- Gillon M., et al., *Nature* **542** 456 (2017)
- Grasset, O., Schneider, J., Sotin, C. *ApJ* **693** 722 (2009)
- Greene, T. P., et al., *ApJ* **817** 17 (2016)
- Grillmair, et al., *Nature* **456**, 767 (2008)
- Guillot, T., Gladman, B.: Disks, Planetesimals, planets, ASP conference proc. **219** (2000)
- Guillot, T., Showman, A., *A&A* **385**, 156 (2002)
- Gustafsson B., et al., *A&A* **486** 951 (2008)
- Habets, and Heintze, *A&AS* **46** 193 (1981)
- Hansen et al., *MNRAS* **450** 4505 (2015)
- Helled, R., Lunine, J., *MNRAS* **441** 2273 (2014)
- Herrero, E. et al., *Exp. Astron.*, **40** 695 (2015)
- Hertzsprung, E., *Publ. Astrophys. Observ. Potsdam*, **22** 1 (1911)
- Holman, M.J., et al. *Science* **330** 51 (2010)
- Howell S. B. et al. *PASP* **126** 398 (2014)
- Huber, D., et al. *ApJ* **767** 127 (2013)
- Ikoma M., Hori, Y., *ApJ* **753**, 66 (2012)
- Irwin, P., et al., *JQSRT* **109** 1118 (2008)
- Kataria, T. et al., **801** 86 (2015)
- Kim S. J., et al., *Icarus* **257** 217 (2015)
- Kite, E. S., et al., *ApJ* **828** 80 (2016)
- Kipping, D. M., et al., *ApJ* **750** 115 (2012)
- Kjeldsen H. & Bedding T. R., *A&A* **529** 8 (2011)
- Kley, W., Nelson, R.P.: *ARAA* 50, 211 (2012)
- Knutson, H. A., et al., *Nature* **447** 183 (2007)
- Knutson, H. A. et al., *Nature* **505** 66 (2014)
- Konopacky, Q. *MEMSAI* **84** 1005 (2013)
- Kreidberg, L., et al. *Nature* **505**, 69 (2014)
- Kreidberg, L., et al. *ApJL* **793** LL27 (2014b)
- Konopacky, Q. *MEMSAI* **84** 1005 (2013)
- Ingalls J. G. et al., *AJ* **152** 44 (2016)
- Laughlin, G., et al. *Nature* **457** 562 (2009)
- Leconte, J., et al., *Exp. Astron.* **40** 449 (2015)
- Leconte, J. & Chabrier, G., *A&A* **540** 20 (2012)
- Leconte, J. & Chabrier, G., *NatGe* **6** 347 (2013)
- Leconte, J., Forget, F., Lammer, H.: *Exp. Astron.* **40** 449 (2015)
- Lee, J.-M., Fletcher, L. N. and Irwin, P., *MNRAS* **420** 170 (2012)
- Léger, A., et al. *Icarus* **213** 1 (2011)
- Léger, A., Selsis, F., Sotin, C. et al. *Icarus* **169** 499 (2004)
- Levison, H.F., et al, *Astron. J.* **142** 152 (2011)
- Lindegren, L., et al., *IAU Symp.*, **248** 217 (2007)
- Line, M.R., Yung, Y. *ApJ* **779**, 6 (2013)
- Line, M.R., et al., *AJ* **152** 203 (2016)
- Linsky, J. L. et al., *ApJ* **717** 1291 (2010)
- Lissauer J. et al., *Nature* **470** 53 (2011)
- Lodders & Fegley, 'Chemistry of Low Mass Substellar Objects', Springer (2006)
- Macintosh, B. et al., *Science* **350** 64 (2015)
- Madhusudhan, N., Seager, S., *ApJ* **707** 24 (2009)
- Majeau, C., et al., *ApJ* **747** L20 (2012)
- Marty, B., *Science Letters*, **313** 56 (2012)
- Matter, A., Guillot, T., Morbidelli, A., *Planet. Space Sci.* **57** 816 (2009)
- Matthews, J.M., et al. *Nature* **430** 51 (2004)
- McCullough, P., et al., *ApJ* **791**, 55 (2014)
- Micela, G., et al., *Exp. Astron.* **40** 577 (2015)
- Micela, G., *Exp. Astron.* **40** 723 (2015)
- Miguel, Y., et al., *ApJL* **742** L19 (2011) Miguel, Y., et al., *MNRAS* **446** 345 (2015)
- Morales, J.C., et al., *Exp. Astron.* **40** 655 (2015)
- Morbidelli A. et al., *Ann. Rev. Earth & Plan. Sci.* **40** 251 (2012)
- Morello, G., et al., *ApJ* **786** 22 (2013)
- Morello, et al., *ApJ*, **786** 22 (2014)
- Morello, G. et al., *ApJ* **802** 117 (2015)

- Morello, G., *ApJ* **808** 56 (2015)
- Morello, G., et al., *ApJ* **820** 86 (2016)
- Moses, J., et al. *ApJ* **737** 15 (2011)
- Nutzman, P., Charbonneau, D., *PASP* **120** 317 (2008)
- Palle, P. L., et al. *ApJ* **441** 952 (1995)
- Parmentier, V. et al., *ApJ* **828** 22 (2016)
- Pascale, E., et al., *Exp. Astron.* **40** 601 (2015)
- Perryman, M. A. C. et al., **797** 14 (2014)
- Pickles, A. J. *PASP* **110** 863 (1998)
- Pillitteri, I. & Micela, G., *ARIEL-INAF-SCI-TN-002* (2017)
- Pollacco, D.L., et al., *PASP* **118** 1407 (2006)
- Puig, L., et al., *Proc. SPIE* **9904** 99041W (2016); doi:10.1117/12.2230964
- Puig, L., et al. *Exp. Astron.* **40** 393 (2015)
- Queloz, D. et al., *A&A* **354** S. 99 (2000)
- Rauer, H., et al. *Exp. Astron.*, 38, 249 (2014)
- Rauscher, E., et al. *ApJ* **662** L115 (2007)
- Raymond S. N., et al.; *Icarus* **183** 265 (2006)
- Rein, H., arXiv:1211.7121 (2012)
- Ricker et al., *SPIE* **9143** 20 (2014)
- Rowe, J., et al., *ApJ* **689** 1345 (2008)
- Russell, H. N.: *Popular Astronomy* **22** 275 (1914)
- Sarkar, S., et al., *SPIE* **9904** 138 (2016)
- Sarkar, S., et al., *ARIEL-CRDF-PL-AN-001*;  
*ARIEL-CRDF-PL-TN-002* (2017)
- Scandariato, G. et al., *Exp. Astron.* **40** 711 (2015)
- Seager, S., Sasselov, D.D., *ApJ* **537**, 916 (2000)
- Sharp, C. M., Burrows, A. *ApJS*, **168**, 140 (2007)
- Sing, D. K., et al. *Nature* **529** 59 (2016)
- Snellen, I. A. G., et al., *Nature* **465** 1049 (2010)
- Snellen, I. A. G., et al., *Nature* **509** 63 (2014)
- Solanki, S. K., Unruh, Y. C., *MNRAS*, **348** 307 (2003)
- Sozzetti, A., et al. *Exp. Astron.* **40** 595 (2015)
- Stevenson, K. B., et al. *Science* **346** 838 (2014)
- Swain, M. R. et al., *Nature* **463**, 637 (2010)
- Swain, M. R., Vasisht, G., Tinetti, G., *Nature* **452**, 329 (2008)
- Swain, M. R., et al. *ApJ* **690**, L114 (2009)
- Taylor, F. W. et al.: ed. F. Bagenal, T. E. Dowling, & W. McKinnon (Cambridge: Cambridge Univ. Press), Chapter 4 (2004)
- Tinetti G. et al., *Proc. SPIE* **9904** 99041X (2016); doi:10.1117/12.2232370
- Tinetti, G., Encrenaz E., Coustenis A., *Astron Astrophys Rev.* **21**, 63 (2013).
- Tinetti, G., Deroo, P., Swain, M., et al. *ApJ* **712** L139 (2010)
- Tinetti, G., et al. *Nature* **448** 169 (2007)
- Todorov, K. O. et al., *ApJ* **796** 100 (2014)
- Tofflemire et al., *AJ* **143**12 (2012)
- TriAUD A. et al., *MNRAS* **444** 711 (2014)
- Tsiganis, K., et al., *Nature* **435** 459 (2005)
- Turrini, D., et al., *Exp. Astron.* **40** 501 (2015)
- Turrini, D., Svetsov, V.: *Life* **4** 4 (2014). doi:10.3390/life4010004
- Valencia, D., et al., *Icarus* **181** 545 (2006)
- Valencia, D., et al., *ApJ* **665** 1413 (2007)
- Valencia, D., et al., *ApJ* **775** 10 (2013)
- Varley, R. et al., *Exp. Astron.*, **40** 621 (2015)
- Vazan, A. et al., *ApJ* **829** 118 (2016)
- Venot, O., et al., *A&A* **546**, A43 (2012)
- Venot, O., et al., *A&A* **577** A33 (2015)
- Venot, O., et al., *ApJ* **830** 77 (2016)
- Venturini, J., et al., *A&A* **596** 90 (2016)
- Vidal-Madjar, A. et al., *Nature*, **422**, 143 (2003)
- Waldmann, I.P., *ApJ* **747** 12 (2012)
- Waldmann I. P., et al. *ApJ* **744** 35 (2012)
- Waldmann, I. P. et al., *ApJ*, **766** 7 (2013)
- Waldmann, I. P. *ApJ* **780** 23 (2014)
- Waldmann, I.P., Pascale, E., *Exp. Astron.* **40** 639 (2015)
- Waldmann, I.P., et al., *ApJ* **802** 107 (2015a)
- Waldmann, I.P., et al., *ApJ* **813** 13 (2015b)
- Weidenschilling, S.J. et al. *Nature* **384** 619 (1996)
- Wordsworth, R.D., et al., *A&A* **522**, A22 (2010)
- Yurchenko, S.N., et al., *Proc. Nat. Acad. Sci.* **111**, 9379 (2014)
- Zingales, T. et al., *Exp. Astron.* Submitted,

ARIEL-UCL-SCI-TN-002, 2017

Zurlo A. et al., *A&A*, **587** A57 (2016)

## 9.2 References for Section 4 & 5 – Payload, Mission and Spacecraft Design

Bagnasco, G., et al., *SPIE* **6692** (2007)

Bishop, G., et al., ARIEL-RAL-PL-PL-002, ARIEL Design, Development, Verification and Engineering Plan, Iss 1.0 (2017)

Bowles, N., et al., ARIEL-OXF-PL-TN-001, ARIEL Payload Calibration OGSE Conceptual Design, Iss 1.0 (2017)

Crouzet, P-E., et al. *Proc. of SPIE* Vol. 9639, 9639OX-1, (2015)

Da Deppo, V., et al., ARIEL-INAF-PL-TN-004, ARIEL Telescope Material Trade-Off Analysis, Iss 2.0 (2017)

Eccleston, P. et al., ARIEL-RAL-PL-DD-001, ARIEL Payload Design Description, Iss 2.0 (2017)

Focardi, M., et al., ARIEL-INAF-PL-TN-001, ARIEL ICU Detailed Design Description, Iss 2.0 (2017)

Hunt, T., et al., ARIEL-MSSL-PL-AN-001, ARIEL PLM Mechanical Analysis Report, Iss 2.0 (2017)

McMurty, C., et al., *Optical Engineering* **52**, 9 (2013)

Middleton, K., et al., ARIEL-RAL-PL-TN-001, ARIEL Baseline Telescope Optical Prescription, Iss 3.2 (2017)

Morgante, G., et al., ARIEL-INAF-PL-TN-003, ARIEL PLM Thermal Analysis Report, Iss 2.0 (2017)

Nascimbeni, V., & Piotto, G., ARIEL-INAF-SCI-TN-004, Signal Contaminant analysis for ARIEL, Iss 0.1 (2017)

Papageorgiou, A., et al., ARIEL-CRDF-PL-ML-001, ARIEL Performance Model, Iss 2.0 (2017)

Pascale, E., et al., ARIEL-CRDF-PL-TN-003, ARIEL Wavefront Distortion Analysis, Iss 1.2 (2017)

Ray, T., et al., ARIEL-DIAS-PL-PL-001, ARIEL Dichroic Study Results and Development Plan, Iss 1.0 (2017)

Ross, R.; “Recent Long-life Space Cryocooler Flight Operating Experience as of May 2016”, JPL, Priv. Comm.

Sarkar, S., et al., ARIEL-CRDF-PL-AN-001, ARIEL Performance Analysis Report, Iss 2.2 (2017)

Wright, G., et al, *PASP* **127**, 595 (2015)

## 9.3 References for Section 6 – Mission Operations

Garcia-Piquer, A., et al., *SPIE* **9152**, 21 (2014)

Garcia-Piquer, A., et al., *Exp. Astron.* **40**, 671 (2015)

Garcia-Piquer, A. et al, *A&A*, submitted (2017)

Kohley, R., et al, ESA-ARIEL-ESAC-SOC-AD-001, ARIEL Science Operations Assumptions Document (SOAD), Iss 1.0 (2017)

Morales, J.C., et al. 2015. “Scheduling the EChO survey with known exoplanets”, *Experimental Astronomy*, **40**, 655

Morales, J.C., et al., ARIEL-ICE-GS-TN-001, ARIEL Long Term Planning, Iss 1.0 (2017).

Pearson, C., et al, ARIEL-RAL-PL-PL-005, ARIEL Ground Calibration Plan, Iss 1.0 (2017)

Petralia, A., Micela, G., ARIEL-INAF-SCI-TN-003, Sky Calibrators for ARIEL, Iss 0.1 (2017)

## 10 List of Acronyms

ACS	Active Cooling System
ADS	Airbus Defence and Space
AIRS	ARIEL InfraRed Spectrometer
AIV	Assembly, Integration and Verification
AO	Announcement of Opportunity
AOCS	Attitude and Orbit Control System
AOR	Astronomical Observation Request
APE	Absolute Pointing Error
ARIEL	Atmospheric Remote-sensing Infrared Exoplanet Large survey
ASIC	Application-Specific Integrated Circuit
AU	Astronomical Units
AVM	Avionics Model
CAD	Computer-Aided Design
CDE	Cooler Drive Electronics
CDF	Concurrent Design Facility
CDMS	Command and Data Management System
CDR	Critical Design Review
cFEE	Cold Front End Electronics
CHEOPS	Characterizing Exoplanets Satellite
CTE	Coefficient of Thermal Expansion
DCU	Detector Control Unit
DM	Development Model
DPU	Data Processing Unit
DRM	Design Reference Mission (document)
EChO	Exoplanet Characterisation Observatory
ECSS	European Cooperation for Space Standardization
EID-A	Experiment Interface Document-A
(E)-ELT	(European) Extremely Large Telescope
EM	Engineering Model
ESA	European Space Agency
ESAC	European Space Astronomy Centre
ESOC	European Space Operations Centre
FAR	Flight Acceptance Review
FCU	FGS Control Unit
FDIR	Fault Detection, Isolation and Recovery
FGS	Fine Guidance Sensor / System
(p)FM	(proto-)Flight Model
FoV	Field of View

FPA	Focal Plane Array / Assembly
FPU	Focal Plane Unit
FWHM	Full Width Half Maximum
GFRP	Glass Fibre Reinforced Polymer
GMM	Geometrical Mathematical Model
GS	Ground Segment
HARPS	High Accuracy Radial-velocity Planet Searcher
HCU	Housekeeping and Calibration Source Unit
HGA	High Gain Antenna
HK	HouseKeeping
HX	Heat eXchanger
ICU	Instrument Control Unit
IOB	Instrument Optical Bench
IOSDC	Instrument Operations and Science Data Centre
IRAC	InfraRed Array Camera
ISO	Infrared Space Observatory
ITAR	International Traffic in Arms Regulations
ITT	Invitation to Tender
IVOA	International Virtual Observatory Alliance
JPL	Jet Propulsion Lab
JT	Joule Thompson
JUICE	JUPITER Icy Moons Explorer
JWST	James Webb Space Telescope
KBO	Kuiper Belt Object
L2	Second Lagrangian Point
LED	Light Emitting Diode
LEO	Low Earth Orbit
LEOP	Launch and Early Operations Phase
LFSA	Large-Format Sensor Array
LGA	Low Gain Antenna
LoS	Line of Sight
(N)LTE	(Non)-Local Thermodynamic Equilibrium
LV	Launch Vehicle
LWS	Long Wave Spectrometer (ISO)
M2M	M2 mirror Mechanism
MCT	Mercury Cadmium Telluride
MICD	Mechanical Interface Control Drawing
MIRI	Mid-InfraRed Instrument
MLI	Multi-Layer Insulation

MOC	Mission Operations Centre
MPE	Mean Pointing Error
MRD	Mission Requirements Document
MRS	Mission Reference Sample
MRS	Medium Resolution Spectrometer (JWST-MIRI)
NEMESIS	Non-linear optimal Estimator for Multivariate Spectral analysis
NEOCam	Near Earth Object Camera
NGTS	Next Generation Transit Survey
NIR	Near InfraRed
NIRSpec	Near IR Spectrometer
OBC	On-Board Computer
OBCU	On-Board Calibration Unit
OBS	On-Board Software
OGSE	On-ground Support Equipment
PCDU	Power Control and Distribution Unit
PDE	Pointing Drift Error
PDR	Preliminary Design Review
PI	Principal Investigator
PLM	Payload Module
PM	Project Manager
POS	Planned Observation Sequence
PS	Project Scientist
PSF	Point Spread Function
PSU	Power Supply Unit
PTM	Pathfinder Telescope Mirror
PVM	Performance Verification Model
QE	Quantum Efficiency
QLA	Quick Look Analysis
QM	Qualification Model
R	Resolving power
RM	Radiometric Model
ROIC	Read-Out Integrated Circuits
RPE	Relative Pointing Error
RSP	Routine Science Phase
S/C	Spacecraft
S/W	SoftWare
SAA	Solar Aspect Angle

SCA	Sensor Chip Assembly
SciRD	Science Requirements Document
SDP	Science Demonstration Phase
SED	Spectral Energy Distribution
SMP	Science Management Plan
SNR	Signal-to-Noise Ratio
SOC	Science Operations Centre
SPC	Science Programme Committee
SPIRE	Spectral and Photometric Imaging Receiver (Herschel)
SRP	Solar Radiation Pressure
SRR	System Requirements Review
SST	Study Science Team
STM	Structural and Thermal Model
SVM	SerVice Module
TAC	Time Allocation Committee
TAS	Thales Alenia Space
TBC	To Be Confirmed
TBD	To be Determined
TCM	Transfer Correction Manoeuvre
TCU	Telescope Control Unit
TDA	Technology Development Activity
TESS	Transiting Exoplanet Survey Satellite
TM/TC	TeleMetry/TeleCommand
TMM	Thermal Mass Model
TN	Technical Note
TOB	Telescope Optical Bench
TRL	Technology Readiness Level
TRP	Technology Research Programme
TT&C	Tracking, Telemetry and Commanding
VG(s)	V-Groove(s)
VISPhot	Visible Photometer
VLT	Very Large Telescope
VM	Virtual Machine
WFC	Wide Field Camera
WFE	WaveFront Error

# 11 Appendix A: ARIEL Payload Consortium

## 11.1 Consortium Management Team

### 11.1.1 Co-PI's & Co-I's

Giovanna Tinetti, University College London, UK; Jean-Philippe Beaulieu, Institut d'Astrophysique de Paris, France; Giusi Micela, INAF – Osservatorio Astronomico di Palermo, Italy; Manuel Guedel, University of Vienna, Austria; Bart Vandenbussche, University of Leuven, Belgium; Hans Ulrik Nørgaard-Nielsen, DTU, Denmark; Paul Hartogh, Max Planck Sonnensystem, Germany; Tom Ray, Dublin Institute for Advanced Studies, Ireland; Michiel Min, SRON Netherlands Institute for Space Research, the Netherlands; Mirek Rataj, Space Research Centre, Polish Academy of Science, Poland; Ignasi Ribas, IEEC – CSIC, Spain; Matt Griffin, University of Cardiff, UK.

### 11.1.2 National Project Managers

Paul Eccleston, STFC – RAL Space, UK; Jean-Louis Auguères, CEA, France; Emanuele Pace, Uni di Firenze, Italy; Josep Colomé, IEEC – CSIC, Spain; Deirdre Coffey, DIAS, Ireland; Martin Frericks, SRON, the Netherlands; Hans Ulrik Nørgaard-Nielsen, DTU, Denmark; Roland Ottensamer, Uni of Vienna, Austria; Mirek Rataj, Space Research Centre, Polish Academy of Science, Poland; Miriam Rengel, MPS, Germany; Etienne Renotte, CSL, Belgium.

## 11.2 Consortium Technical Team Coordinators

Paul Eccleston, RAL Space, UK; Kevin Middleton, RAL Space, UK; Jerome Amiaux, CEA, France; Naidu Bezawada, UKATC, UK; Georgia Bishop, RAL Space, UK. Neil Bowles, University of Oxford, UK; Deirdre Coffey, DIAS, Ireland; Josep Colomé, IEEC-CSIC, Spain; Martin Crook, RAL TD, UK; Vania Da Deppo, CNR-IFN Padova, Italy; Mauro Focardi, INAF-OAA; Tom Hunt, MSSL, UK; Pino Malaguti, INAF - IASF Bologna, Italy; Andrea Moneti, IAP, France; Gianluca Morgante, INAF - IASF Bologna, Italy; Marc Ollivier, IAS Paris, France; Roland Ottensamer, University of Vienna, Austria; Emanuele Pace, Università di Firenze, Italy; Enzo Pascale, Cardiff University, UK; Chris Pearson, RAL Space, UK; Mirek Rataj, Space Research Centre, Polish Academy of Science, Poland; Richard Stamper, RAL Space, UK;

## 11.3 Consortium Science Team Coordinators

**ESA Science Study Team** – Giovanna Tinetti, UCL, UK; Pierre Drossart, LESIA, France; Paul Eccleston, RAL Space, UK; Paul Hartogh, MPS Germany; Jérémy Leconte, Laboratoire d'Astrophysique de Bordeaux, France; Giusi Micela, INAF, Palermo, Italy; Marc Ollivier, IAS Paris, France; Diego Turrini, INAF-IAPS, Italy; Paulina Wolkenberg, CBK-PAN, Poland.

**Science Team Working Group Leads** – Joanna Barstow, UCL, UK; Jean-Philippe Beaulieu, IAP, France; Matt Burleigh, University of Leicester; James Cho, QMUL, UK; Vincent Coudé du Foresto, LESIA, France; Athena Coustenis, LESIA, France; Leen Decin, University of Leuven, Belgium; Therese Encrenaz, LESIA, France; Marina Galand, Imperial College, UK; Michael Gillon, ULG, Belgium; Juan Carlos Morales, IEEC-CSIC, Spain; Pierre-Olivier Lagage, CEA, France; Giuseppe Malaguti, INAF-IASF Bologna, Italy; Antonio García Muñoz, Technische Universität Berlin, Germany; Ravit Helled, University of Zurich, Switzerland; Michiel Min, SRON, the Netherlands; Andrea Moneti, IAP, France; Isabella Pagano, OAct, Italy; Enzo Pascale, Sapienza Università di Roma, Italy; Giuseppe Piccioni, INAF/IAPS, Italy; David Pinfield, UH, UK; Ignasi Ribas, IEEC – CSIC, Spain; Subhjit Sarkar, Cardiff University, UK; Franck Selsis, Université de Bordeaux, France; Jonathan Tennyson, UCL, UK; Amaury Triaud, Cambridge University, UK; Olivia Venot, LISA, France; Ingo Waldmann, UCL, UK; David Waltham, RHUL, UK; Gillian Wright, UKATC, UK.

## 11.4 Consortium Contributing Scientists & Engineers

**Austria** – University of Vienne – F. Kerschbaum, A. Luntzer, R. Ottensamer, T. Rank-Lüftinger

**Belgium** – University of Leuven – Ioannis Argyriou; Université de Liège – B. Bonfond, J.-C. Gerard, Denis Grodent, J. Gustin, B. Hubert, A. Radioti, L. Soret, A. Stiepen; Xenics – Pieter Deroo;

**Denmark** – DTU – Allan Hornstrup

**France** – CEA – Sacha Brun, Emeline Bolmont, Antoine Strugarek, Vincent Minier, Stephane Mathis; CNES – Yves André, Rodolphe Clédassou, Bastien Duong, Hervé Geoffroy, Jean Jaubert, Queyrel Julien; LAM – Alexandre Santerne; IAP – Christophe Alard, Virginie Batista, Jean-Pierre Maillard, Jean-Baptiste Marquette; Observatoire de la

Cote d'Azur – Yamila Miguel; Observatoire de Paris – Nicole Allard, Camilla Danielski; LESIA – Bruno Bézard, Benjamin Charnay, Emanuel Lellouch, Pierre Kervella, Bruno Sicardy, Sabine Vinatier; Pernelle Bernardi, Y. Hello, Jean-Michel Réess, N. Nguyen Tong;

**Germany** – Vanessa Doublier; MPS – Markus Fränz, Christopher Jarchow, Norbert Krupp, Urs Mall, Alexander Medvedev, Ladislav Rezac; Hamburg University – Nicolas Iro.

**Italy** – INAF-IASF Bologna – Luca Terenzi; INAF-IAPS, Rome – Francesca Altieri, Giancarlo Bellucci, Anna Maria Di Giorgio, Maria Farina, Alessandro Mura, Fabrizio Oliva, Stefano Pezzuto, Giuseppe Sindoni; INAF-OAA, John Robert Brucato, Vladimiro Noce, Federico Landini, Nicoletta Sanna; INAF-OACt – Gaetano Scandariato; INAF Astronomical Observatory of Padova – Serena Benatti, Riccardo Claudi, Jesus Maldonado; INAF-OAPa – Laura Affer, Rosaria Bonito, Cesare Cecchi Pestellini, Angela Ciaravella, Ettore Flaccomio, Mario Giuseppe Guarcello, Antonio Maggio, Antonino Petralia, Ignazio Pillitteri, Loredana Prisinzano; INAF/OATo – Aldo S. Bonomo, Mario Damasso, Alessandro Sozzetti; Università di Firenze – Cristian Baccani, Giuseppe Leto, Maurizio Pancrazzi; Università di Padova – Valerio Nascimbeni; Giampaolo Piotto;

**The Netherlands** – SRON – Martin Frericks, Rens Waters, Frans Zwart; UvA, Carsten Dominik, Allona Vazan; University of Delft – Daphne Stam; University of Leiden – Ignas Snellen

**Poland** – CBK-PAN – Marek Banaszekiewicz, Maria Blecka, Anna Wawrzaszek; Piotr Wawer, Mateusz Sobiecki, Konrad Skup, Rafał Graczyk, Waldemar Bujwan

**Spain** – CAB (INTA-CSIC) – María Rosa Zapatero Osorio; IEEC-CSIC – Carles Sierra, Álvaro García-Piquer, Lluís Gesa, Francesc Vilardell, Enrique Herrero, Manuel Perger, Albert Rosich, Marina Lafarga; IAC – Enric Palle, Guo Chen

**Switzerland** – University of Bern – Kevin Heng

**UK** – University of Cardiff – Peter Ade, S. Doyle, S. Eales, W. Gear, H. Gomez, P. Hargrave, Andreas Papageorgiou, G. Pisano, C. Tucker, A. Whitworth; University of Exeter – Benjamin Drummond; University of Keele – Pierre Maxted; University of Leicester – Sarah Casewell, Leigh Fletcher; University of Oxford – Patrick Irwin, Ray Pierrehumbert; UCL – Claudio Arena, Alan Aylward, Mario Damiano, Steve Fossey, Anita Heward, Giuseppe Morello, Marco Rocchetto, Giorgio Savini, Marcell Tessenyi, Angelos Tsiaras, Serena Viti, Sergey N. Yurchenko, Tiziano Zingales; UH – Hugh Jones; UK ATC – Ian Bryson, William Taylor, UK ATC;

## 11.5 International Participating Scientists

US – ASU – Mike Line; Caltech – Renyu Hu, Yuk L. Yung; UA–LPL – Caitlin Griffith, Tommi Koskinen, Vivien Parmentier; JPL – Mark Swain (for and on behalf of the CASE team), Gautam Vasisht, Robert Zellem; LPI – Julianne Moses; NMSU – Patrick Gaulme; Princeton University – Gaspar Bakos; University of Chicago – Jacob Bean;

Japan – ELSI – Shigeru Ida; Tokyo Institute of Technology – Masahiro Ikoma; University of Osaka – Taro Matsuo;

Canada – Université de Montréal – René Doyon; University of Toronto – Diana Valencia;

Mexico – UNAM, Christophe Morisset;